Edited by
Ivan Nazarenko

DYNAMIC PROCESSES IN TECHNOLOGICAL TECHNICAL SYSTEMS

Monograph

Technology Center

2021

Reviewers:
Bogdan Korobko, Doctor of Technical Sciences, Associate Professor, Vice-Rector for Scientific-Pedagogical and Educational, Department of Construction Machinery and Equipment, National University «Yuri Kondratyuk Poltava Polytechnic»;
Oleksii Lanets, Doctor of Technical Sciences, Professor, Director of Institute, Institute of Mechanical Engineering and Transport, Lviv Polytechnic National University;
Victor Gaidaichuk, Doctor of Technical Sciences, Professor, Head of Department of Theoretical Mechanics, Kyiv National University of Construction and Architecture.

D98   **Authors:**
Edited by **Ivan Nazarenko**
Ivan Nazarenko, Oleg Dedov, Iryna Bernyk, Andrii Bondarenko, Andrii Zapryvoda, Maxim Nazarenko, Ivan Pereginets, Yevhen Mishchuk, Mykola Kyzminec, Serhii Oryshchenko, Oleg Fedorenko, Sergii Tsepelev, Artur Onyshchenko, Liudmyla Titova, Ivan Rogovskii, Mykola Ruchynskyi, Anatoly Svidersky, Volodymyr Slipetskyi, Maksym Delembovskyi, Igor Zalisko, Mykola Nesterenko
Dynamic processes in technological technical systems: monograph / I. Nazarenko and others. – Kharkiv: PC TECHNOLOGY CENTER, 2021. – 196 p.

The monograph is devoted to the study of dynamic processes in technical systems for industrial machine building. Models and equations of motion of discrete and continuous dynamic systems, dispersed media in the spectrum of their processing are considered. Changes in the parameters of subsystems are revealed: working mediums, mechanical systems, the processes of their interaction are investigated on the basis of taking into account their stress-strain state. The processes of grinding, sorting, mixing, compaction of materials and media are considered. The given algorithms and methods of calculations of technical systems of different technological designation.
Figures 118, Tables 14, References 145 items.

9 786177 319497

AUTHORS

IVAN NAZARENKO
Doctor of Technical Sciences, Professor, Head of Department
Department of Machinery and Equipment of Technological Processes
Kyiv National University of Construction and Architecture
ORCID ID: https://orcid.org/0000-0002-1888-3687

OLEG DEDOV
Doctor of Technical Sciences, Associate Professor
Department of Machinery and Equipment of Technological Processes
Kyiv National University of Construction and Architecture
ORCID ID: https://orcid.org/0000-0001-5006-772X

IRYNA BERNYK
Doctor of Technical Sciences, Associate Professor
Department of Food Technology and Microbiology
Vinnytsia National Agrarian University
ORCID ID: https://orcid.org/0000-0002-1367-3058

ANDRII BONDARENKO
PhD, Associate Professor, Head of Department
Department of Mechanical Engineering
Odessa State Academy of Civil Engineering and Architecture
ORCID ID: https://orcid.org/0000-0002-4594-6399

ANDRII ZAPRYVODA
PhD, Associate Professor
Department of Architectural Constructions
Kyiv National University of Construction and Architecture
ORCID ID: https://orcid.org/0000-0001-9171-9325

MAXIM NAZARENKO
PhD, Director
Limited Liability Company ACADEMBUDSERVICE
ORCID ID: https://orcid.org/0000-0003-1463-1789

IVAN PEREGINETS
PhD, Associate Professor
Department of Machines and Equipment of Technological Processes
Kyiv National University of Construction and Architecture
ORCID ID: https://orcid.org/0000-0003-3812-6509

YEVHEN MISHCHUK
PhD, Associate Professor
Department of Machines and Equipment of Technological Processes
Kyiv National University of Construction and Architecture
ORCID ID: https://orcid.org/0000-0002-7850-0975

MYKOLA KYZMINEC
Doctor of Technical Sciences, Professor
Department of Computer, Engineering Graphics and Design
National Transport University
ORCID ID: https://orcid.org/0000-0002-9636-919X

SERHII ORYSHCHENKO
PhD, Associate Professor
Department of Machines and Equipment of Technological Processes
Kyiv National University of Construction and Architecture
ORCID ID: https://orcid.org/0000-0002-5359-5285

OLEG FEDORENKO
Head of Department
Department of Road Maintenance
State Agency of Automobile Road of Ukraine
ORCID ID: https://orcid.org/0000-0003-3628-4298

SERGII TSEPELEV
Director of Department
Department of Road Network Development
State Agency of Automobile Road of Ukraine
ORCID ID: https://orcid.org/0000-0001-7232-4651

ARTUR ONYSHCHENKO
Doctor of Technical Sciences, Professor
Department of Bridges, Tunnels and Hydraulic Structures
National Transport University
ORCID ID: https://orcid.org/0000-0002-1040-4530

LIUDMYLA TITOVA
PhD, Associate Professor
Department of Technical Service and Engineering Management named after M. P. Momotenko
National University of Life and Environmental Sciences of Ukraine
ORCID ID: https://orcid.org/0000-0001-7313-1253

IVAN ROGOVSKII
Doctor of Technical Sciences, Senior Researcher
Department of Technical Service and Engineering Management named after M. P. Momotenko
National University of Life and Environmental Sciences of Ukraine
ORCID ID: https://orcid.org/0000-0002-6957-1616

MYKOLA RUCHYNSKYI
PhD, Professor
Department of Machinery and Equipment of Technological Processes
Kyiv National University of Construction and Architecture
ORCID ID: https://orcid.org/0000-0002-9362-292X

ANATOLY SVIDERSKY
PhD, Professor
Department of Machinery and Equipment of Technological Processes
Kyiv National University of Construction and Architecture
ORCID ID: https://orcid.org/0000-0002-0005-7969

VOLODYMYR SLIPETSKYI
Deputy Director
Department of Procurement and Contract Policy
Corporation «DSK – ZHITLOBUD»
ORCID ID: https://orcid.org/0000-0002-9539-6022

MAKSYM DELEMBOVSKYI
PhD, Associate Professor
Department of Machines and Equipment Processes
Kyiv National University of Construction and Architecture
ORCID ID: https://orcid.org/0000-0002-6543-0701

IGOR ZALISKO
PhD, Associate Professor
Limited Liability Company «Drogobych Truck Crane Plant»
ORCID ID: https://orcid.org/0000-0002-8353-9524

MYKOLA NESTERENKO
PhD, Associate Professor
Department of Construction Machinery and Equipment
National University «Yuri Kondratyuk Poltava Polytechnic»
ORCID ID: https://orcid.org/0000-0002-4073-1233

ABSTRACT

The monograph is devoted to the study of dynamic processes in technical systems for various technological purposes. A new approach and methodology is proposed for a systemic, synergistic approach, taking into account the influence of energy fields of physical and mechanical effects, transformation and inversion of types of energy action. Models and equations of motion of discrete and continuous dynamic systems, dispersed media in the spectrum of their processing are considered. Changes in the parameters of subsystems are revealed: working mediums, mechanical systems, the processes of their interaction are investigated on the basis of taking into account their stress-strain state. The processes of grinding, sorting, mixing, compaction of materials and media are considered. The intensification of physical and mechanical processes, methods and means of their creation was achieved by the systematization and complexity of approaches due to the joint consideration of the mutual influence of the internal properties of subsystems. The processes of material processing by superresonant, subresonant and multi-mode parameters are investigated. Methods for determining effective parameters and modes of their operation are proposed. The processes of grinding, sorting, mixing, compaction of the processing medium in the field of vibration load are described. As a result of the research carried out, new properties of the behavior of discrete-continuous systems under power load conditions are revealed. For the first time, the stresses and deformations of both working bodies and media were taken into account to create energy-saving vibration systems for various technological processes. The carried out scientific research makes it possible to obtain the laws of change in the state of dispersed media under the action of power loads by technical systems, new technological and design solutions were proposed.

KEYWORDS

Technical systems, technological media, grinding, sorting, mixing, compaction, cavitation, models, continuous and discrete parameters, force loads, stresses, deformations, energy, synergetics, vibration amplitude, vibration frequency, laws of motion.

CONTENTS

LIST OF TABLES

LIST OF FIGURES

CIRCLE OF READERS AND SCOPE OF APPLICATION

It is intended for students, masters, post-graduate students, doctoral students of higher educational institutions of a technical profile, and can also be useful for designers, research workers of industrial mechanical engineering.

The processes of material processing by superresonant, subresonant and multimode parameters are investigated. Methods for determining effective parameters and modes of their operation are proposed. The processes of grinding, sorting, mixing, compaction of the processing medium in the field of vibration load are described. As a result of the research carried out, new properties of the behavior of discrete-continuous systems under power load conditions are revealed. For the first time, the stresses and deformations of both working bodies and media were taken into account to create energy-saving vibration systems for various technological processes. The carried out scientific research makes it possible to obtain the laws of change in the state of dispersed media under the action of power loads by technical systems, new technological and design solutions were proposed.

The monograph will be of interest to the countries of Europe, America, Asia.

INTRODUCTION

I. Nazarenko

Technological technical systems occupy a leading place in many technological processes in various sectors of the national economy. The classification features and the proposed criteria have been determined, according to which the assessment of the design and technological parameters of the existing technical systems of industrial engineering has been carried out. A method for studying technical systems for technological purposes has been developed, which provides for the implementation of analytical studies and the rational use of the regularities of changes in the internal properties of the machine-medium system based on the joint use of models with discrete and distributed parameters.

The study of the dynamic parameters of the vibration crusher has been carried out and the dependences of the influence of the ratio of vibration masses on the grinding process have been established, and algorithms for calculating the parameters of a vibration three-mass crusher have been formulated.

The physical and mathematical model of the screen is substantiated, on the basis of which the equations of motion of the material over the sieve are compiled and the distribution of the amplitude of oscillations of the material particles from the oscillation frequency of the sieve is obtained. The influence of the vibration frequency and the angle of inclination on the sorting efficiency have been established. An algorithm and method for calculating the main parameters of a vibration screen have been developed.

It has been determined that the use of a vibration concrete mixer makes it possible to reduce the duration of mixing by 2.5–3 times in comparison with conventional free mixing concrete mixers. It has been proven that the process of preparing hard concrete mixtures and improving the quality of concrete mixtures occurs due to the destruction of defective aggregates and a more uniform distribution of the binder throughout the mixed mixture.

An algorithm and method for calculating the main parameters of a vibration concrete mixer have been developed.

A model of the hybrid system «vibration plant – medium» is proposed, in which active and reactive resistances to wave coefficients are taken into account. The results of calculations of changes in the parameters of vibration machines for the processes of compaction of concrete mixture confirm the implementation of accounting for the reactive and active resistance of the concrete mixture.

Predictive mathematical models have been created to determine the stress state of the soil during compaction at characteristic points of the massif under the pipelines, which make it possible to obtain rational values of the parameters of the working bodies for soil compaction. An algorithm and method for calculating the main parameters of vibration systems for compaction of working media have been developed.

The assessment and substantiation of methods for studying the parameters of acoustic treatment of technological media have been done. The functional relationships between the acoustic parameters of the cavitation apparatus and the rheological properties of the processing technological media have been revealed. The process of staged acoustic treatment of technological media is described. Analytical dependences are obtained for determining the main parameters of the cavitation apparatus and the regularities of the processes of staged acoustic treatment of technological media under conditions of energy minimization are established. An algorithm for substantiating the rational choice of the structural-parametric system «acoustic apparatus – technological medium» is proposed.

The main states of reliability of a technical system and its elements are investigated by the example of vibration platforms for compacting concrete mixtures. A model for assessing reliability based on fuzzy logic, implemented in the MATLAB b2020 medium, has been developed. When processing statistical data on the MTBF of the propeller shafts of vibration platforms, the Weibull distribution law was established and the possibility of failure-free operation of such structural elements was determined.

In the course of the research, finite element models of vibration machines were developed to implement the transmission of energy in the vertical direction with a fixed frequency, with a polyphase direction of the action of external forces, with the spatial direction of movement in the vertical and horizontal planes.

Investigations of the nature of distribution and numerical values of stresses and strains in the forming structure of the unit are carried out, depending on the angle of instantaneous action of the external force of vibrators and variable frequencies.

Stress concentrators in structural elements of machines for technological purposes are determined, taking into account the workloads.

The static and dynamic loads of the support contour of a truck crane have been investigated.

The obtained research results are taken into account for making further design decisions when creating such machines.

1 ASSESSMENT OF THE CURRENT STATE OF PARAMETERS AND OPERATING MODES OF TECHNOLOGICAL TECHNICAL SYSTEMS

I. Nazarenko, O. Dedov, I. Bernyk, A. Bondarenko,
A. Zapryvoda, M. Nazarenko, I. Pereginets

ABSTRACT

The classification features of technological technical systems, the further development of the theory of the working process are given. The classification features are determined. Only the classification features that determine their purpose and the nature of the work they perform are considered. An assessment of the design and technological parameters of the existing technical systems of industrial engineering has been carried out. New and improved evaluation criteria have been used. Reliable assessment and analysis made it possible to formulate more reasonably methods for solving the problem. Continuously improving, the technology leaves a reflection on the directions of development of technical system designs. On the basis of this, working hypotheses were formulated, the essence of which lies in modeling the medium and technical system as a single system with their own dynamic individuality. The system «technical system – medium» is represented by a complex hybrid (mixed) dynamic system, in which the technical system is a system with discrete parameters, and the medium is with distributed parameters, and this system is reduced to the calculated one in the form of a system with discrete parameters.

KEYWORDS

Technical system, medium, classification, criteria, assessment, analysis, modeling, discrete, distributed parameters, hypotheses.

1.1 DETERMINATION OF THE CLASSIFICATION CHARACTERISTICS OF TECHNICAL SYSTEMS AND PROCESSING MEDIUMS IN THESE STUDIES

Technical systems can be processes and objects, depending on the nature of the connections between the elements of the system. The main goal of the development of technical systems is to eliminate the contradiction between the growing needs of society and the capabilities of today's technical systems. Any technical system is primarily a physical object. And the correct choice of fundamental, that is, physical, foundations of functioning will lead to its viability and efficiency. The dialectic of the development of technical systems lies in the fact that new and well-known technical solutions are effectively combined in a newly created or improved system.

The technical systems of industrial engineering include machines (equipment), which include a number of elements, devices designed to perform certain technological operations and functions (**Fig. 1.1**).
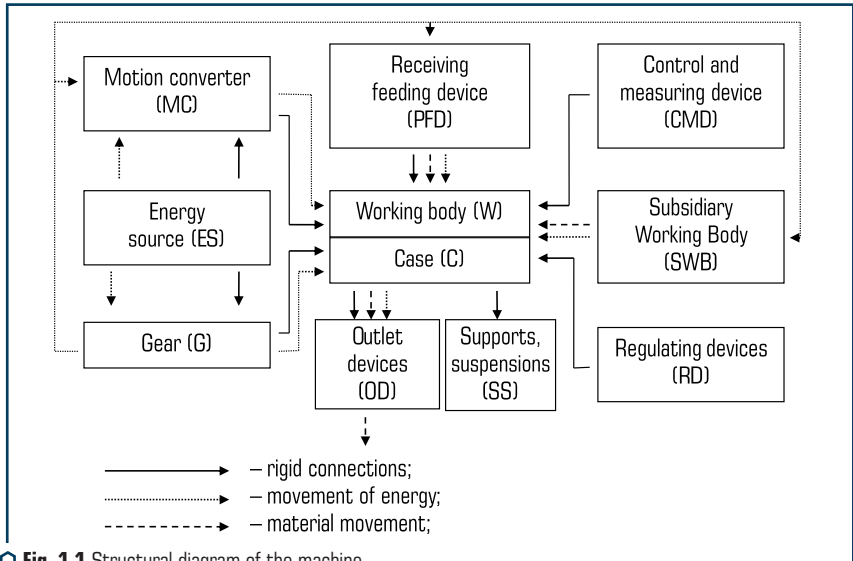
Fig. 1.1 Structural diagram of the machine

For the development of general principles for the creation of machines, for the further development of the theory of their working process, the classification features of these machines have been determined. The classification signs take into account the fundamental and design features of the structure of vibration machines, their purpose and the nature of the work they perform.

In this work, the most significant two classifications of machines are used: constructive-technological and structural. Structural and technological classification implies the determination of the use of a machine for performing a particular work process (crushing, sorting, compaction, etc.) with a note of the design features of their working bodies.

Structural classification characterizes the general fundamental features of the structure of machines of dynamic action and the nature of the interaction of their working bodies with the processed medium. This classification creates the necessary prerequisites for the development of a unified theory of machines, guides and facilitates their further development.

The parameters of work (the magnitude of the amplitude and the type of trajectory of oscillations of the working body) of dynamic machines are determined by the nature of the working forces, the frequency of oscillations, a feature of elastic links and the ratio of the masses of individual parts of the system. Therefore, the structural classification in the monograph is determined by the signs of the degree of freedom of the dynamic scheme of the machine, the nature of its drive, the characteristics of elastic links.

The type of work performed by machines and the peculiarities of the interaction of their working bodies with the processed medium determine, on the one hand, the fundamental structure of

the machine, and on the other hand, put them in an equivalent relationship in assessing the working conditions. In this regard, one of the main classification features of a machine is the nature of the work it performs (features of the interaction of its working body with the medium being processed and the type of overcoming different types of resistance).

All machines are divided into several groups that are fundamentally similar in structure and nature of interaction with the processed medium.

The following operations, which are homogeneous with respect to the nature of external resistance to the working bodies, can be noted: the transfer of energy to different media during their processing.

In the classical theory of oscillations, all dynamical systems are usually divided into systems with one, two, three, n and an infinite number of degrees of freedom (systems with distributed parameters). Such a distribution of dynamical systems presents certain conveniences with regard to their theoretical study. Dynamical systems with an equal number of degrees of freedom are described by the same number of differential equations solved by similar methods.

By the type of drive, which is the third classification feature, the monograph examines vibration machines with a power drive. Currently, machines with a kinematic drive have little application and are not used in research.

The fourth classification feature is based on the characteristics of elastic links, which determine the nature of the restoring forces and internal resistances of the vibration machine. According to the characteristics of elastic connections, all investigated vibration machines are divided into machines with linear and nonlinear characteristics of stiffness [1].

A feature of these studies is taking into account the conditions of interaction with the processing medium [2], as a result of which there is a need to determine the classification features of such mediums. Such information is necessary for the justified direction of the formation of the algorithm and methods of technical systems of dynamic action. In such conditions, the key features of the classification are the state of the medium, the nature of the qualitative behavior of the medium, rheological properties and dynamic parameters. Depending on the ratio of the yield point τ at pure shear to atmospheric pressure p_a, the process medium in its state can be [3]:

– hard plastic $\tau/P_a \geq 1$;
– liquid-plastic $\tau/P_a = 1$;   (1.1)
– liquid at: $\tau/P_a \leq 1$.

By the nature of the qualitative behavior under dynamic load in the medium (1.1), wave phenomena may appear or these phenomena are absent. Accounting for wave phenomena in the working medium can be estimated from the ratio of the wave propagation time t_{min} and the oscillation period T [4] under the following conditions:

$$\left.\begin{array}{c} \tau < T \\ \tau > T \end{array}\right\}. \qquad (1.2)$$

5

Under the first condition (1.2), the process of oscillation of the medium can be considered slow and the elastic wave can be neglected. In this case, accelerations and deformations are determined exclusively by forces that are constant and unchanged in the direction of the action of external forces on such a medium.

When the second condition (1.2) is satisfied, the motion of the medium is determined not only by forces, but also by elastic waves. Movement, speed and acceleration along the majestic change and depend not only on time, but also on the coordinate in the direction of which external forces act on such a medium.

So, in the first case, inertial forces dominate, and in the second, elastic ones. In most cases, real mediums to be investigated fall between these conditions (1.2). That is, as a rule, it is necessary to take into account the elastic, inertial and dissipative properties, which is accepted in this work.

1.2 ASSESSMENT OF DESIGN AND TECHNOLOGICAL PARAMETERS OF EXISTING TECHNICAL SYSTEMS OF INDUSTRIAL ENGINEERING

The design and technological parameters are assessed using functional criteria according to the appropriate method [5]. The methodology is based on the principles of parameter assessment (**Fig. 1.2**) of the same type of machines using the technical characteristics of existing technological technical systems. Subsequently, depending on the purpose of the technical system, the numerical values of the criteria are determined (**Table 1.1**) and, on their basis, conclusions are drawn on the formulation of research tasks for certain processes.

The application of the above criteria, fulfilled for machines for crushing, sorting, mixing and compaction, are taken into account in the corresponding sections of the monograph. Their analytical form is shown in **Table 1.1**.

Table 1.2 shows the numerical values of the main parameters of vibration crushers.

Calculations according to this **Table 1.2** obtained numerical criteria for evaluating the parameters of vibration crushers, confirming significant differences (**Table 1.3**).

The main parameters of resonant technical systems for sorting materials are presented in **Table 1.4**.

As follows from **Table 1.4,** resonant screens, having a one-two-mass structure according to the screening scheme, are three and four-mass. The screen parameters are also different: the vibration amplitude (**Table 1.4**) has a wide range from 0.6 to 10 mm, foreign production – 5–14 mm. They are also excellent in vibration frequency, which is reflected in one of the main indicators – vibration acceleration. In terms of the power of a foreign-made rotor for such parameters (amplitude and frequency of oscillations), they have lower values, which indicates a possible greater oscillation amplification factor, and therefore greater efficiency.

Technical characteristics of gravity concrete mixers are given in **Tables 1.5, 1.6**.
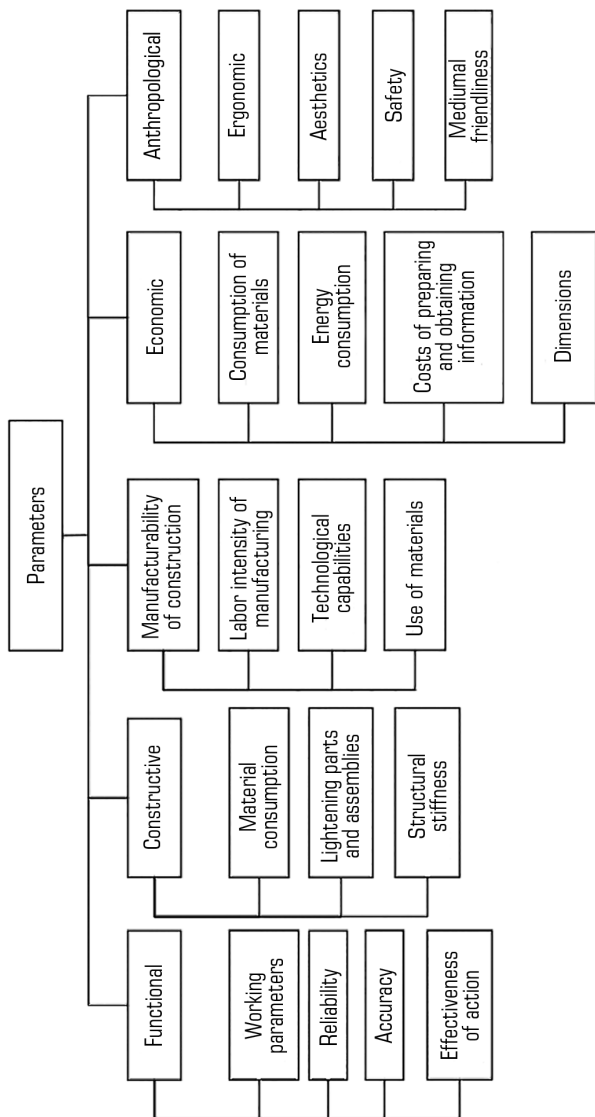
○ **Fig. 1.2** Classification of technical system parameters

7

● **Table 1.1** Criteria for evaluating technological and design parameters of technical systems for dynamic processes of processing technological media

No.	Criterion	Analytical dependence
1	Effect of mass on performance	$K_m = P/m$
2	Impact of energy consumption on performance	$k_e = P/R$
3	Effect of power on ground	$k_p = P/m$
4	System synergy factor (efficiency)	$K_s = E_s/E_{p.k.}$
5	The rate of change in the stress state of the medium in time	$\upsilon_{s.s} = d\sigma/dt$
6	Speed	$k_s = \mathbf{X}_0 \cdot \omega$
5	Acceleration	$k_a = \mathbf{X}_0 \cdot \omega^2$
6	Dynamism of the system	$k_d = a/g$
7	Mixing drum volume ratio	$K_z = V_s/V_g$
8	The ratio of the mass of the medium to the mass of the technical system	$K_m = m_m/m_{t.s.}$

● **Table 1.2** Numerical values of the main parameters of vibration crushers

Type	Productivity, m³/h	Mass, kg	Power, kWt	The largest size of the input material, mm	The smallest size of the source material, mm	Machine volume, m³
VSHCHD 440×800 (REC «Mechanort-tekhnika)	22	1 500	60	350	40	10.92
VSHCHD 65×400 2 chambers (REC «Mechanort-tekhnika)	2.5	1 400	14	50	10	3.6
VSHCHD 130×300 (REC «Mechanort-tekhnika)	1	1 500	22	110	20	2.89
VSHCHD 600×150 (Mining Academy in Krakiw)	1.56	1 082	7.5	120	15	1.35
VSHCHD 600×800 (REC «Mechanort-tekhnika)	47	2 500	60	5 00	70	17.95
VSHCHD 1200×1500 (REC «Mechanort-tekhnika)	188	5 400	110	1 000	100	59.2
SVDA-1000 (Skochinsky Institute of Mining)	938	8 116	480	1 000	300	–

● **Table 1.3** The value of the criteria for evaluating the parameters of vibration crushers

Type	K1	K2	K3	K4	K5
VSHCHD 440×800 (REC «Mechanort-tekhnika)	0.0015	0.3667	250.00	8.75	2.0147
VSHCHD 65×400 2 chambers (REC «Mechanort-tekhnika)	0.0018	0.1786	100.00	5.00	0.6940
VSHCHD 130×300 (REC «Mechanort-tekhnika)	0.0007	0.0455	68.18	5.50	0.3460
VSHCHD 600×150 (Mining Academy in Krakiw)	0.0014	0.2080	144.27	8.00	1.1556
VSHCHD 600×800 (REC «Mechanort-tekhnika)	0.0019	0.7833	416.67	7.14	2.6184
VSHCHD 1200×1500 (REC «Mechanort-tekhnika)	0.0035	1.7091	490.91	10.00	3.1757
SVDA-1000 (Skochinsky Institute of Mining)	0.0116	1.9542	169.08	0.01	–

● **Table 1.4** Parameters of resonant technical systems for sorting materials

Type	Scheme	Amplitude of vibrations, mm	Vibration frequency rad/i	Power, kWt	Maximum acceleration, m/s²
VR-50	One-mass unbalanced	4.0	78.5	10	24
VUR-80	Two-mass balanced	4.0	97.4	10	38
VKVS	Two-mass balanced	0.65	294	1.6	55
PEV-1-0,5×3,6	Two-mass	0.60	314	0.5	60
PEV-2-0,5×5	Two-mass	0.70	314	0.5	70
PEV-3-9×2,5	Two-mass	0.80	314	2.0	80
79-TS	Two-mass	0.80	314	2.0	80
PVG-2	Two-mass balanced	4.0	78.5	30	24
GRL62	Two-mass balanced	10	52.3	13	27
PEV-2-4×12	Two-mass	0.90	314	4.0	90
EV	Two-mass	5...15	52.3...105	5...8	39...51
EF	Two-mass	5...15	105...209	6	39...51
RJ	Two-mass	5...14	105...209	6	36...51
S	Two-mass	5...14	105...209	6	36...51
RMS-2,25	Two-mass	5...14	105...209	3.5...5	36...51
RMN-4,5	Two-mass	5...14	105...209	5...9	36...51
RS	Three-mass	5...14	105...209	6	36...51
DV	Four-mass	5...15	105...209	5...8	39...51
GC	Four-mass	10...12	105...209	6...8	51...72

● **Table 1.5** Technical characteristics of Johnson-Ross gravity concrete mixers

Standard size and loading volume			Drum rotation drive power, kW		Number of mixing blades	Mass, t
yd³	m³	l	engine power	total		
4.5	3.44	3 440.7	1×29.8	29.8	3	6.804
6	4.59	4 587.6	2×22.4	44.8	3	12.701
8	6.12	6 116.8	2×29.8	59.6	4	14.515
10	7.65	7 646.0	2×37.3	74.6	4	16.33
12	9.18	9 175.2	2×44.8	89.6	4	17.917
15	11.47	11 469.0	2×56.0	112	4	19.958

● **Table 1.6** Specifications of BMH Systems of The Roll Master Gravity Reversible Mixers

Loading volume, m³	Drum diameter, m	Drive power, kW	Productivity, m³/hour	Mass, kg
3	2.5	2×22	85	12 000
4.5	2.8	4×18	112	15 000
6	3.15	4×22	165	18 000
9	3.35	4×37	245	21 000

The variety of currently used concrete mixers can also be explained by an unreliable comparative assessment of their technical, technological and operational parameters. Based on a review of the designs of prototypes of concrete mixing machines (**Tables 1.5, 1.6**), the key parameters were identified that affect the mixing process. According to the analysis of technical and economic indicators and parameters, the tasks of researching vibration concrete mixers are determined.

Thus, studies using the above technique have established that for the processes of grinding [6, 7], sorting [8], mixing [9], compaction [10, 11], cavitation treatment [12–14], research of parameters, modes and reliability machines [15–20] there is a significant difference in the numerical values of the criteria of the studied class of technical systems. The main reason lies in the use of simplified models, the absence of modeling and consideration of the joint movement of the working bodies of the technical system and the processed medium or material.

1.3 DISCUSSION OF RESULTS AND IDENTIFICATION OF MAIN DIRECTIONS OF RESEARCH

For the development of general principles for the creation of technological technical systems, for the further development of the theory of the working process, classification signs are determined. The monograph considers only the classification features that determine their purpose and the nature of the work they perform. This has some limitations of the existing classification signs.

An important point in the analysis of existing works is the assessment of the design and technological parameters of the existing technical systems of industrial engineering. New and improved evaluation criteria have been used. Reliable assessment and analysis made it possible to formulate more reasonably methods for solving the problem. Continuously improving, the technology leaves a reflection on the directions of development of technical system designs. On the basis of this, working hypotheses and research methods were formulated, the results of which are presented in the corresponding sections of the monograph.

Working hypotheses for researching technical systems for technological purposes:

– consideration (modeling) of the medium and the technical system as a single system with its own dynamic personality. The embodiment of this principle guarantees the movement of the studied systems in a given or established mode of operation;

– «technical system – medium» system is a complex hybrid (mixed) dynamic system, in which the technical system is a system with discrete parameters, and the medium is with distributed

parameters, and this system is reduced to the calculated one in the form of a system with discrete parameters, in which wave phenomena of the medium and are represented by contact force;

— an increase in the efficiency of technical systems for various technological purposes is achieved through the efficient use of energy supplied to the medium both on the main and on the superharmonic resonance mode of oscillations of the system under study, as well as with a variable, time-controlled mode of operation;

— reliability of the machine is ensured by a rational combination of the effect of shock and vibration at low frequencies, as well as the use of reliable vibration exciters.

Research methodology for technical systems for technological purposes:

— analytical research and rational use of the regularities of changes in the internal (elastic-inertial and dissipative) properties of the «machine — medium» system;

— conducting experimental studies based on the determination of rational operating modes of technical systems for various technological purposes;

— reliability assessment based on a small number or absence of failures;

— study of the stress-strain state of metal structures of machines of static and dynamic action;

— establishment of regularities in the distribution of normal and contacting stresses for different shapes of the cross-section of elements of metal structures.

The proposed method of compiling a mathematical model [1, 2] is based on the idea of considering at the first stage a separate medium, the stress-strain state of which is under the load of the force of any law of its change.

The next stage of the analytical solution of the motion of the medium is based on the premise that the structure of the dependence reflecting its state at any moment of motion consists of two components — one is capable of accumulating energy that passes from one form to another (reactance), and the other is energy dissipation (active resistance). The resulting formula has a discrete form in structure, however, its constituent parameters and characteristics take into account wave processes in the medium.

The final stage is the drawing up of the equation of the joint motion of the vibration system «machine — medium» by the appropriate combination of reactive and active components of the resistance of the machine and the medium, for which the method of vector diagrams is used.

CONCLUSIONS TO SECTION 1

1. For the development of general principles for the creation of technical systems for technological purposes, the further development of the theory of their working process, classification features and proposed criteria have been determined, according to which the assessment of the design and technological parameters of the existing technical systems of industrial engineering is carried out.

2. Working hypotheses of research of technological technical systems are formulated, the implementation of which is a guarantee of the reliability of the obtained results of the movement of the systems under study in a given or established operating mode.

3. A method for researching technological technical systems has been developed, which provides for the implementation of analytical research and the rational use of the regularities of changes in the internal properties of the machine-medium system based on the joint use of models with discrete and distributed parameters.

REFERENCES

1. Nazarenko, I., Gaidaichuk, V., Dedov, O., Diachenko, O. (2017). Investigation of vibration machine movement with a multimode oscillation spectrum. Eastern-European Journal of Enterprise Technologies, 6 (1 (90)), 28–36. doi: http://doi.org/10.15587/1729-4061.2017.118731

2. Nazarenko, I., Gaidaichuk, V., Dedov, O., Diachenko, O. (2018). Determination of stresses and strains in the shaping structure under spatial load. Eastern-European Journal of Enterprise Technologies, 6 (7 (96)), 13–18. doi: http://doi.org/10.15587/1729-4061.2018.147195

3. Nazarenko, I. I., Harnets, V. M., Sviderskyi, A. T., Pentiuk, B. M. (2009). Systemnyi analiz tekhnichnykh obiektiv. Kyiv: KNUBA, 164.

4. Mishchuk, Y., Nazarenko, I., Mishchuk, D. (2021). Definition of rational operating modes of a vibratory jaw crusher. Naukovyi Visnyk Natsionalnoho Hirnychoho Universytetu, 4, 56–62. doi: http://doi.org/10.33271/nvngu/2021-4/056

5. Nazarenko, I., Mishchuk, Y., Mishchuk, D., Ruchynskyi, M., Rogovskii, I., Mikhailova, L. et. al. (2021). Determiantion of energy characteristics of material destruction in the crushing chamber of the vibration crusher. Eastern-European Journal of Enterprise Technologies, 4 (7 (112)), 41–49. doi: http://doi.org/10.15587/1729-4061.2021.239292

6. Nazarenko, I. I., Oryshchenko, S. V. (2009). Modeliuvannia protsesu rukhu materialu po hrokhotu. Tekhnika budivnytstva. Naukovo-tekhnichnyi zhurnal, 22, 81–84.

7. Ruchynskyi, M. M., Svyrydiuk, D. Ya. (2013). Doslidzhennia kolyvan vibratsiinoho betonozmishuvacha z urakhuvanniam vplyvu peremishchuvanoho materialu. Tekhnika budivnytstva. Naukovo-tekhnichnyi zhurnal, 31, 35–42.

8. Nazarenko, I., Ruchynskyi, M., Delembovskyi, M. (2018). The Basic Parameters of Vibration Settings for Sealing Horizontal Surfaces. International Journal of Engineering & Technology, 7 (3.2), 255–259. doi: http://doi.org/10.14419/ijet.v7i3.2.14415

9. Bernyk, I., Luhovskyi, O., Nazarenko, I. (2018). Effect of rheological properties of materials on their treatment with ultrasonic cavitation. Materiali in Tehnologije, 52 (4), 465–468. doi: http://doi.org/10.17222/mit.2017.021

10. Nesterenko, M., Nazarenko, I., Molchanov, P. (2018). Cassette Installation with Active Working Body in the Separating Partition. International Journal of Engineering & Technology, 7 (3.2), 265–268. doi: http://doi.org/10.14419/ijet.v7i3.2.14417

11. Nazarenko, I. I., Ruchynskyi, M. M., Sviderskyi, A. T., Kobylanska, I. M., Harasim, D., Kalizhanova, A., Kozbakova, A. (2019). Development of energy-efficient vibration machines for the buiding-and-contruction industry. Przeglad Elektrotechniczny, 95 (4), 53–59. doi: http://doi.org/10.15199/48.2019.04.10

12. Bernyk, I., Luhovskyi, O., Wojcik, W., Shedreyeva, I., Karnakova, G. (2019). Theoretical Investigations of the Interaction of Acoustic Apparatus with Technological Environment Working Process. Przeglad Elektrotechniczny, 1 (4), 32–37. doi: http://doi.org/10.15199/48.2019.04.06

13. Luhovskyi, O., Bernyk, I., Gryshko, I., Abdulina, D., Zilinskyi, A.; Stryczek, J., Warzyńska, U. (Eds.) (2021). Mobile Equipment for Ultrasonic Cavitation Inactivation of Microorganisms in the Liquid Environment. NSHP 2020. Lecture Notes in Mechanical Engineering. Cham: Springer, 272–281. doi: http://doi.org/10.1007/978-3-030-59509-8_24

14. Babič, M., Cali, M., Nazarenko, I., Fragassa, C., Ekinovic, S., Mihaliková, M. et. al. (2018). Surface roughness evaluation in hardened materials by pattern recognition using network theory. International Journal on Interactive Design and Manufacturing, 13 (1), 211–219. doi: http://doi.org/10.1007/s12008-018-0507-3

15. Nesterenko, M. P., Molchanov, P. O., Savyk, V. M., Nesterenko, M. M. (2019). Vibration platform for forming large-sized reinforced concrete products. Naukovyi Visnyk Natsionalnoho Hirnychoho Universytetu, 5, 74–78. doi: http://doi.org/10.29202/nvngu/2019-5/8

16. Nesterenko, M., Nesterenko, T., Skliarenko, T. (2018). Theoretical Studies of Stresses in a Layer of a Light-Concrete Mixture, Which is Compacted on the Shock-Vibration Machine. International Journal of Engineering & Technology, 7 (3.2), 419–424. doi: http://doi.org/10.14419/ijet.v7i3.2.14564

17. Dmitrenko, A., Lebedyk, G., Nesterenko, M. (2018). Product Cost Calculation Methods in Construction. International Journal of Engineering & Technology, 7 (3.2), 6–11. doi: http://doi.org/10.14419/ijet.v7i3.2.14367

18. Nazarenko, I., Dedov, O., Bernyk, I., Rogovskii, I., Bondarenko, A., Zapryvoda, A. et. al. (2020). Determining the regions of stability in the motion regimes and parameters of vibratory machines for different technological purposes. Eastern-European Journal of Enterprise Technologies, 6 (7 (108)), 71–79. doi: http://doi.org/10.15587/1729-4061.2020.217747

19. Nazarenko, I., Svidersky, A., Kostenyuk, A., Dedov, O., Kyzminec, N., Slipetskyi, V. (2020). Determination of the workflow of energy-saving vibration unit with polyphase spectrum of vibrations. Eastern-European Journal of Enterprise Technologies, 1 (7 (103)), 43–49. doi: http://doi.org/10.15587/1729-4061.0.184632

20. Nazarenko, I., Gavryukov, O., Klyon, A., Ruchynsky, N. (2018). Determination of the optimal parameters of a tubular belt conveyor depending on such an economical. Eastern-European Journal of Enterprise Technologies, 3 (1 (93)), 34–42. doi: http://doi.org/10.15587/1729-4061.2018.131552

2 RESEARCH OF PROCESSES OF PRODUCING MATERIALS BY TECHNICAL POWER LOADING SYSTEMS

I. Nazarenko, Ye. Mishchuk, M. Kyzminec,
S. Oryshchenko, O. Fedorenko, S. Tsepelev

ABSTRACT

An increase in the effective working process of the crusher is achieved when it operates in the vicinity of resonance, i.e. at a high value of the coefficient of resonant amplification of oscillations. The optimal values of the amplitude of the oscillations of the masses have the greatest values, provided that the coefficient of regulation of elasticity in frequency n is in the range of $0.6 \leq n \leq 1$. Within the frequency range of 14.5 Hz$<f<$26 Hz, material is effectively crushed. The numerical values of the coefficient are established, which determine the rational ratios of vibration masses. The studies carried out and their results indicate that the main stresses causing the destruction of the material are shear stress. Analytical equations are obtained that reflect the picture of energy consumption for the destruction of the material. Such studies are planned as a continuation of the topic under consideration through experimental studies and consideration of several members of the series and optimization of the parameters of crushing machines. The proposed approach to studying the energy characteristics of material destruction in the crusher chamber with a guaranteed zone of stability of parameters in the resonance zone can be used for other processes. Such processes include the destruction of materials during dynamic cutting of soils, processing of materials in mills and sorting of materials, which are widely used in Ukraine abroad. An algorithm and method for calculating the main parameters of a vibration crusher have been developed.

KEYWORDS

Vibration crusher, material, grinding, physical, mathematical model, equation, resonance, parameters, destruction, stability zone, stress, deformation, energy consumption.

2.1 SELECTION AND JUSTIFICATION OF PHYSICAL AND MATHEMATICAL MODELS OF TECHNICAL SYSTEMS FOR MATERIALS GRINDING PROCESSES

Vibration jaw crushers are a relatively new direction in the development of crushing technology, which are highly energy efficient and are used in various industries, including construction. The most promising of the known vibration jaw crushers are crushers with two movable jaws and crushers with a heavy body and a pendulum. On the other hand, the creation of such machines is hindered by the severity of providing a resonant mode of operation in which the efficiency of crushers increases significantly.

Let's consider a model of a working fluid in terms of interaction with a machine. Let's consider the layout of the elements of the vibration system under study in the following order (**Fig. 2.1**): vibration exciter – machine body – working medium – striker. Let's take: m – total mass of the machine; c – coefficient of elasticity of elastic connections; m_m – mass of the material; $F_0(t)$ – driving force; x_n – movement of individual elements of the crusher structure; D – average diameter of the input material.
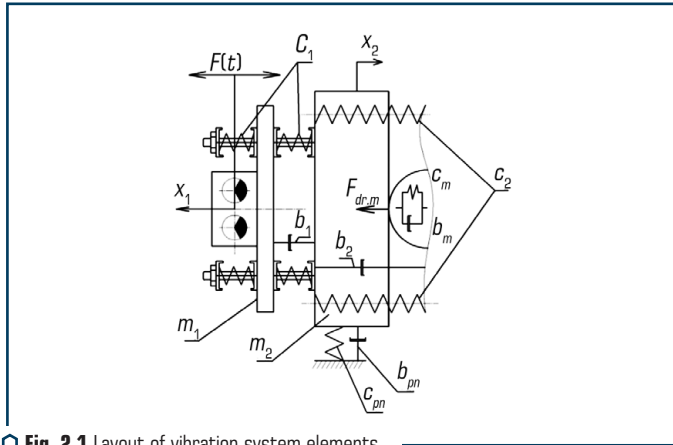
○ **Fig. 2.1** Layout of vibration system elements

The equation of motion of our system will be an equation of the form [1]:

$$\frac{\partial^2 x}{\partial u^2} = \frac{1}{c^2}\frac{\partial^2 x}{\partial t^2}, \tag{2.1}$$

where c – speed of the wave propagating in the medium.

The solution to equation (2.1) will be the dependence [1]:

$$x(u,t) = \left(A\cos\frac{\omega}{c}v + B\sin\frac{\omega}{c}v\right)\sin\omega t. \tag{2.2}$$

Coefficients A and B are determined by the boundary conditions and, by their physical content, reflect the vibration amplitudes in the corresponding contact zones.

Forces acting on the contact between the crushing plate and the material:

$$-F_{cr.m} = F_0\sin\omega t - \left(m_1\ddot{x}_1 + 2x_1c_1 - x_2c_1 + m_2\ddot{x}_2 + x_2c_1 - x_1c_1 + 2c_2x_2 - 2c_2x_3 + x_3c_f\right), \tag{2.3}$$

where $F_{cr.m}$ – reaction force of the material from the action of the crushing jaw (equal to the crushing force with the opposite sign);

$$F_0 \sin \omega t - \left(m_1 \ddot{x}_1 + 2x_1 c_1 - x_2 c_1 + m_2 \ddot{x}_2 + x_2 c_1 - x_1 c_1 + 2c_2 x_2 - 2c_2 x_3 + x_3 c_f \right)$$

– crusher motion equation.

On the other hand, the expression for the reaction of the material to the crushing plate can be written as follows:

$$F_{cr.m} = \sigma s = ES \left(\frac{\partial x}{\partial u} \right). \tag{2.4}$$

Equating expressions (2.3) and (2.4) let's obtain:

$$ES \left(\frac{\partial x}{\partial u} \right) = F_0 \sin \omega t - \left(\begin{array}{c} m_1 \ddot{x}_1 + 2x_1 c_1 - x_2 c_1 + m_2 \ddot{x}_2 + \\ + x_2 c_1 - x_1 c_1 + 2c_2 x_2 - 2c_2 x_3 + x_3 c_{on} \end{array} \right). \tag{2.5}$$

Let's find the unknown derivatives $\partial x / \partial u$ and $\ddot{x} = \partial x^2 / \partial^2 t$ by differentiating equation (2.2):

$$\frac{\partial x_2}{\partial u} = \left(-A \frac{\omega}{c} \sin \frac{\omega}{c} v + B \frac{\omega}{c} \cos \frac{\omega}{c} v \right) \sin \omega t, \tag{2.6}$$

$$\frac{\partial x_2^2}{\partial^2 t} = - \left(A \cos \frac{\omega}{c} v + B \sin \frac{\omega}{c} v \right) \omega^2 \sin \omega t. \tag{2.7}$$

To find the displacements of the first and third masses included in equation (2.5), let's use the solution in the form of the following functions:

$$\begin{cases} x_1 [t] = A_1 \sin \omega t; \\ x_3 [t] = A_3 \sin \omega t. \end{cases} \tag{2.8}$$

Thus, an equation can be derived to determine the vibration amplitudes of the contact zone:

$$B_2 = A_2 \tan \left(\frac{r\omega}{c} \right), \tag{2.9}$$

$$A_2 = - \frac{A_1 c_1 - 2A_3 c_2 + A_3 c_{on} - F_0 - \omega^2 A_1 m_1}{2c_2 - \omega^2 m_2 + ES \left(\frac{\omega}{c} \right) \tan \left(\frac{r\omega}{c} \right)}. \tag{2.10}$$

As can be seen from equation (2.10), the effect of the material on the dynamics of the mouse is determined by a parameter $ES (\omega/c) \tan (r\omega/c)$ that can be turned into the following form [1]:

$$m_m \omega^2 \left(\frac{\text{tg}\psi}{\psi} \right), \tag{2.11}$$

where m – the mass of the material.

The ratio $(\text{tg}\psi / \psi) = \gamma$ is called the coefficient of added mass. It takes into account the difference between the mass m_m and its static value m_{ms} [1].

When designing any machine, great attention should be paid to the rational selection of kinematic parameters. The kinematic parameters mainly include the geometric characteristics of the machine as a whole and its individual parts.

One of the features in the design of vibration crushers is the presence of vertical movements of the crusher relative to the falling material.

Expanded, the dependency for defining the material path will be as follows:

$$l_1 = \frac{g(\sin[\alpha] - \mu_f \cos[\alpha])}{4f} + \frac{F}{m_{cr} \omega^2}, \tag{2.12}$$

where μ_f – coefficient of friction; m_{cr} – the mass of the vibration parts of the machine (mass of the crusher).

Knowing the total length of the crushing plate, let's find the number of cycles of application of loading to the material during its stay in the crushing chamber $(h/l_1) = n_i$.

On the other hand, the required number of load cycles for material destruction is calculated by the formula [2]:

$$n_i' = (\delta_d / \delta_e), \tag{2.13}$$

where δ_d – depth of entry of the crushing plate into the body of the crushed material, at which the material is destroyed, m; δ_e – depth of entry of the crushing plate into the body of the material at a given energy of a single impact.

The value δ_e depends on the dependence [2]:

$$\delta_e = (2 \, _i v) / (c_w k_d S_c), \tag{2.14}$$

where $E_i = mv^2/2$ – impact energy, J; v – speed of application of the load to the material, m/s; c_w – wave propagation speed, m/s; k_d – dynamic factor; S_c – contact area, m^2.

2.2 INVESTIGATION OF THE STRESS-STRAIN STATE OF THE MATERIAL

Study of the stress-strain state of a solid material.

The stresses arising on the platforms of the selected element are shown in **Fig. 2.2**.
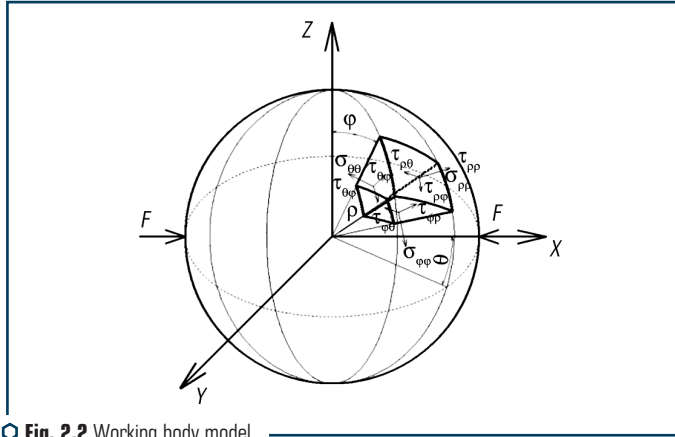
○ **Fig. 2.2** Working body model

A complete description of the stress-strain state in the linear theory of elasticity (spherical coordinates) includes the following dependences [3]:

— static equations:

$$
\begin{cases}
\dfrac{\partial \sigma_{\rho\rho}}{\partial \rho} + \dfrac{1}{\rho\sin(\varphi)}\dfrac{\partial \tau_{\rho\theta}}{\partial \theta} + \dfrac{1}{\rho}\dfrac{\partial \tau_{\rho\varphi}}{\partial \varphi} + \dfrac{1}{\rho}\left(2\sigma_{\rho\rho} - \sigma_{\theta\theta} - \sigma_{\varphi\varphi} + \tau_{\rho\varphi}\operatorname{ctg}(\varphi)\right) + M = 0; \\[2mm]
\dfrac{\partial \tau_{\rho\theta}}{\partial \rho} + \dfrac{1}{\rho\sin(\varphi)}\dfrac{\partial \sigma_{\theta\theta}}{\partial \theta} + \dfrac{1}{\rho}\dfrac{\partial \tau_{\theta\varphi}}{\partial \varphi} + \dfrac{1}{\rho}\left(\tau_{\theta\varphi}\left(3 + 2\operatorname{ctg}(\varphi)\right)\right) + N; \\[2mm]
\dfrac{\partial \tau_{\varphi\rho}}{\partial \rho} + \dfrac{1}{\rho\sin(\varphi)}\dfrac{\partial \tau_{\theta\varphi}}{\partial \theta} + \dfrac{1}{\rho}\dfrac{\partial \sigma_{\varphi\varphi}}{\partial \varphi} + \dfrac{1}{\rho}\left(\left(\sigma_{\rho\rho} - \sigma_{\theta\theta}\right)\operatorname{ctg}(\varphi) - 3\tau_{\varphi\rho}\right) + L = 0;
\end{cases}
\tag{2.15}
$$

— deformation equations:

$$
\begin{cases}
\varepsilon_{\rho\rho} = \dfrac{\partial u}{\partial \rho};\ \varepsilon_{\varphi\varphi} = \dfrac{1}{\rho}\dfrac{\partial w}{\partial \varphi} + \dfrac{u}{\rho};\ \varepsilon_{\theta\theta} = \dfrac{1}{\rho}\left(\dfrac{1}{\sin(\varphi)}\dfrac{\partial v}{\partial \theta} + u + w\operatorname{ctg}(\varphi)\right); \\[2mm]
\gamma_{\rho\theta} = \dfrac{1}{\rho}\dfrac{1}{\sin(\varphi)}\dfrac{\partial u}{\partial \theta} + \rho\dfrac{\partial}{\partial \rho}\left(\dfrac{v}{\rho}\right);\ \gamma_{\rho\varphi} = \rho\dfrac{\partial}{\partial \rho}\left(\dfrac{w}{\rho}\right) + \dfrac{1}{\rho}\dfrac{\partial u}{\partial \varphi}; \\[2mm]
\gamma_{\theta\varphi} = \dfrac{1}{\rho}\dfrac{1}{\sin(\varphi)}\left(\dfrac{\partial}{\partial \varphi}\left(v\sin(\varphi)\right) + \dfrac{\partial w}{\partial \theta}\right);
\end{cases}
\tag{2.16}
$$

— stress equations:

$$
\begin{cases}
\sigma_{\rho\rho} = 2G\varepsilon_{\rho\rho} + \lambda e;\ \tau_{\rho\theta} = G\gamma_{\rho\theta}; \\[2mm]
\sigma_{\theta\theta} = 2G\varepsilon_{\theta\theta} + \lambda e;\ \tau_{\rho\varphi} = G\gamma_{\rho\varphi}; \\[2mm]
\sigma_{\varphi\varphi} = 2G\varepsilon_{\varphi\varphi} + \lambda e;\ \tau_{\theta\varphi} = G\gamma_{\theta\varphi},
\end{cases}
\tag{2.17}
$$

where ρ, θ, φ – suitable coordinates for the placement of the stressed body element; u, v, w – movement in the direction of the corresponding coordinate axes; $\sigma_{\rho\rho}, \sigma_{\theta\theta}, \sigma_{\varphi\varphi}$ – normal stresses at the respective sites; $\tau_{\rho\theta}, \tau_{\rho\varphi}, \tau_{\theta\varphi}$ – shear stresses at the respective sites; M, N, L – volumetric forces; $G = E/2(1+\nu)$ – shear modulus; $\nu = \lambda/2(\lambda+G)$ – Poisson's ratio; $\lambda = E\nu/((1+\nu)(1-2\nu))$ – Lame constant; $e = 1/\rho^2 \partial(\rho^2 u)/\partial\rho + (1/\rho\sin(\varphi))((\partial(w\sin(\varphi))/\partial\varphi) + \partial v/\partial\theta)$ – volumetric relative deformation; $\varepsilon_{\rho\rho}$, $\varepsilon_{\theta\theta}$, ε_{ff} – linear deformations; $\gamma_{\rho\theta}$, $\gamma_{\rho f}$, $\gamma_{\theta f}$ – shear deformation.

To solve the problem, let's use the displacement method.

Combining equations (2.15)–(2.17) by alternate substitution, and performing some mathematical transformations, let's obtain the equation of elastic balance of the body in displacements [4]:

$$\begin{cases} (\lambda+2G)\rho\sin(\varphi)\partial e/\partial\rho - 2G\left[\partial\xi_\varphi/\partial\theta - \partial(\xi_\theta\sin(\varphi))/\partial\varphi\right] = 0; \\ (\lambda+2G)(1/\sin(\varphi))\partial e/\partial\theta - 2G\left[\partial\xi_\rho/\partial\varphi - \partial(\rho\xi_\varphi)/\partial\rho\right] = 0; \\ (\lambda+2G)\sin(\varphi)\partial e/\partial\varphi - 2G\left[\partial(\rho\xi_\theta\sin(\varphi))/\partial\rho - \partial\xi_\rho/\partial\theta\right], \end{cases} \quad (2.18)$$

where $\xi_\rho, \xi_\theta, \xi_f$ – components of rotation, determined by the following formulas:

$$\begin{cases} \xi_\rho = 1/2\rho\sin(\varphi)\left[\partial w/\partial\theta - \partial(v\sin(\varphi))/\partial\varphi\right]; \\ \xi_\theta = 1/2\rho\left[\partial u/\partial\varphi - \partial(\rho w)/\partial\rho\right]; \\ \xi_\varphi = 1/2\rho\sin(\varphi)\left[\partial(\rho v\sin(\varphi))/\partial\rho - \partial u/\partial\theta\right]. \end{cases} \quad (2.19)$$

Therefore, to solve this problem, it is necessary to find the displacement functions. These functions must satisfy three main conditions [4]:

1) be harmonious or biharmonic functions;

2) transform equation (2.18) into an identity;

3) stresses, expressed in terms of displacement functions, must satisfy the compatibility equations on the surface, which are written as follows [5]:

$$\begin{cases} \sigma_{\rho v} = \sigma_{\rho\rho}l + \tau_{\rho\theta}m + \tau_{\rho\varphi}n; \\ \sigma_{\theta v} = \tau_{\theta\rho}l + \sigma_{\theta\theta}m + \tau_{\varphi\varphi}n; \\ \sigma_{\varphi v} = \tau_{\varphi\rho}l + \tau_{\varphi\theta}m + \sigma_{\varphi\varphi}n, \end{cases} \quad (2.20)$$

where l, m, n – direction cosines.

In expanded form, the displacement functions for a spherical coordinate system are written as follows [6]:

$$\begin{cases} 2Gu_1 = 4(1-\nu)\left[(\chi_1\cos\theta + \chi_2\sin\theta)\sin\varphi + \chi_3\cos\varphi\right] - \partial M/\partial\rho; \\ 2Gw_1 = 4(1-\nu)\left[(\chi_1\cos\theta + \chi_2\sin\theta)\cos\varphi - \chi_3\sin\varphi\right] - (1/\rho)(\partial M/\partial\varphi); \\ 2Gv_1 = 4(1-\nu)\left[(-\chi_1\sin\theta + \chi_2\cos\theta)\right] - (1/\rho\sin\varphi)(\partial M/\partial\theta), \end{cases} \quad (2.21)$$

where $M = \chi_0 + \rho\left[(\chi_1\cos\theta + \chi_2\sin\theta)\sin\varphi + \chi_3\cos\varphi\right]$.

In this problem, the body forces are insignificant, so they can be neglected.

Therefore, from the above, it is possible to conclude that the solution of equations (2.21) is reduced to finding three harmonic functions χ_1, χ_2, χ_3.

Such functions are volumetric spherical functions, which, in general, can be written as follows:

$$\chi = \sum (A_n\,\rho^n + B_n\,\rho^{-n-1})(C_m\cos(m\theta) + D_m\sin(m\theta))(L_{nm}P_{nm}(\mu) + F_{nm}Q_{nm}(\mu)), \qquad (2.22)$$

where $\mu = \cos[\varphi]$ – module; $P_{nm}(\mu)$ – Legendre function of the first kind, degree n and order m; $Q_{nm}(\mu)$ – Legendre function of the second kind, degree n and order m; $Q_n(\mu)$ – Legendre function of the second kind; $P_n(\mu)$ – Legendre function of the first kind; A_n, B_n, C_m, D_m, $L_{n,m}$, $F_{n,m}$ – constants.

Now, knowing the displacement by formulas (2.16), (2.17), it is possible to find deformations and stresses. Let's consider the most atypical condition under which $n1$–$n3$, $m1$–$m3$ are different integers, for this $-1 < \mu < 1$. For subsequent calculations, let's take: $n1 = 4$, $m1 = 1$; $n2 = 5$, $m2 = 2$; $n3 = 6$, $m3 = 3$. Then equations (2.22) can be written as follows:

$$\chi_{1(m1,n1)} = -\left((\rho^9 A_4 + B_4)(\sin[\theta]H_1 + \cos[\theta]M_1)\big/12\sqrt{1-\mu^2}\rho^5\right)\times$$
$$\times\left(\begin{pmatrix}-32+230\mu^2-210\mu^4+\\+15\mu(3-10\mu^2+7\mu^4)\mathrm{Log}\left[\dfrac{1+\mu}{1-\mu}\right]\end{pmatrix}F_{4,1}+30\mu(3-10\mu^2+7\mu^4)L_{4,1}\right);$$

$$\chi_{2(m2,n2)} = -\frac{(\rho^{11}A_5 + B_5)(\sin[2\theta]H_2 + \cos[2\theta]M_2)}{4(-1+\mu^2)\rho^6}\times$$
$$\times\left(\begin{pmatrix}64-686\mu^2+1260\mu^4-630\mu^6+105\mu(-1+\mu^2)^2(-1+3\mu^2)\mathrm{Log}\left[\dfrac{1+\mu}{1-\mu}\right]\end{pmatrix}F_{5,2}+\\ +210\mu(-1+\mu^2)^2(-1+3\mu^2)L_{5,2}\end{pmatrix}\right);$$

$$\chi_{3(m3,n3)} = -\left((\rho^{13}A_6 + B_6)(\sin[3\theta]H_3 + \cos[3\theta]M_3)\big/4(1-\mu^2)^{3/2}\rho^7\right)\times$$
$$\times\left(\begin{pmatrix}-512+7326\mu^2-20286\mu^4+\\+20370\mu^6-6930\mu^8+315\mu(-1+\mu^2)^3\times\\ \times(-3+11\mu)^2\mathrm{Log}\left[\dfrac{1+\mu}{1-\mu}\right]\end{pmatrix}F_{6,3}+630\mu(-1+\mu^2)^3(-3+11\mu^2)L_{6,3}\right). \quad (2.23)$$

Study of the stress-strain state taking into account the rupture zone in the body of destruction.

The realistic crack shape is an elliptical shape. In this form, by changing the ellipticity, it is possible to realize different degrees of curvature of the crack boundary.

The solution to this problem is complex and very voluminous, due to the use of biharmonic functions. Therefore, for further research, let's use the technique proposed for solving the stress-strain state of a body near the rupture zone, which has the shape of an ellipse [3, 4].

In general, the problem is divided into two separate ones:
1) an elliptical crack under internal pressure;
2) an elliptical crack under shear conditions.

For a better understanding of the problem statement, let's present a diagram of the location of a plane crack in a three-dimensional body (**Fig. 2.3**).

The limiting conditions for solving the problem of an elliptical crack under the action of loading are as follows:

$$\sigma_z = -F, \quad \xi = 0, \quad w = 0, \quad \varrho = 0. \tag{2.24}$$

To solve the problem, the gravitational potential outside a homogeneous elliptical plate of the following form was used [4]:

$$\varphi = \frac{3}{2} \int_{\xi}^{\infty} \left[\frac{x^2}{a^2 + \int} + \frac{y^2}{b^2 + \int} + \frac{z^2}{\int} - 1 \right] \frac{d\int}{V(\int)}, \tag{2.25}$$

where $V(\int) = \left[\int (a^2 + \int)(b^2 + \int) \right]^{1/2}$ – function of $\int$; $\int$ – continuous integration; a, b – respectively large and having semi-axes of an ellipse.

Constant A is found by the following formula [4]:

$$A = -ab^2 F / 4\mu E(m), \tag{2.26}$$

where $E(m) = \int_0^{\pi/2} \sqrt{1 - k^2 (\sin[\varphi])^2} \, d\varphi$ – complete elliptic integral of the second kind; φ – amplitude of the integral; $m = \sin[\alpha]$ – modulus of the integral; α – modular angle.
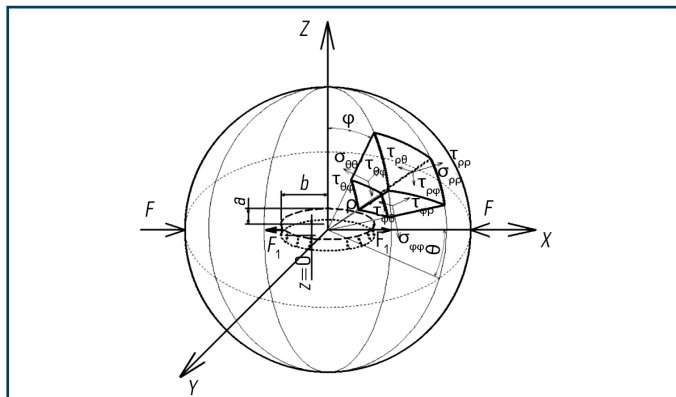
○ **Fig. 2.3** Scheme for determining the stress-strain state in the presence of a rupture in the crushing material

After some transformations and calculations, the displacements from the action of normal forces through the elliptical coordinates will have the following form [4]:

$$u_n = \frac{2Ax}{ab^2}\left\{(1-2v)\left[u_f + E[u_f]\left(\frac{m'}{m}\right)^2\right] - \frac{bz\left[(b^2+\xi)\varrho\vartheta\right]^{1/2}}{(\xi-)(\xi-\vartheta)(a^2+\xi)^{1/2}}\right\},$$

$$v_n = \frac{2Ay}{ab^2}\left\{(1-2v)\left[E[u_f]-m'^2 u_f - m^2\frac{snu_f \cdot cnu_f}{dnu_f}\right]\frac{1}{m^2} - \frac{bz\left[(a^2+\xi)\varrho\vartheta\right]^{1/2}}{(\xi-\varrho)(\xi-\vartheta)(b^2+\xi)^{1/2}}\right\},$$

$$w_n = \frac{2Az}{ab^2}\left[\begin{array}{c}(1-2v)E[u_f]+\left[\dfrac{cnu_f}{dnu_f}-2(1-v)\dfrac{dnu_f}{cnu_f}\right]snu_f + \\[2mm] +\dfrac{\xi^{1/2}\left[\xi(a^2b^2-\varrho\vartheta)-a^2b^2(\varrho+\vartheta)-(a^2+b^2)\varrho\vartheta\right]}{a(\xi-\varrho)(\xi-\vartheta)(a^2+\xi)^{1/2}(b^2+\xi)^{1/2}}\end{array}\right],$$

$$(2.27)$$

where ξ, ϱ, ϑ – elliptical coordinates; $\xi = \text{const}$ – family of ellipsoids; ϱ – hyperboloid with one cavity; ϑ – hyperboloids with two cavities; $E[u_f]=\int_0^{u_f} dn^2\beta\,d\beta$ – function; u_f – variable; m' – argument of elliptic functions (modulus of the integral), $(m')^2 + (m)^2 = 1$; snu_f, cnu_f, dnu_f – elliptic functions of C. Jacobi.

Now let's return to solving the general problem of a body with a crack. Using the principle of superposition of the stress states of two problems, namely, the stress-strain state of a body without a crack and in the vicinity of a crack, it is possible to write the following equations:

$$u_{tot} = u_i + u_{ni};\ \sigma_{tot} = \sigma_i + \sigma_{ni},$$

$$(2.28)$$

where u_i, σ_i – displacement and stress, respectively, calculated for a body without a crack; u_{ni}, σ_{ni} – corresponding displacements and stresses calculated for bodies with a rupture zone.

Since the displacements indicated in formulas (2.27) were determined for elliptical coordinates, and preliminary calculations were performed for a spherical system, therefore, when performing further calculations, it is necessary to switch to a single coordinate system. Let's accept the spherical coordinate system as more convenient for further operation.

After simple transformations of the system of equations (2.27), let's obtain the value of the displacements in spherical coordinates:

$$u_n = \frac{A}{3r^7}\left(\begin{array}{c}21r^5 - 70r^4\rho + 105r^3\rho^2 - \\ -84r^2\rho^3 + 35r\rho^4 - 6\rho^5\end{array}\right)\left(-3+(-5+4v)\cos[2\varphi]\right)+O[\rho-r]^6;\ v_n = 0;$$

$$w_n = -\frac{2A}{3r^7}(-1+2v)\left(\begin{array}{c}21r^5 - 70r^4\rho + 105r^3\rho^2 - \\ -84r^2\rho^3 + 35r\rho^4 - 6\rho^5\end{array}\right)\sin[2\varphi]+O[\rho-r]^6.$$

$$(2.29)$$

It should be noted that these equations were obtained on the basis of the expansion of formulas (2.27) in power series. The calculations took into account the condition $-\xi \approx \rho^2$; $\varrho \approx \vartheta \approx 0$.

To obtain the stress components, it is necessary to substitute formulas (2.29) into the equation for determining the stresses.

Finally, the stresses in the body in the presence of a rupture zone will be equal:

$$\sigma_{\rho\rho} = \frac{1}{3r^7} 2A \left(\begin{array}{l} G\left(\begin{array}{l} -70r^4 + 210r^3\rho - 252r^2\rho^2 + \\ +140r\rho^3 - 30\rho^4 \end{array}\right)\left(-3 + (-5 + 4v)\cos[2\varphi]\right) - \\ -1/\rho\lambda\left(\begin{array}{l} \left(\begin{array}{l} 42r^5(1+v) - 35r^4(7+4v)\rho + 105r^3(5+2v)\rho^2 - \\ -42r^2(13+4v)\rho^3 + 70r(4+v)\rho^4 - 3(19+4v)\rho^5 + \end{array}\right) \\ +3\left(\begin{array}{l} 14r^5(1+v) - 105r^4\rho - 35r^3(-7+2v)\rho^2 + \\ +14r^2(-19+8v)\rho^3 - 70r(-2+v)\rho^4 + \\ +(-29+16v)\rho^5 \end{array}\right)\cos[2\varphi] \end{array}\right) \end{array} \right);$$

$$\sigma_{\theta\theta} = \frac{1}{3r^7\rho} 2A \left(\begin{array}{l} -G\left(\begin{array}{l} 21r^5 - 70r^4\rho + 105r^3\rho^2 - \\ -84r^2\rho^3 + 35r\rho^4 - 6\rho^5 \end{array}\right)\left(1 + 4v + 3\cos[2\varphi]\right) - \\ -\lambda\left(\begin{array}{l} \left(\begin{array}{l} 42r^5(1+v) - 35r^4(7+4v)\rho + 105r^3(5+2v)\rho^2 - \\ -42r^2(13+4v)\rho^3 + 70r(4+v)\rho^4 - 3(19+4v)\rho^5 + \end{array}\right) \\ +3\left(\begin{array}{l} 14r^5(1+v) - 105r^4\rho - 35r^3(-7+2v)\rho^2 + \\ +14r^2(-19+8v)\rho^3 - 70r(-2+v)\rho^4 + \\ +(-29+16v)\rho^5 \end{array}\right)\cos[2\varphi] \end{array}\right) \end{array} \right);$$

$$\sigma_{\varphi\varphi} = -\frac{1}{3r^7\rho} 2A \left(\begin{array}{l} 3G\left(21r^5 - 70r^4\rho + 105r^3\rho^2 - 84r^2\rho^3 + 35r\rho^4 - 6\rho^5\right) + \\ +\lambda\left(\begin{array}{l} 42r^5(1+v) - 35r^4(7+4v)\rho + 105r^3(5+2v)\rho^2 - \\ -42r^2(13+4v)\rho^3 + 70r(4+v)\rho^4 - 3(19+4v)\rho^5 \end{array}\right) + \\ \left(\begin{array}{l} G(1+4v)\left(\begin{array}{l} 21r^5 - 70r^4\rho + 105r^3\rho^2 - \\ -84r^2\rho^3 + 35r\rho^4 - 6\rho^5 \end{array}\right) + \\ 3\lambda\left(\begin{array}{l} 14r^5(1+v) - 105r^4\rho - 35r^3(-7+2v)\rho^2 + \\ +14r^2(-19+8v)\rho^3 - 70r(-2+v)\rho^4 + \\ +(-29+16v)\rho^5 \end{array}\right)\cos[2\varphi] \end{array}\right) \end{array} \right);$$

$$\tau_{\rho\theta} = 0; \quad \tau_{\rho\varphi} = -\frac{4AG}{3r^7\rho}\left(\begin{array}{l} 21r^5(-2+v) - 35r^4(-5+4v)\rho + \\ +315r^3(-1+v)\rho^2 - 42r^2(-7+8v)\rho^3 + \\ +35r(-4+5v)\rho^4 + 9(3-4v)\rho^5 \end{array}\right)\sin[2\varphi]; \quad \tau_{\theta\varphi} = 0. \quad (2.30)$$

Thus, knowing all the components of stresses and displacements for two stress-strain states, it is possible to determine the total energy of destruction.

Based on the superposition of equations for determining displacements without a crack and equations for determining the displacements of a body with a crack, the corresponding graphs were constructed [4]. The graphs of the dependence of the principal stresses on the size of the major semiaxis of the crack ellipse are shown in **Fig. 2.4**. The graph of stress versus zenith angle φ is shown in **Fig. 2.5**. The change in stress $\sigma\rho$ depending on the radius r is shown in **Fig. 2.6**.
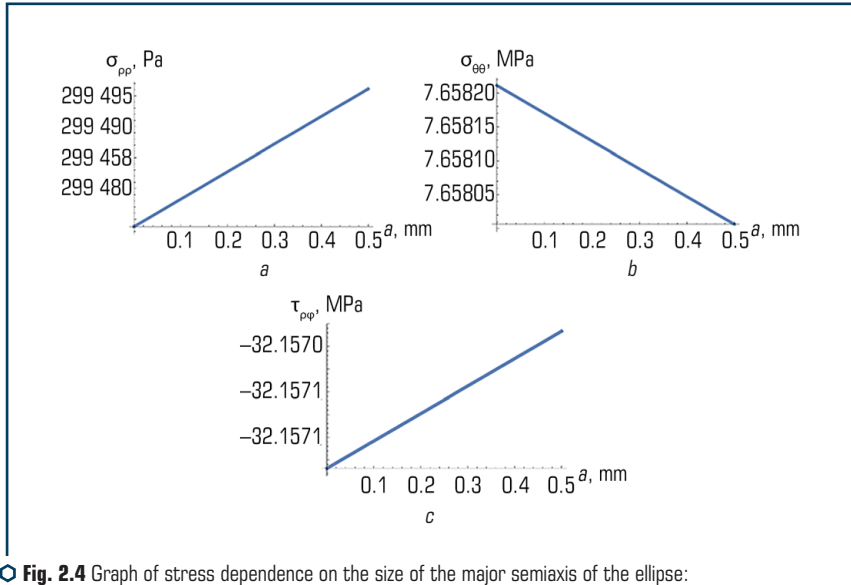
Fig. 2.4 Graph of stress dependence on the size of the major semiaxis of the ellipse: $a - \sigma\rho{-}a$; $b - \sigma\theta{-}a$; $c - \tau\rho\varphi{-}a$
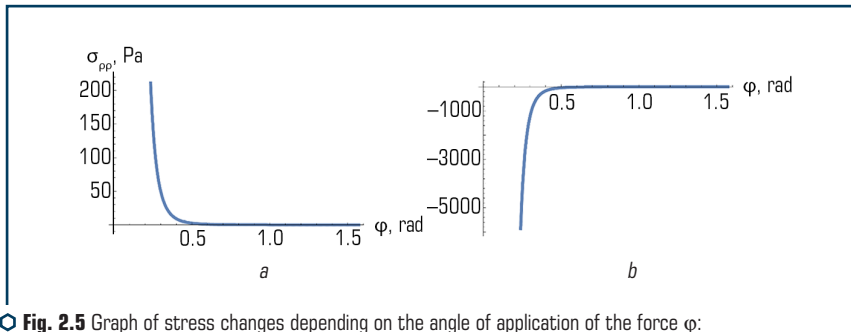
Fig. 2.5 Graph of stress changes depending on the angle of application of the force φ: $a - \sigma\rho{-}\varphi$; $b - \tau\rho\varphi{-}\varphi$
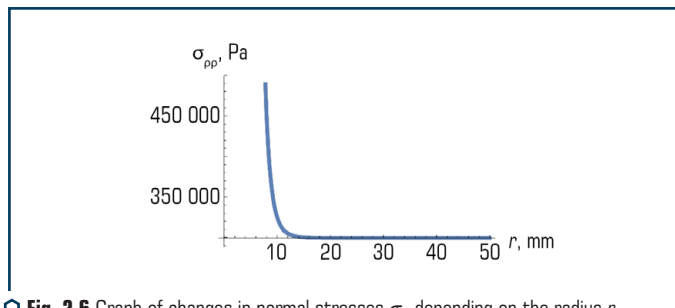
○ **Fig. 2.6** Graph of changes in normal stresses σ_p depending on the radius r

As follows from the graphs (**Fig. 2.4**), the dependences of stresses on the size of the major semiaxis of the ellipse have a linear characteristic within the framework of the calculations, the numerical values of which were used to determine the parameters of the crusher.

The significant influence of the angle of application of the force on the change in stresses is noted in the range of 0.3–0.5 (**Fig. 2.5**).

A more complex law of variation of normal stresses depending on the radius r is noted in the range of 9–12 mm (**Fig. 2.6**).

2.3 RESEARCH AND ANALYSIS OF MATERIAL GRINDING MACHINE PARAMETERS

A mathematical model of an experimental jaw crusher. The physical model of a vibration jaw crusher is shown in **Fig. 2.7**. When considering the physical model, the structural elements of the machine take an elementary form, the gravity forces of individual links are applied at certain points, the forces of resistance to destruction are presented in the form of a total force applied to the jaw center [7, 8].
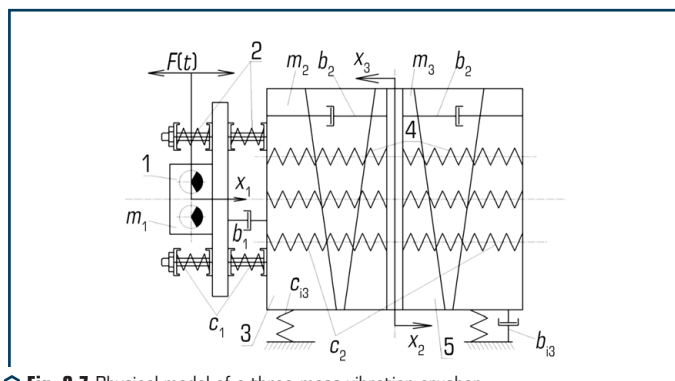
○ **Fig. 2.7** Physical model of a three-mass vibration crusher

When compiling the equations of motion of the vibration system of a jaw crusher, let's use Hamilton's variational principle. It establishes that the variation in kinetic and potential energy plus variation in the work of non-conservative forces during any time interval should be equal to zero [9–11].

To compose the equations of motion, let's consider the structural diagram of a vibration jaw crusher. The investigated jaw crusher is made in the form of a three-mass resonance system (**Fig. 2.7**), in which rectilinear vibrations are realized and the dynamics of which occurs according to a three-mass scheme.

The vibration exciter 1 with the base plate is the first or active mass, the movable body 3 is the second mass, the middle plate with inner armor 5 is the third mass. Each mass performs horizontal oscillations along the x-axis along the generalized coordinates, respectively, and has its own inertial parameter.

The active mass is set in motion by the centrifugal force arising from the rotation of the unbalanced masses of the vibration exciter. The crusher is adjusted in such a way that during operation the first and third masses oscillate in phase, and the second in antiphase, that is, when one chamber approaches in another, the jaw diverge.

All masses of the crusher are connected in pairs by elastic systems 2 and 5 (**Fig. 2.7**) with stiffnesses and. The vibration machine is isolated from the foundation by vibration dampers with stiffness on which the second mass rests. Resistance forces act in the system, but these forces can be neglected to simplify calculations.

The system of equations of motion for the model using the Lagrange equation of the second kind will take the form [5]:

$$\begin{cases} m_1\ddot{x}_1 + 2x_1c_1 - x_2c_1 = F_0\sin\omega t; \\ \left(m_2 + km_m\right)\ddot{x}_2 + x_2c_1 - x_1c_1 + 2c_2x_2 - 2c_2x_3 + x_2c_f = 0; \\ \left(m_3 + km_m\right)\ddot{x}_3 + 2c_2x_3 - 2c_2x_2 = 0; \\ F_{cr} \le c_2x_n; \\ x_1 > 0;\ x_3 > 0;\ x_2 < 0; \\ x_2 + x_3 = \xi \cdot D_{max}, \end{cases} \qquad (2.31)$$

where F_0 — centrifugal force ($F_0 = m_0r_0\omega^2$); r_0 — eccentricity, distance from the center of gravity of the mass m_0 to the center of the axis of rotation, m; ω — angular speed of unbalance rotation, s^{-1}; m_1, m_2, m_3 — the first, second and third mass of the crusher, kg; c_1, c_2 — stiffness of the springs connecting the masses of the crusher; x_1, x_2 and x_3 — corresponding displacement of the masses of the crusher, mm; c_f — stiffness of the connections of the system connecting the machine to the foundation; F_{cr} — crushing force formula, N; ξ — relative compression of the material; D_{max} — the maximum size of the crushed material, mm.

The solution to the system of equations (2.30) and (2.31) is obtained in the form:

$$\begin{cases} x_1 = X_1 \sin \omega t; \\ x_2 = X_2 \sin \omega t; \\ x_3 = X_3 \sin \omega t, \end{cases} \qquad (2.32)$$

where X_1, X_2, X_3 – amplitudes of mass displacement.

Substituting (2.32) into (2.18) and carrying out the appropriate transformations, let's obtain the dependences for determining the values of the amplitudes of the displacement of the masses X_1, X_2, X_3.

The energy consumed by the electric motor is spent on the work on crushing the material, on the potential energy of deformation of the elastic system, on overcoming friction forces, on heat losses, on the deformation of the crusher parts and other losses. The greatest energy consumption during the operation of the crusher is spent on crushing the material, the kinetic energy of the crushing plates and the potential energy of deformation of the springs.

$$X_1 = \frac{F_0\left(\omega^2\left(-c_f+\omega^2 m_2\right)m_3 + c_1\left(2c_2-\omega^2 m_3\right)+2c_2\left(c_f-\omega^2\left(m_2+m_3\right)\right)\right)}{c_1^2\left(2c_2-\omega^2 m_3\right)+\omega^2 m_1\left(\omega^2\left(c_f-\omega^2 m_2\right)m_3 + 2c_2\binom{-c_f+}{+\omega^2\left(m_2+m_3\right)}\right)+c_1\left(\omega^2\binom{-2c_f+}{+\omega^2\left(m_1+2m_2\right)}m_3 - 2c_2\binom{-2c_f+}{+\omega^2\binom{m_1+}{+2\left(m_2+m_3\right)}}\right)};$$

$$X_2 = \frac{c_1 F_0\left(2c_2-\omega^2 m_3\right)}{c_1^2\left(2c_2-\omega^2 m_3\right)+\omega^2 m_1\left(\omega^2\left(c_f-\omega^2 m_2\right)m_3 + 2c_2\binom{-c_f+}{+\omega^2\left(m_2+m_3\right)}\right)+c_1\left(\omega^2\binom{-2c_f+}{+\omega^2\left(m_1+2m_2\right)}m_3 - 2c_2\binom{-2c_f+}{+\omega^2\binom{m_1+}{+2\left(m_2+m_3\right)}}\right)};$$

$$X_3 = \frac{2c_1 c_2 F_0}{c_1^2\left(-2c_2+\omega^2 m_3\right)+\omega^2 m_1\left(\omega^2\left(-c_{o?}+\omega^2 m_2\right)m_3 + 2c_2\binom{c_{o?}-}{-\omega^2\left(m_2+m_3\right)}\right)+c_1\left(-\omega^2\binom{-2c_{o?}+}{+\omega^2\left(m_1+2m_2\right)}m_3 + c_2\binom{-4c_{o?}+}{+2\omega^2\binom{m_1+}{+2\left(m_2+m_3\right)}}\right)}. \qquad (2.33)$$

Thus, the total energy consumed by the crusher for crushing the material will look like this:

$$E_{tot} = C + P, \tag{2.34}$$

where C – kinetic energy of the system; P – potential energy of the system.

Part of the potential energy is spent on the destruction of the material. Knowing the general displacements arising in the material during its destruction and applying the condition of the minimum potential energy of deformation, it is possible to write the following:

$$U_p = G\iiint \left[\varepsilon_{\rho\rho}^2 + \varepsilon_{\theta\theta}^2 + \varepsilon_{\varphi\varphi}^2 + \frac{\nu}{1-2\nu}e^2 + \frac{1}{2}\left(\gamma_{\rho\theta}^2 + \gamma_{\theta\varphi}^2 + \gamma_{\rho\varphi}^2\right) \right]\rho^2 \sin\varphi d\rho d\theta d\varphi. \tag{2.35}$$

Knowing the energy consumption for the destruction of the material, one can proceed to determining the energy consumption for the process as a whole.

Let's consider two vibration-driven crushing systems shown in **Fig. 2.8**.

The vibration jaw crusher (**Fig. 2.8, *a***) is made in the form of a three-mass resonance system, in which rectilinear vibrations are realized and the dynamics of which occurs according to a three-mass scheme. The vibration exciter 1 with the base plate is the first or active mass, the movable body 5 is the second mass, the middle plate with the inner armor 4 is the third mass. All masses of the crusher are connected in pairs by elastic systems 2 and 3.
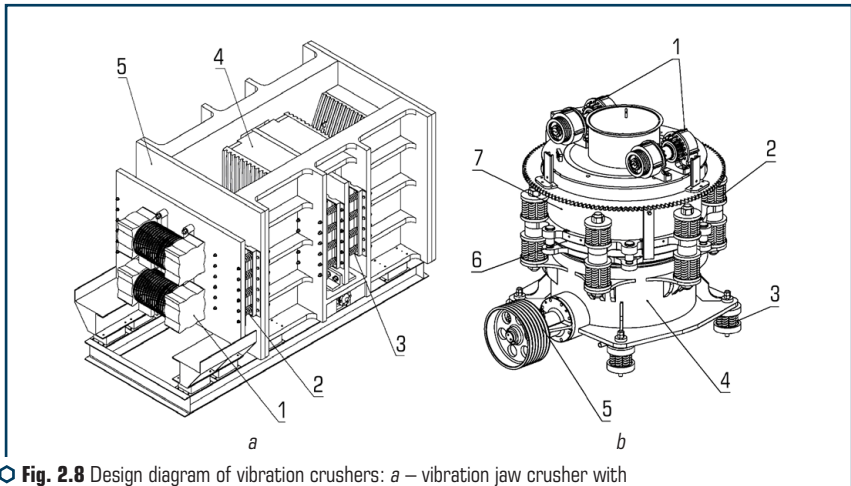
○ **Fig. 2.8** Design diagram of vibration crushers: *a* – vibration jaw crusher with three vibration masses; *b* – cone crusher with vibrators on the body

Vibration cone crusher (**Fig. 2.8, *b***) consists of vibration exciters 1 installed on a stationary cone 7 of the crusher. The fixed cone 7 is connected to the crusher body 4 through the adjusting

ring 6 and the elastic system 2. The crusher body 4 is installed on the foundation through the elastic system 3. The movable crusher cone is driven through the drive 5.

The energy consumed by the electric motors of the crushers (**Fig. 2.8, *a*, *b***) is spent on the work on crushing the material. Additionally, energy costs are spent on deformation of the elastic system, overcoming friction forces, heat losses, deformation of crusher parts and other losses. However, the greatest energy consumption during the operation of crushers is spent on the kinetic energy of crushing plates and the potential energy of deformation of the springs [2].

Based on the general equation of energy consumption for a vibration jaw crusher with three vibration masses (2.32), the following equation was derived:

$$E_{tot} = \left[\sum_{n=1}^{3} \frac{m_n \dot{x}_n^2}{2} \right] + \left[\frac{1}{2} \left(c_f x_2^2 + c_1 \left(3x_1^2 - 4x_1 x_2 + 2x_2^2 \right) + 4c_2 \left(x_2 - x_3 \right)^2 \right) \right], \tag{2.36}$$

where m_n – respectively n-mass of the crusher, kg; c_1, c_2 – stiffness of the springs connecting the masses of the crusher; x_1, x_2 and x_3 – corresponding displacements of the masses of the crusher, mm; c_f – the stiffness of the connections of the system connecting the machine to the foundation.

When determining the total energy of a vibration cone crusher (**Fig. 2.8, *b***), let's assume that the movable cone is an absolutely rigid cylinder rolling on a solid undeformed body in the shape of an ellipse. In turn, let's assume that the crusher body with vibrators is a solid body with mass m_{tot} and moment of inertia *I*, which is fixed on a fixed base by springs with stiffness c_{is} [1]:

$$E_{tot} = \left[\frac{1}{2} m_{mc} \times \left(v_x^2 + v_y^2 \right) + \frac{I_{mc} \times \dot{\varphi}^2}{2} + \frac{1}{2} m_{sc} v_{sc}^2 \right] + \left[\frac{c_{cr} \left(n \times x_1 \right)^2}{2} + \frac{c_1 x_1^2}{2} \right], \tag{2.37}$$

where $T_1 = 1/2 m_{mc} \times (v_x^2 + v_y^2) + (I_{mc} \times \dot{\varphi}^2)/2$ – kinetic energy of rolling a movable cone [4]; $T_2 = 1/2 m_{sc} v_{sc}^2$ – kinetic energy of vibrations of a stationary cone; m_{sc} – the mass of the movable cone; I_{mc} – central moment of inertia of the cone; x_1, y_1 – Cartesian coordinates of the center of the cone; φ – angle of rotation of the movable cone around its own axis; m_{sc} – total mass of the stationary cone; v_{sc} – speed of vertical displacements of a fixed cone; c_{cr} – material stiffness coefficient; c_1 – the stiffness coefficient of the elastic system connecting the stationary cone and the crusher body.

Sandstone with a strength limit of up to 20 MPa was taken as the model of the material of destruction. Based on the equations of motion of a vibration jaw crusher (2.31), the speeds of movement of the vibration masses of the crusher shown in **Fig. 2.9**.

Regarding **Fig. 2.9**, it should be noted that these speeds of mass fluctuations are valid at the frequency of the disturbing force $f = 19$ Hz and the total mass of the laboratory unit $m_{tot} = 334$ kg.

Using the first part of equation (4) and the equations of motion of the masses of the vibration jaw crusher (2.31), graphs of the consumption of kinetic energy were built, which is spent on moving the vibration masses of the vibration crusher **Fig. 2.10**.
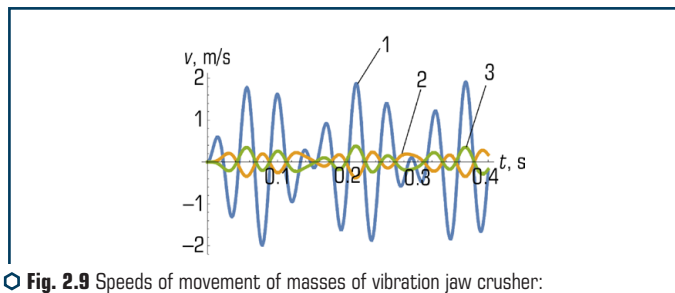
Fig. 2.9 Speeds of movement of masses of vibration jaw crusher:
1 – first mass; 2 – second mass; 3 – third mass
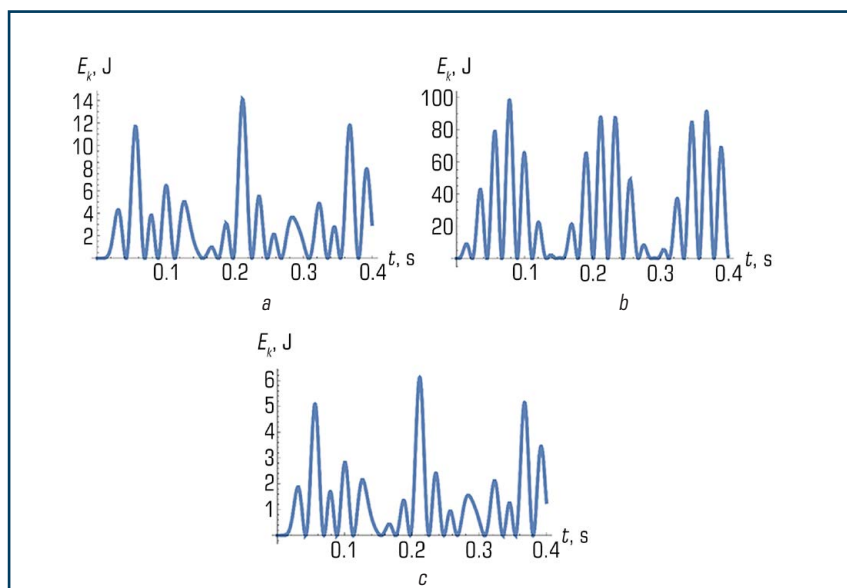
Fig. 2.10 Graph of changes in the kinetic energy of vibration masses of a vibration jaw crusher: a – first mass; b – second mass; c – third mass

From the graphs in **Fig. 2.10**, it is clear that the total kinetic energy of the motion of the masses is within 120 J. However, equations (2.36) used to plot the graphs in **Fig. 2.10** do not take into account the loss of dry and viscous friction force.

To construct graphs of potential energy consumption for the crushing process, let's use equation (2.31).

The movement of vibration masses of the crusher, determined numerically based on the equation of motion, is shown in **Fig. 2.11**.
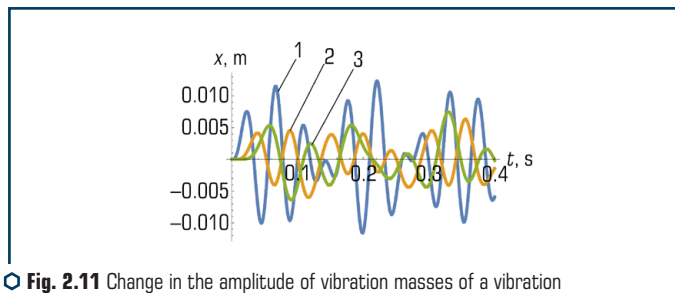
Fig. 2.11 Change in the amplitude of vibration masses of a vibration jaw crusher: 1 – first mass; 2 – second mass; 3 – third mass

From the graph in **Fig. 2.11** it can be seen that the system setting is correct, that is, the second and third masses oscillate in antiphase. The total amplitude of displacement of the second and third vibration masses is in the range of 8–10 mm. The minimum required value of the amplitude of vibration of the crushing plates of a vibration crusher, at which destruction occurs, is within 3–5 mm.

The graph of the total costs of potential energy for the destruction process in the crushing chamber of a vibration jaw crusher is shown in **Fig. 2.11**. This graph was constructed by numerous methods using equations (2.31) and (2.36).

The graphs in **Fig. 2.10** and **Fig. 2.12** indicate an insignificant expenditure of energy for the destruction process. It should be noted here that the system is tuned for resonant operation. That is, in the graphs in **Fig. 2.10** and **Fig. 2.12** does not reflect the energy consumption for the system to enter the resonance mode and maintain its operation in this mode. In addition, it should be borne in mind that, in order to simplify, the equation of motion (2.31) does not take into account energy dissipation.

To assess the energy of destruction of a body containing a crack, graphs of the instantaneous force arising when the crushing plates of the second and third masses of the vibration crusher collide with the material in **Fig. 2.13**. To construct this graph, equations (2.31) and (2.36) were used.

The given graph (**Fig. 2.13**) testifies to the adequacy of the calculation scheme to the accepted premises. So, the first mass moves in antiphase with the second mass. The third mass, accumulating energy, is an auxiliary source of energy transfer to the material crushing process.
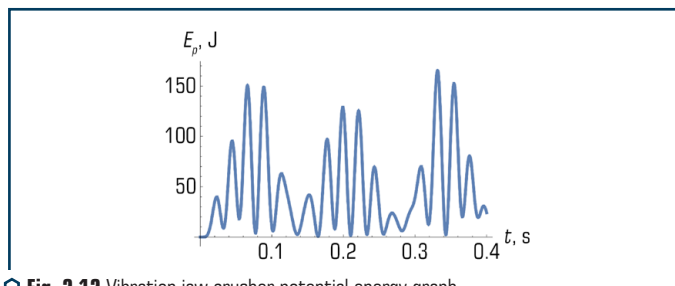
Fig. 2.12 Vibration jaw crusher potential energy graph
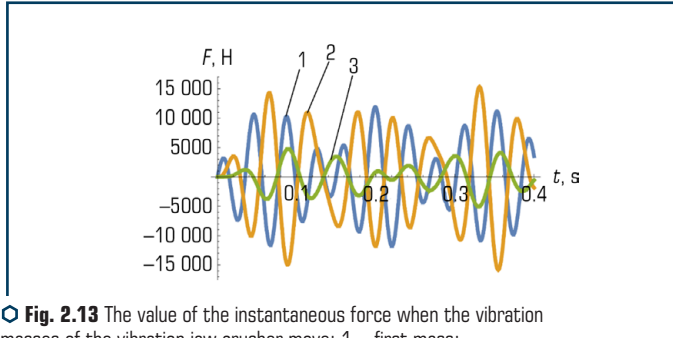
○ **Fig. 2.13** The value of the instantaneous force when the vibration masses of the vibration jaw crusher move: 1 – first mass; 2 – second mass; 3 – third mass

In equation (2.36), to determine the energy consumption of a vibration jaw crusher, the fracture resistance of the material is considered as the added mass. That is, the indicator of the stiffness of the material is the parameter that includes energy consumption at the micro level. In equation (2.37) for a vibration cone crusher, this parameter is directly the stiffness coefficient of the material. Thus, the obtained analytical dependences (2.36), (2.37) reveal the physical essence of the grinding process, take into account the conditions of interaction between the crusher and the material to be crushed. The practical application of the obtained dependences requires the numerical values of the characteristics of a particular material, which is the subject of further research.

2.4 DETERMINING THE OPTIMAL CHARACTERISTICS OF MATERIAL GRINDING PROCESSES

Study of the influence of the stiffness index on the amplitude. When designing vibration machines, two modes are recognized as expedient: resonant (near resonance), with a frequency ratio $\omega/\omega_0 = 0.85...0.95$; overresonant (only for centrifugal vibration exciters) with a significant distance from resonance, when $\omega/\omega_0 > 7$ [12, 13].

The advantage of the resonant mode is to achieve a given amplitude with less forced force. The resonant mode is characterized by the stability of the amplitude in case of random changes in resistance and frequencies of natural and forced oscillations.

The operation of a vibration crusher in one of the listed modes is achieved by choosing elastic links that provide a vibration frequency, which may differ from the frequency of the forcing vibrations. The stiffness of the system depends on two main parameters of mass and vibration frequency. By manipulating these parameters, it is possible to determine the optimal stiffness value for the corresponding mode.

To begin with, for given values of the masses of the system, let's change the value of the frequency. It should be noted that the stiffness of the system should help to ensure an effective

grinding regime for the material. To determine the stiffness of the system, let's use the following relationship [5]:

$$c_{ij} = \left(\omega_0 n\right)^2 \frac{m_i m_j}{m_i + m_j},$$
(2.38)

where ω – natural angular frequency of oscillations (resonant frequency); n – coefficient of stiffness regulation in frequency. Substituting the corresponding values of the stiffness calculated by the formula (2.38) into the equation of the amplitudes of the displacement of masses (2.37), let's obtain the graphs of the dependence of the amplitude on the coefficient n (**Fig. 2.14**) for the corresponding frequency modes [6, 8].
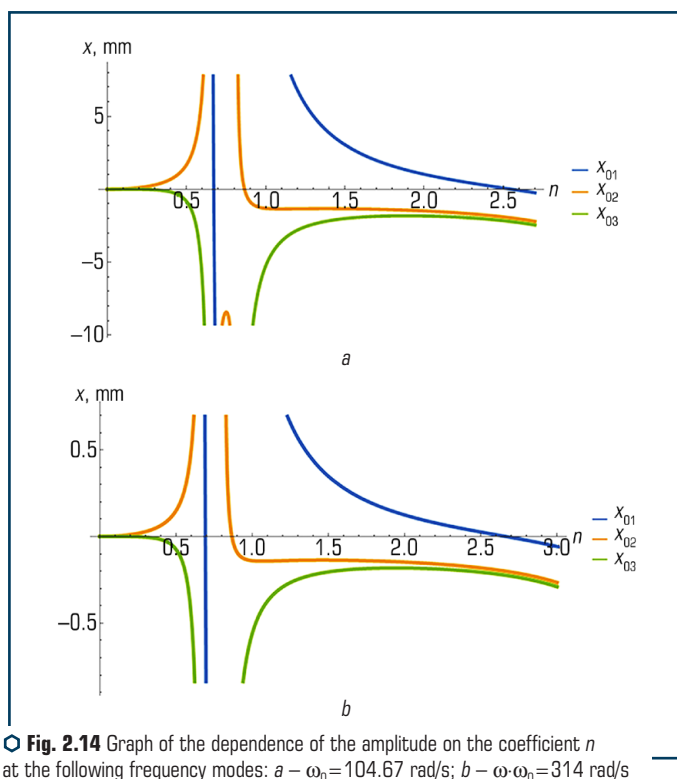
○ **Fig. 2.14** Graph of the dependence of the amplitude on the coefficient n at the following frequency modes: $a - \omega_0 = 104.67$ rad/s; $b - \omega \cdot \omega_0 = 314$ rad/s

The following conclusion can be drawn from the graphs in **Fig. 2.14**. The rational value of the coefficient n is within $0.6 \le n \le 1$. With an increase in the value of the coefficient $(1 \le n < 2.5)$, the effective range of the crusher narrows and shifts towards higher frequencies. Graphs **Fig. 2.14**

show that the stiffness of the elastic bonds of the crusher ensures its efficient operation in the resonance and near-resonance modes, namely, between the second and third resonances. With the value of the coefficient $0.6 \leq n \leq 1$, the amplitudes of the masses have the greatest values and decrease as n approaches 1.4. With an increase in $n > 1$, the change in the amplitude of the second mass is insignificant, and for $n > 1.4$, the change in the amplitudes of the first and third masses is insignificant. The amplitude of the first mass reaches zero in the vicinity of the point $n = 2.52$.

Study of the effect of mass on the amplitude. Rationally selected ratios of vibration masses provide the required operating mode of the crusher (in-phase, anti-phase) and provide the required vibration amplitudes of these masses [13].

When choosing the ratio of mass m_2 and m_2, the value of the mass m_1 is taken constructively, the value of the stiffness of the systems c_1, c_2 is taken taking into account formulas (2.31), (2.38). To introduce the mass ratio coefficient depending on the equations of motion (2.37), let's use the following logical transformations [7]:

$$N_{23} = m_2 + m_3; \; k_{23} = m_2/m_3. \tag{2.39}$$

Based on this:

$$m_2 = (N_{23}k_{23})/(1 + k_{23}); \; m_3 = N_{23}/(1 + k_{23}). \tag{2.40}$$

On the basis of the above material, the graphs of the dependence of the amplitude on the mass ratio for different frequency spectra were plotted in **Fig. 2.15**. Analyzing the graphs in **Fig. 2.15** the following can be noted. The effective value of the coefficient k_{23} for the resonant angular frequency $\omega_0 = 104.667 \, \text{rad/s}$ is within the limits $0 < k_{23} \leq 2.5$, for $\omega_0 = 314 \, \text{rad/s} -$ $1.5 < k_{23} \leq 2.45$ [14–18].

Analyzing each graph separately, **Fig. 2.15**, the following conclusions were made. At the resonant frequency $\omega_0 = 104.667 \, \text{rad/s}$, the maximum value of the amplitude of the third mass is reached in the vicinity of the point $k_{23} = 1.3$. And the maximum values of the amplitudes of the first and second masses are in the vicinity of the point $k_{23} = 0.75$. For the resonant frequency $\omega_0 = 314 \, \text{rad/s}$, the maximum values of the amplitudes of all three masses are achieved under the condition of the point k_{23} lying in the vicinity $k_{23} = 1.5$.

Let's use the same approach to find the optimal ratio of masses m_2 and $m_1 - k_{21}$.

Construction of the amplitude-frequency characteristics of the vibration jaw crusher. Knowing all the unknown parameters of the equations of motion, graphs of the dependence of the amplitude of displacement of the crushing plates on the frequency of change in the disturbing force were built (**Fig. 2.16, 2.17**) [3, 5].

Based on the graphs (**Fig. 2.16, 2.17**), the following conclusions were made:

– the effective mode of operation of the crusher is realized in the zone of the second resonance and in the range between the second and third resonances;

– with an increase in the calculated value of the resonant frequency of wheel vibrations ω_0 (2.38), the range of effective operation of a three-mass vibration jaw crusher shifts towards an increase in frequency;

– the effective ranges of the crusher operation at the system stiffness values calculated at the corresponding resonant frequencies of natural vibrations ω_0 (2.38) will be as follows:

$100\,\text{rad/s} < \omega < 180\,\text{rad/s};\ \omega_0 = 104.667\,\text{rad/s};$

$97\,\text{rad/s} < \omega < 121\,\text{rad/s};\ 186\,\text{rad/s} < \omega < 234\,\text{rad/s};$

$\omega_0 = 314\,\text{rad/s};\ 291\,\text{rad/s} < \omega < 322\,\text{rad/s};\ 365\,\text{rad/s} < \omega < 400\,\text{rad/s}.$
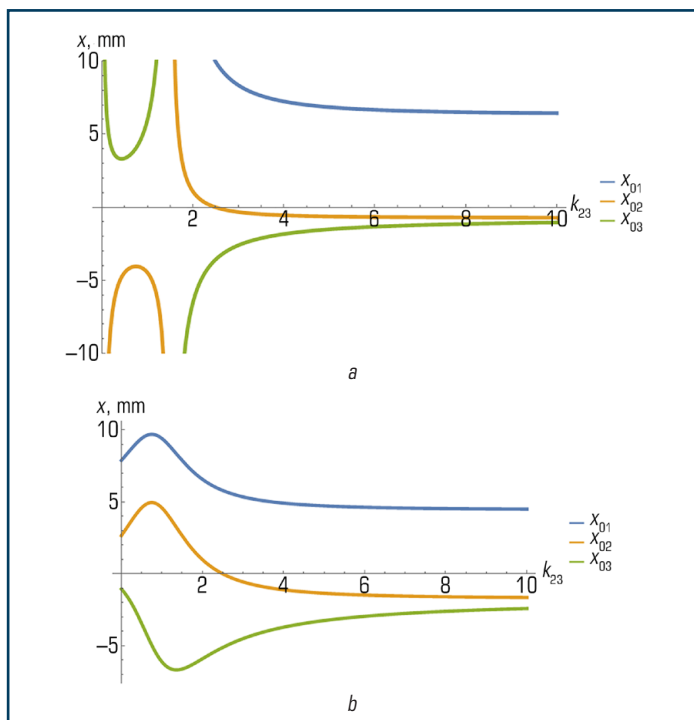
○ **Fig. 2.15** Graphs of the dependences of the amplitude change on the mass ratio k_{23} at different frequency ranges: $a - \omega_0 = 104.67$ rad/s; $b - \omega_0 = 314$ rad/s

To ensure the operation of the crusher at the values of the stiffness of the system, calculated from the resonant frequency of natural vibrations of the $\omega_0 = 104.67$ rad/s (2.38), in the lower

frequency ranges, it is necessary to increase the masses of the vibration parts of the machine. The increased masses should not exceed the permissible limits, exceeding which will lead to the economic inexpediency of this machine design [3, 5].
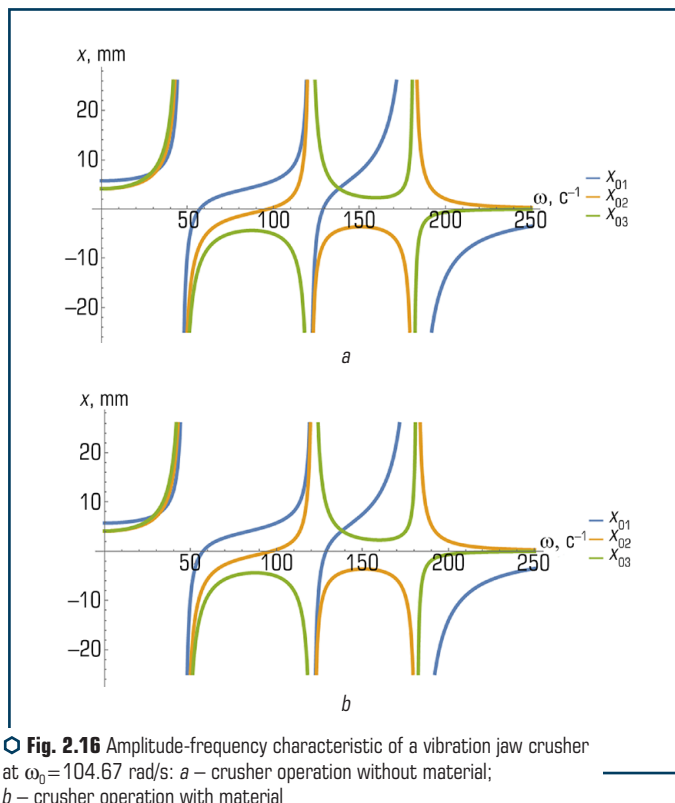
○ **Fig. 2.16** Amplitude-frequency characteristic of a vibration jaw crusher at $\omega_0 = 104.67$ rad/s: *a* – crusher operation without material; *b* – crusher operation with material

The study of the effect of frequency on the operation of the crusher with changing parameters of the disturbing force and stiffness is presented in the form of vibrograms in **Fig. 2.18, 2.19**.

The range at which the experimental studies of the operation of the three-mass vibration jaw crusher were carried out covers three modes: pre-resonant, near-resonant and over-resonant. As the work of the crusher approaches resonance, the difference between the values of the theoretically calculated and experimentally determined amplitudes slightly increases, which is explained by not taking into account the theoretical calculations of dissipative resistances. When the crusher is operating at low frequencies up to $f = 7$ Hz, that is, before the first resonance, there is a fluctuation of the masses in one phase. It follows from this that this mode is not effective.
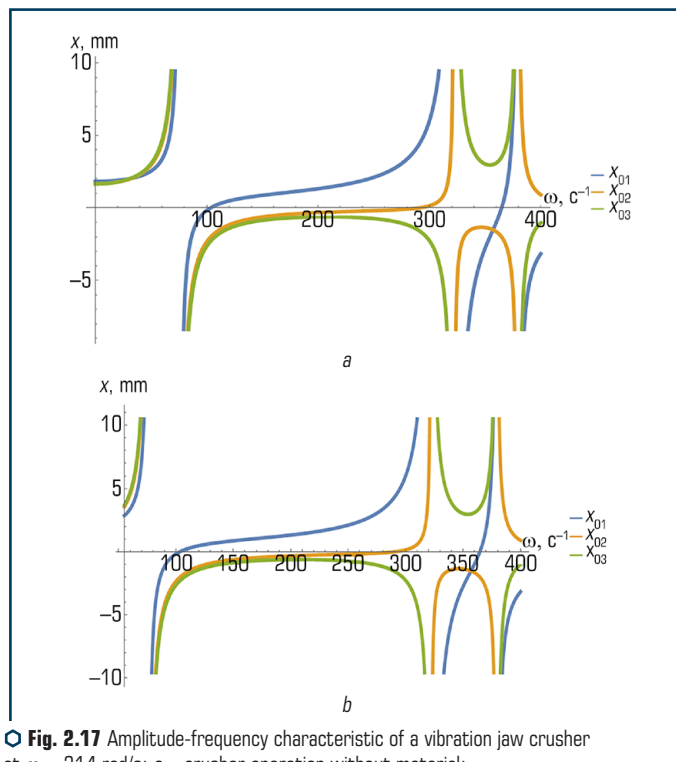
○ **Fig. 2.17** Amplitude-frequency characteristic of a vibration jaw crusher at $\omega_0 = 314$ rad/s: *a* – crusher operation without material; *b* – crusher operation with material

When the crusher is operating in the vicinity of a frequency of 12 Hz, there is almost no crushing of the material. This can be explained by the fact that the vibrator does not create forces at a given frequency that could effectively destroy the material.

In the frequency range 14.5 Hz < *f* < 26 Hz, the material is efficiently comminuted. The efficiency of crushing is somewhat reduced when the crusher is operating in the vicinity of a frequency of 22 Hz. This can be explained by a decrease in the amplitude of oscillation of the second and third masses and a decrease in vertical oscillations of the crusher body, which increases the residence time of the material in the crushed chamber.

When studying the influence of the stiffness of the elastic systems of the crusher on the crushing process, the following features were established. As the stiffness of the system increases, the effective range of the crusher shifts towards an increase in the angular frequency. This is due to the shift of the resonance point towards an increase in the angular frequency of the crusher vibrations. This property can be used to create a crusher control system.
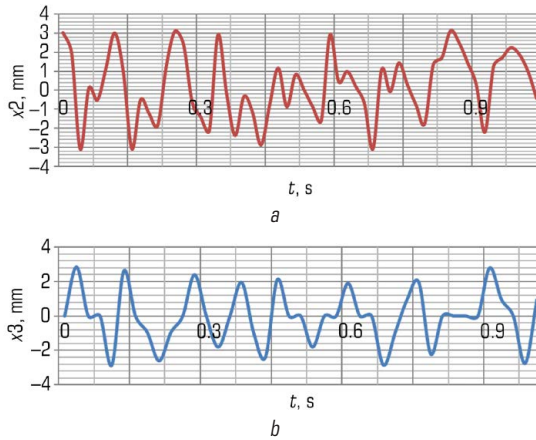
Fig. 2.18 Vibrograms of vibrations of the masses of the crusher when working with material ($F=4\ 111$ N, $c_2=219\ 052$ N/m): a – displacement of the second mass; b – displacement of the third mass
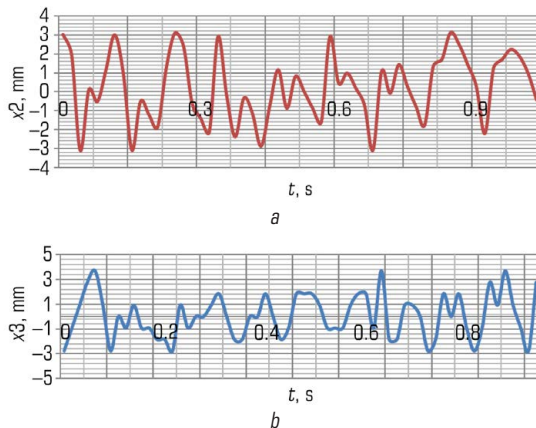
Fig. 2.19 Vibrograms of vibrations of the crusher masses when working with material ($F=4\ 111$ N, $c_2=234\ 438$ N/m): a – displacement of the second mass; b – displacement of the third mass

However, too much increase or decrease in stiffness adversely affects the performance of the machine. So, with a stiffness N/m, in the frequency range, the second and third masses move in phase, and the first in antiphase. Thus, the operation of the crusher at low frequencies is not

efficient at a given stiffness. At very low stiffness, the efficiency of energy transfer from the vibrator to the third mass deteriorates, as evidenced by experimental data. The vibration amplitudes of the third mass, provided that N/m are insignificant. The features of the impact of stiffness are as follows. As stiffness increases, the crusher's effective operating range shifts towards zero. If the stiffness is increased too much, the three-mass system turns into a two-mass one. With a decrease in stiffness, the range of effective operation of the crusher narrows, and in conditions of too large a decrease in stiffness, the system leaves the state of equilibrium, which has a negative effect on the crushing process.

2.5 DISCUSSION OF RESEARCH RESULTS

An efficient crusher operation can be achieved by operating it in the vicinity of resonance, i.e. at a high value of the coefficient of resonant amplification of oscillations. However, this mode is sensitive to changes in external influences on the workflow. It is possible to reduce external influences by automatically adjusting the operating mode of the machine.

The control of the vibration machine is to ensure the optimal operating mode, in which the specified displacements, speeds and accelerations are achieved [6–8]. The set values of displacements, speeds and accelerations of a vibration jaw crusher can be achieved both in pre-resonant and over-resonant operating modes.

The creation of a control system for the amplitude-frequency characteristic and taking into account the dependences of the moment of resistance on the frequency of the driving force underlies the method of regulating the working process of the crusher. This task can be achieved by correctly calculating the parameters of the three-mass vibration jaw crusher.

The second way to regulate the operating mode of a three-mass vibration crusher is to adaptively change the stiffness of the system. The third way to regulate the operating modes of the crusher is to change the vibration frequency.

On the basis of the above studies, algorithms were formulated for calculating the main parameters and controlling the working process of a vibration three-mass jaw crusher (**Fig. 2.20, 2.21**), respectively.

A physical model and a mathematical model of a vibration jaw crusher have been developed, taking into account the elastic – inertial properties, power and geometric characteristics of the «jaw – fractional material» system.

One of the main research tools were the amplitude – frequency characteristics of the system movement. The studies have established the regularities of the change in the elasticity coefficients depending on the frequency, the coefficients that determine the rational ratios of the vibration masses.

The optimal values of the amplitude of the oscillations of the masses have the greatest values, provided that the coefficient of regulation of elasticity in frequency n is in the range of $0.6 \leq n \leq 1$. Within the frequency range of 14.5 Hz$<f<26$ Hz, material is effectively crushed. The numerical values of the coefficient k_{23} are established, which determine the rational ratios of vibration masses.

The studies carried out and their results indicate that the main stresses causing the destruction of the material are shear stress. With an increase in the size of the major semiaxis of the crack ellipse, the total stresses decrease, which indicates the destruction of the brittle body. However, the stresses σρ acting along the radius slightly increase. The graphs (**Fig. 2.4**) reflect the picture of the stress distribution in a spherical body relative to the point of application of the force along the angle φ. The graph (**Fig. 2.5**) shows the change in normal stresses depending on the distance r. Analysis of the graph (**Fig. 2.6**) makes it possible to conclude that at $r->0$, the stresses increase indefinitely. As a result of this, the stresses and strains in the cracked body must be determined in the vicinity of the center of the body. In addition, it was found that the complete elliptical integral of the second kind has an insignificant effect on the change in the stress pattern in the body. It should be noted that when solving the problem using the Legendre functions, 15 constants appear in the stress equations, which together have a significant effect on the stress pattern in the body. These constants were a numerous method based on the equations of the potential energy of a deformed body.

Equations (2.21), (2.23) and (2.30) fully reflect the picture of energy consumption for material destruction. Such studies are planned as a continuation of the topic under consideration through experimental studies and consideration of several members of the series and optimization of the parameters of crushing machines. The proposed approach to studying the energy characteristics of material destruction in the crusher chamber with a guaranteed zone of stability of parameters in the resonance zone can be used for other processes. Such processes include the destruction of materials during dynamic cutting of soils, processing of materials in mills and sorting of materials, which are gaining widespread use in various European countries.

CONCLUSIONS TO SECTION 2

1. A physical model and a mathematical model of a vibration jaw crusher have been developed.

2. The stress-strain state of the material in the process of its destruction for a continuous medium and surrounded by an existing crack has been investigated.

3. The efficiency of the crusher's working process is proved by the practical achievement of its work in the vicinity of resonance. That is, at a high value of the resonant amplification factor of the oscillations.

4. It has been determined that the optimal values of the amplitude of the oscillations of the masses have the greatest values, provided that the coefficient of regulation of elasticity in frequency n is within $0.6 \leq n \leq 1$. Within the frequency range of 14.5 Hz$<f<$26 Hz, material is effectively crushed.

5. The proposed approach to study the energy characteristics of material destruction in the crusher chamber with the provision of a guaranteed zone of stability of parameters in the resonance zone.

6. The studies carried out and their results indicate that the main stresses that lead to the destruction of the material are shear stress.

7. Algorithms for calculating the parameters of a vibration three-mass crusher have been formulated.

REFERENCES

1. Baladinskyi, V. L., Nazarenko, I. I., Onyshchenko, O. H. (2002). Budivelna tekhnika. Kyiv – Poltava: KNUBA-PNTU, 463.
2. Nazarenko, I. I. (2010). Prykladni zadachi teorii vibratsiinykh system. Kyiv: Vydavnychyi Dim «Slovo», 440.
3. Mishchuk, Y., Nazarenko, I., Mishchuk, D. (2021). Definition of rational operating modes of a vibratory jaw crusher. Naukovyi Visnyk Natsionalnoho Hirnychoho Universytetu, 4, 56–62. doi: http://doi.org/10.33271/nvngu/2021-4/056
4. Nazarenko, I., Mishchuk, Y., Mishchuk, D., Ruchynskyi, M., Rogovskii, I., Mikhailova, L. et. al. (2021). Determiantion of energy characteristics of material destruction in the crushing chamber of the vibration crusher. Eastern-European Journal of Enterprise Technologies, 4 (7 (112)), 41–49. doi: http://doi.org/10.15587/1729-4061.2021.239292
5. Nazarenko, I., Mishchuk, E., Kuchinsky, V. (2019). Assessment and analysis of basic design the cone crushers. Girnichi, budivelni, dorozhni ta meliorativni mashini, 94, 5–15. Available at: http://gbdmm.knuba.edu.ua/article/view/216440
6. Lapin, R., Kuzkin, V. (2019). Calculation of the normal and shear compliances of a three-dimensional crack taking into account the contact between the crack surfaces. Letters on Materials, 9 (2), 234–238. doi: http://doi.org/10.22226/2410-3535-2019-2-234-238
7. Zou, J., Han, J., Yang, W. (2020). Investigating the Influences of Indentation Hardness and Brittleness of Rock-Like Material on Its Mechanical Crushing Behaviors. Mathematical Problems in Engineering, 2020. doi: http://doi.org/10.1155/2020/4713532
8. Nazarenko, I., Gaidaichuk, V., Dedov, O., Diachenko, O. (2018). Determination of stresses and strains in the shaping structure under spatial load. Eastern-European Journal of Enterprise Technologies, 6 (7 (96)), 13–18. doi: http://doi.org/10.15587/1729-4061.2018.147195
9. Nazarenko, I. I., Ruchynskyi, M. M., Sviderskyi, A. T., Kobylanska, I. M., Harasim, D., Kalizhanova, A., Kozbakova, A. (2019). Development of energy-efficient vibration machines for the buiding-and-contruction industry. Przeglad Elektrotechniczny, 95 (4), 53–59. doi: http://doi.org/10.15199/48.2019.04.10
10. Nazarenko, I., Svidersky, A., Kostenyuk, A., Dedov, O., Kyzminec, N., Slipetskyi, V. (2020). Determination of the workflow of energy-saving vibration unit with polyphase spectrum of vibrations. Eastern-European Journal of Enterprise Technologies, 1 (7 (103)), 43–49. doi: http://doi.org/10.15587/1729-4061.0.184632
11. Vasiliev, L. M., Vasiliev, D. L., Malich, M. G. (2021). Modeling the process of disintegration of solid materials by asymmetric loading in crushing machines in order to find ways to reduce energy costs. Energy- and resource-saving technologies of developing the raw-material base of mining regions. Petroşani: UNIVERSITAS Publishing, 457–473. doi: http://doi.org/10.31713/m1028
12. Hong, S. J., Yang, H. J. (2019). A Study on the Impact Load Quantification of the Jaw Crusher. Journal of Drive and Control, 16 (2), 1–7. doi: https://doi.org/10.7839/KSFC.2019.16.2.001

13. Blokhin, V. S., Bolshakov, V. I., Malich, N. G. (2006). Osnovnye parametry tekhnologicheskikh mashin. Mashiny dlia dezintegratsii tverdykh materialov. Part. I. Dnepropetrovsk: IMA-press, 404.

14. Vaisberg, L. A., Zarogatskii, L. P., Turkin, V. Ia. (2004). Vibratsionnye drobilki. Osnovy rascheta, proektirovaniia i tekhnologicheskogo primeneniia. Saint Petersburg: Izd-vo VSEGEI, 306.

15. Nazarenko, I., Dedov, O., Bernyk, I., Rogovskii, I., Bondarenko, A., Zapryvoda, A. et. al. (2020). Determining the regions of stability in the motion regimes and parameters of vibratory machines for different technological purposes. Eastern-European Journal of Enterprise Technologies, 6 (7 (108)), 71–79. doi: http://doi.org/10.15587/1729-4061.2020.217747

16. Nesterenko, M., Nazarenko, I., Molchanov, P. (2018). Cassette Installation with Active Working Body in the Separating Partition. International Journal of Engineering & Technology, 7 (3.2), 265–268. doi: http://doi.org/10.14419/ijet.v7i3.2.14417

17. Bernyk, I., Luhovskyi, O., Nazarenko, I. (2018). Effect of rheological properties of materials on their treatment with ultrasonic cavitation. Materiali in Tehnologije, 52 (4), 465–468. doi: http://doi.org/10.17222/mit.2017.021

18. Nazarenko, I., Gavryukov, O., Klyon, A., Ruchynsky, N. (2018). Determination of the optimal parameters of a tubular belt conveyor depending on such an economical. Eastern-European Journal of Enterprise Technologies, 3 (1 (93)), 34–42. doi: http://doi.org/10.15587/1729-4061.2018.131552

3 RESEARCH OF TECHNICAL SYSTEMS OF MATERIALS SORTING PROCESSES

I. Nazarenko, A. Onyshchenko, S. Oryshchenko,
O. Fedorenko, S. Tsepelev, L. Titova

ABSTRACT

The studies carried out revealed the influence of the vibration frequency and the angle of inclination on the efficiency of sorting. It was found that with an increase in the vibration frequency and vibration amplitude of the box, the separation of the material and the sorting speed increase. The proposed model made it possible to determine the transport speed in the case when the sieve screen carries out a circulating movement, which is the application of two independent vibrations with different amplitudes and frequencies. The number of throws of the material to be sorted is influenced by the transport time of this material over the surface of the sieve and the amount of vibration excitation to this material. The dependence of the used power on the design and technological parameters of the vibration screen was revealed. An algorithm and method for calculating the main parameters of a vibration screen were developed.

KEYWORDS

Vibration screen, material, sorting, grain composition, physical, mathematical model, equation, resonance, parameters, experimental setup, sieve, particles, amplitude, vibration frequency, productivity.

3.1 SELECTION AND JUSTIFICATION OF PHYSICAL AND MATHEMATICAL MODELS OF TECHNICAL SYSTEMS FOR MATERIALS SORTING PROCESSES

As a technical system for the processes of sorting materials, let's take a vibration screen, which is widely used in industry [1–6]. Let's imagine the sorting process as some ordered process of movement of a large number of different parts in a layer on a sieve (**Fig. 3.1**). Each share with size d characterizes its size, which does not change during movement, and is a value that can have a discrete set of values: d_1, d_2,..., d_n. Since the number of particles in the layer is large, then d can be assigned arbitrary values in the interval of a given layer of fractions, and thus its value can be considered continuous.

H_{sup}, h_{sub} — the height of the superlattice and sublattice product; S — sieve area; Δl — sieve section; D, d — average diameter of superlattice and sublattice products; Δ — thickness of the sieve wires; V_{sup}, V_{sub} — volume of the superlattice and sublattice product.

Based on this assumption, the particle system can be replaced with a continuous model, and the productivity P will be determined by the formula:

$$P = V/t = bhv = bhl/t = sh/t, \tag{3.1}$$

where V – volume of the material layer on the sieve, m³; t – time of transporting the material over the sieve, s; b – sieve width, m; v – sieve length, m; S – sieve area, m²; h – average layer height on a sieve, m; v – transport speed, m/s.
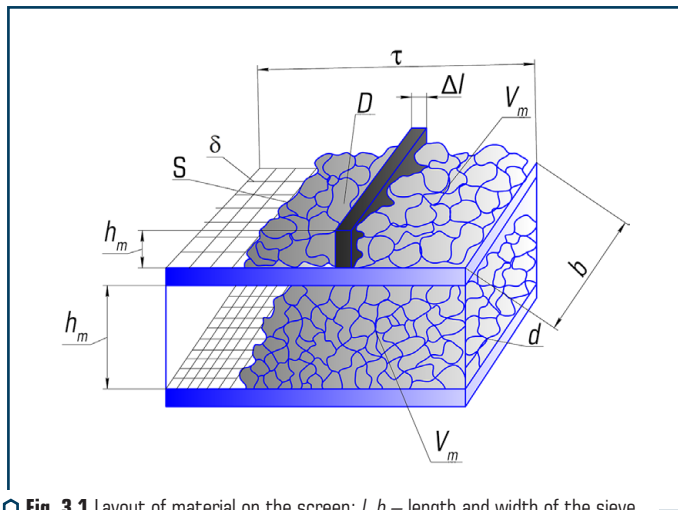
○ **Fig. 3.1** Layout of material on the screen: l, b – length and width of the sieve

The volume can be represented as the sum of the volumes of the superlattice and sublattice materials:

$$V = V_{sup} + V_{sub} = S_{sup}h_{sup} + S_{sub}h_{sub}. \tag{3.2}$$

If to divide the sieve along its length at the level of the section Δl (**Fig. 3.1**), then:

$$\Delta l = l/n = \text{const}, \tag{3.3}$$

where n – an arbitrary number. Then the volume V_p will be distributed in equal portions V_c by Δl:

$$V_c = \Delta l_c h_{sup} b_{sup} = \text{const}, \tag{3.4}$$

where c – the number of the segment Δl.

Using the main provisions of the theory of probability [3], the process of separation into fractions can be represented as the probability p of the passage of grains d through cells D:

$$p_i = (D - d_i)^2 / (D + \delta)^2, \tag{3.5}$$

where $i = 1,2,3...m$ – the serial number of the fraction, counted according to the characteristic of the size of the undersize product in the direction of growth d; d_i – the average grain size of the i-th fraction, corresponding to the characteristics of the size of half of its output; Δ – sieve wire thickness. The volume V_n distributed in this way along the length l forms a layer with the dimensions of a parallelepiped, averaging the inhomogeneity of its constituent grains. For a product with a volume of V_n, this means that all the sieve cells through which it is obtained, for the case of close alignment, a rectangle is formed, the area of which is S_n.

According to (3.4):

$$V_n = \Delta l \sum_{k=1}^{n} h_k b_k, \tag{3.6}$$

where h_k and b_k is the average value of the height and width of the layers V_k, depending on the probability p.

Consequently, the grain composition of each portion volume differs from the grain composition of similar portions of the undersize product and is a value:

$$V_k = \sum_{i=1}^{m} V_{i,k}, \tag{3.7}$$

where $V_{i,k}$ – part of the volume of the i-th fraction V_i sorted at the section Δl_k.

Under condition (3.4), the height of the i-th layer:

$$h_{i,k} = d_i p_{\min,k} / p_{bc}, \tag{3.8}$$

where $p_{\min,k}$ – probability of sieving the largest grains belonging to the composition V_c.

Considering that there is a probability that parts of the material do not pass the parts of the material $l_{i(sup)}$ ($l - l_i = l_{i(sup)}$) and condition that $1/p_{\min,k} = l_k / \Delta l$, it is possible to obtain an expression for the volume of material passage, which will be proportional to:

$$V_{i,k} = V_k \left(V_i - \sum_{i=1}^{k} V_{i,k-1} \right) \Big/ \left(\sum_{i=1}^{k} \left(V_i - V_{i,k-1} \right) \right). \tag{3.9}$$

Expression (3.9) is dependence for determining the rational load of the sieve during sorting based on a continuous model obtained on the probability of sorting grains.

For practical calculations, the considered model can be replaced by an adequate discrete model. For this purpose, let's express S_i, taking into account S_{sup}, through the area occupied by the fraction of grains, which are located near D in size. Let's call this fraction «heavy», that is, boundary in the general fractional composition. Then there are the following relations:

$$S_{sup} = S_2 \Delta h_{sup} \Delta C_{sup},$$
$$S_1 = S_2 \Delta h_1 \Delta C_1,$$
$$.........................,$$
$$S_{sub} = S_2 \Delta h_{sub} \Delta C_{sub},$$

(3.10)

where Δh – ratio of heights h_B/h_{sub}; ΔC – ratio of C_{sup}/C_h in percentage of the initial product (C_h is the yield of «heavy» grains).

From the relation (3.10) it is possible to determine the area of «heavy» grains:

$$S_2 = \left(S_{sup} + S_{sub}\right) \big/ \left(C_1 \Delta h_B + C_{sub} \Delta h_n + C_B\right).$$

(3.11)

Using the probability of passing (3.5) and assuming that with each throw V_t of the layer V_h onto the sieve, «heavy» grains are sown along its width $n = b_s/d_{bc}$ and along the length of the sieve $n = 1/d_{bc}$, let's obtain the volume of limiting grains sorted in one throw of the layer on the sieve:

$$V_h = \left(\pi d_{bc} b_h \cdot l\right) \big/ 6.$$

(3.12)

Then the capacity for sorting heavy grains will be:

$$P_h = V_h/T = 0.08 d_{bc} C_h l \omega.$$

(3.13)

Accordingly, the overall optimal power performance:

$$P = 100 P_h / C_h.$$

(3.14)

Taking into account (3.11), let's finally get the formula for determining the performance:

$$P = \left(S_o d \omega \left[1 - d/D\right]^2\right) \Big/ \left[\left(C_{min} \Delta h_{Tin} + C_{av} \Delta h_{av} + C_h\right) \cdot (1 - \lambda)\right],$$

(3.15)

where S_o – area of the open section of the sieve; λ – voidness of the material; $\Delta h_{Tin} = h_{heavy}/h_{min}$; $\Delta h_{av} = h_h/h_{av}$.

3.2 INVESTIGATION OF THE DYNAMICS OF THE RESONANT SCREEN, ANALYSIS AND ASSESSMENT OF ITS PARAMETERS

The proposed model [6] allows to indicate the speed of transport in the case when the sieve shaker carries out a circulating movement, which is the application of two independent vibrations with different amplitudes and frequencies. The design scheme for determining the rational

parameters of screens (**Fig. 3.2**) displays a single particle on the surface of the sieve, which vibrates according to the most general laws [7, 8].
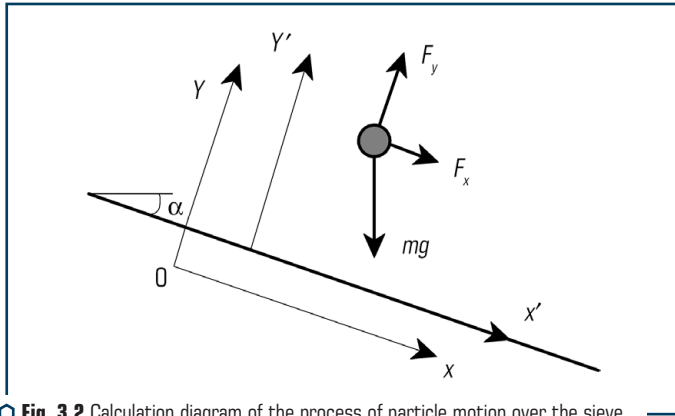
○ **Fig. 3.2** Calculation diagram of the process of particle motion over the sieve

Differential equations for the relative motion of a particle over the sieve surface in a movable coordinate system associated with it:

$$\dot{V}_{y'} = -g\cos\alpha + X_y\omega_y^2\sin(\omega_y t + \varphi_c), \tag{3.16}$$

$$\dot{y}' = V_{y'}, \tag{3.17}$$

$$\dot{V}_{x'} = g\sin\alpha + X_x\omega_x^2\cos(\omega_x t + \varphi_x), \tag{3.18}$$

$$\dot{x}' = V_{x'}, \tag{3.19}$$

where $V_{x'}$ and $V_{y'}$ – projections of the visualization speed of the relative motion of the particle, and the last terms in (3.16) and (3.17) correspond to the inertial force of the translational motion:

$$F_x = m\omega_x^2 X_x \sin(\omega_x t + \varphi_x), \tag{3.20}$$

$$F_y = m\omega_y^2 X_y \sin(\omega_y t + \varphi_y). \tag{3.21}$$

Equations (3.16) and (3.18) do not take into account the forces of air resistance to the motion of the particle. A particle lying on the sieve surface passes into the station field predetermined by the field (3.16)–(3.19), provided that:

$$X_y\omega_y^2\sin(\omega_y t + \varphi_y) > g\cos\alpha. \tag{3.22}$$

Upon reaching the surface of the sieve in free flight ($y' = 0$), the particle strikes the surface of the sieve. The change in speed from impact can be described by the ratios of inelastic impact.

$$V_{y'}^+ = -RV_{y'}^-,$$
(3.23)

$$V_{x'}^+ = v_{x'}^- - f(R+1)V_{y'}^-,$$
(3.24)

where R – coefficient of speed recovery from the impact, f – coefficient of friction of the particle with the sieve surface, the subscripts «–» and «+» correspond to the states immediately before and after the impact. On the one hand, there is a significant uncertainty in the experimental determination of these coefficients, and on the other hand, in real conditions the particle strikes not against the sieve surface, but against the layer of particles on it, after which its relative speed is practically zero. Therefore, with an accuracy acceptable for practical calculations, it can be considered $V_{y'}^+ = V_{x'}^+ = 0$ with each impact. The coefficient of friction f will be defined as the coefficient of internal friction or the angle of natural slope of the bulk material. After a particle hits the surface of a sieve with layers of particles on it, several options for its further behavior are possible:

– if $X_y \omega_y^2 \sin(\omega_y t + \varphi_y) > g\cos\alpha$, then the particle is detached from the surface and continues to move above the surface in accordance with equations (3.16)–(3.19);

– if at the moment of attachment of the particle to the surface and for some next period of time $X_y \omega_y^2 \sin(\omega_y t + \varphi_y) < g\cos\alpha$, then the particle remains on the surface until the sign of the roughness changes. Its movement along the surface of the sieve during this period of time is determined by the following conditions:

if

$$\left| \left(g\cos\alpha - X_y \omega_y^2 \sin(\omega_y t + \varphi_y) \right) \right| f > \left| g\sin\alpha + X_x \omega_x^2 \sin(\omega_x t + \varphi_x) \right|,$$
(3.25)

then

$$V_{x'} = 0,$$
(3.26)

and the particle is stationary on the surface of the sieve;

if

$$\left| \left(g\cos\alpha - X_y \omega_y^2 \sin(\omega_y t + \varphi_y) \right) \right| f < \left| g\sin\alpha + X_x \omega_x^2 \sin(\omega_x t + \varphi_x) \right|,$$
(3.27)

then

$$\dot{V}_{x'} = g\sin\alpha + X_x \omega_x^2 \sin(\omega_x t + \varphi_x) - f\left(g\cos\alpha - X_y \omega_y^2 \sin(\omega_y t + \varphi_y) \right),$$
(3.28)

$$\dot{x}' = V_{x'}.$$
(3.29)

Consequently, the particle moves along the surface under the action of the projection of the gravity force, the variable friction force due to the variable pressing of the particle to the surface, and the longitudinal exchange force of inertia of the translational motion. The system of equations (3.16)–(3.19) with nonlinear conditions (3.25)–(3.29) can be solved only by a numerous method.

With an independent disturbance of the vibrations of the sieve in the longitudinal and transverse directions, the movement of the particle above and along the surface is rather complicated. In some practically important cases, which are necessary for evaluating certain parameters of vibration sorting, the system of equations of motion can be significantly simplified. Experiments with the model described above allow one to determine the characteristics of the motion of a particle over a horizontal surface, performing vertical oscillations, necessary for considering periodic sorting. Of these characteristics, the vibration amplitude and frequency of contacts are important, the vibration amplitude determines the increase in the layer height due to the effect of its «swelling». The frequency of contact of particles with the surface determines the conditions for their passage through the openings of the sieve. Calculations show that, regardless of the initial phase, a steady cycle of a share is formed rather quickly. From this, the amplitude of the particle tosses over the surface and the period of contacts with it are determined.

Fig. 3.3 shows the effect of the angular frequency and the amplitude of surface vibrations on the amplitude of particle motion.
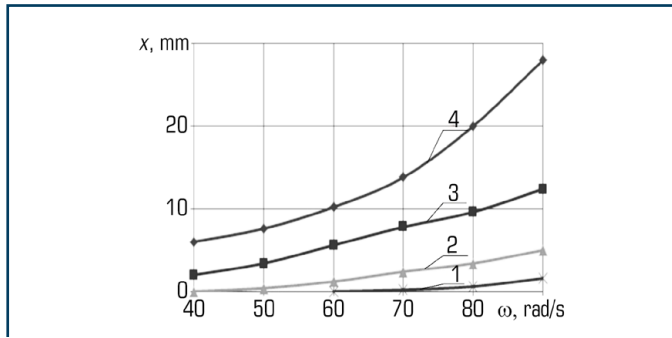
○ **Fig. 3.3** Changing the vibration amplitude of x material particles from frequency ω: $1 - x=4$ mm; $2 - x=6$ mm; $3 - x=8$ mm; $4 - x=10$ mm

With an amplitude of 5 mm, the separation of a particle from the surface of the sieve begins at a circular frequency of 45 rad/s, and for an amplitude of 2.5 mm – generally at a frequency of 63 rad/s. The effect of circular frequency and surface amplitude on the frequency of particle-surface contacts is shown in **Fig. 3.4**.

Each amplitude has its own rotation frequency corresponding to the maximum frequency of contacts, that is, the fastest passage of particles through the holes. At a frequency of 50 rad/s, the effect of the surface amplitude on the contact frequency is not significant.
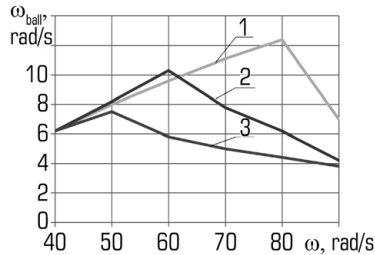
○ **Fig. 3.4** Influence of the vibration frequency of the screen on the frequency of contacts of particles with its surface at different amplitudes: 1 – 10 mm; 2 – 2–8 mm; 3 – 3–6 mm

The sorting process is influenced by the likelihood of the passage of the grains through the openings of the sieve. This probability depends on the size of the particles, the dynamic parameters of the vibrations of the screen, the design of the screen, and the shape of the holes in the screen. The average speed of passage of particles through the sieve is determined by the frequency of contacts of the particles with the surface and the ratio of the sizes of the particle and the hole. The frequency of particle-sieve contact is influenced by the amplitude and frequency of vibrations of the screen surface. An estimate of the probability of a particle passing through the sieve opening in one collision can be carried out on the basis of the design scheme shown in (**Fig. 3.5**).
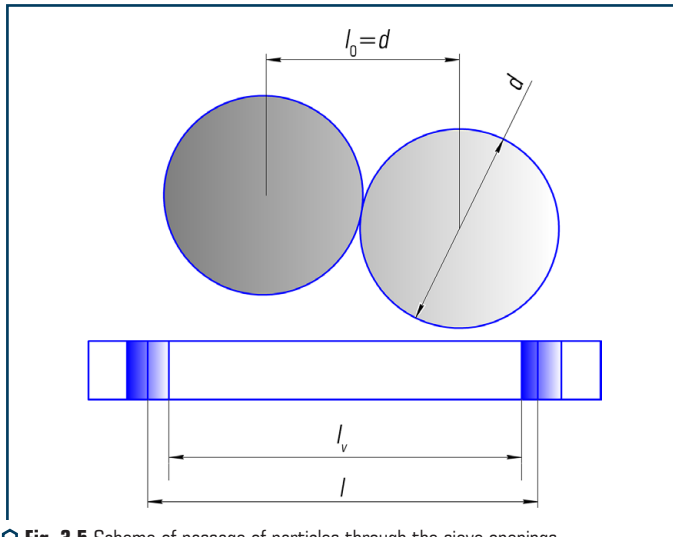
○ **Fig. 3.5** Scheme of passage of particles through the sieve openings

Taking into account the direction of impact of particles on the surface perpendicular to it, it can be assumed that only particles which centers are inside the square $(l_0 - d) \times (l_0 - d)$ will pass into the hole. In general, particles can reach the surface anywhere in the $l \times l$ square. The probability of particles passing through the holes is determined by the relationship:

$$p = n\Delta t K_g \left(1 - d/l_0\right)^2, \tag{3.30}$$

where $n = n(X_0, \omega)$ – the number of contacts of the particle with the sieve surface per time unit; φ – coefficient of the open section of the sieve; d – particle diameter; l_0 – hole size; Δt – time of one transition in the matrix of transition probabilities g of the cellular model of the periodic sieving process.

The angle of inclination of the sieving surface α determines the probability of particles penetrating through its holes p_f, which is determined by the angle at which the particles attack the sieve surface. This angle depends on the parameters of the vibrations of the sieve, the trajectory of the screening surface and the angle of its inclination to the horizon; it can vary within wide limits.

For experimental research, a model of a vibration screen has been developed and manufactured (**Fig. 3.6**) [9–12].
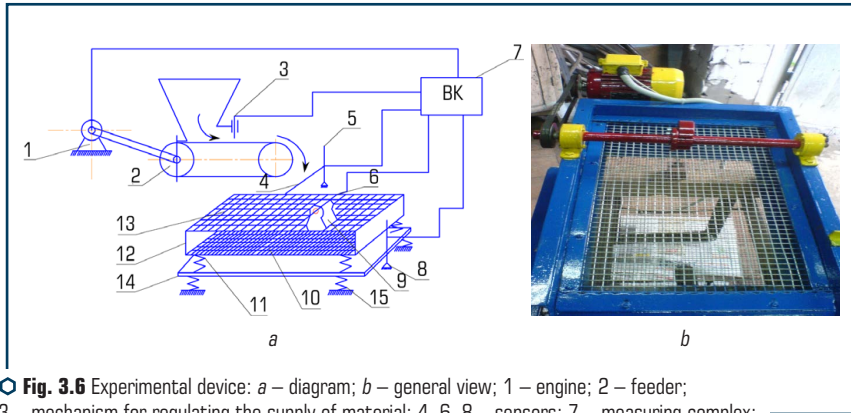
○ **Fig. 3.6** Experimental device: a – diagram; b – general view; 1 – engine; 2 – feeder; 3 – mechanism for regulating the supply of material; 4–6, 8 – sensors; 7 – measuring complex; 9 – oscillator; 10, 13 – sieves; 12 – box; 14 – reactive mass; 11, 15 – elastic elements

The model, in terms of its design and technological parameters, is analogous to a serial vibration screen, and the ratio of the length to width of the screen was taken according to the standard ratios of 2:1.

In the course of the experiments, the search for the most efficient sorting modes was carried out.

With a certain number of throws $n_{k\,max}$ and sizes of boundary grains, experimental 1 and calculated 2 graphs were built (**Fig. 3.7**).
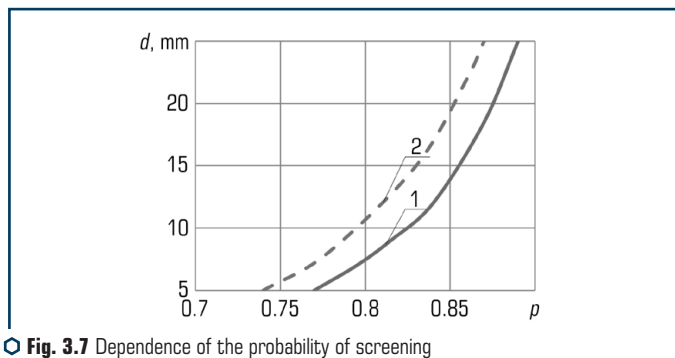
○ Fig. 3.7 Dependence of the probability of screening
grains (the number of throws) on their size: 1 — calculated; 2 — experimental

The position of curve 2 corresponds to the position of curve 1 in terms of the proportionality coefficient $K_p = 0.95$. The probability of sorting the boundary grains of the crushed mixture according to the formula (3.5) is determined by the ratio:

$$P_{sor} = \frac{(l - K_n d_{bc})^2 K_g}{(l + d)^2}. \tag{3.18}$$

In accordance with this correction, let's perform calculations of the optimal productivity and the corresponding screening efficiency for experimental screening units. At the same time, let's neglect a similar correction for light grains, taking into account the insignificant size dl.

Let's find the average value of the grain size composition of the material in each experiment and the empirical dispersion S^2 for each fraction. As an estimate of variances, let's take the weighted average number of individual empirical variances.

Let's compare the obtained permissible measurement accuracy, having previously determined the nature of the variance discrepancies by the ratio.

The critical value of these ratios for the degrees of freedom $K_1 = 49$ and $K_2 = 13$, $F \approx 2.3$. This confirms the random nature of the variance discrepancies and the absence of a significant difference in the measurement accuracy in individual experiments. Hence, with a reliability $P = 0.95$ and an accuracy S' for the actual grain size composition of the material, one can take the average, compiled according to the data of all experiments. As the result shows, the initial characteristic of the size of the material practically did not change during the experiments. Using the experimental and calculated points, let's build the graphs of the dependence (**Fig. 3.8**).

Analysis of experimental data on the number of throws $n_{k\,max}$ revealed the following. The value $n_{k\,max}$ is influenced by two main parameters: the time of transporting the material over the sieve t and the frequency of forced vibrations of the vibrator. The time of transporting the material t increases the screening efficiency E even in the case when the limiting grain size d_{bc} is

large, i.e. $d_{bc}/D > 0.9$. On the other hand, an increase in the parameter t reduces its vibration transport speed v, which reduces the total amount of material passing through the screen per unit time. For example, at $t=5$ s, $P=26...43$ kg/min; for $t=6$ s, $P=21...38$ kg/min; for $t=7$ s, $P=16...24$ kg/min; for $t=12$ s, $P=9...21$ kg/min; for $t=16$ s, $P=3...14$ kg/min; for $t=26$ s, $P=4...9$ kg/min. The graphical meaning is shown in **Fig. 3.9**.
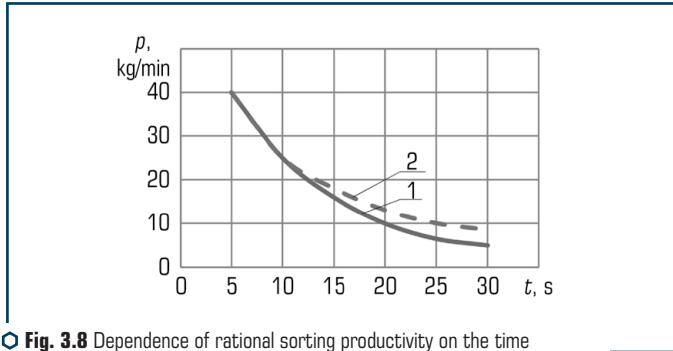
Fig. 3.8 Dependence of rational sorting productivity on the time of material transportation over the sieve: 1 – calculated; 2 – experimental
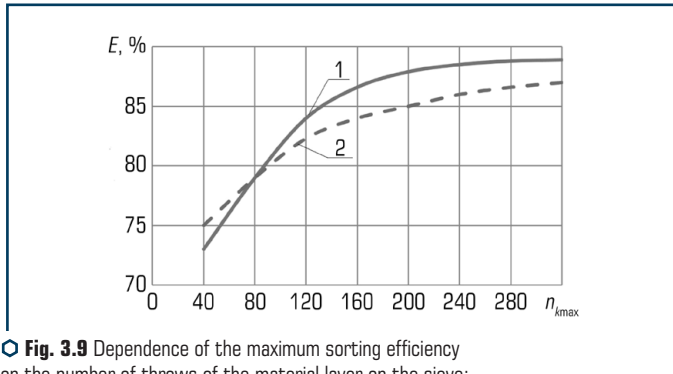
Fig. 3.9 Dependence of the maximum sorting efficiency on the number of throws of the material layer on the sieve: 1 – calculated curve; 2 – experimental curve

As can be seen from the above examples, with an increase in the residence time of the material on the sieve t_m, an inversely proportional decrease in the productivity of the vibration screen is observed. The size of the sorted material has a significant effect on the value of productivity. In this case, the productivity P can vary up to 42 %. For example, in the case of transportation during the time of material $t=12$ s at $d_{bc}=8.4$ mm, at $d_{bc}/D = 0.907$ and $S_h=9.64$ %, the productivity of the screen $P=10.2$ kg/min, and at $d_b=8.32$ at $d_{bc}/D = 0.924$ and $S_h=10.8$ % screening capacity is 12 kg/min.

Analysis of the experimental data (**Fig. 3.9**) on the number of material throws $n_{k\,max}$ over the sorted material and their influence on the main technological parameters showed that the discrepancy is 5.3–8.1 %.

3.3 DISCUSSION OF RESEARCH RESULTS

The studies carried out revealed the influence of the vibration frequency and the angle of inclination on the efficiency of sorting. So, with an increase in the frequency of vibration and the amplitude of vibration of the box, the separation of the material and the speed of sorting increase. The particle speed is of greater importance at the frequency of the box vibrations, $\omega = 45...85$ rad/s. When changing the angle of inclination from $\alpha = 2°...204°$ it was obtained that with an increase in the angle of inclination of the sieve from $14°$ to $20°$, the concentration, speed and power are more stable. The dependence of the used power on the design and technological parameters of the vibration screen is revealed. The number of throws to be sorted is influenced by the transport time t of this material over the surface of the sieve and the amount of vibration excitation to this material. These parameters are due to the magnitude of the forced vibrations of the vibration system, with an increase in both of these parameters [13–16].

An increase in the number of throws of material $n_{k\,max}$ increases the residence time of the material on the surface of the sieve, reduces the speed of passage of the material and, in general, reduces the productivity of the screen. For example, for $n_{k\,max} = 49$, $P = 26...43$ kg/min with an increase $n_{k\,max}$ to 67, the productivity of the screen P decreases to 16...24 kg/min, for $n_{k\,max} = 211$ it decreases to 3...14 kg/min, and with a value of $n_{k\,max} = 367$, the productivity of the screen is only about 8.1 kg/min.

The efficiency of the sorting process E is also affected by $n_{k\,max}$ as follows: with the number of throws $n_{k\,max}$ indicated in the previous paragraph, the efficiency of screening E is respectively: 87.9 %, 89 %, 91.5 %, 94.7 % (**Fig. 3.9**, curve 2). The increase in the efficiency of screening E in accordance with the increase $n_{k\,max}$ is explained by the increase in the time of vibration exposure to the medium being separated. This is confirmed by the close placement of curves 1 and 2 (**Fig. 3.9**).

CONCLUSIONS TO SECTION 3

1. The physical and mathematical model of the screen has been substantiated, on the basis of which the equations of material movement over the sieve are compiled.

2. Distribution of the vibration amplitude of the material particles from the vibration frequency of the sieve has been determined.

3. An experimental model of a vibration screen has been developed and experimental studies of its operation have been carried out.

4. Dependence of the used power on the design and technological parameters of the vibration screen has been revealed.

5. The influence of the vibration frequency and the angle of inclination on the sorting efficiency has been determined. So, with an increase in the frequency of vibrations and the amplitude of vibrations of the box, the separation of the material increases and the particle speed is of greater importance at a frequency of vibrations of the box of 45…85 rad/s.

REFERENCES

1. Blekhman, I. I., Dzhanelidze, G. Iu. (1964). Vibratsionnoe peremeschenie. Moscow: Nauka, 412.
2. Vaisberg, L. A. (1986). Proektirovanie i raschety vibratsionnykh grokhotov. Moscow: Nedra, 144.
3. Venttsel, E. S., Ovcharov, L. A. (2000). Teoriia veroiatnosti i ee inzhenernye prilozheniia. Moscow: Vysshaia shkola, 480.
4. Nadutyi, V. P., Kalinichenko, V. V. (2004). Vibratsionnoe grokhochenie gornoi masy povyshenoi vlazhnosti. Dnepropetrovsk: NGU Ukrainy, 135.
5. Nazarenko, I. I. (1999). Mashyny dlia vyrobnytstva budivelnykh materialiv. Kyiv: KNUBA, 488.
6. Nazarenko, I. I., Oryshchenko, S. V. (2009). Modeliuvannia protsesu rukhu materialu po hrokhotu. Tekhnika budivnytstva. Naukovo-tekhnichnyi zhurnal, 22, 81–84.
7. Nazarenko, I. I. (2010). Prykladni zadachi teorii vibratsiinykh system. Kyiv: Vydavnychyi dim «Slovo», 440.
8. Oryshchenko, S. V. (2010). Teoretychni doslidzhennia ta vyznachennia osnovnykh etapiv rukhu vibratsiinoho hrokhota. Tekhnika budivnytstva, 24, 44–47.
9. Oryshchenko, S. V. (2009). Eksperymentalni doslidzhennia robochykh parametriv vibratsiinoho hrokhota. Tekhnika budivnytstva, 23, 88–91.
10. Nazarenko, I., Dedov, O., Bernyk, I., Rogovskii, I., Bondarenko, A., Zapryvoda, A. et. al. (2020). Determining the regions of stability in the motion regimes and parameters of vibratory machines for different technological purposes. Eastern-European Journal of Enterprise Technologies, 6 (7 (108)), 71–79. doi: http://doi.org/10.15587/1729-4061.2020.217747
11. Nazarenko, I., Svidersky, A., Kostenyuk, A., Dedov, O., Kyzminec, N., Slipetskyi, V. (2020). Determination of the workflow of energy-saving vibration unit with polyphase spectrum of vibrations. Eastern-European Journal of Enterprise Technologies, 1 (7 (103)), 43–49. doi: http://doi.org/10.15587/1729-4061.0.184632
12. Nazarenko, I. I., Ruchynskyi, M. M., Sviderskyi, A. T., Kobylanska, I. M., Harasim, D., Kalizhanova, A., Kozbakova, A. (2019). Development of energy-efficient vibration machines for the buiding-and-contruction industry. Przeglad Elektrotechniczny, 95 (4), 53–59. doi: http://doi.org/10.15199/48.2019.04.10

13. Nesterenko, M., Nazarenko, I., Molchanov, P. (2018). Cassette Installation with Active Working Body in the Separating Partition. International Journal of Engineering & Technology, 7 (3.2), 265–268. doi: http://doi.org/10.14419/ijet.v7i3.2.14417

14. Nazarenko, I., Gaidaichuk, V., Dedov, O., Diachenko, O. (2018). Determination of stresses and strains in the shaping structure under spatial load. Eastern-European Journal of Enterprise Technologies, 6 (7 (96)), 13–18. doi: http://doi.org/10.15587/1729-4061.2018.147195

15. Bernyk, I., Luhovskyi, O., Nazarenko, I. (2018). Effect of rheological properties of materials on their treatment with ultrasonic cavitation. Materiali in Tehnologije, 52 (4), 465–468. doi: http://doi.org/10.17222/mit.2017.021

16. Nazarenko, I., Gavryukov, O., Klyon, A., Ruchynsky, N. (2018). Determination of the optimal parameters of a tubular belt conveyor depending on such an economical. Eastern-European Journal of Enterprise Technologies, 3 (1 (93)), 34–42. doi: http://doi.org/10.15587/1729-4061.2018.131552

4 RESEARCH OF TECHNICAL SYSTEMS OF PROCESSES OF MIXING MATERIALS

I. Nazarenko, I. Bernyk, O. Dedov,
I. Rogovskii, M. Ruchynskyi, I. Pereginets, L. Titova

ABSTRACT

The process of a vibration concrete mixer has been investigated. Well-coordinated equations of motion of the system «mixer – concrete mixture» and their solutions have established the regularities of changing the parameters of the mixer at different angles of inclination. An experimental design of vibration-gravitational mixing has been developed and manufactured, and studies of the working process of mixing efficiency have been carried out on it. Research carried out at three warehouses of concrete mixtures confirmed the assumptions accepted in the work, the assumption and the selected physical and mathematical model of the «Mixer – concrete mixture» system. The use of a vibration concrete mixer made it possible to reduce the duration of mixing by 2.5–3 times in comparison with conventional free mixing concrete mixers. Provides the preparation of hard concrete mixtures and improving the quality of concrete mixtures due to the destruction of defective aggregates and a more uniform distribution of the binder throughout the volume of the mixed mixture.

An algorithm and method for calculating the main parameters of a vibration concrete mixer have been developed.

KEYWORDS

Vibration mixer, material, physical, mathematical model, equation, resonance, parameters, experimental setup, vibration frequency, productivity.

4.1 JUSTIFICATION OF THE CONSTRUCTIVE DIAGRAM OF THE TECHNICAL SYSTEM FOR THE PROCESSES OF MIXING MATERIALS

The technical systems for the processes of mixing materials include mixers, which are classified according to the characteristics: the principle of mixing, the nature of work, the method of installation [1, 2]. According to the principle of mixing the components, concrete mixers are divided into two classes: with free mixing of materials (gravitational) and with forced [3]. It is most expedient to use gravity mixers to prepare more plastic mixtures with lower resistivity when mixing them [4]. For the preparation of hard concrete mixes, mixers with forced mixing of materials are most effective. At the same time, modern requirements for the quality of concrete mixtures require the use of more efficient mixing equipment. Such equipment includes mixers using vibration effect [5]. In such a mixer, up to five component movements take place, and mixing is carried out simultaneously

by translational and rotational movements of the components of the mixture. A free-mixing vibration concrete mixer (**Fig. 4.1**) includes a cone-cylindrical mixing drum 1, which is mounted on a base plate 3 with the help of elastic shock absorbers 2.
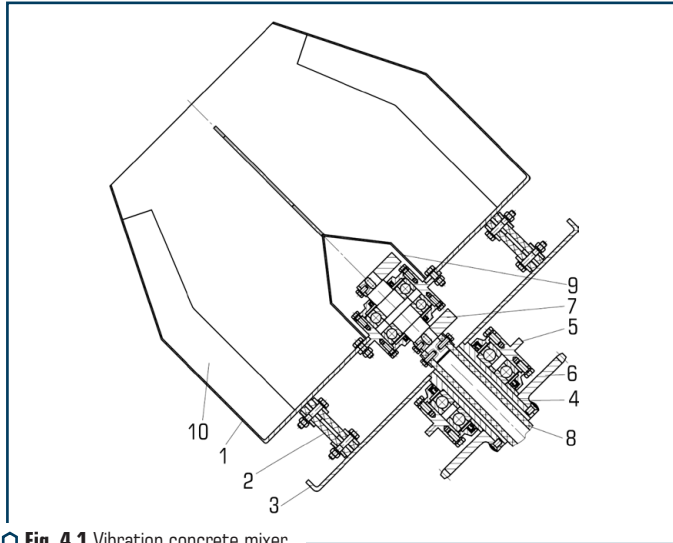
○ **Fig. 4.1** Vibration concrete mixer

This base plate 3 is rigidly connected in its central part to a hollow drive shaft 4, mounted in a bearing support 5. At the end of the drive shaft 4, a sprocket 6 is mounted, connected to an electromechanical drive (not shown). On the bottom of the mixing drum 1, a circular vibration exciter 7 is mounted, which is half mounted in the inner cavity of the mixing drum. In this case, the vibration exciter of circular vibrations 7 is connected to the drive motor (not shown in the **Fig. 4.1**) using a flexible shaft 8 passing inside the hollow drive shaft 4. Inside the mixing drum, the vibration exciter of circular vibrations 7 is closed with a cone-cylinder protective cap. drum. Blades 10 are located inside the mixing drum 1. The bearing support 5 is mounted on the traverse of the fixing and tipping mechanism.

Free mixing vibration concrete mixer works as follows.

Mixing drum 1 is installed at an angle of 40–45 degrees to the horizon and is loaded with a portioned amount of sand, crushed stone and cement. Pour in the required amount of water. The mixer drum drive is included. In this case, the rotating mixing drum using the blades 10 provides mechanical mixing of the mixture. This preliminary mixing of the components of the mixture continues for 15–20 s.

Then, with the help of the fixing and tipping mechanism, the mixing drum is set in a vertical position and the vibration exciter of circular vibrations 7. Under the influence of vibration,

the mixing drum performs complex vibration movements that cause variable amplitude-frequency deformations in the concrete mixture. The vibration action of the applied simultaneous torsional and circular vibrations ensures efficient mixing of the concrete mixture. The duration of vibromechanical mixing, vibration treatment and vibration activation is 15–25 s, depending on the concrete mix. After the end of vibromechanical mixing, the vibration exciter of vibrations is turned off and, using the fixing and overturning mechanism, the mixing drum is transferred to its original position. The drum is installed at an angle of 40–45 degrees to the horizon and the process of mixing the mixture continues for 10–12 seconds until a homogeneous state is obtained. Then the concrete mixture is discharged from the mixing drum.

4.2 DETERMINATION OF THE PARAMETERS OF THE MATHEMATICAL MODEL OF THE VIBRATION MIXER

The main parameters influencing the choice of the mathematical model of the vibration mixer are the nature of the mixing drum vibrations, the coordinates of the center of gravity of the mixing drum, the physical and mechanical characteristics of the mixture, the geometric dimensions of the mixing drum and the volume of filling it with the concrete mixture.

When vibration in the vertical direction on the bottom of the mixing drum from the side of the processed concrete mixture, support forces will act, which can be represented in the form of inertial forces F_{in1} and dissipative forces F_{ds1}, i.e. forces of inelastic resistance F_{ds1}. These forces can be described by the following dependencies:

$$F_{in1} = m_{pr1} \frac{d^2z}{dt^2};$$
(4.1)

$$F_{ds1} = b_{pr1} \frac{dz}{dt},$$
(4.2)

where m_{pr1} – reduced mass of the concrete mixture interacting with the bottom of the mixing drum during vertically directed vibrations; b_{pr1} – reduced coefficient of inelastic resistance of the concrete mixture.

In this case, the value of the reduced mass of the concrete mixture can be determined from the dependence, modified as a result of the refinement, given in [6]:

$$m_{pr1} = \frac{\rho F_1}{k_1} tg k_1 H_r,$$
(4.3)

where ρ – dynamic density of the concrete mixture; F_1 – the area of the bottom of the mixing drum in contact with the concrete mixture; k_1 – the wavenumber;

$$k_1 = \frac{\omega}{a_1}; \tag{4.4}$$

a_1 – phase speed of propagation of the disturbance in the treated layer:

$$a_1 = \sqrt{\frac{E}{\rho}}; \tag{4.5}$$

E – dynamic modulus of elastic deformation of the processed concrete mixture; H_r – estimated thickness of the processed layer, selected from the condition:

$$\text{at } h \le \frac{\pi}{4\omega}\sqrt{\frac{E}{\rho}}, \ H_r = h; \tag{4.6}$$

$$\text{at } h > \frac{\pi}{4\omega}\sqrt{\frac{E}{\rho}}, \ H_r = \frac{\pi}{4\omega}\sqrt{\frac{E}{\rho}}, \tag{4.7}$$

where h – thickness of the processed layer.

The coefficient of inelastic resistance of the concrete mixture is determined from the following relationship:

$$b_{pr1} = \eta_1 k_1 F_1 \text{tg} k_1 H_r, \tag{4.8}$$

where η_1 – coefficient of dynamic viscosity of the concrete mixture;

$$\eta_1 = f_{v1} H_r \sqrt{E\rho}, \tag{4.9}$$

where f_{v1} – coefficient of internal friction of the concrete mixture.

From the given dependences (4.2) and (4.8), let's find the specific values of the reduced mass and the coefficient of inelastic resistance:

$$m_{ypr1} = \frac{\rho}{k_1} \text{tg} k_1 m H_r, \tag{4.10}$$

$$b_{ypr1} = \eta_1 k_1 \text{tg} k_1 H_r. \tag{4.11}$$

The specific values of the reduced mass and the coefficient of inelastic resistance of the concrete mixture interacting with the cylindrical walls of the mixing drum during horizontal vibrations are determined from the following dependencies:

$$m_{ypr2} = \frac{m_{ypr1}}{2(1+\mu)} = \frac{\rho}{2k_1(1+\mu)} \text{tg} k_1 L_r; \tag{4.12}$$

$$b_{ypr2} = \frac{b_{ypr1}}{2(1+\mu)} = \frac{\eta_1 k_1}{2(1+\mu)} tg k_1 L_r, \tag{4.13}$$

where μ – Poisson's ratio; L_r – length of the processed layer in the horizontal direction.

To determine the nature of the motion of the mixing drum in the vibration operating mode, let's consider the design diagram of the dynamic system «mixing drum – processed medium» (**Fig. 4.2**).
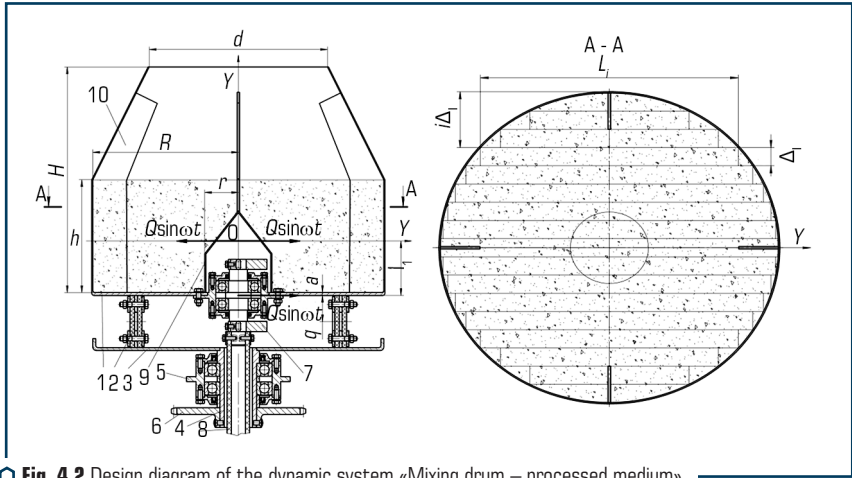
○ **Fig. 4.2** Design diagram of the dynamic system «Mixing drum – processed medium»

To determine the value of the reduced mass and the coefficient of inelastic resistance of the concrete mixture interacting with the cylindrical walls of the mixing drum during horizontal vibrations in the direction of the coordinate, let's conventionally divide the entire mixed concrete mixture located in the cylindrical part of the mixing drum into a number of elementary vertical volumes. the same width (**Fig. 4.2**). From **Fig. 4.2**:

$$\Delta_l = \frac{2R}{n}. \tag{4.14}$$

The length of each i-th volume with the width Δ_l located at a distance $i\Delta_l$ from the drum shell is determined from the following relationship:

$$L_i = \sqrt{R^2 + (R - i\Delta_l)^2}. \tag{4.15}$$

Based on the obtained expressions (4.12), (4.13) and (4.15), let's determine the values of the reduced mass and the coefficient of inelastic resistance of the concrete mixture for each elementary volume interacting with the cylindrical walls of the mixing drum during horizontally directed vibrations:

$$m_{ipr2} = \frac{h\Delta_i\rho}{2k_1(1+\mu)}\,\mathrm{tg}k_1L_i; \tag{4.16}$$

$$b_{ipr2} = \frac{h\Delta_i\eta_1k_1}{2(1+\mu)}\,\mathrm{tg}k_1L_i. \tag{4.17}$$

4.3 EQUATION OF MOTION AND ANALYTICAL DESCRIPTION OF VIBRATION MIXER MOTION

Based on the obtained expressions (4.10), (4.11), (4.18) and (4.19) of the calculation scheme shown in **Fig. 4.2** and the method described above, vibrations of a mixing drum loaded with concrete can be represented in the form of the following system of differential equations:
– vibrations in the horizontal direction along the coordinate axis:

$$(m + m_{pr2})\frac{d^2y_{1r}}{dt^2} + (b_2 + b_{pr2})\frac{dy_{1r}}{dt} + c_2y_{1r} = Q\sin\omega t; \tag{4.18}$$

– angular (torsional) vibrations about the X coordinate axis:

$$(m + m_{pr2})\frac{d^2x_{1r}}{dt^2} + (b_3 + b_{pr2})\frac{dx_{1r}}{dt} + c_3x_{1r} = Q\cos\omega t; \tag{4.19}$$

– angular (torsional) vibrations about the X coordinate axis:

$$(J_x + J_{b1})\frac{d^2\psi_{xr}}{dt^2} + (n_2 + n_{b2})\frac{d\psi_{xr}}{dt} + k_2\psi_{xr} = Ql_1\sin\omega t; \tag{4.20}$$

– angular (torsional) vibrations about the Y coordinate axis:

$$(J_y + J_{b1})\frac{d^2\psi_{yr}}{dt^2} + (n_3 + n_{b2})\frac{d\psi_{yr}}{dt} + k_3\psi_{yr} = Ql_1\cos\omega t; \tag{4.21}$$

– vertical vibrations in the direction of the Z coordinate axis along the X axis:

$$z_{xr} = x\psi_{yr}; \tag{4.22}$$

– vertical vibrations in the direction of the Z coordinate axis along the Y axis:

$$z_{yr} = y\psi_{xr}, \tag{4.23}$$

where x_{1r}, y_{1r}, y_{1r}, z_{yr} – linear displacements of the mixing drum in the direction of the coordinate axes X, Y and Z under the action of harmonic exciting forces $Q\cos\omega t$ and $Q\sin\omega t$ in the operating mode; ψ_{xr}, ψ_{yr} – angular displacements of the mixing drum relative to the coordinate

axes X, Y, respectively, under the action of the moments of exciting forces $Q \sin \omega t$ and $Q \cos \omega t$ in the operating mode; l_1 – distance from the center of application of the exciting force of the vibration exciter of vibrations to the center of gravity of the vibration dynamic system in the operating mode in the direction of the coordinate Z_1,

$$l_1 = \frac{ml + m_{pr1}(0.5h + a)}{m + m_{pr1}};$$
(4.29)

J_{b1} – moment of inertia of the concrete mixture relative to the horizontal axis of gravity passing through the center of weight:

$$J_{b1} = \frac{1}{2}m_{pr2}R^2 + \frac{1}{12}m_{pr2}h^2 + m_{pr2}(0.5h + a - l_1)^2;$$
(4.30)

– coefficient of inelastic resistance of the concrete mixture at angular displacements of the oscillating system relative to the horizontal axis;

$$n_{b2} = 0.5hb_{pr2}.$$
(4.31)

The solution to the system of differential equations (4.18)–(4.21) for stationary oscillations describing the steady motion of a vertically installed mixing drum in operating mode is presented in the following form:

$$y_{1r}(t) = A_{1r} \sin(\omega t - \varphi_{1r});$$
(4.32)

$$x_{1r}(t) = A_{2r} \cos(\omega t + \varphi_{2r});$$
(4.33)

$$\psi_{xr}(t) = \Psi_{1r} \sin(\omega t - \xi_{1r});$$
(4.34)

$$\psi_{yr}(t) = \Psi_{2r} \cos(\omega t + \xi_{2r}),$$
(4.35)

where A_{1r} – amplitude of harmonic oscillations of the oscillating center of gravity of the system in the direction of the coordinate Y in the operating mode; A_{2r} – amplitude of harmonic oscillations of the center of gravity of the oscillating system in the direction of the coordinate X in the operating mode; Ψ_{1r} – amplitude of angular (torsional) harmonic vibrations of the mixing drum relative to the axis X passing through the center of gravity of the oscillating system in the operating mode; Ψ_{2r} – amplitude of angular (torsional) harmonic vibrations of the mixing drum relative to the axis Y passing through the center of gravity of the oscillating system in the operating mode; φ_{1r}, φ_{2r} – phase shift angle between the amplitudes of the exciting forces and the amplitudes of the forced vibrations; ξ_{1r}, ξ_{2r} – phase shift angle between the amplitudes of the moments of the exciting forces and the amplitudes of the angular forced vibrations;

$$A_{1r} = \frac{Q}{\sqrt{[c_2 - (m + m_{pr2})]^2 + (b_2 + b_{pr2})^2 \omega^2}}; \qquad (4.36)$$

$$A_{2r} = \frac{Q}{\sqrt{[c_3 - (m + m_{pr2})]^2 + (b_2 + b_{pr2})^2 \omega^2}}; \qquad (4.37)$$

$$\Psi_{1r} = \frac{Ql_1}{\sqrt{[k_2 - (J_x + J_{b1})]^2 + (n_2 + b_{b2})^2 \omega^2}}; \qquad (4.38)$$

$$\Psi_{2r} = \frac{Ql_1}{\sqrt{[k_3 - (J_x + J_{b1})]^2 + (n_3 + b_{b2})^2 \omega^2}}; \qquad (4.39)$$

$$\varphi_{1r} = \operatorname{arctg} \frac{(b_2 + b_{pr2})\omega}{c_2 - (m + m_{pr2})}; \qquad (4.40)$$

$$\varphi_{2r} = \operatorname{arctg} \frac{(b_3 + b_{pr2})\omega}{c_3 - (m + m_{pr2})}; \qquad (4.41)$$

$$\xi_{1r} = \operatorname{arctg} \frac{(n_2 + b_{b2})\omega}{k_2 - (J_x + J_{b1})}; \qquad (4.42)$$

$$\xi_{2r} = \operatorname{arctg} \frac{(n_3 + b_{b2})\omega}{k_3 - (J_x + J_{b1})}. \qquad (4.43)$$

Using the obtained solutions (4.32)–(4.43) of the system of equations (4.18)–(4.28) of the considered dynamic system, let's successively determine the laws of motion of the bottom and walls of the mixing drum, as well as the protective cap, affecting the processed concrete mixture both in vertical and horizontal directions, and causing normal and tangential stresses in the processed medium, significantly affecting the destruction of internal bonds in the concrete mixture and, accordingly, the efficiency of vibration processing and mixing of the prepared concrete mixture.

The law of motion of the bottom of the mixing drum interacting with the processed concrete mixture horizontally in the direction of the coordinate can be described by the following equation:

$$X_{dr}(t) = x_{1r}(t) + (l - a)\psi_{yr}(t) = A_{2r} \cos(\omega t + \varphi_{2r}) + \Psi_{2r}(l - a)\cos(\omega t + \xi_{2r}), \qquad (4.44)$$

where $X_{dr}(t)$ – horizontal displacement of the mixing drum bottom in the direction of the coordinate X, which causes contacting stresses in the concrete medium.

After transformations of expression (4.44), let's obtain a dependence convenient for analysis and computer simulation:

$$X_{dr}(t) = A_{2d} \cos(\omega t + \theta_2), \qquad (4.45)$$

where A_{2d} – amplitude of harmonic vibrations of the bottom of the mixing drum in the direction of the coordinate axis,

$$A_{2d} = \sqrt{A_{2r}^2 + [\Psi_{2r}(l-a)]^2 + 2A_{2r}\Psi_{2r}(l-a)]\cos(\varphi_{2r} - \xi_{2r})};$$ (4.46)

θ_2 – angle of phase displacement between the amplitude of the exciting force and the amplitude of the forced vibrations of the bottom of the mixing drum in the direction of the coordinate axis X,

$$\theta_1 = \text{arctg}\frac{A_{2r}\sin\varphi_{2r} + \Psi_{2r}(l-a)\sin\xi_{2r}}{A_{2r}\cos\varphi_{2r} + \Psi_{2r}(l-a)\cos\xi_{2r}}.$$ (4.47)

The law of motion of the bottom of the mixing drum interacting with the processed concrete mixture horizontally in the direction of the coordinate can be described by the following equation:

$$Y_{dr}(t) = y_{1r}(t) + (l-a)\psi_{xr}(t) = A_{1r}\sin(\omega t - \varphi_{1r}) + \Psi_{1r}(l-a)\sin(\omega t - \xi_{1r}),$$ (4.48)

where $Y_{dr}(t)$ – horizontal displacement of the mixing drum bottom in the direction of the coordinate Y, which also causes contacting stresses in the concrete medium.

Transforming expression (4.48), let's obtain a dependence convenient for analysis and computer simulation:

$$Y_{dr}(t) = A_{1d}\sin(\omega t - \theta_1),$$ (4.49)

where A_{1d} – amplitude of harmonic vibrations of the bottom of the mixing drum in the direction of the coordinate axis Y,

$$A_{1d} = \sqrt{A_{1r}^2 + [\Psi_{1r}(l-a)]^2 + 2A_{1r}\Psi_{1r}(l-a)]\cos(\varphi_{1r} - \xi_{1r})};$$ (4.50)

θ_1 – angle of phase displacement between the amplitude of the exciting force and the amplitude of the forced vibrations of the bottom of the mixing drum in the direction of the coordinate axis X,

$$\theta_1 = \text{arctg}\frac{A_{1r}\sin\varphi_{1r} + \psi_{1r}(\ell-a)\sin\xi_{1r}}{A_{1r}\cos\varphi_{1r} + \psi_{1r}(\ell-a)\cos\xi_{1r}}.$$ (4.51)

The law of motion of the bottom of the mixing drum interacting with the processed concrete mixture in the vertical direction along the coordinate Y can be described by the following equation:

$$Z_{dr}(y,t) = y\psi_{xr}(t) = \Psi_{1r}y\sin(\omega t - \xi_{1r}) \text{ at } -R \le y \le -r, r \le y \le R.$$ (4.52)

The law of motion of the bottom of the mixing drum interacting with the processed concrete mixture in the vertical direction along the coordinate X can be described by the following equation:

$$Z_{dr}(x,t) = x\psi_{yr}(t) = x\psi_{2r}\cos(\omega t + \xi_{2r}) \text{ at } -R \leq x \leq -r, r \leq x \leq R. \tag{4.53}$$

Here $Z_{dr}(y,t)$ and $Z_{dr}(x,t)$ — displacement of the bottom of the mixing drum in the vertical direction along the coordinates X and Y, causing normal stresses in the concrete medium.

The law of motion of the mixing drum shell interacting with the processed concrete mixture horizontally in the coordinate X direction can be described by the following equation:

$$X_{obr}(z,t) = x_{1r}(t) + z\psi_{yr}(t) =$$
$$= A_{2r}\cos(\omega t + \varphi_{2r}) + \Psi_{2r}z\cos(\omega t + \xi_{2r}) \text{ at } -(l-a) \leq z \leq (H-l+a), \tag{4.54}$$

where $X_{obr}(z,t)$ — movement of the shell of the mixing drum in the horizontal direction along the coordinate X, which causes normal stresses in the medium being processed.

After transformations of expression (4.54), let's obtain a dependence convenient for analysis and computer simulation:

$$X_{obr}(z,t) = A_{3ob}(z)\cos[\omega t + \theta_3(z)], \tag{4.55}$$

where A_{3ob} — variable amplitude of harmonic vibrations of the mixing drum shell in the direction of the coordinate axis,

$$A_{3ob} = \sqrt{A_{2r}^2 + (\psi_{2r}z)^2 + 2A_{2r}\psi_{2r}z\cos(\varphi_{2r} - \xi_{2r})}; \tag{4.56}$$

$\theta_3(z)$ — variable phase angle between the amplitude of the exciting force and the amplitude of forced vibrations of the shell of the mixing drum in the direction of the coordinate axis:

$$\theta_3(z) = \text{arctg}\frac{A_{2r}\sin\varphi_{2r} + \Psi_{2r}z\sin\xi_{2r}}{A_{2r}\cos\varphi_{2r} + \Psi_{2r}z\cos\xi_{2r}}. \tag{4.57}$$

The law of motion of the mixing drum shell interacting with the processed concrete mixture horizontally in the coordinate direction can be described by the following equation:

$$Y_{obr}(z,t) = y_{1r}(t) + z\psi_{xr}(t) =$$
$$= A_{1r}\sin(\omega t - \varphi_{1r}) + \Psi_{1r}z\sin(\omega t - \xi_{1r}) \text{ at } -(l-a) \leq z \leq (H-l+a), \tag{4.58}$$

where $Y_{obr}(z,t)$ — movement of the shell of the mixing drum in the horizontal direction along the coordinate, causing normal stresses in the medium being processed.

Transforming expression (4.58), let's obtain a dependence convenient for analysis and computer simulation:

$$Y_{obr}(z,t) = A_{4ob}(z)\sin[\omega t - \theta_4(z)], \tag{4.59}$$

where A_{4ob} — variable amplitude of harmonic vibrations of the mixing drum shell in the direction of the coordinate axis Y,

$$A_{4ob} = \sqrt{A_{1r}^2 + (\Psi_{1r}z)^2 + 2A_{1r}\Psi_{1r}z\cos(\varphi_{1r} - \xi_{1r})}; \tag{4.60}$$

$\theta_3(z)$ — variable phase angle between the amplitude of the exciting force and the amplitude of forced vibrations of the shell of the mixing drum in the direction of the coordinate axis Y,

$$\theta_4(z) = \text{arctg}\frac{A_{1r}\sin\varphi_{1r} + \Psi_{1r}z\sin\xi_{1r}}{A_{1r}\cos\varphi_{1r} + \Psi_{1r}z\cos\xi_{1r}}. \tag{4.61}$$

The law of motion of the shell of the mixing drum interacting with the processed concrete mixture in the vertical direction along the coordinates Y and X can be described by the following equations:
— for the cylindrical part:

$$Z_{obyr}(t) = R\psi_{xr}(t) = \Psi_{1r}R\sin(\omega t - \xi_{1r}); \tag{4.62}$$

$$Z_{obxr}(t) = R\psi_{yr}(t) = \Psi_{2r}R\cos(\omega t + \xi_{2r}); \tag{4.63}$$

— for the tapered part:

$$Z_{obxr}(y,t) = R\psi_{xr}(t) =$$
$$= \Psi_{1r}\left[R - \frac{y - (h - \ell - a)}{\text{tg}\beta}\right]\sin(\omega t + \xi_{1r}) \text{ at } (h - \ell + a) \leq y \leq (H - \ell + a); \tag{4.64}$$

$$Z_{obxr}(x,t) = R\psi_{yr}(t) =$$
$$= \Psi_2\left[R - \frac{y - (h - l + a)}{\text{tg}\beta}\right]\cos(\omega t + \xi_{2r}) \text{ at } (h - l + a) \leq y \leq (H - l + a), \tag{4.65}$$

where $Z_{obyr}(t)$ and $Z_{obxr}(t)$ — displacement of the cylindrical part of the mixing drum in the vertical direction along the coordinates Y and X, causing tangential stresses in the concrete medium; $Z_{oby}(y,t)$ and $Z_{obx}(x,t)$ — displacement of the tapered part of the mixing drum in the vertical direction along the coordinates Y and X.

4.4 DETERMINATION OF THE MAIN PARAMETERS OF THE WORKING PROCESS OF AN OPERATION OF CONCRETE MIXER

Based on the obtained theoretical dependencies (4.1)–(4.65), describing the vibrations of the vibration drum in the operating mode, a program was created in the TurboPascal system designed to simulate the laws of motion of the mixing drum under the action of disturbing forces generated by the displaced vibration exciter of circular vibrations.

Fig. 4.3–4.6 show the theoretical values of the vibration amplitudes of the surfaces of a vibration drum in contact with a concrete mixture of different consistency in the horizontal plane and in the vertical direction. Used cement-concrete mixtures with a cone subsidence $OK=3.5–4$ cm and a stiffness of 30 s, 60 s and 90 s.

The data of the vibration amplitudes of the bottom of the mixing drum (**Fig. 4.3, a**) and the shell of the mixer drum (**Fig. 4.3, b**) with horizontal (1) and vertical (2) movements in the operating mode are given. The calculations were performed for the preparation of a concrete mixture with a cone subsidence $OK=3.5–4$ cm.
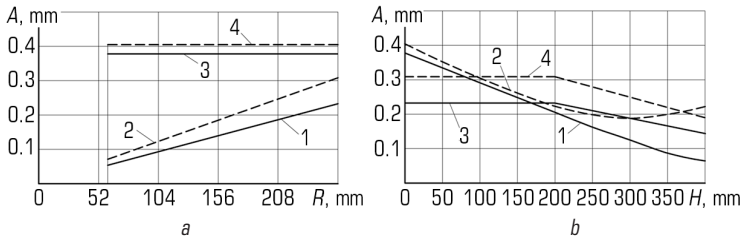
Fig. 4.3 Amplitudes of vibrations of the surfaces of the mixing drum (mixture with cone subsidence $OK=3.5–4$ cm)
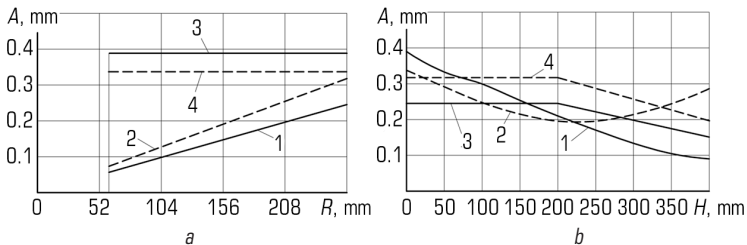
Fig. 4.4 Amplitudes of vibrations of the surfaces of the mixing drum (mixture with a hardness of 30 s)
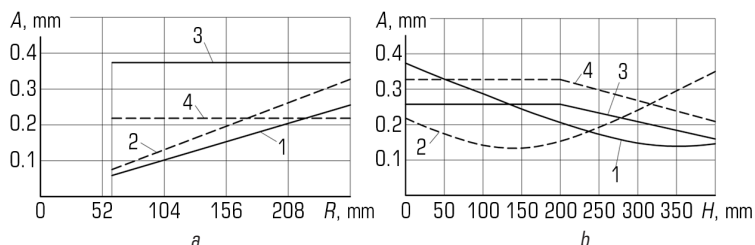
Fig. 4.5 Amplitudes of vibrations of the surfaces of the mixing drum (mixture with a hardness of 60 s)
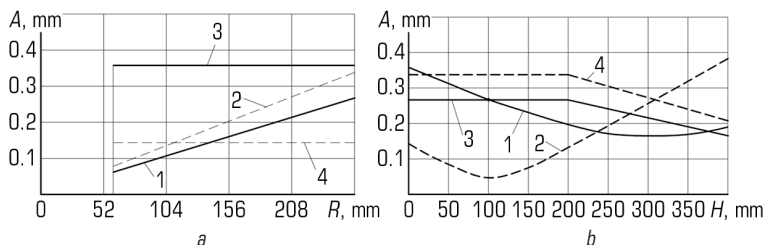
Fig. 4.6 Amplitudes of vibrations of the surfaces of the mixing drum (mixture with a hardness of 90 s)

When preparing hard concrete mixes, the distribution of amplitudes is somewhat different from mobile mixes. Yes, in **Fig. 4.5, 4.6** show the results of calculations for mixtures with stiffness of 60 s and 90 s for the bottom of the mixer drum (*a*) with horizontal (1) and vertical (2) and the shell of the mixer drum (*b*) with horizontal (1) and vertical (2) movements.

The data presented show that during the preparation process concrete mixtures are subjected to vibration action with sufficiently high amplitudes in the horizontal plane and in the vertical direction at a frequency of angular vibrations of 292 rad/s, sufficient for effective mixing and vibration activation of the concrete mixture.

Thus, the obtained expressions (4.1)–(4.65) make it possible to establish the law of motion of all surfaces of the inner surface of the mixer interacting with the processed cement-concrete mixture during its preparation, to determine the main parameters of the proposed vibration device depending on the physical and mechanical characteristics of the processed mixture, to justify rational modes. actions on the concrete mix during its vibration processing and preparation.

For experimental research, a vibration mixer was developed and manufactured (**Fig. 4.7**).
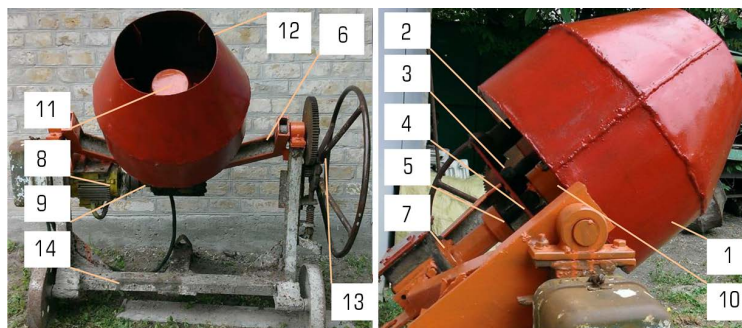
○ **Fig. 4.7** Design of the experimental device

It is a cone-cylindrical mixing drum 1, which is mounted on a base plate 3 with the help of elastic shock absorbers 2. This base plate 3 is rigidly connected in its central part to a drive shaft 4 installed in a bearing support 5. A worm is built into the cross-beam 6 a gearbox 7 connected to an electric motor 8 through a clutch 9. On the bottom of the mixing drum 1, a circular vibration exciter 10 is mounted, which is half mounted in the inner cavity of the mixing drum. Inside the mixing drum, the circular vibration exciter 10 is closed with a conical protective cap 11, which is hermetically attached to the bottom of the drum. Inside the mixing drum 1 there are blades 12. The traverse 6 and the locking and tipping mechanism 13 are mounted on the frame 14.

The process of testing the operation of the mixer with the necessary instruments for measuring parameters was carried out in accordance with the requirements of the interstate standard (GOST 16349-85).

– error of power measuring instruments – no more than 2.5 %;

– rotational speed of the mixing bodies was checked under load;

– weight of the mixer was determined by weighing on a balance;

– total time of one mixing cycle was determined by a stopwatch and was counted from the beginning of loading the mixture to the end of unloading the mixed mixture;

– composition, grade of the concrete mixture was determined at the test site;

– during the tests, three batches of mixtures of the same composition were prepared. The amount of the mixture was sufficient for testing. A total of three mixtures were used.

All indicators provided by the interstate standard, including vibration parameters (amplitude and frequency of oscillations), were recorded through the appropriate equipment on the computer display (**Fig. 4.8**).

On the foundation on the side of the vibration mixer (**Fig. 4.8**) there is a fixed stand of the tripod, in which the sensor is fixed on a special clamp. The other end of the sensor is attached to the bottom of the mixing drum through a special bracket. The length of the sensor base and

its thickness are selected from the condition that the natural oscillation frequency of the sensor ω_{0d} exceeds the value of the oscillation frequency by 8...10 times.

As a result of the experiments, the value of the vibration amplitude is recorded on the computer screen in the form of vibrograms. Based on the results of the analysis and processing of vibration records, both the mutual influence of the working body and the medium and the determination of optimal modes are established. The analysis of the records was carried out in two stages: preliminary analysis of the oscillogram; complete control processing.

By processing a series of typical vibrograms according to the above method, the numerical values of the vibration amplitudes of the bottom of the mixing drum and shell were obtained for mixtures with different cone draft and different stiffness. Based on the results of data processing, graphs were constructed with the repetition of each experiment in three dimensions. **Fig. 4.9** shows graphs comparing the theoretical and experimental values of the amplitude of oscillations of horizontal and vertical oscillations of the bottom and shell, depending on the radius, measured from the axis of rotation of the drum to the shell of the drum.

○ **Fig. 4.8** Measurement scheme: X_H – horizontal movements of the mixing drum; X_V – vertical movements of the mixing drum

○ **Fig. 4.9** Comparison of theoretical and experimental values of the amplitude:
a – horizontal vibrations of the bottom and shell, depending on the radius;
b – vertical vibrations of the bottom and shell for the mixture $G=30$ s
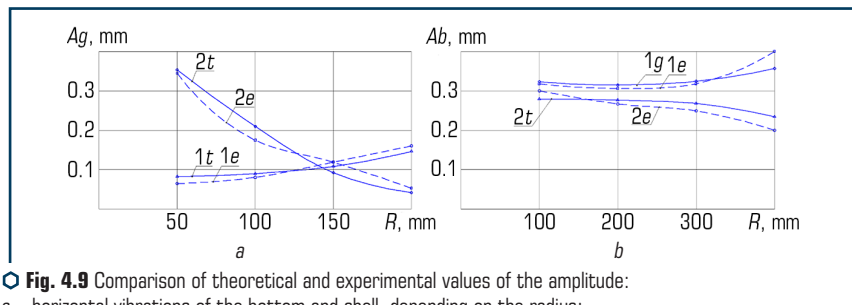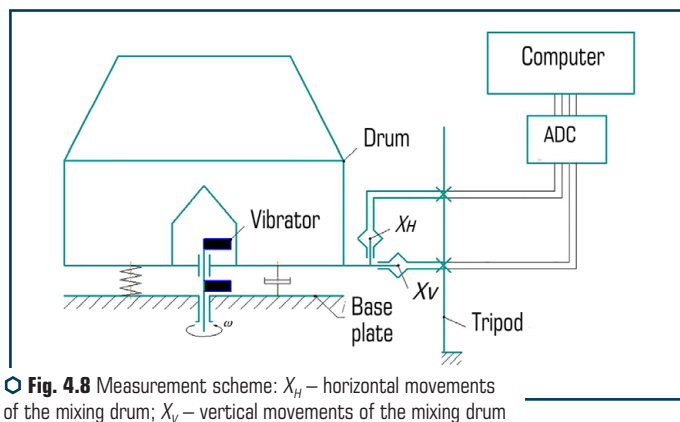
An assessment of the performed studies has established that the discrepancy between the theoretical and experimental numerical values in the vibration amplitudes is 11–15 %.

4.5 METHODOLOGY AND ALGORITHM FOR CALCULATING THE MAIN PARAMETERS OF A VIBRATION CONCRETE MIXER

The initial parameters are the amplitude, the vibration frequency, set depending on the composition of the mixture. An important indicator of the vibration process is the selected type and direction of vibrations and the nature of vibrations. If, according to the condition of the problem, the values of the amplitudes and frequencies of oscillations are absent, then their values can be determined based on the fact that the dominant parameter is acceleration. Then such properties as amplitude, speed, frequency, acceleration must be considered together.

For harmonic oscillations with frequency, the oscillation amplitude is optimal [7]:

$$X_{OPT} = \frac{(4-6)g}{\omega^2},$$ (4.66)

where g — acceleration due to gravity ($g = 9.8$ m/s). For the frequency $\omega = 3.14\ \text{s}^{-1}$, the optimal vibration amplitude is determined by the lower and upper acceleration, i.e. $X_{OPT} = 0.4 - 0.6$ mm.

The second parameter is the drive power of the concrete mixer, which is spent on vibrations of the mixture P_v and friction in the bearings of the vibration exciter P_{FR}.

The vibration power is calculated according to the maximum value that the existing driving force can develop with an increase in the dissipative resistance of the system.

Power per vibration, W, is determined by the dependence [7]:

$$\max P_{av} = \frac{1}{4}F_0 x_c' \, \omega,$$ (4.67)

where F_0 — driving force necessary to maintain a given amplitude is calculated taking into account the effect of the concrete mixture on the working body of the machine; x_c' — amplitude of displacements of the working body, taking into account only the reactive forces of the system:

$$x_c' = \frac{m_0 r_0}{m_c a + m}, \quad m_c = \frac{\rho F}{k}\text{tg}kH,$$ (4.68)

where ω — frequency of forced vibrations.

Friction force power in vibration exciter bearings, W,

$$P_{FR} = F_0 \mu \frac{d_j}{2}\omega,$$ (4.69)

where $\mu = 0.005...0.008$ — coefficient of friction in the bearings; d_j — diameter of the bearing journal.

Motor power for vibration exciter, kW:

$$P_M = \frac{\max P_{AV} + P_{FR}}{1000\eta},$$ (4.70)

where μ – transmission efficiency.

The main parameters of the gravitational action, as components of the general process of mixing the concrete mixture, is the drum rotation frequency, which is determined by the dependence:

$$\omega = \sqrt{2g/D}.$$ (4.71)

The algorithm for calculating the main parameters and characteristics of a vibration mixer based on gravitational and vibration components is shown in **Fig. 4.10**.
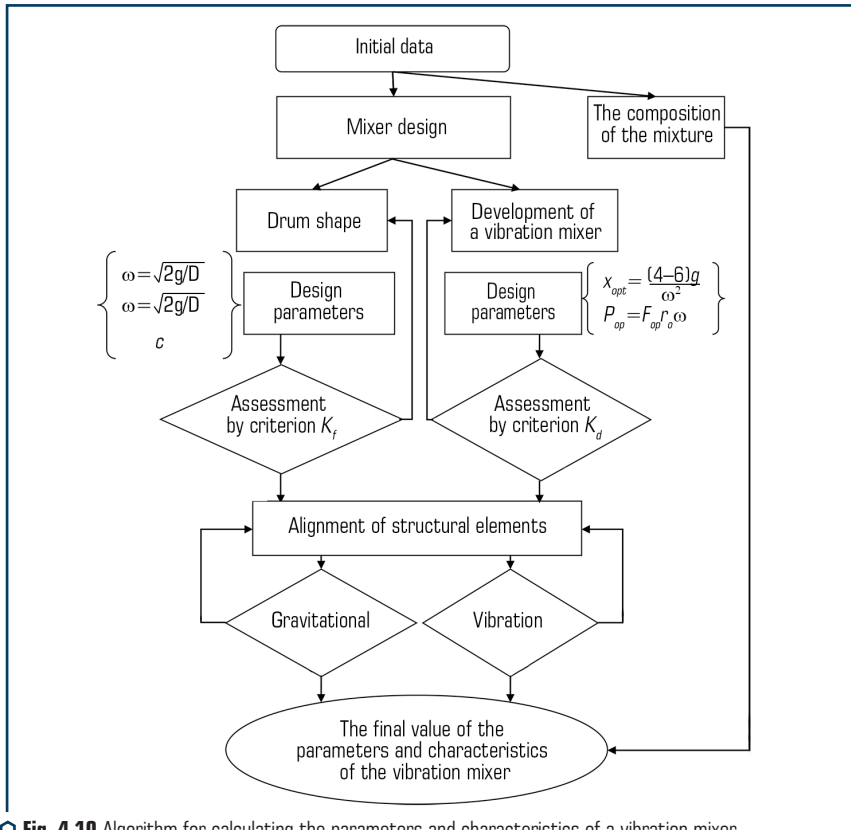
○ **Fig. 4.10** Algorithm for calculating the parameters and characteristics of a vibration mixer

4.6 DISCUSSION OF RESEARCH RESULTS

The analysis of the obtained expressions (4.32)–(4.65) shows that the mixing drum in the process of operation makes complex spatial vibrations, designed to provide an effective vibration action on the mixed concrete mixture. Moreover, each point located on the inner surface of the mixing drum has its own law of motion. As a result, the mixed concrete mixture will experience an alternating amplitude-frequency action, which causes multidirectional normal and tangential stresses in the mixture, which ensures the ultimate destruction of internal bonds and greater mobility in it, which contributes to an increase in mass transfer and effective mixing [8–13].

The use of a vibration concrete mixer makes it possible to reduce the mixing time by 2.5–3 times in comparison with conventional free mixing concrete mixers. Provides the preparation of hard concrete mixes and improving the quality of concrete mixes due to the destruction of defective aggregates and a more uniform distribution of the binder throughout the volume of the mixed mix. An experimental design of vibration-gravitational mixing has been developed and manufactured, and studies of the working process of mixing efficiency have been carried out on it. Research carried out at three warehouses of concrete mixtures confirmed the assumptions accepted in the work, the assumption and the selected physical and mathematical model of the «Mixer – concrete mixture» system. It was found that the use of vibration and gravitational action makes it possible to reduce the mixing time from 90 to 60 s. The strength of control concrete cubes is 17–18 % higher than in a gravity mixer. The discrepancy between the theoretical and experimental numerical values for the vibration amplitudes is 11–15 %. The proposed design and the studies carried out on it have confirmed the effectiveness of the vibration mixing method. As a result of the studies performed, it was found that the nature of the vibration of the mixing drum is close to harmonious [14]. The amplitude of vertical oscillations of the bottom varies in the range of 0.3–0.4 mm at a distance $R=208$–220 mm from the drum bottom. At a distance of $R=120$ mm, the vibration amplitude slightly decreased and its average value is 0.2 mm. Horizontal displacements of the drum bottom have huge vibration amplitudes – 0.02 mm. When loading with a concrete mixture, the amplitudes of vibrations at the same radius have significantly decreased, and their average value fluctuates between 0.2–0.25 mm and 0.14–0.16 mm.

CONCLUSIONS TO SECTION 4

1. Well-coordinated equations of motion of the system «mixer – concrete mixture» and their solutions established the regularities of changing the parameters of the mixer at different angles of inclination.

2. The distribution of the amplitudes of vibrations of the working body of the vibration solvent has been obtained, depending on the distance of application of the energy source.

3. An experimental design of vibration-gravitational mixing has been developed and manufactured, and studies of the working process of mixing efficiency have been carried out on it.

4. It has been determined that the use of a vibration concrete mixer makes it possible to reduce the duration of mixing by 2.5–3 times in comparison with conventional free mixing concrete mixers. Provides the preparation of hard concrete mixes and improving the quality of concrete mixes due to the destruction of defective aggregates and a more uniform distribution of the binder throughout the volume of the mixed mix.

5. The results of experimental studies are presented and a comparative analysis based on theoretical data has been carried out.

It has been found that the use of vibration and gravitational action can reduce the mixing time from 90 to 60 s. The strength of control concrete cubes is 17–18 % higher than in a gravity mixer.

6. An algorithm and method for calculating the main parameters of a vibration concrete mixer have been developed.

REFERENCES

1. Nazarenko, I. I. (1999). Mashyny dlia vyrobnytstva budivelnykh materialiv. Kyiv: KNUBA, 488.

2. Nazarenko, I. I., Tumanska, O. V. (2004). Mashyny i ustatkuvannia pidpryiemstv budivelnykh materialiv. Konstruktsii ta osnovy ekspluatatsii. Kyiv: Vyshcha shkola, 590.

3. Emelianova, I. A., Dobrokhodova, O. V., Anischenko, A. I. (2010). Sovremennye stroitelnye smesi i oborudovanie dlia ikh prigotovleniia. Kharkiv: Timchenko, 146.

4. Bogomolov, A. A. (2010). Teoreticheskie i tekhnicheskie osnovy sovershenstvovaniia smesitelnykh mashin dlia prigotovleniia stroitelnykh smesei. Belgorod: Iz-vo BGTU, 151.

5. Ruchynskyi, M. M., Svyrydiuk, D. Ya. (2013). Doslidzhennia kolyvan vibratsiinoho betonozmishuvacha z urakhuvanniam vplyvu peremishchuvanoho materialu. Tekhnika budivnytstva. Naukovo-tekhnichnyi zhurnal, 31, 35–42.

6. Maslov, A. G., Ponomar, V. M. (1985). Vibratsionnye mashiny i protsessy v dorozhnom stroitelstve. Kyiv: Budivelnik, 128.

7. Nazarenko, I. I. (2007). Vibratsiini mashyny i protsesy budivelnoi industrii. Kyiv: KNUBA, 230.

8. Bernyk, I., Luhovskyi, O., Nazarenko, I. (2018). Effect of rheological properties of materials on their treatment with ultrasonic cavitation. Materiali in Tehnologije, 52 (4), 465–468. doi: http://doi.org/10.17222/mit.2017.021

9. Nazarenko, I. I., Ruchynskyi, M. M., Sviderskyi, A. T., Kobylanska, I. M., Harasim, D., Kalizhanova, A., Kozbakova, A. (2019). Development of energy-efficient vibration machines for the buiding-and-contruction industry. Przeglad Elektrotechniczny, 95 (4), 53–59. doi: http://doi.org/10.15199/48.2019.04.10

10. Nazarenko, I., Dedov, O., Bernyk, I., Rogovskii, I., Bondarenko, A., Zapryvoda, A. et. al. (2020). Determining the regions of stability in the motion regimes and parameters of vibratory machines for different technological purposes. Eastern-European Journal of Enterprise Technologies, 6 (7 (108)), 71–79. doi: http://doi.org/10.15587/1729-4061.2020.217747

11. Nesterenko, M., Nazarenko, I., Molchanov, P. (2018). Cassette Installation with Active Working Body in the Separating Partition. International Journal of Engineering & Technology, 7 (3.2), 265–268. doi: http://doi.org/10.14419/ijet.v7i3.2.14417
12. Nazarenko, I., Gaidaichuk, V., Dedov, O., Diachenko, O. (2018). Determination of stresses and strains in the shaping structure under spatial load. Eastern-European Journal of Enterprise Technologies, 6 (7 (96)), 13–18. doi: http://doi.org/10.15587/1729-4061.2018.147195
13. Nazarenko, I., Svidersky, A., Kostenyuk, A., Dedov, O., Kyzminec, N., Slipetskyi, V. (2020). Determination of the workflow of energy-saving vibration unit with polyphase spectrum of vibrations. Eastern-European Journal of Enterprise Technologies, 1 (7 (103)), 43–49. doi: http://doi.org/10.15587/1729-4061.0.184632
14. Nazarenko, I., Gavryukov, O., Klyon, A., Ruchynsky, N. (2018). Determination of the optimal parameters of a tubular belt conveyor depending on such an economical. Eastern-European Journal of Enterprise Technologies, 3 (1 (93)), 34–42. doi: http://doi.org/10.15587/1729-4061.2018.131552

5 STUDY OF TECHNICAL SYSTEMS OF MATERIALS COMPACTION PROCESS

I. Nazarenko, O. Dedov, A. Bondarenko, A. Zapryvoda,
M. Kyzminec, M. Nazarenko, M. Ruchynskyi, A. Svidersky, V. Slipetskyi

ABSTRACT

The working process of concrete mixture compaction is investigated. The model of the processing medium is determined, which is characterized by three stages. At the first stage of compaction it is a free-flowing medium, at the second and third stages of compaction it is an elastic-viscoplastic medium. This result lies in the definition of the physical and mathematical model, the equations of motion. The vibration system «machine-medium» at any moment of movement consists of two components – one is capable of accumulating energy that passes from one form to another (reactance), and the second is energy dissipation (active resistance). The influence of active and reactive forces on the general movement of the system under study has been investigated and determined. By solving the equations, analytical dependencies were obtained, which established the laws of motion of the «Vibration machine – sealing medium» system. Practical implementation for technical systems for the formation of concrete products and soil compaction processes under the main pipeline has been carried out. An algorithm and method for calculating the main parameters of vibration systems for compaction of working media have been developed.

KEYWORDS

Vibration system, medium, compaction process, concrete mix, soil, physical, mathematical model, reactance, active resistance, equation, analytical dependences, parameters, experimental units, amplitude, vibration frequency.

5.1 DETERMINATION OF PHYSICAL MODELS OF THE PROCESS OF VIBRATION COMPACTION OF MATERIALS

The vibration effect on the concrete mix is of great practical importance and forms the basis of all modern technology for compaction of consistencies [1–3]. The essence of the vibration action lies in the fact that during vibrations, the concrete mixture acquires the properties of fluidity due to the violation of bonds between the particles. The compaction process is characterized by the following movement of concrete mixture particles: individual, general (general) vibration of concrete mixture particles as a continuous system. The uniform movement of particles from one equilibrium position to another occurs predominantly in the surface layer.

Based on a general view of the compaction process, it can be noted that the concrete mix at different stages obeys different laws. At first, it can be represented as a free-flowing medium, where the vibration movement of its particles occurs, that is, the forces of dry friction mainly affect. With subsequent compaction, the mixture becomes more mobile and behaves like an elastic viscoplastic body. Along with the properties of a viscous liquid, the mixture is clearly elastic. Thus, the physical model of the mixture should take into account three stages of the compaction process (**Fig. 5.1**).
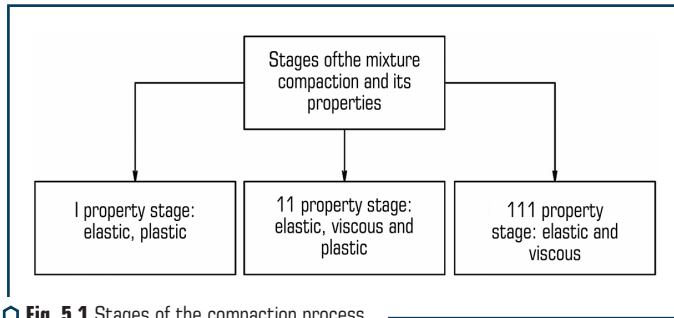
○ **Fig. 5.1** Stages of the compaction process

The elastic properties according to Hooke's law (**Table 5.1**) are presented in the form of a linear (linear model) or nonlinear (nonlinear model) layer of a concrete mixture.
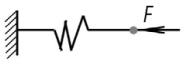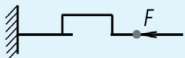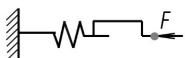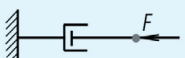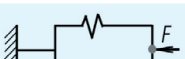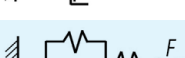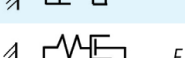
Viscous properties according to Newton's law (**Table 5.1**) are modeled by a damper consisting of a piston moving in a cylinder with a liquid. Other connections of elements with each other are possible, which is due to the need to take into account certain properties and composition of the components of a real mixture. The equations describing the propagation of a wave process in a mixture can be represented as follows:

$$\frac{\partial^2 u}{\partial t^2} = c^2 \frac{\partial^2 u}{\partial z^2}; \ \frac{\partial^2 u}{\partial t^2} = c^2 \frac{\partial^2 u}{\partial z^2} + \frac{\eta}{\rho} \frac{\partial^3 u}{\partial z^2 \partial t}; \ \frac{\partial^2 u}{\partial t^2} = c^2 (1 + i\gamma) \frac{\partial^2 u}{\partial z^2}. \tag{5.1}$$

The first equation (5.1) describes the displacement of the layer of the mixture $u(z, t)$ as an elastic body with density at a speed c. The second equation (5.1) describes the motion of the mixture as an elastic-viscous body with density with a frequency-dependent dissipation of energy taken into account in the equation by the coefficient η. The third equation (5.1) describes the motion of the mixture as an elastic – viscous body with density ρ with a frequency-independent dissipation of energy taken into account in the equation by the coefficient γ. At different stages of the concrete compaction process (**Fig. 5.1**), all equations (5.1) can be applied. The first equation (5.1) is not applicable in the case of a possible resonance, since the absence of a dissipative component in the resonance zone gives a solution for the amplitude of oscillations $A \to \infty$. Therefore, the second and third equations (5.1) are left to choose from. At the present stage of development of vibration

technology for compaction of building mixtures, the third equation (5.1) is more applied due to the fact that for a specific vibration frequency, the stress state is determined by the vibration amplitude. Therefore, in further analytical studies, the third equation (5.1) is used.

● **Table 5.1** The main types of physical models

Model properties	Physical model		Model name
	scheme	Mathematical notation	
Elastic		$\sigma = \varepsilon E;\ \tau = xG$	Hooke
Plastic		$\tau = \tau_{pl}$	Saint-Venant
Elastic-plastic		$\tau = \tau_{pl};\ \tau = xG$	Prandtl
Viscous		$\tau = \eta \dfrac{dV}{dz}$	Newton
Elastoviscous with stress relaxation		$\tau = \eta \dfrac{dV}{dz};\ \tau = xG$	Maxwell
Elastoviscous with delayed deformations		$\tau = xG + \eta \dfrac{dV}{dz}$	Voigt
Elastoviscous with creep phenomenon		$\tau = xG;\ \tau = x_1 G_1 + \eta \dfrac{dV}{dz}$	Kelvin
Elasto-visco-plastic		$\tau = xG;\ \tau = x_1 G_1 + \tau_{pl}$	Bingham
Elasto-visco-plastic with relaxation		$\tau = xG;\ \tau = x_1 G_1 + \tau_{pl};\ \tau = \tau_{pl} + \eta \dfrac{dV}{dz}$	Shvedov
Elasto-visco-plastic in the process of shear deformation		$\tau = xG;\ \tau = x_1 G_1 + \eta \dfrac{dV}{dz};\ \tau = \tau_{pl} + \eta_1 \dfrac{dV}{dz}$	Generalized Kelvin and Shvedov

When vibrations are transmitted from the working body to the mixture (**Fig. 5.2**), elastic waves propagate in the latter, which carry the energy that goes to the compaction of the mixture layers.
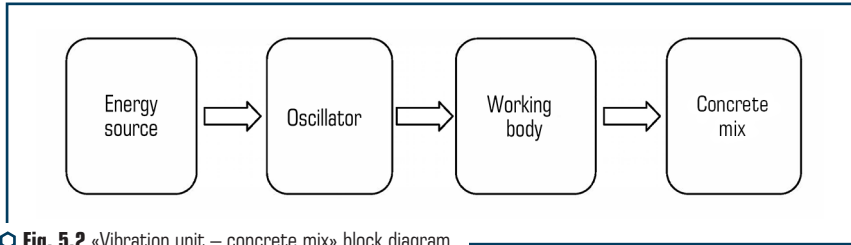
Fig. 5.2 «Vibration unit – concrete mix» block diagram

Based on the above reasoning, the «machine – medium» vibration system by different signs of their behavior will be represented from the point of view of modeling as subsystems with discrete (machine) and distributed (medium) parameters.

The next premise is based on the fact that the «machine – medium» vibration system at any moment of movement consists of two components – one is capable of accumulating energy that passes from one form to another (reactance), and the second is energy dissipation (active resistance) [3].

Thus, the task of accounting for the medium to be processed is reduced to determining the active and reactive forces in the contact zone and introducing them into the equation of motion of the vibration unit.

For this purpose, the «vibration unit – concrete mix» design diagram according to the method [2] is shown in **Fig. 5.3**.
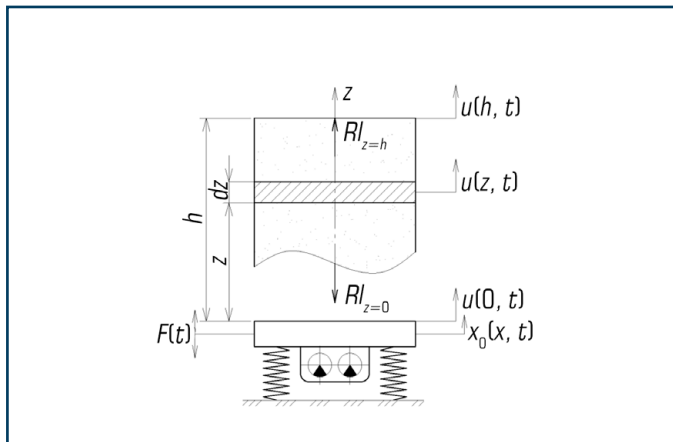
Fig. 5.3 Design diagram of the «vibration plant – concrete mix» system: x – displacement; $F(t)$ – external forced force; $u(z, t)$ – longitudinal displacement of the current section of the concrete mixture column; $R_{z=0}$ – reaction of the concrete mixture in the section, provided that $z=0$; $R_{z=h}$ – reaction of the concrete mixture in the cross section of the column, provided that $z=h$

The wave equation of displacement of the current section of the column of concrete mixture is taken in the form (5.1):

$$\frac{\partial^2 u}{\partial t^2} = c^2 (1 + i\gamma) \frac{\partial^2 u}{\partial z^2}.$$

Here $\partial^2 u / \partial t^2$ – acceleration of the concrete mixture layer; $\partial^2 u / \partial z^2$ – the second derivative of the displacement of the concrete mixture layer u along the coordinate of the mixture column z; c – speed of the mixture layer; γ – coefficient of resistance of the concrete mixture, which characterizes the quantitative value of energy dissipation; i – imaginary unit showing the rotation between the elastic and dissipative components by the angle $\varpi/2$.

The solutions of the wave equation (5.1) will be used in the form:

$$u(z,t) = \left(u_1 e^{kz} + u_2 e^{-kz} \right) e^{i\omega t}. \tag{5.2}$$

The displacement u is determined by the product of two functions, one of which depends on the arguments $z(z)$ and $T(t)$:

$$z(z) = u_1 e^{kz} - u_2 e^{-kz}, \tag{5.3}$$

$$T(t) = e^{i\omega t}.$$

In solution (5.2) u_1 and u_2 are constants determined by the boundary conditions, k – complex wavenumber: $k = (\alpha + i\beta)$, where α, β – coefficients [1–3]:

$$\alpha = \mu \frac{\omega}{c_2}; \ \beta = \nu \frac{\omega}{c_2}, \tag{5.4}$$

where $\mu = \sqrt{\dfrac{\sqrt{1+\gamma^2} - 1}{2(1+\gamma^2)}}$; $\nu = \sqrt{\dfrac{\sqrt{1+\gamma^2} + 1}{2(1+\gamma^2)}}$.

The coefficient α determines the attenuation of the wave propagated in the layer of the medium, and the coefficient β determines the attenuation of the same wavelength. Indeed, if there is no resistance ($\gamma=0$), then $\alpha=0$, $\beta = \omega/c_o$, that is, the wave under this condition propagates without extinction, which corresponds to the first equation (5.1).

The main task is to provide an analytical description of the dynamics of the «vibration unit – concrete mix» hybrid system.

The design diagram of the vibration system (**Fig. 5.4**) is described by the equation obtained on the basis of the use of the reaction method [4–6]:

$$(m + m_c a)\ddot{x} + (b + m_c \omega d)\dot{x} + c_o x = Fo \cdot \sin \omega t. \tag{5.5}$$

The solution to this equation gives an expression $x = x_o \sin(\omega t + \gamma)$ for determining the vibration amplitude of a vibration machine, taking into account the entire complex of resistance forces:

$$x_o = \frac{Fo}{\sqrt{\left[\left(c - mw^2\right) + m_c\omega^2 a\right]^2 + \left(b\omega + m_c w^2 d\right)^2}},$$ (5.6)

where a – wave coefficient of the reactance of the concrete mixture; d – wave coefficient of the active resistance of the concrete mixture;

$$a = \frac{\alpha \, \text{sh} 2\alpha h + \beta \sin 2\beta h}{h\left(\alpha^2 + \beta^2\right)\left[\text{ch} 2\alpha h + \cos 2\beta h\right]}; \quad d = \frac{\alpha \sin 2\beta h - \beta \, \text{sh} 2\alpha h}{h\left(\alpha^2 + \beta^2\right)\left[\text{ch} 2\alpha h + \cos 2\beta h\right]}.$$ (5.7)

Because of the task at hand, it is important to determine not only the influence of the nominal resistance forces on the amplitude value of displacement in the contact zone, but also to find an expression for determining the nature and magnitude of the distribution of the amplitudes of displacement over the layers of the mixture $z = z(h)$.

Using the solution of the wave equation, let's find an expression for finding the displacement of any layer of the mixture:

$$x(z,t) = \frac{x_o \text{ch}(h-z)(\alpha_1 + i\beta_1)}{\text{ch}\left[h(\alpha_1 + i\beta_1)\right]} e^{i(wt+\varphi)}.$$ (5.8)

The modulus of expression (5.8) gives a formula for the amplitude of the displacement of the mixture layer:

$$x(z,t) = \frac{x_o \text{ch}(h-z)(\alpha_1 + i\beta_1)e^{i(wt+\varphi)}}{\text{ch}\left[h(\alpha_1 + i\beta_1)\right]}.$$ (5.9)

When to enter an additional element, for example when loading, the limit conditions are changed. Now the stress on the upper contacting surface will not be equal to zero. It is obvious that the surcharge, like the working body, in its motion will also perceive the influence of the active and reactive resistances of the medium. By analogy, the force of resistance to surcharge fluctuations can be expressed as:

$$R(h,t) = ES(1+i\gamma)\left(\frac{\partial u}{\partial z}\right)_{z=h} =$$
$$= \rho c_b^2 S\left(\frac{k^2}{\delta^2}\right)\delta\left[u_1 e^{z\delta} - u_2 e^{-z\delta}\right]_{z=h} e^{iwt} = \frac{m_c w^2}{h} \cdot \frac{e^{iwt}}{\delta}\left(u_1 e^{h\delta} - u_2 e^{-h\delta}\right).$$ (5.10)

The notation is accepted here $k = w/c$; $m_A = \rho Sh$; $\delta = \alpha + i\beta$.

5.2 INVESTIGATION OF THE PARAMETERS OF VIBRATION MACHINES FOR THE COMPACTION OF CONCRETE MIX

To study the parameters of vibration machines for the compaction of a concrete mixture according to the obtained formulas, calculations were made according to the following variable parameters: the height of the mixture column $h = 0.1...1.5$ m; the frequency of the oscillations $w = 100..300$ 1/c; the speed of propagation of vibrations in the concrete mixture $C_c = 30...50$ m/s; the loss factor $\gamma = 0.05...1.0$; the ratio of the masses of the concrete mixture m_c to the mass of the vibration machine m: $m_c/m = 0.4...1.0$; static pressure. **Fig. 5.4** shows the results calculations.
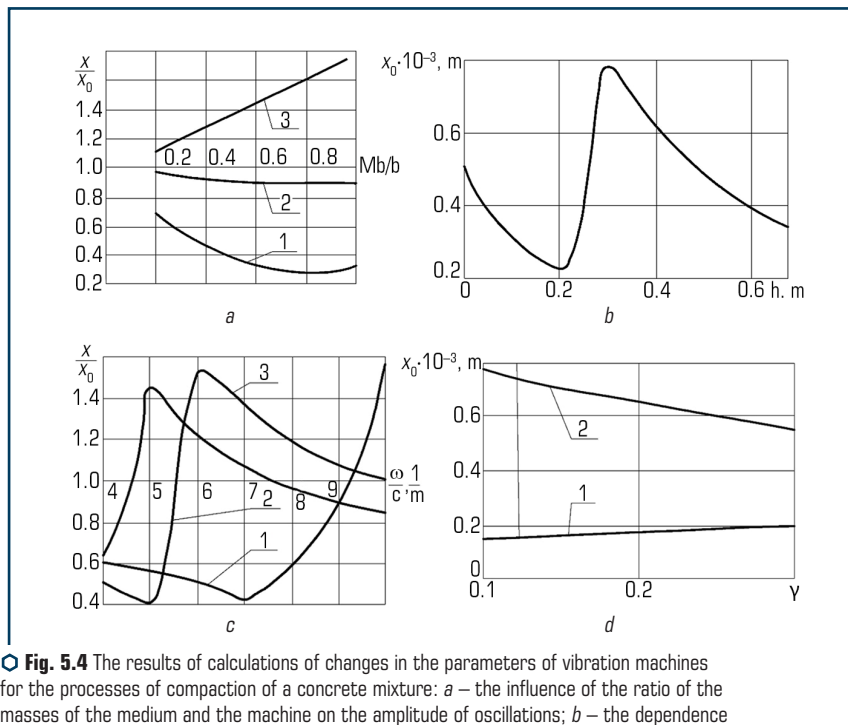
○ **Fig. 5.4** The results of calculations of changes in the parameters of vibration machines for the processes of compaction of a concrete mixture: a – the influence of the ratio of the masses of the medium and the machine on the amplitude of oscillations; b – the dependence of the amplitude of the oscillations on the height of the mixture column; c – the influence of the wave number on the amplitude of the oscillations; d – the influence of the loss factor on the vibration amplitude of the working body

The effect of the mass ratio of the medium and the machine on the vibration amplitude depends on the specific height of the mixture column. So, in zones far from resonance, these are the heights of the mixture column $h=0.2$ g and $h=0.5$ m (**Fig. 5.4, a**, curve 1 and curve 2), the amplitude

of the oscillations decreases. In the resonance zone $h=0.3$ m (**Fig. 5.4**, curve 3), the amplitude of oscillations increases, which is confirmed by the graph (**Fig. 5.4, b**). A noticeable effect on the amplitude has the speed of propagation of oscillations (**Fig. 5.4**), the value of which is included in the determination of the numerical values of the wave coefficients a and d (5.7). So, an error in determining the vibration speed by 10 % can lead to a discrepancy between the calculated and actual vibration amplitudes by 150 % (**Fig. 5.4**, curve 2).

The degree of influence of active resistance forces (**Fig. 5.4, d**) is determined by the height of the mixture column. In the zone of the greatest value of the vibration amplitude for a height of $h=0.3$ m (curve 1, **Fig. 5.4, d**), an increase γ leads to a natural decrease x_o. For the height (curve 1, **Fig. 5.4, d**), the picture is the opposite: here an increase γ leads to an increase in the amplitude of oscillations x_o.

The change γ from 0.1 to 0.3 led to an increase in the x_o amplitude from 0.156 to 0.173 mm.

The considered examples clearly confirm the taken into account the reactive and active resistance of the concrete mixture.

5.3 STUDY OF THE PARAMETERS OF SOIL COMPACTION PROCESSES UNDER THE MAIN PIPELINE

Main pipelines are rightly considered the energy arteries of Ukraine, because they provide energy resources not only for the needs of the state's own economy, but also for the transportation of oil and gas to more than 15 European countries. The current state of ensuring reliable and safe operation of trunk pipelines requires the urgent development and implementation of new equipment and technologies for capital repairs of pipelines, the use of which will significantly accelerate the pace of repair work with a decrease in material and labor costs for their implementation [7–9].

A feature of the new technology is that after a complex of works on replacing insulation under the repaired pipeline, soil is poured and compacted under the pipe to such an extent that it excludes subsidence of the latter after repair.

A schematic diagram of soil compaction under the pipeline by two surfaces symmetrically located relative to the longitudinal axis of the pipeline, synchronously moving against each other along the required trajectory, is shown in **Fig. 5.5**. In the process of compaction, there is a mutual influence of stress diagrams in the soil from both soil-compaction surfaces, which leads to the formation of a generalized stress diagram in the zone of the vertical soil mass under the main pipeline.

The stress state of the massif depends on many factors, primarily on the magnitude of the applied external loads, load modes, physical and mechanical characteristics of the compacting soil, the size of the soil mass under the pipe, the shape and size of the trench, and the design parameters of the soil compacting working equipment.

The values of technological factors in this study are taken to be fixed. The diameter of the pipeline is taken $D_p=1220$ mm, as the most common in Ukraine. The weight of one running meter of the pipeline is assumed unchanged and maximum in value, for the case when the pipe is filled with

oil q_p=14.3 kN/m. The height of the soil mass under the pipeline (the height of the placement of the lower point of the pipe relative to the bottom of the trench) is taken no more than H=820 mm. The geometrical dimensions of the trench for pipeline repair D_p=1220 mm, the following: depth h=3000 mm, width of the trench at the top b_t=4400 mm and at the bottom b_b=2620 mm (**Fig. 5.5**).

The speed of application of loads to the soil-packing surfaces V_l reflects the mode of operation of the soil-packing equipment. It must be consistent with the overlap factor of the compaction zone [10, 11]. Soil moisture W has a significant effect on the characteristics of its compaction. Let's believe that the compacted soil has an optimal moisture content W_o [12, 13].

The structural and force factors that significantly affect the soil compaction process under the pipelines include the geometric dimensions of the sealing surfaces, their relative position in the trench relative to the pipeline and the pressure they create on the compacted soil mass. Flat undeformed surfaces (blades) of rectangular shape are taken as working surfaces.

Determining the approach to the study of the stress-strain state of the soil mass under the pipeline, let's note that in the elastic region the stresses are directly proportional to the value of the applied loads. With a known value of stresses in the soil mass from the action of each fixed pressure of the sealing blades on the soil, it is possible to determine the value of stresses for another value of the applied pressure to the soil mass [14, 15]. Thus, with a known stress in the soil mass under the action of a fixed pressure P created by the working surfaces, it is possible to find new stresses in the soil mass for other values of the applied pressure of the blades on the soil:

$$\sigma' = \frac{P'}{P} \cdot \sigma, \tag{5.11}$$

where P – fixed pressure created by the blades on the soil mass; σ – known value of stresses in the soil mass from the action of a fixed pressure.
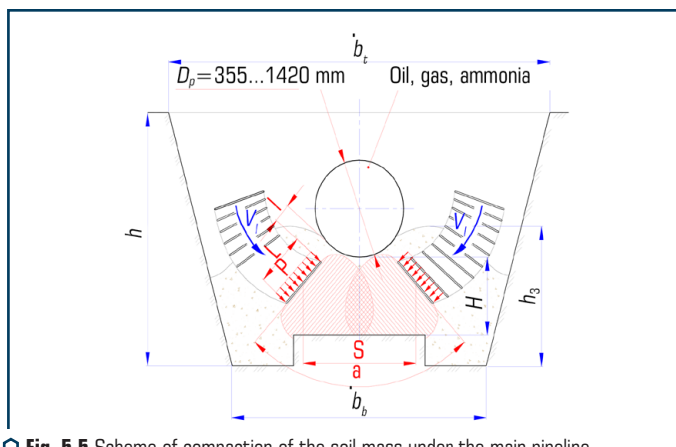
○ **Fig. 5.5** Scheme of compaction of the soil mass under the main pipeline

It follows from this that the pressure P created by the blades on the soil can be excluded from the number of variable factors.

Since the pressure on the soil from the blade is distributed evenly both along the length and along its width, the problem of determining the stress-strain state of the soil under the pipe in the direction along the pipeline can be considered as flat. Consequently, the stresses in the soil, when they are determined within the framework of flat surrender, will depend on the value of the pressure under the blades, regardless of the width of the blades B. On the other hand, under all equal loading conditions (fixed pressures), when the width of the blade changes, the stresses in the soil mass will change proportional to the width of the blade B:

$$\sigma' = \frac{B'}{B} \cdot \sigma, \tag{5.12}$$

where σ' – stress at an arbitrary blade width; σ – stress determined for a fixed blade width.

Therefore, such a geometric parameter as the width of the blade B is also referred to as constant factors.

Combining formulas (5.11) and (5.12), let's obtain the dependence of the stress σ' for arbitrary P' and B' at a known stress σ arising in a flat body with thickness B and a given load P:

$$\sigma' = \sigma \cdot \frac{P'B}{PB'}. \tag{5.13}$$

Thus, on the basis of consideration and analysis of the factors affecting the stress-strain state of the soil under the pipeline, it was established that the unchanged (constant) ones should include: $h = 3000$ mm, $b_t = 4400$ mm, $b_b = 2620$ mm, $H = 820$ mm, $D_p = 1220$ mm, $q_p = 14.3$ kN/m, $h_d = H + 0.5D_p$, $P = 10$, $\mu = 0.37$.

Consequently, the constant factors, the value of which must be determined experimentally, include: the compression rate V_l, the compaction delay time t_d, the compaction overlap coefficient K_o, the elastic modulus E, the optimal moisture content Wo.

In the process of studying the stress-strain state of the soil under the pipeline, it is necessary to determine the effect on the characteristics of the stress state of the following parameters: blade angle α, blade length L and width B, blade pressure P on the ground, distance l from blade to pipe, as well as distance S between blades (**Fig. 5.6**). Determination of the rational values of these factors and their interaction in the process of soil compaction is the main task of the study.

The essence of the study is to determine the effect of changes in the linear parameters L and B of the sealing blades, the pressure P they create on the ground, on the provision of the necessary stresses in the soil mass under the pipeline, taking into account the parameters α, l and S, characterizing the position of the blades in the trench relative to the pipeline of a given diameter.

To construct a mathematical model of the stress state of the soil mass under the pipeline, let's select the values of the variable factors characterizing the compaction process for the zero level and the limits of change of these values are the intervals of variation of the factors. The value

of the variation intervals is chosen based on the following considerations and requirements. The compression angle was chosen $\alpha=90°...70°$, based on the values of the angle of the prism of the soil massif under the pipeline, at which a sufficient stability coefficient of the massif will be ensured. When choosing the intervals for changing the linear parameters of the blades L and B, we leave, first of all, from the position of ensuring guaranteed non-damage of the pipeline insulation coating during soil compaction $L=450...650$ mm.

Based on the results of studies of soil compaction with stamps, the recommended width of the stamp should be equal to half of its length, because it is with this ratio that the maximum depth of the active compaction zone, $B=225...325$ mm, is achieved during the compaction process. In further studies, let's take the value of the blade width to be constant and equal to $B=300$ mm.

Since it is known that the depth of the core during soil compaction [13] is equal to two dimensions of the smaller side of the stamp [11], and taking into account the predicted increase in the active zones as a result of their overlap as a result of the oncoming motion of the sealing blades, let's take $S=1200...1600$ mm. The levels of the selected factors and the intervals of their variation are presented in **Table 5.2**.

● **Table 5.2** Factor levels and intervals of their variation study of the stress state of the MP soil bed

Independent variables		Variation levels			Variation intervals Δi
		Upper +1	**Basic 0**	**Low −1**	
X1	α, degree	90	80	70	10
X2	S, mm	1600	1400	1200	200
X3	L, mm	650	550	450	100
X4	l, mm	250	200	150	50

The design diagram of soil compaction under the pipeline is shown in **Fig. 5.6**. The geometrical dimensions of the investigated soil massif were determined on the basis of the dimensions b_t, b_b, h of the trench profile, built by the pipeline opening machine $D_p=1220$ mm. The height of the soil massif under the pipe H is taken in accordance with the size of the developed soil massif under the pipe $H=820$ mm.

The soil mass, compacted under the pipeline, is bounded by two inclined surfaces symmetrical about the vertical axis passing through the center of the pipeline, the positions of which are regulated by the values of the compression angle $X1$ and the distance between the blades $X2$ (**Fig. 5.7**). It is accepted that the value of the parameter $X2$ is calculated horizontally, located relative to the lower point of the pipeline at a distance of 1/3H.

In this case, the mass of compacted soil is limited from the top of the generatrix of the pipe of a given diameter D_p, and from the bottom by the bottom of the excavated recess, which is located at a distance H from the lower point of the generatrix of the pipeline. Since the pipeline wall and trench walls have significantly higher elastic moduli than the compacted soil mass, they can be

considered undeformed surfaces. Therefore, in the zones where the compacted soil borders on the generatrix of the pipeline and the walls of the trench, it is legitimate to impose boundary conditions for the movement of the soil perpendicular to the undeformed surfaces.
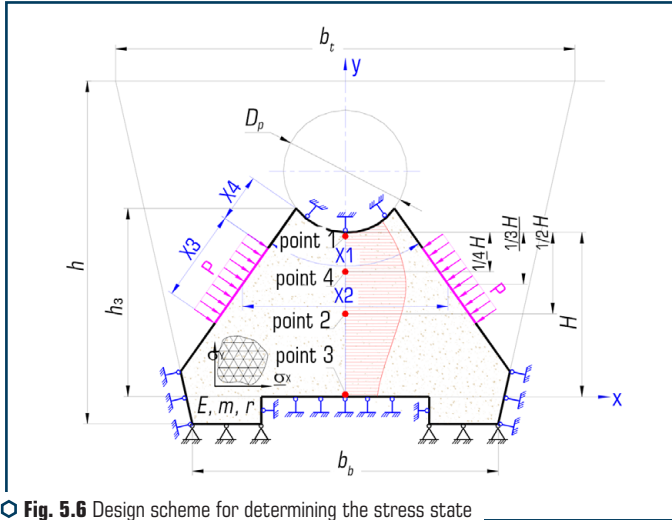
○ Fig. 5.6 Design scheme for determining the stress state of the soil mass under the pipeline
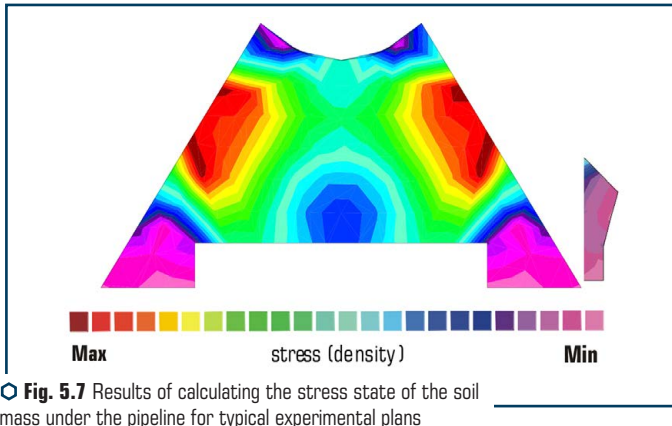
○ Fig. 5.7 Results of calculating the stress state of the soil mass under the pipeline for typical experimental plans

Taking into account the above, for further research let's take soil compacted isotropic in volume.

The sizes, which are determined (reviews) in the study, are equivalent stresses at the characteristic points of the soil mass along the axis under the pipeline. Typical points are considered (**Fig. 5.7**):

$Y1$ – the magnitude of stresses in the soil mass in the area under the pipeline; $Y2$ – the value of stresses in the middle part of the soil massif at a distance of $1/2N$ from the pipeline; $Y3$ – the magnitude of stresses in the lower part of the massif at the level with the bottom of the trench; $Y4$ – the value of stress in the soil at a distance of $1/4H$ from the pipeline.

Determination of the rational values of the parameters $X1...X4$, B and P, their functional interdependence and influence on the stress state of the soil compacted under the pipeline made it possible to provide the necessary values of the soil compaction coefficients and the uniformity of its compaction.

The visual presentation of the results of calculating the stress state of the soil [8] under the pipeline using the finite element method made it possible to evaluate the influence of the interaction of compaction nuclei in the soil mass created by the blades of the working body, under the action of various combinations of values of the initial parameters that determine the compaction process. Typical results of calculating the stress state of the soil indicate that there may be combinations of initial parameters at which the expected effect of superposition of compaction nuclei is not observed, the stresses in the soil mass at different depths under the pipeline are insignificant, therefore, the coefficients of soil compaction remain minimal. The combination of the initial parameters (**Fig. 5.8**) provides a more uniform soil compaction under the pipeline, which indicates the presence of the effect of the interaction of compaction nuclei in the soil.

Thus, it can be argued that by changing the combinations of the initial parameters that determine the process of soil compaction under the pipeline, it is possible to control the interaction of soil compaction nuclei, as well as to influence the value of the final indicators of this process [11, 12, 16–18].

As a result of processing the data of numerical experiments [10], in accordance with the folded matrix, mathematical models were obtained to determine the stress state of the soil at the characteristic points of the massif under the pipelines, which are predictive models. Their adequacy was confirmed by the Fisher test with a confidence level of 0.95 [11].

$$\sigma_1 = \frac{P'B}{PB'} \cdot \begin{pmatrix} 0.08637 - 0.01696 \cdot x_1 + 0.02101 \cdot x_2 - \\ -0.02524 \cdot x_3 - 0.00306 \cdot x_1^2 + 0.00367 \cdot x_4^2 \end{pmatrix}; \tag{5.14}$$

$$\sigma_2 = \frac{P'B}{PB'} \cdot \left(0.09741 - 0.0027 \cdot x_1 - 0.00798 \cdot x_2 + 0.01312 \cdot x_3 + 0.0024 \cdot x_2^2 \right); \tag{5.15}$$

$$\sigma_3 = \frac{P'B}{PB'} \cdot \left(0.0725 - 0.00509 \cdot x_2 - 0.01162 \cdot x_3 - 0.00276 \cdot x_1^2 \right); \tag{5.16}$$

$$\sigma_4 = \frac{P'B}{PB'} \cdot \left(0.09889 - 0.00642 \cdot x_1 + 0.00605 \cdot x_3 - 0.01496 \cdot x_4 + 0.00306 \cdot x_2^2 \right). \tag{5.17}$$

Thanks to the predictive models (5.14)–(5.17), it became possible to control the process of interaction of the compaction nuclei by changing the linear dimensions of the blades, the parameters

of their installation, namely: the compression angle $\alpha=X1$, the distance between the blades $S=X2$, the blade length $L=X3$ mm, the distance from the blade to the pipeline $l=X4$, blade width B.

Based on the solution of the system of equations (5.14)–(5.17), a rational combination of the output parameters of the soil compaction process under the pipelines was found: $\alpha=75°$, $S=1400$ mm, $L=600$ mm, $l=180$ mm, $B=300$ mm, as well as the dependence for the characteristic points 1…4 of the change in the values of the compaction coefficients on the pressure of the blades on the ground is built (**Fig. 5.8**).
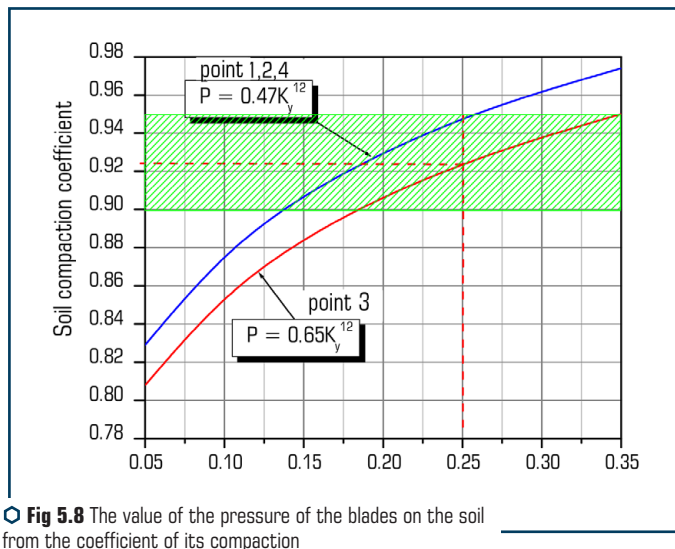
○ **Fig 5.8** The value of the pressure of the blades on the soil from the coefficient of its compaction

This made it possible to obtain the value of the pressure of the blades on the soil $P=0.2…0.35$ MPa, at which the necessary values of the soil compaction coefficients under the pipeline will be provided within the range of $K_y=0.9…0.95$.

Rational values of the parameters of the working body and operating modes under which the interaction of soil compaction nuclei under the pipeline is guaranteed, adopted for subsequent research and for use in the design of working equipment for soil compaction under the pipeline.

5.4 DISCUSSION OF RESEARCH RESULTS

A certain model of the processing medium, based on a general view of the compaction process, is characterized by three stages. This is at the first stage of compaction of a granular medium (**Fig. 5.1**), at the second and third stages of compaction, an elastic-viscoplastic medium.

This important result requires a clear definition of the physical and mathematical model, which is suggested by equations (5.1). Further studies are required to determine the temporal assessment of the course of these stages. Application of the idea of considering the «technical system – medium» system as a system that at any moment of movement consists of two components. One is capable of storing energy that passes from one form to another (reactance), and the other is capable of dissipating energy (resistance). A certain significant influence of the components of resistance on the movement of a technical system (**Fig. 5.4**) testifies to the hypothesis put forward about the need to take into account the forces of resistance of the medium. A technical system is a system with discrete parameters, and a medium – with distributed parameters. In this case, this general system is reduced to a computational system in the form of a system with discrete parameters, in which the wave phenomena of the medium are preserved and are represented by a contact force. The obtained wave coefficients (5.7) have general properties. They can be used in any equations of motion for such technical systems. This is the novelty of the method of analytical study of vibration systems for compaction of mixtures.

The presentation of the results of calculating the stress state of the soil under the pipeline using the finite element method made it possible to assess the influence of the interaction of compaction of nuclei in the soil mass. By changing the combinations of the initial parameters that determine the process of soil compaction under the pipeline, it allows to control the interaction of soil compaction nuclei, as well as to influence the value of the final indicators of this process. Based on the results of studies of soil compaction with stamps, the width of the stamp was determined ($B=225...325$ mm). Its value is equal to half of its length, since according to this ratio, the maximum depth of the active zone of compaction is achieved during the compaction process. A rational combination of the initial parameters of the soil compaction process under the pipelines ($\alpha=75°$, $S=1400$ mm, $L=600$ mm, $l=180$ mm, $B=300$ mm) has been established under which the interaction of soil compaction nuclei under the pipeline is guaranteed.

CONCLUSIONS TO SECTION 5

1. The model of the processing medium, characterized by three stages of compaction, has been determined.

2. The review and analysis of physical and mathematical models of the process of compaction of technological media has been carried out.

3. A model of the «vibration plant – medium» hybrid system is proposed, in which active and reactive resistances to wave coefficients are taken into account.

4. The results of calculations of changes in the parameters of vibration machines for the processes of compaction of concrete mixture have been obtained, confirming the implementation of accounting for the reactive and active resistance of the concrete mixture.

5. Predictive mathematical models have been created to determine the stress state of the soil during compaction at the characteristic points of the massif under the pipelines, which make it possible to obtain rational values of the parameters of the working bodies for soil compaction.

6. Regularities of movement of technical systems for compacting concrete mixtures and soils and their rational parameters have been established.

7. An algorithm and methodology for calculating the main parameters of vibration systems for compaction of working media have been developed.

REFERENCES

1. Nazarenko, I., Gaidaichuk, V., Dedov, O., Diachenko, O. (2017). Investigation of vibration machine movement with a multimode oscillation spectrum. Eastern-European Journal of Enterprise Technologies, 6 (1 (90)), 28–36. doi: http://doi.org/10.15587/1729-4061.2017.118731

2. Nazarenko, I., Gaidaichuk, V., Dedov, O., Diachenko, O. (2018). Determination of stresses and strains in the shaping structure under spatial load. Eastern-European Journal of Enterprise Technologies, 6 (7 (96)), 13–18. doi: http://doi.org/10.15587/1729-4061.2018.147195

3. Nazarenko, I., Ruchynskyi, M., Delembovskyi, M. (2018). The Basic Parameters of Vibration Settings for Sealing Horizontal Surfaces. International Journal of Engineering & Technology, 7 (3.2), 255–259. doi: http://doi.org/10.14419/ijet.v7i3.2.14415

4. Nesterenko, M., Nazarenko, I., Molchanov, P. (2018). Cassette Installation with Active Working Body in the Separating Partition. International Journal of Engineering & Technology, 7 (3.2), 265–268. doi: http://doi.org/10.14419/ijet.v7i3.2.14417

5. Nazarenko, I. I., Ruchynskyi, M. M., Sviderskyi, A. T., Kobylanska, I. M., Harasim, D., Kalizhanova, A., Kozbakova, A. (2019). Development of energy-efficient vibration machines for the buiding-and-contruction industry. Przeglad Elektrotechniczny, 95 (4), 53–59. doi: http://doi.org/10.15199/48.2019.04.10

6. Klets, D., Gritsuk, I. V., Makovetskyi, A., Bulgakov, N., Podrigalo, M., Kyrychenko, I. et. al. (2018). Information Security Risk Management of Vehicles. SAE Technical Paper Series. doi: http://doi.org/10.4271/2018-01-0015

7. Dubovenko, Y. I., Kuzminets, M. P. (2017). The experience of integrating of GIS techniques in the construction of digital maps of geophysical fields. 16th International Conference on Geoinformatics – Theoretical and Applied Aspects. doi: http://doi.org/10.3997/2214-4609.201701851

8. Dubovenko, Y. I., Shumlianska, L. A., Kuzminets, M. P. (2020). Seismic velocity gradient stratification of the mantle at Ukrainian Shield. Geoinformatics: Theoretical and Applied Aspects 2020. doi: http://doi.org/10.3997/2214-4609.2020geo063

9. Dubovenko, Y. I., Chorna, O. A., Kuzminets, M. P. (2020). Modeling of the potential fields transformants for the ring structure Illinetska. Geoinformatics: Theoretical and Applied Aspects 2020. doi: http://doi.org/10.3997/2214-4609.2020geo062

10. Nazirova, A. B., Dubovenko, Y. I., Abdoldina, F. N., Kuzminets, M. P. (2021). Optimization of GIS modules for processing data of gravity monitoring of subsoil in the Republic of Kazakhstan. Geoinformatics. doi: http://doi.org/10.3997/2214-4609.20215521136

11. Nazarenko, I., Svidersky, A., Kostenyuk, A., Dedov, O., Kyzminec, N., Slipetskyi, V. (2020). Determination of the workflow of energy-saving vibration unit with polyphase spectrum of vibrations. Eastern-European Journal of Enterprise Technologies, 1 (7 (103)), 43–49. doi: http://doi.org/10.15587/1729-4061.0.184632

12. Onishchenko, A., Koretskyi, A., Bashkevych, I., Ostroverkh, B., Bieliatynskyi, A. (2020). Dam Failure Model and Its Influence on the Bridge Construction. Advances in Intelligent Systems and Computing, 229–237. doi: http://doi.org/10.1007/978-3-030-57450-5_21

13. Onishchenko, A., Lapchenko, A., Fedorenko, O., Bieliatynskyi, A. (2020). Research of the Properties of Bitumen Modified by Polymer Latex. Advances in Intelligent Systems and Computing, 104–116. doi: http://doi.org/10.1007/978-3-030-57450-5_10

14. Kovalchuk, V., Kravets, I., Nabochenko, O., Onyshchenko, A., Fedorenko, O., Pentsak, A. et. al. (2021). Devising a procedure for assessing the subgrade compaction degree based on the propagation rate of elastic waves. Eastern-European Journal of Enterprise Technologies, 1 (5 (109)), 6–15. doi: http://doi.org/10.15587/1729-4061.2021.225520

15. Luchko, J., Kovalchuk, V., Kravets, I., Gajda, O., Onyshchenko, A. (2020). Determining patterns in the stresseddeformed state of the railroad track subgrade reinforced with tubular drains. Eastern-European Journal of Enterprise Technologies, 5 (7 (107)), 6–13. doi: http://doi.org/10.15587/1729-4061.2020.213525

16. Lantukh-Lyashchenko, A., Onishchenko, A., Davydenko, O. (2020). Problem of the degradation criteria for transportation construction elements. E3S Web of Conferences, 164, 03014. doi: http://doi.org/10.1051/e3sconf/202016403014

17. Nazarenko, I., Dedov, O., Bernyk, I., Rogovskii, I., Bondarenko, A., Zapryvoda, A. et. al. (2020). Determining the regions of stability in the motion regimes and parameters of vibratory machines for different technological purposes. Eastern-European Journal of Enterprise Technologies, 6 (7 (108)), 71–79. doi: http://doi.org/10.15587/1729-4061.2020.217747

18. Nazarenko, I., Gavryukov, O., Klyon, A., Ruchynsky, N. (2018). Determination of the optimal parameters of a tubular belt conveyor depending on such an economical. Eastern-European Journal of Enterprise Technologies, 3 (1 (93)), 34–42. doi: http://doi.org/10.15587/1729-4061.2018.131552

6 RESEARCH OF THE PROCESSES OF ACOUSTIC CAVITATION TECHNOLOGY FOR PROCESSING DISPERSED MEDIA

I. Nazarenko, I. Bernyk

ABSTRACT

The operation process of acoustic treatment of technological media is investigated. The assessment and substantiation of methods for studying the parameters of acoustic treatment of technological media is done. The functional relationships between the acoustic parameters of the cavitation apparatus and the rheological properties of the processing technological media have been revealed. The process of staged acoustic treatment of technological media is described. A number of criteria and key parameters were determined, the use of which was carried out as an assessment in the calculation algorithm, depending on certain known initial data of the cavitator and the medium. The values of the input resistance of the compensator are determined and the condition for the maximum transfer of energy from the acoustic apparatus to the technological medium is obtained. To calculate the parameters of the «cavitator – technological medium» ultrasonic cavitation system, an algorithm and method for creating a synergistic system were developed.

KEYWORDS

Acoustic system, cavitator, medium, bubble, stage, cavitation process, physical, mathematical model, rheological properties, equations, analytical dependences, parameters, amplitude, vibration frequency, intensity, energy, wave resistance.

6.1 ASSESSMENT AND JUSTIFICATION OF THE CHOICE OF METHODS FOR STUDYING THE PARAMETERS OF ACOUSTIC TREATMENT OF TECHNOLOGICAL MEDIA

Cavitation technology occupies a leading place in a number of advanced and effective methods for processing liquid media and creating new materials. This technology is being implemented for a number of different technological processes, including dispersion, emulsification, homogenization, degassing, and others [1–6]. Cavitation refers to vibration processes widely used in food [1–3], chemical [4, 5], mechanical engineering [6], construction [7], and other industries. The generally accepted definition of cavitation as a physical phenomenon is the process of the formation of cavities (of a certain size of bubbles) in a fluid flow under the influence of external pressure. Depending on the method of pressure formation in the medium, cavitation can be hydrodynamic or acoustic.

In hydrodynamic cavitation, a decrease in pressure occurs due to an increase in the local speeds of the liquid flow [5]. If a decrease in pressure is due to the passage of acoustic waves of a sound or supersonic spectrum of vibration frequencies, cavitation is considered acoustic [6].

During cavitation, the energy density of the sound field is transformed into a high energy density inside and around the bubble, which collapses over time. Consequently, energy is spent on the formation of shock waves, thermal energy, local electrification of bubbles, excitation of sonoluminescence, and the formation of free radicals [8]. In this case, during cavitation, there is a change in the rheological properties of the technological medium, such as viscosity, plasticity and elasticity [9]. Therefore, the determination of the parameters of acoustic treatment of technological media and energy requires the use of a computational model [10], which takes into account these changes. The key parameter of the evolution of gas and air bubbles in the acoustic field is the pressure that is formed in the contact zone of the «cavitator – medium» system [11–14]. The specified parameters and characteristics (**Fig. 6.1**) [15, 16].
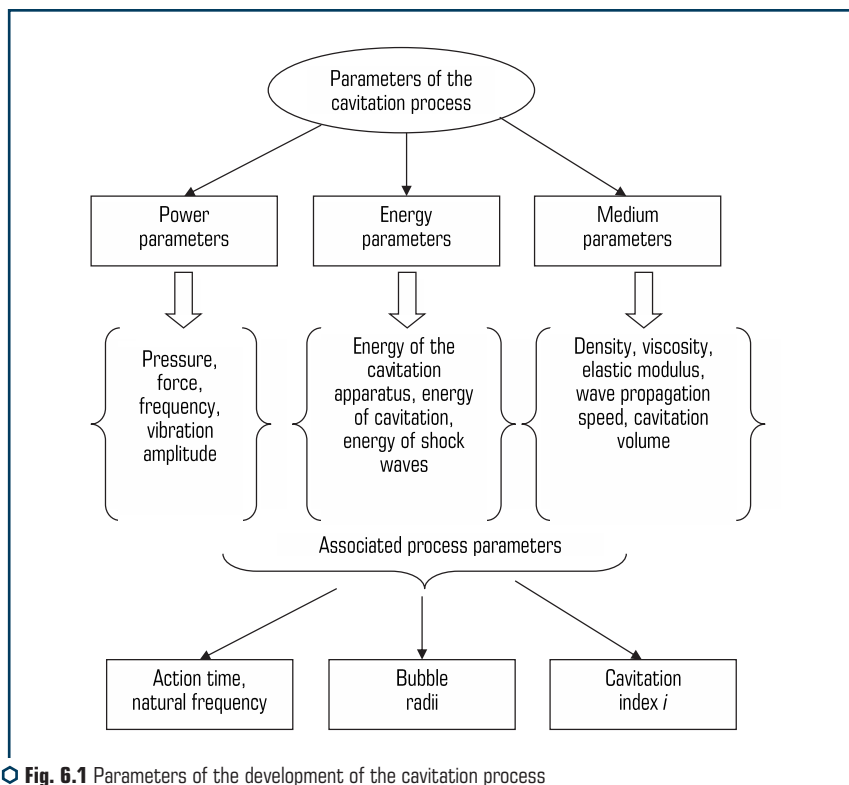
○ **Fig. 6.1** Parameters of the development of the cavitation process when processing technological media

The dominant influence on the sequence of the cavitation process is exerted by the following acoustic parameters and properties of the medium [17, 18]:

$$F = f\{A, A_i, f, v, W, P, L, t, l, p, \sigma, c, E, \rho, \mu\},\qquad(6.1)$$

where F – functional (integral criterion for evaluating a process); A – amplitude of oscillations of the contact zone «acoustic apparatus – medium» zone; A_i – flow amplitude of medium oscillations at a distance x_i from the boundary of the contact zone «acoustic apparatus – medium»; f – vibration frequency of the acoustic apparatus; v – speed of vibrations of the contact zone «acoustic apparatus – medium»; W – energy, P – power; L – intensity; t – time; l – characteristic size of the medium in the direction of propagation of the acoustic wave in it; p – the pressure on the medium; σ – stress in the medium; c is the speed of propagation of an acoustic wave in a medium; E – modulus of elasticity of the medium; ρ – density of the medium; μ – coefficient of viscosity of the medium.

Integral parameters of function (6.1) are energy, intensity and power. Ultrasonic energy from the emitting surface of the ultrasonic apparatus to the medium undergoes several stages of transformation:

– accumulation of energy in cavitation bubbles during their formation and expansion;

– transformation of energy into energy of a shock wave during a burst of a cavitation bubble.

6.2 DETERMINATION OF FUNCTIONAL DEPENDENCIES BETWEEN THE ACOUSTIC PARAMETERS OF THE CAVITATION APPARATUS AND THE RHEOLOGICAL PROPERTIES OF THE PROCESSING TECHNOLOGICAL MEDIA

Let's consider the influence of the parameters of the cavitation process on the formation of the volume of the cavitating technological medium. By analogy with the general functional (6.1), the rate of change in the volume of bubbles V can be represented by the following functional dependence:

$$V(t) = f(t, R_0, l, n, \rho_l, \mu_l, \sigma, \rho_g, \mu_g, p_e, p_i).\qquad(6.2)$$

Taking time t, bubble radius R_0, density ρ_l as the main independent parameters in terms of dimension and using the basic provisions of the theory of dimensions [19], let's reduce all parameters (6.2) to a dimensionless form with respect to the formed bubble volume: t – time, $[T]$; l – characteristic length in the direction of the wave motion of the bubbles, $[L]$; R_0 – initial bubble radius, $[L]$; n – the number of bubbles per unit volume, $[1/L^3]$; ρ_l – density of the medium, $[M/L^3]$; μ_l – viscosity, $[M/LT]$; σ – surface tension, $[M/T^2]$; ρ_g – gas density, $[M/L^3]$; μ_g – gas viscosity, $[M/LT]$; p_e – external pressure, $[M/LT^2]$; p_i – pressure inside the bubbles, $[M/LT^2]$. Then the functional dependence (6.2) can be represented in dimensionless form:

$$\frac{V}{\frac{4}{3}\pi R_0^3/t} = f\left(\frac{l}{R_0}; nR_0^3; \frac{\mu_l}{\rho_l R_0^2/t}, \frac{\sigma}{\rho_l R_0^3/t^2}, \frac{\rho_g}{\rho_l}, \frac{\mu_g}{\rho_l R_0^2/t}, \frac{p_e}{\rho_l R_0^2/t^2}, \frac{p_e-p_i}{\rho_l R_0^2/t^2}\right). \tag{6.3}$$

The next analysis procedure (6.3) is to assess the importance of taking into account the components of this dependence on the rate of formation of the volume of the cavitating technological medium. If to accept the condition of bubble bursting time τ_B in the form [20]:

$$\tau_B = 0.915R_0\sqrt{\frac{\rho_l}{p_e-\rho_i}}, \tag{6.4}$$

then dependence (6.3) can be re-formed into the following form:

$$\frac{V}{\frac{4}{3}\pi R_0^3/\tau_B} = f\left(l; N; \frac{\mu_l}{\rho_L R_0^2/\tau_B}, \frac{\sigma}{\rho_l R_0^3/\tau_B^2}, \frac{\rho_g}{\rho_l}, \frac{\mu_g}{\rho_l R_0^2/\tau_B}, \frac{p_e}{p_e-p_i}, \frac{t^2}{\tau_B^2}\right). \tag{6.5}$$

For media with low viscosity at the stage of bubble burst, according to the data of [20], the viscosity and surface tension can be neglected. Then dependence (6.5) for such conditions can be simplified to the form:

$$\frac{V}{\frac{4}{3}\pi R_0^3/\tau_B} = f\left(l; N; \frac{p_e}{p_e-p_i}, \frac{t^2}{\tau_B^2}\right). \tag{6.6}$$

The obtained dependence testifies to the importance of the influence of pressure, bubble diameter and burst time on the rate of formation of a volume of a cavitating medium with low viscosity. For other technological media, dependence (6.3) is used. The calculations of the numerical values of the volume of the cavitation zone depending on the intensity are given in **Table 6.1**.

● **Table 6.1** Numerical value of the formation of the volume of the cavitation zone, depending on the intensity

Intensity, W/cm²	5.0	10.0	20.0	30.0	40.0	50.0
The volume of the cavitation zone, m³·10⁻⁴	0.10	0.30	0.40	0.42	0.44	0.46

The importance of the data in this table lies in the fact that the ratio of the volume of non-bursting ΔV_l (long-lived bubbles) to the volume of bubbles that burst ΔV_b is an estimate of the efficiency of the cavitation process:

$$K_V = \Delta V_l/\Delta V_b. \tag{6.7}$$

In general, a number of criteria and key parameters have been determined, the use of which is proposed as an estimate in the calculation algorithms, depending on certain known initial data of the cavitator and the medium (**Table 6.2**). of the cavitation process of processing technological media The main set of criteria involves the assessment of the energetics of the process as a key characteristic, and taking into account possible changes in key parameters from the stage of nucleation of bubbles to the final stage – a burst of bubbles. Criteria that directly determine the reliability of the choice of the mode (harmonic or pulsed mode) are extremely important. These include criteria 8, 9 and 12. The importance of criterion 8 lies in the reliability of the selected speed of the cavitation apparatus, and criterion 9 is a direct indicator of the ratio of the burst time and the period of the technological process. The most numerical value of this criterion determines the provision of the minimum value of the ratio (6.7) and the possible expediency of using a pulsed mode of loading on the technological medium.

● **Table 6.2** Criteria and key parameters for evaluating the effectiveness of the cavitation process of processing technological media

No.	Criterion, parameter	Analytical dependence
1	2	3
1	The intensity of the cavitation process by the type of vibration	
1.1	Sinusoidal vibrations, I, W/cm²	$I = \dfrac{p^2}{2\rho c}$; $I = A^2 \times f^3$
1.2	Two-frequency oscillations, I, W/cm²	$I = \dfrac{\alpha \times A}{4\pi^2 T} \times \dfrac{(1+kn)^2}{2}$
1.3	Multifrequency oscillations, I, W/cm²	$I = \dfrac{\alpha \times A}{4\pi^2 T} \times \dfrac{\left(1 + \sum k_i n_i\right)^2}{2}$
1.4	Non-linear (non-sinusoidal) fluctuations, I, W/cm²	$I = \dfrac{\alpha \times A}{4\pi^2 T}$
2	System synergy coefficient (efficiency), k_s	$k_s = E_s / E_{n.x.}$
3	The rate of change in the stress state of the medium in time $\upsilon_{s.s}$, N/m²s	$\upsilon_{s.s} = \dfrac{d\sigma}{dt}$
4	Coefficient of the ratio of the volumes of long-lived and cavitating bubbles, K_v	$K_v = \Delta V_d / \Delta V_c$
5	Coefficient of energy change over time for the entire period of bubble processing, μ, J/s	$\mu = 1/T(\ln E_0 / E_k)$
6	Energy absorption coefficient, ap, m⁻¹	$A_p = P_{sp}/I$
7	Coefficient of the ratio of wave resistances of the cavitation medium, k_r	$k_r = \dfrac{\rho_k c_k}{\rho_c c_c} = \left[\dfrac{1}{1 + \dfrac{K\beta_n}{\beta_0}}\right]^{1/2}$

● **Continuation of Table 6.2**

1	2	3
8	Speed ratio, k_v	$K_s = v_0/c_k$
9	Coefficient of the ratio of the burst time to the time of the oscillation period, k_t	$k_t = \tau/T$
10	Contact zone work, A_{cz}, J	$A_{cz} = \pi m_c x_0^2 \omega^2 \mu$
11	Work on the formation of cavitation bubbles, A_{cb}, J	$A_{cb} = \dfrac{4}{3}\pi R_m^3 P_0 N$
12	Specific work of the cavitator, $\overline{A}$, J	$\overline{A} = \overline{P} \cdot t$
13	Specific work of volume, A_c cavitating medium, J	$A_c = E_c \Delta V$
14	Coefficient of conversion of acoustic energy into energy of shock waves, η_y	$\eta_y = \eta \dfrac{E_y}{E_k}\dfrac{T}{\tau}$
15	Productivity of the cavitation process, ΔP, m³/s	$\Delta P = kP/E_c$
16	Bubble displacement amplitude, A_b, µm	$A_b = \dfrac{1}{\omega}\sqrt{\dfrac{2I}{\rho c}}$
17	Bubble speed amplitude, v_b, µm/s	$v_b = \sqrt{\dfrac{2I}{\rho c}}$
18	Bubble acceleration amplitude, a_b, µm/s²	$a_b = \omega\sqrt{\dfrac{2I}{\rho c}}$
19	Natural bubble oscillation frequency: discrete model, ω_n, rad/s	$\omega_n = \sqrt{\left[\dfrac{3\gamma}{\rho R_0^2}\left(P_0 + \dfrac{2\sigma}{R_0}\right) - \dfrac{2\sigma}{\rho R_0^3} + \dfrac{2c_{np}}{\rho R_0^3}\right] - \left(\dfrac{2\pi\delta_{np}}{\omega}\right)^2}$
20	Natural bubble oscillation frequency: continuous model, ω_n, rad/s	$\omega_n = \dfrac{\pi}{2I}\sqrt{\dfrac{(E' + iE'')(t_c)}{\rho(t_c)}}$
21	Relative bubble size, kr	$K_b = R_m/R_0$

The application of this or that criterion is due to the initial information and the set goal formulated before the researcher to select the model and parameters, or by the engineer to create the necessary acoustic wave system for a specific technological processing process or create a new technological medium.

A similar example can be given for creating the required acoustic wave system. To implement the criteria-based assessment of the justification of the rational choice of the structural-parametric system «acoustic apparatus – technological medium», an algorithm has been developed (**Fig. 6.2**).

The essence of the algorithm lies in the ability to vary not only the initial parameters and the layout of the cavitator relative to the processing medium, but also to determine the influence of

variable parameters on the maximum value of a particular criterion (**Table 6.2**). Depending on the formulation of the problem, a criterion is selected, which is fixed in block 8. Further, in block 2 «Formation of the technological scheme», preliminary calculations are made for the mode of energy transfer to the medium in accordance with the selected criterion. An important stage of the algorithm is blocks 3 and 5, which determine the physical and mathematical models based on the research results [7–9, 12–18]. It is in blocks 4, 6, 7 that the initial data are formed to determine the numerical values of the impact parameters and the limits of their rational use. The completion of the calculation is the parameters that serve as the initial information for making decisions to improve the rational design and technological parameters of the acoustic cavitator.
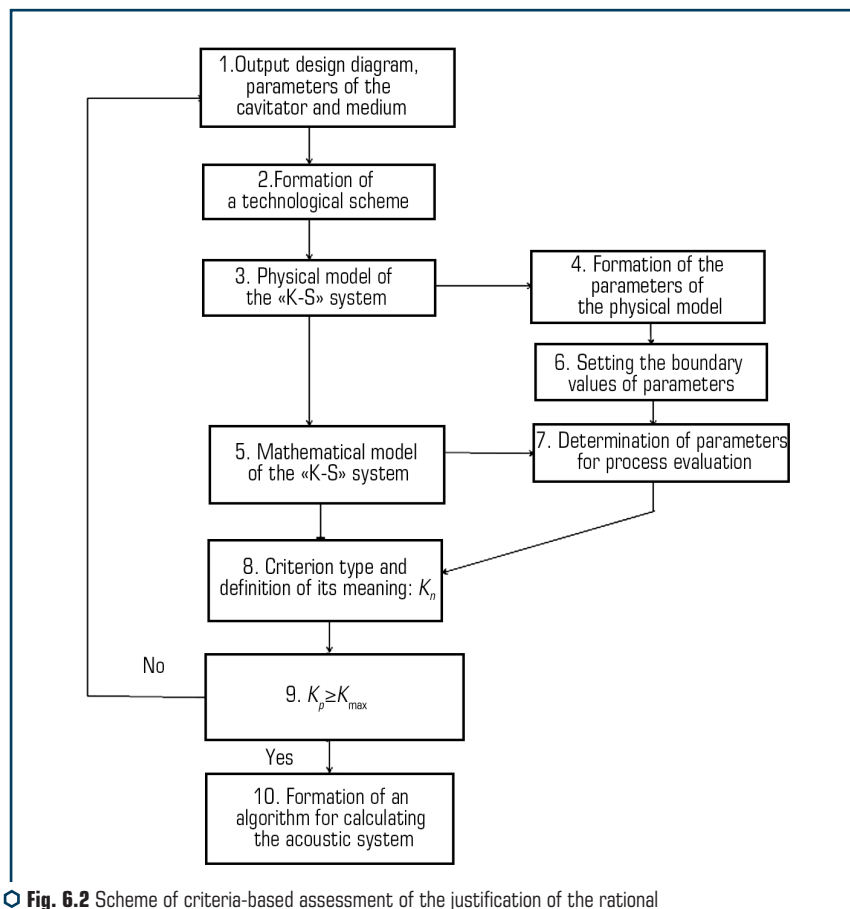
○ **Fig. 6.2** Scheme of criteria-based assessment of the justification of the rational choice of the «acoustic apparatus – technological medium» structural-parametric system

This technology of the proposed algorithm is a fundamentally new system of automatic enumeration of parameters to fulfill the condition for ensuring the criterion of block 9. The second important aspect of this algorithm is the creation of a control system for the processing of objects by an ultrasonic cavitation unit in the optimal operating mode. The energy absorption coefficient (criterion 6), which characterizes the change in the specific energy P_{sp} and the ultrasound intensity I in the irradiated medium, serves as a criterion for evaluating the efficiency of the acoustic treatment of this medium.

6.3 DETERMINATION AND ASSESSMENT OF THE INFLUENCE OF THE WAVE IMPEDANCE OF THE MEDIUM ON THE ACTION OF THE ACOUSTIC APPARATUS

An important parameter of the cavitation process is the wave resistance of the medium of the acoustic apparatus. The characteristic impedance is the ratio of the acoustic pressure P_a to the vibration speed of the particles in the medium υ:

$$Z_a = \pm P_a / \upsilon. \tag{6.8}$$

The importance of knowing the coefficient Z_a is that it is an important characteristic of the interaction of the «acoustic apparatus – medium» system, not only as a resistance, but also as a characteristic of wave motion. Therefore, the obvious task of an effective acoustic device is its design, which ensures the transfer of maximum energy for the implementation of the cavitation process. That is why the signs should be taken into account in formula (6.9): the upper (plus) identifying the wave transmitted from the radiation surface into the medium (incident wave), and the lower (minus) for the wave traveling in the opposite direction, i.e. from the border of the system «apparatus – technological medium» (wave). Obviously, for efficient transmission of the energy of an acoustic wave, the properties of the apparatus and the medium must be consistent with each other.

This consistency consists in the fact that their wave supports must be the same, which is practically impossible in real conditions of the cavitation process. Indeed, the acoustic resistances for solid materials from which the emitting surface of the acoustic device is made, and the resistance of the technological medium, differ significantly from each other.

For example, such a hard material as sapphire has an acoustic resistance for longitudinal waves: $Z_a = 44.3 \cdot 10^6$ kg/(m². s), and for water $Z_a = 1.5 \cdot 10^6$ kg/(m². s), for air $Z_a = 4.27 \cdot 10^2$ kg/(m². s) [21]. Comparing these digital values, it becomes obvious that in order to solve the problems of rational design of an acoustic apparatus and determine its parameters, it is necessary to analytically investigate the sequence of acoustic matching of the apparatus and the technological medium in order to obtain the conditions for maximum energy transfer to the processing medium. For this, the process of propagation of an acoustic wave from the radiation surface of the apparatus to the processing medium is considered (**Fig. 6.3**).
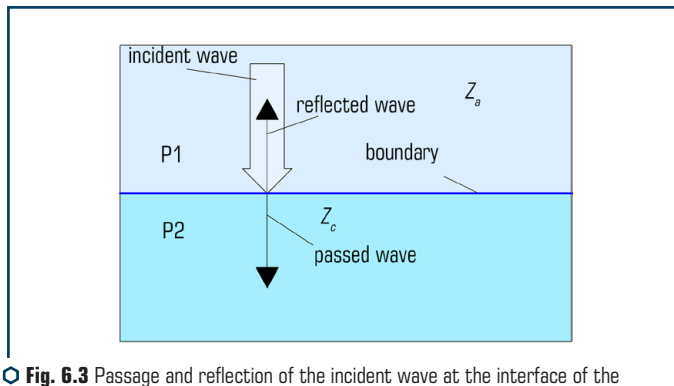
○ **Fig. 6.3** Passage and reflection of the incident wave at the interface of the «emitting surface of the cavitation apparatus – process medium» system

Let's assume that a plane acoustic wave along the X-axis from the apparatus to the boundary with the medium propagates with acoustic resistance Z_a, and in the medium at the border with the radiation surface of the apparatus along the same X-axis, due to the action of this resistance, wave resistance Z_c arises. It is quite obvious that, in addition to the wave transmitted into the medium, a wave moving in the opposite direction arises at the interface between the radiation surface and the medium. Thus, a complex wave field is formed, which can be represented by the transmission and reflection coefficients of the wave in the form:

$$K_{ref} = P_{aref} / P_{ainc} ; \ K_{pas} = P_{ainc} / P_{aref} . \tag{6.9}$$

By analogy with solving the equation of motion, it is possible to write expressions for the incident and reflected waves of pressure and speed:

$$P(x) = P_{ainc} e^{-ik_1 x} + P_{aref} e^{ik_1 x}; \ \upsilon(x) = \upsilon_{xinc} e^{-ik_1 x} + \upsilon_{xref} e^{ik_1 x}, \tag{6.10}$$

where $k_1 = \omega_1 / c_1$ – the wavenumber; i – imaginary unit.

Applying the condition of continuity of motion parameters in the contact zone of the «apparatus – medium» system (no violation of continuity):

$$P_a = P_e; \ \upsilon_a = \upsilon_e, \tag{6.11}$$

let's obtain:

$$\frac{P_{ainc}}{Z_a} - \frac{P_{aref}}{Z_a} = \frac{P_{apas}}{Z_e} . \tag{6.12}$$

Dividing the left and right sides by the amplitude of the acoustic pressure P_{ainc} and using (6.9) let's obtain expressions for determining the reflection and transmission coefficients of the wave:

$$K_{ref} = (Z_e - Z_a)/(Z_e + Z_a); \quad K_{pas} = 2Z_e/(Z_e + Z_a).$$

(6.13)

The condition for determining the wave impedance for its maximum transmission can be realized by introducing a compensator between the boundary of the radiation surface of the apparatus and the medium, which plays the role of resistance to the load and the reflection of acoustic waves exclusively in the zone of the apparatus (**Fig. 6.4**).
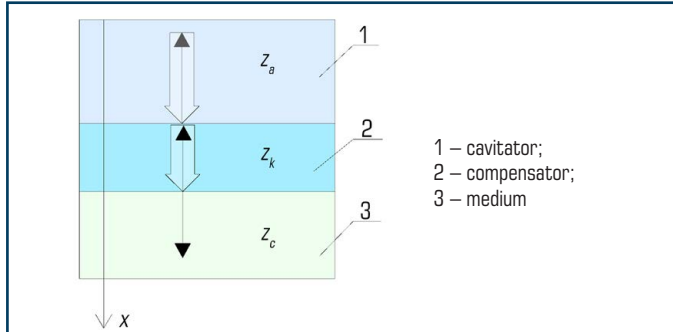
○ **Fig. 6.4** Passage and reflection of the incident wave in the system «radiation surface of the cavitation apparatus – compensator – technological medium»

In this case, the load resistance must be equal to the wave resistance of the medium: $Z_k = Z_e$.

Using solution (6.10) with the replacement $x = l$, where l – the length of the radiation surface of the apparatus, where the wave propagates, let's obtain the resistance in the section $(x = -l)$:

$$Z_{in}(x = -l) = \frac{P_a(-l)}{\upsilon(-l)} = Z_a \left[\frac{e^{ik_1 l} + k_{ref}5^{-ik_1 l}}{e^{ik_1 l} - k_{ref}5^{-ik_1 l}} \right].$$

(6.14)

Taking into account expression (6.14):

$$Z_{in} = -l = Z_a \frac{Z_e \cos k_1 l + i Z_a \sin k_1 l}{Z_a \cos k_1 l + i Z_e \sin k_1 l}.$$

(6.15)

If to assume that a compensator with a length is installed between the radiation surface of the apparatus and the medium $l = \lambda/4$, where λ – the wavelength in the compensator, then let's obtain the following dependence:

$$k_1 l = (2\pi/\lambda)/(\lambda/4) = \pi/2.$$

(6.16)

Substituting (6.16) into (6.15), let's obtain an expression for determining the input wave impedance:

$$Z_{in}\left(\lambda/4\right) = Z_a^2/Z_e. \tag{6.17}$$

So, choosing the value of the input resistance of the compensator with a length of $\lambda/4$, let's obtain the condition for maximum transmission, according to which the characteristic impedance of the apparatus and the compensator is in agreement. Indeed, by placing an auxiliary layer of material with such an acoustic impedance between the boundary of the apparatus and the medium, it is possible to ensure the equality of the acoustic impedance of the apparatus and the equivalent transmission line. Then the waves of reflection from both boundaries of the additionally installed layer will be equal to the amplitude and will move in antiphase direction, which will lead to their mutual compensation. And the shift between the phases of movement for $180°$ is provided by the difference in wave path between the boundaries at half the wavelength. Equality of amplitudes is ensured by the optimal choice of the wave impedance of the compensator. If the compensator has its own parameters: resistance Z_k, wavenumber k_k and thickness lk, then provided that $l_k = \lambda_k/4$ is the input resistance at the boundary $x = -l_k$:

$$Z_{in} = Z_k^2 / Z_e. \tag{6.18}$$

To fulfill the condition under which there were no reflected waves from the section $x = -l_k$, the input impedance (6.17) must be equal to the acoustic impedance of the apparatus Z_1:

$$Z_a = Z_k^2/Z_e. \tag{6.19}$$

From (6.19) let's obtain an expression for calculating the acoustic resistance of the compensator:

$$Z_k = \sqrt{Z_a Z_e}. \tag{6.20}$$

To apply dependence (3.72), which allows matching the acoustic impedance of the apparatus and the medium, it is necessary to determine the real numerical values of the wave impedance of technological media under conditions of their cavitation treatment.

One of the most important parameters, on which the wave impedance of the technological medium depends, is the wave propagation speed c. In terms of physical content, the dependence of the wave propagation speed determines the ratio of elastic (E) and inertial (mass ρ) characteristics of the technological medium:

$$c = \sqrt{E/\rho}. \tag{6.21}$$

An experimental device was created to measure the speed of wave propagation in a technological medium (**Fig. 6.5**).
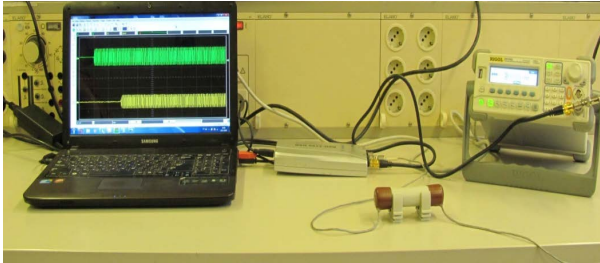
○ Fig. 6.5 Experimental device for measuring the speed of propagation of waves in a technological medium

The essence of the device is as follows. An electrical signal of a fixed ultrasonic frequency is referenced from the pulse generator to the transmitter. The sensor, which in this case is a transmitter and receiver, converts the incoming signal into elastic vibrations of the same frequency (inverse piezoelectric effect) passing through the layer of the technological medium. The receiver converts elastic vibrations of ultrasonic frequency into an electrical signal of the same frequency (direct piezoelectric effect) and sends the signal to the computer screen. The computer screen displays the generator impulse and the signal transmitted through the tube with the process medium (**Fig. 6.6**).

a *b*
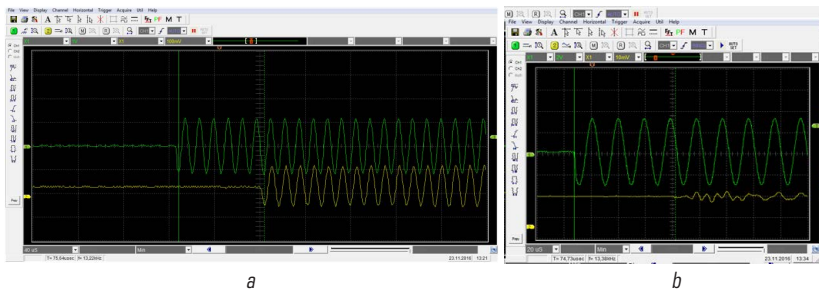
○ Fig. 6.6 Vibrograms for measuring acoustic parameters: *a* – water: $f=2.58$ MHz; *b* – $f=52$ kHz

The distance between them h characterizes the time t of passage of elastic vibrations from the source to the reflector and back. Consequently, the speed of propagation of waves in the technological medium is determined by the formula:

$$c=h/t. \tag{6.22}$$

6.4 METHODOLOGY AND ALGORITHM FOR DETERMINING THE RATIONAL PARAMETERS OF THE WORKING PROCESS OF ACOUSTIC TREATMENT OF TECHNOLOGICAL MEDIA

An algorithm was developed to calculate the parameters of the «cavitator – technological medium» ultrasonic cavitation system (**Fig. 6.7**).
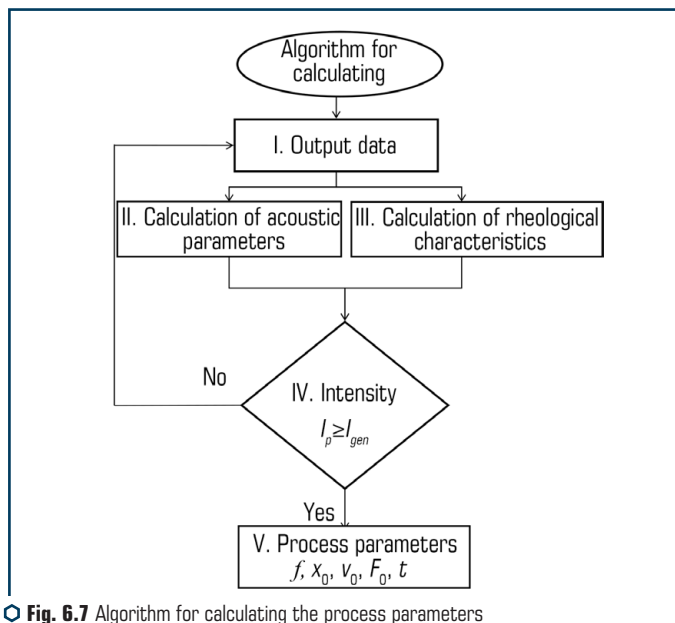
○ **Fig. 6.7** Algorithm for calculating the process parameters of the «cavitator – technological medium» ultrasonic cavitation system

The initial parameters used for the calculation are formed depending on the specific processing process or the creation of a new technological medium. The first step in the process of selecting the initial parameters is to substantiate the general scheme of the structural-parametric system «acoustic apparatus – technological medium» (**Fig. 6.1**) and the mode of action of the transducer on the medium. The structural-parametric scheme selected according to the algorithm (blocks 2–4, **Fig. 6.1**) requires specification of the limiting values of the parameters (block 6, **Fig. 6.1**) and the choice of a mathematical model of the «K-S» system (block 5, **Fig. 6.1**). In the future, the procedure for formulating the initial data, the calculation of acoustic parameters and the calculation of the rheological characteristics of the medium are carried out [4, 7–9, 11–15, 18–20, 22–26]. The criterion for the reliability of the calculation is the intensity (block IV, **Fig. 6.7**). When the numerical value of the intensity is provided, the procedure for calculating the process parameters is completed (block V, **Fig. 6.7**).

6.5 DISCUSSION OF RESEARCH RESULTS

The value of the input resistance of the compensator of length $\lambda/4$ is determined and the condition of maximum transmission is obtained, according to which the wave impedance of the apparatus and the compensator is in agreement. By placing an auxiliary layer of material with such an acoustic impedance between the boundary of the apparatus and the medium, equality of the acoustic impedance of the apparatus and the equivalent transmission line is ensured. Then the waves of reflection from both boundaries of the additionally installed layer will be equal to the amplitude and will move in antiphase direction, which will lead to their mutual compensation. And the shift between the phases of movement for 180° is provided by the difference in wave path between the boundaries at half the wavelength. As a result, the maximum transfer of energy from the acoustic device to the technological medium is created. For the implementation of the criterion assessment of the justification of the rational choice of the «acoustic apparatus – technological medium» structural-parametric system, an algorithm is proposed (**Fig. 6.1**). The essence of the algorithm lies in the ability to vary not only the initial parameters and the layout of the cavitator relative to the processing medium, but also to determine the influence of variable parameters on the maximum value of a particular criterion (**Table 6.2**). The necessary degree of influence and consideration of stages, rational modes and parameters for the development of techniques that implement an increase in the efficiency of the cavitation process in conditions of minimizing energy costs have been determined.

CONCLUSIONS TO SECTION 6

1. The estimation and methods of research of parameters of acoustic treatment of technological media have been carried out. The functional relationships between the acoustic parameters of the cavitation apparatus and the rheological properties of the processing technological media have been revealed. The process of staged acoustic treatment of technological media is described.

2. The analytical dependences of the determination of the main parameters of the cavitation apparatus have been obtained and the regularities of the processes of staged acoustic treatment of technological media in conditions of energy minimization have been established.

3. A number of criteria and key parameters have been determined, the use of which is carried out as an assessment in the calculation algorithm, depending on certain known initial data of the cavitator and the medium. The values of the input resistance of the compensator have been determined and the condition for the maximum transfer of energy from the acoustic apparatus to the technological medium has been obtained.

4. An algorithm is proposed to substantiate the rational choice of the «acoustic apparatus – technological medium» structural-parametric system, which allows to vary not only the initial parameters and the layout of the cavitator relative to the processing medium, but also to determine the effect of variable parameters on the maximum value of a particular criterion.

REFERENCES

1. Kaletnik, H., Sevostianov, I., Bulgakov, V., Holovach, I., Melnik, V., Ihnatiev, Ye., Olt, J. (2020). Development and examination of high-performance fluidised-bed vibration drier for processing food production waste. Agronomy Research, 18 (4), 2391–2409. doi: http://doi.org/10.15159/ar.20.234

2. Bulgakov, V., Sevostianov, I., Kaletnik, G., Babyn, I., Ivanovs, S., Holovach, I., Ihnatiev, Y. (2020). Theoretical Studies of the Vibration Process of the Dryer for Waste of Food. Rural Sustainability Research, 44 (339), 32–45. doi: http://doi.org/10.2478/plua-2020-0015

3. Kaletnik, G., Tsurkan, O., Rimar, T., Stanislavchuk, O. (2020). Determination of the kinetics of the process of pumpkin seeds vibrational convective drying. Eastern-European Journal of Enterprise Technologies, 1 (8 (103)), 50–57. doi: http://doi.org/10.15587/1729-4061.2020.195203

4. Bernyk, I. M. (2011). Osnovni zasady proektuvannia mashyn i obladnannia pererobnykh vyrobnytstv. Teoriia i praktyka budivnytstva, 8, 6–9.

5. Vitenko, T. M. (2009). Hidrodynamichna kavitatsiia u masoobminnykh, khimichnykh i biolohichnykh protsesakh. Ternopil: Vydavnytstvo TDTU im. I Puliuia, 224.

6. Khmelev, V. N., Slivin, A. N., Barsukov, R. V., Tsyganok, S. N., Shalunov, A. V. (2010). Primenenie ultrazvuka vysokoi intensivnosti v promyshlennosti. Biisk: Izd-vo Alt. gos. tekhn. un-ta, 203.

7. Nazarenko, I., Dedov, O., Bernyk, I., Rogovskii, I., Bondarenko, A., Zapryvoda, A. et. al. (2020). Determining the regions of stability in the motion regimes and parameters of vibratory machines for different technological purposes. Eastern-European Journal of Enterprise Technologies, 6 (7 (108)), 71–79. doi: http://doi.org/10.15587/1729-4061.2020.217747

8. Luhovskyi, O. F., Bernyk, I. M. (2014). Vstanovlennia osnovnykh parametriv vplyvu tekhnolohichnoho seredovyshcha na robochyi protses ultrazvukovoi kavitatsiinoi obrobky. Vibratsii v tekhnitsi ta tekhnolohiiakh, 3 (75), 121–126.

9. Bernyk, I. M. (2015). Enerhetyka kavitatsiinoi obrobky tekhnolohichnoho seredovyshcha. Naukovi pratsi ONAKhT, 1 (47), 123–129.

10. Luhovskaia, E. A., Yakhno, O. M., Bernyk, Y. N. (2012). Model of Technological Process of Ultrasonic Clearing of Elastic Surfaces Management. Naukovi pratsi Don NTU. Seriia: Hirnychoelektromekhanichna, 23 (196), 154–166.

11. Luhovskyi, O. F., Gryshko, I. A., Bernyk, I. M. (2018). Enhancing the Efficiency of Ultrasonic Wastewater Disinfection Technology. Journal of Water Chemistry and Technology, 40 (2), 95–101. doi: http://doi.org/10.3103/s1063455x18020078

12. Bernyk, I., Luhovskyi, O., Nazarenko, I. (2018). Effect of rheological properties of materials on their treatment with ultrasonic cavitation. Materiali in Tehnologije, 52 (4), 465–468. doi: http://doi.org/10.17222/mit.2017.021

13. Bernyk, I., Luhovskyi, O., Wojcik, W., Shedreyeva, I., Karnakova, G. (2019). Theoretical Investigations of the Interaction of Acoustic Apparatus with Technological Environment

Working Process. Przeglad Elektrotechniczny, 1 (4), 32–37. doi: http://doi.org/10.15199/48.2019.04.06

14. Luhovskyi, O., Bernyk, I., Gryshko, I., Abdulina, D., Zilinskyi, A.; Stryczek, J., Warzyńska, U. (Eds.) (2021). Mobile Equipment for Ultrasonic Cavitation Inactivation of Microorganisms in the Liquid Environment. NSHP 2020. Lecture Notes in Mechanical Engineering. Cham: Springer, 272–281. doi: http://doi.org/10.1007/978-3-030-59509-8_24

15. Bernyk, I., Luhovskyi, O., Nazarenko, I. (2016). Research staff process of interaction and technological environment in developed cavitation. Journal of Mechanical Engineering the National Technical University of Ukraine «Kyiv Polytechnic Institute», 1 (76), 12–19. doi: http://doi.org/10.20535/2305-9001.2016.76.39735

16. Bernyk, I. M. (2013). Intensification of technological processes of treatment of food environments. Vibratsii v tekhnitsi ta tekhnolohiiakh, 3 (71), 109–115.

17. Bernyk, I. M. (2014). Doslidzhennia parametriv kavitatsiinoho protsesu obrobky tekhnolohichnykh seredovyshch. Naukovo-tekhnichnyi zhurnal Tekhnika budivnytstva, 33, 21–26.

18. Bernyk, I. M. (2018). Investigation of the viscosity of dispersed media under conditions of their intensive processing. Tekhnika, enerhetyka, transport APK, 1 (100), 62–67.

19. Ohirko, O. I., Halaiko, N. V. (2017). Teoriia ymovirnostei ta matematychna statystyka. Lviv: LvDUVS, 292.

20. Sirotiuk, M. G., Gavrilov, L. R. (2008). Akusticheskaia kavitatsiia. Moscow: Nauka, 271.

21. Goliamina, I. P. (Ed.) (1979). Ultrazvuk. Malenkaia entsiklopediia. Moscow: Sovetskaia entsiklopediia, 400.

22. Nazarenko, I., Svidersky, A., Kostenyuk, A., Dedov, O., Kyzminec, N., Slipetskyi, V. (2020). Determination of the workflow of energy-saving vibration unit with polyphase spectrum of vibrations. Eastern-European Journal of Enterprise Technologies, 1 (7 (103)), 43–49. doi: http://doi.org/10.15587/1729-4061.0.184632

23. Nazarenko, I., Gavryukov, O., Klyon, A., Ruchynsky, N. (2018). Determination of the optimal parameters of a tubular belt conveyor depending on such an economical. Eastern-European Journal of Enterprise Technologies, 3 (1 (93)), 34–42. doi: http://doi.org/10.15587/1729-4061.2018.131552

24. Nazarenko, I. I., Ruchynskyi, M. M., Sviderskyi, A. T., Kobylanska, I. M., Harasim, D., Kalizhanova, A., Kozbakova, A. (2019). Development of energy-efficient vibration machines for the buiding-and-contruction industry. Przeglad Elektrotechniczny, 95 (4), 53–59. doi: http://doi.org/10.15199/48.2019.04.10

25. Nazarenko, I., Gaidaichuk, V., Dedov, O., Diachenko, O. (2018). Determination of stresses and strains in the shaping structure under spatial load. Eastern-European Journal of Enterprise Technologies, 6 (7 (96)), 13–18. doi: http://doi.org/10.15587/1729-4061.2018.147195

26. Nazarenko, I., Gaidaichuk, V., Dedov, O., Diachenko, O. (2017). Investigation of vibration machine movement with a multimode oscillation spectrum. Eastern-European Journal of Enterprise Technologies, 6 (1 (90)), 28–36. doi: http://doi.org/10.15587/1729-4061.2017.118731

7

STUDY OF RELIABILITY OF TECHNICAL SYSTEMS RELIABILITY

I. Nazarenko, M. Delembovskyi, O. Dedov,
A. Onyshchenko, I. Rogovskii, M. Nazarenko, I. Zalisko

ABSTRACT

The main states of reliability of a technical system and its elements are investigated by the example of vibration platforms for compacting concrete mixtures. Experimental studies on the development of vibration platforms for failure have been carried out. Complex indicators were used, which were the coefficient of technical utilization, the coefficient of availability and durability. The received data of malfunctions was made by fixing by groups of prefabricated units, parts and elements to determine the data on their operating time. Based on these data, the analysis of the operating time of the main elements to failure and the most frequently out of order was carried out. The conducted research identified the main prefabricated units and failing parts: engine, gearbox, synchronizer, vibration exciter, propeller shafts, couplings. At the same time, propeller shafts and couplings most often failed. In some cases, the destruction of bearings in vibration exciters has been evidenced. The parameters of the Weibull distribution law have been determined and graphs have been constructed for the model of reliability and failures of propeller shafts of vibration platforms. A graph of the dependence of reliability on the operating time and graphs of the regularities of the distribution of resource indicators and the distribution function, which served as information for the development of recommendations, were built.

KEYWORDS

Technical system, reliability, vibration platform, prefabricated units, complex indicators, distribution laws, technical utilization factors, availability and durability.

7.1 STATEMENT OF THE PROBLEM AND ANALYSIS OF METHODS FOR DETERMINING THE RELIABILITY INDICATORS OF VIBRATION PLATFORMS

Ensuring the reliability of vibration platforms in the construction industry [1–3] is an important problem of increasing their efficiency. The process of operating technical systems is impossible without performing technical services, the most important task is to restore the working condition of machines or units by eliminating failures during operation, as well as overhaul or refurbishment at manufacturing enterprises. Repair planning assumes the availability of information on reliability indicators in order to perform high-quality repairs with the least amount of time.

In vibration platforms, when performing work, there is a probability of failure (random and fluctuations) in the process of deviation of specified fluctuations, considered as a result of changes in time of the parameters of the system (amplitude of fluctuations, accelerations, permissible stresses in the structural elements of vibration platforms). The analysis of random events of oscillatory processes [1, 2] makes it possible to assess such deviations associated with the processes of accumulation of failures, which are the subject of the theory of reliability.

Assessment of the reliability of technical systems generally implies an integrated approach to solving the procedure for assessing reliability indicators at all stages of the existence of such systems. Methods for assessing such indicators are based on the use of mathematical models of the existence of a system, depending on the stage of the life cycle of a technical object. The physical essence of the existence of a system is due to the presence of a number of factors and factors that must be taken into account when creating a model.

So at the design stage, methods are used to predict reliability characteristics based on general methods of probability theory, analytical mechanics, theory of machines and devices, resistance of materials, vibration theory, etc.

Structural methods of calculation are characteristic at the stages of manufacturing and operation of technical structures, since they involve the consideration of the system by means of a structural-functional diagram. In such a logical scheme, the transition of a system from one state to another, the relationship between such states, the interaction of system elements, taking into account their functional purpose, manufacturing technologies, and conditions of use are investigated.

Physical methods are used to determine reliability, durability and safety of technical objects for which degradation mechanisms are known under the influence of external and internal factors, which leads to failures – the limiting state during operation. Such methods are based on the representation of processes using mathematical models capable of determining reliability indicators taking into account the design features, manufacturing technology of its individual elements, operating modes, etc.

Each of the methods has its own advantages and disadvantages, therefore, in specific cases, it is more efficient to use a combination of such methods to solve the problem. This approach allows one to obtain a result that has not only an imaginary understanding of the existence of a technical system, but also has a physical essence, confirmed by experimental research.

One of the methods that satisfy an integrated approach to solving the problem is the probabilistic-physical method of reliability analysis. This method of reliability analysis involves the use of probabilistic-physical reliability models, the parameters of which have a specific physical interpretation and relate the value of the probability of failure and the physical (determining) parameter, which leads to failure. Among the advantages of this method, there is a quantitative assessment of the reliability indicators of systems (elements) both on the basis of statistical information about failures and statistical information about physical processes leading to failures. In this case, all data is used in aggregate and separately.

Thus, the application of the above method will make it possible to assess the necessary reliability indicators, including the complete characteristic – the distribution law based on the processing of statistical data on the failure of technical structures.

Prediction of the reliability of vibration platforms occurs at all stages of design, operation and repair [3–5]. At the same time, it is important to obtain the design parameters of parts and assemblies depending on predicting reliability indicators: mean time between failures, reliability, durability and maintainability.

Today in this area the works of such scientists as: I. Kravchenko, V. Bolotin, A. Barash, A. Pronikov, K. Frolov and others are known. As a basis for research for assessing the reliability of vibration platforms, a model was adopted in which the object under study is in one of the following states: serviceable, faulty, efficient, disabled and extreme. The structural and logical diagram of the technical system and the path of transition from one state to another is shown in **Fig. 7.1**.
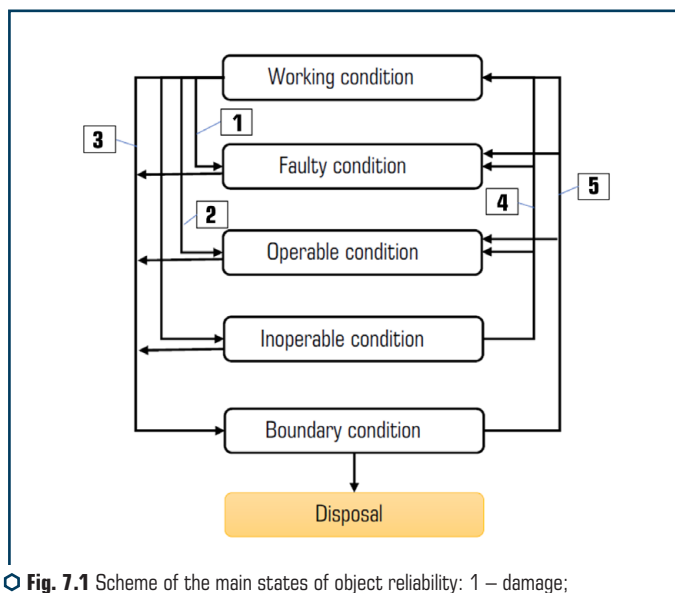
○ **Fig. 7.1** Scheme of the main states of object reliability: 1 – damage; 2 – failure; 3 – transition to the limiting state; 4 – recovery; 5 – repair

For the implementation of research, the following states of the system and their evaluation criteria were adopted:

— working condition – a property of the vibration platform, in which it meets all the requirements of the normative, technical and design documentation;

— faulty condition – a property of a vibration platform, in which it does not meet at least one requirement of regulatory, technical and design documentation;

— operable condition – a property of a vibration platform, at which the value of all parameters, characterizing the properties of performing specified functions, meet the requirements of normative, technical and design documentation;

— condition — a property of a vibration platform, in which the value of at least one parameter characterizing the property of performing a given function does not meet the requirements of regulatory, technical and design documentation;

— boundary condition — a property of a vibration platform [5], in which its further use for its intended purpose is unacceptable and impractical, or the restoration of its serviceable or service-able state is impossible or impractical (**Table 7.1**).

● **Table 7.1** Criteria for the limiting state of the components of the vibration platform

Unit or unit name	Limit state criteria
Frame structures	1. Tiring transverse cracks along the perimeter of more than 40 %. 2. Concavity, twisting and other damage exceeding permissible limits, for elimination of which it is necessary to completely dismantle the frame structure
Gear transmission	1. Limiting wear of teeth. 2. Crumbling of the working surface of the tooth with a total area of more than 25 %
Clutch coupling	Worn splines or bearing seat on the shaft or breakage of the shaft, in which it is necessary to replace it
Propeller shaft	1. Crack in pipes, forks along welded seams. 2. Limiting wear of spline joints. 3. Limit wear of the bores for the bearing shells

Failures are divided by reason of occurrence, nature of manifestation, interrelation, groups of complexity and method of detection. In addition, there are resource and degradation failures. The classification of failures depending on the nature of their occurrence and the course of development processes leading to the onset of failure are shown in **Fig. 7.2**.
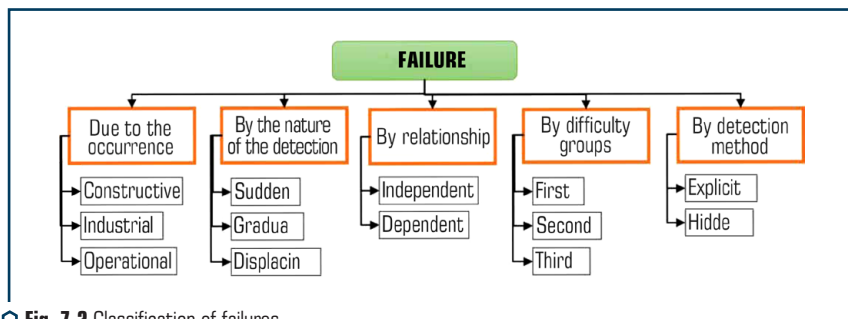
○ **Fig. 7.2** Classification of failures

Thus, improving the quality and reliability of a vibration platform [5] depends on many reasons, the main of which is the quality of vibration equipment. An integral part of quality is the accuracy class of the vibration platform or the error with which the vibrations are simulated. Therefore,

the task of the study is not only to assess the reliability of existing structures, but also in new technical systems of complex structure. To solve such a problem, a set of criteria is proposed, the assessment of which will improve the quality of such technical systems.

7.2 ENSURING THE RELIABILITY OF VIBRATION PLATFORMS IN THE CONSTRUCTION INDUSTRY, TAKING INTO ACCOUNT THE METHODS OF ANALYSIS

Vibration platforms are widely used in the construction industry in the manufacture of concrete and reinforced concrete products. The effectiveness of their work largely depends on a fairly specific accounting of the operating forces of the system and the reliability of the parts of the vibration platforms. Currently, there are practically no works on the development of methods for assessing the reliability of vibration platforms in various modes of their operation. However, the practice of operating vibration platforms in the construction industry testifies to the frequent failure of parts and assemblies of these machines, which significantly reduces their performance in the operating modes provided for by the technology. As a result of this situation, formed goods may be defective. Therefore, the problem of reliability methods, determination of its criteria and improvement of the design of elements of vibration areas is urgent.

In accordance with DSTU 2861-94, reliability analysis for vibration platforms can be carried out in order to:

— checking the feasibility of the established requirements and assessing the likelihood of achieving the required level of reliability of the components and the object as a whole;

— verification of the effectiveness of the proposed (implemented) measures for finalizing the design, manufacturing technology, maintenance and repair strategies to improve reliability;

— predicting reliability and choosing the best ways to ensure or improve reliability.

Considering the above, the methods of analyzing the reliability of vibration platforms [1—6] are used to predict the reliability, maintainability, readiness and measures to guarantee safety, as well as to fulfill the consequences of forecasting with the given requirements.

Consequently, the tasks of reliability analysis and their scope depend on the stage of the life cycle of vibration platforms, the depth of development and reliability, the consequences of failures and their limiting states, and other factors.

The DSTU 2861-94 standard establishes two main approaches to the analysis of the reliability of all objects, including vibration platforms:

— analysis of the reliability of vibration platforms based on the results of measures and methods of ensuring reliability at the stages of design, production and operation in accordance with the reliability assurance program;

— quantitative methods for analyzing the reliability of vibration platforms based on the analysis of operating conditions, causes and mechanisms of failures, reliability indicators of elements, maintenance and repair strategies.

The analysis of the reliability of vibration platforms presupposes a reliability assurance program (**Fig. 7.3**), according to the results of the implementation of which the desired result can be achieved.
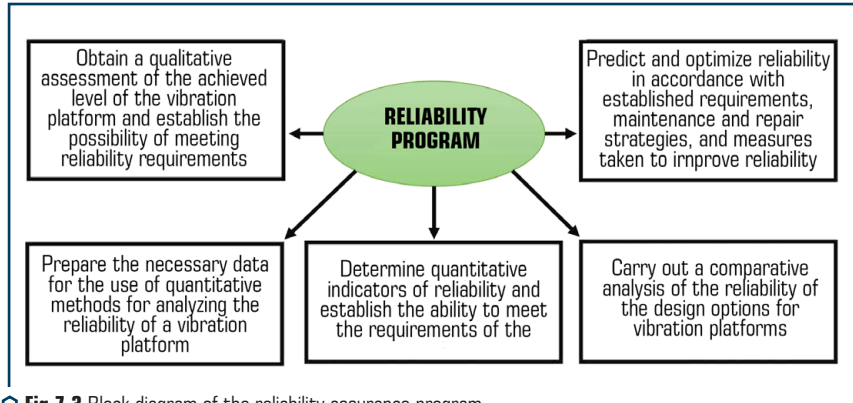
⭘ **Fig 7.3** Block diagram of the reliability assurance program

The analysis of the reliability of the vibration platform system is carried out using the following methods:

— qualitative analysis (determination of types of malfunctions, failure mechanisms of elements and their consequences for the system, analysis of the functional diagram of the system, analysis of the maintenance and repair system, construction of structural diagrams of system reliability);

— quantitative analysis (construction of mathematical models of the reliability of elements and systems according to the indicators under consideration, obtaining quantitative indicators of reliability by calculation or modeling, analysis of the importance of failures and sensitivity, assessment of the possibility of improving the characteristics of the system based on backup subsystems and maintenance and repair strategies).
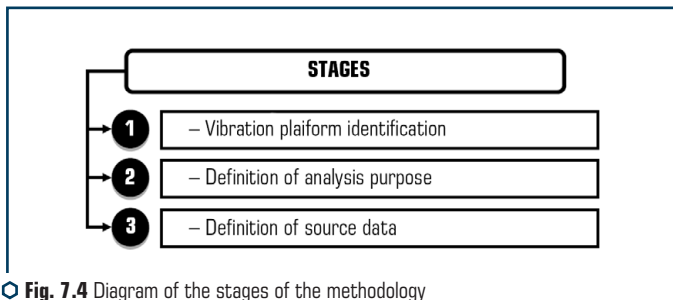
⭘ **Fig. 7.4** Diagram of the stages of the methodology for analyzing the reliability of vibration machines

Accordingly, the assessment of the analysis results involves comparison with the mandatory reliability indicators and recommendations for measures to comply with the mandatory reliability indicators, which may include a design review, identification of weak points, imbalances, modes, replacement of parts with a high risk of malfunctions, development of alternative ways to improve reliability, implementation trade-off analysis and cost estimation of vibration platform design options as a whole.

7.3 EXPERIMENTAL STUDIES OF RELIABILITY ASSESSMENT BASED ON FUZZY LOGIC

The solution to the problem of increasing the reliability and efficiency of vibration machines is achieved by studying the parameters and characteristics of failures of the elements of a vibration machine in the operation stage to develop recommendations for determining the reliability indicators of units and parts of vibration machines with an increase in their efficiency.

To a large extent, the study of reliability indicators requires the involvement of a large number of observations, which in fact takes quite a significant amount of time. Taking this into account, it is necessary to carry out studies of reliability indicators using modern information technologies and alternative solutions to the problem.

When performing work on modeling the assessment of the reliability of vibration machines based on a fuzzy model, it is necessary to represent them in the form of fuzzy networks, the elements and sets of elements of which implement various components of fuzzy models and stages of fuzzy inference.

In his work, Lotfi Asker Zadeh presented a fuzzy productive model as follows [4, 7]:

$$(i): Q; P; A \Rightarrow B: S; F; N, \tag{7.1}$$

where Q – field of application of fuzzy products; P – condition for the activation of the fuzzy production core; A – condition of the kernel (antecedent); B – kernel output (consequent); S – method for determining the quantitative value of the degree of truth of the kernel output; F – coefficient of confidence of fuzzy products; N – post condition of the productive rules.

A fuzzy imitation of the relationship between antecedent and consequent can be viewed as fuzzy production:

if $x \in A$, then $y \in B$;

X – domain of definition of the antecedent;

A – fuzzy set visible on X;

$\mu_A(E) \in [0,1]$ –membership function of an odd set A;

Y – area of definition of the consequent;

B – fuzzy set defined on Y;

$\mu_B(E) \in [0,1]$ – membership function of an odd set B.

If the ratio function of odd sets $A - \mu_A(E)$, is known, then for odd sets B, the ratio function is determined by the composition rule:

$$\mu_B(C) = \sup_{x \in X} \left\{ T \left(\mu_A(x), \mu_B(x,y) \right) \right\},\tag{7.2}$$

where sup — operation of determining the upper limit of the sets of parts; T — T-norm operation.

When modeling the failures of vibration machines as a rule for calculating fuzzy implication, the classical fuzzy implication of L. Zadeh:

$$\mu_B(x,C) = \max \left\{ \min \left[\mu_A(x), \mu_B(y) \right], \left[1 - \mu_A(x) \right] \right\}.\tag{7.3}$$

For the purpose of inference, the main methods in a fuzzy production model are forward and backward inference. Direct inference is based on such a concept as *fuzzy modus ponens*.

In the process of developing a fuzzy production model, the assessment of failures of vibration machines requires the formulation of certain conditions $X = \{ E_i \}, i = \overline{1, n}$ — factors that are the source of failures, and therefore the entire range of conclusions $Y = \{ y_v \}, j = \overline{1, m}$ is an indicator of failures of various elements and components of vibration machines.

Based on the previously established objects and concepts of the systems under consideration, namely vibration platforms, it is necessary to formulate the corresponding linguistic variables:

M — electric motor;

S — synchronizer;

C — clutch;

R — bearing (roller);

P — propeller shaft;

SP — support;

F — frame (vibration plate).

Let's take B as the initial linguistic variable — the level of failure.

Let's define terms for input and output linguistic variables. For input linguistic variables P, R, M let's introduce term-sets {critically low, low, average, high, critically high}, for S, C, SP, F — {low, medium, high}. The term sets of the initial linguistic variable describe the failure detection rate — {absent, unlikely, low, high enough, critically high}.

The level of failure of a vibration platform is estimated in the process of fuzzy inference, using a large number of fuzzy rules that make up the aggregate knowledge base of a given subject area, represented in the form:

If (x_1 is A) and (x_2 is B), then (y is C),

where A, B, C — linguistic values, identified in a fuzzy way through the corresponding membership functions for the variables x_1, x_2 and y.

As a result of the study, a fuzzy knowledge base was determined, presented in the form of certain rules [7].

For further modeling of this kind of system, the Fuzzy Logic Designer software toolkit is used, which is a MATLAB b2020 extension package containing tools for designing a fuzzy logic system [6].

When determining the shapes of the curves of membership functions, it is taken into account that they are constructed subjectively according to the results of a survey of experts, therefore, in a sense, they are «approximate». The most common membership function is of the Gaussian type [8, 9], but in practice, the shape of the membership function curves is chosen based on the complexity of the calculations. The most widespread are triangular and trapezoidal membership functions due to their versatility and lower requirements for computing resources in their hardware implementation.

To display the selected fuzzy subsets of linguistic variables, let's them. The parameters of the input membership functions are shown in **Fig. 7.5**.
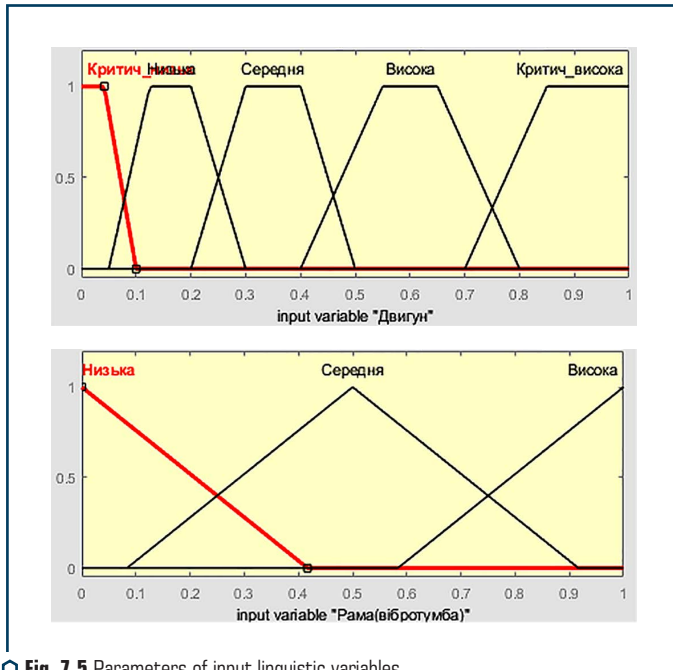
○ **Fig. 7.5** Parameters of input linguistic variables

The Mamdani algorithm, which has received the greatest practical application in fuzzy modeling problems and consists in the application of a mini-maximum composition of fuzzy sets, is used as a mechanism for the fuzzy logical inference being developed.

The process of processing fuzzy inference rules in this case consists of four stages:

1. Fuzzification, which consists in determining the degree of truth, that is, the value of the membership function for the premises (left-hand sides) of each rule.

2. Fuzzy inference, which consists in applying to the conclusions (right side) of the rules of the calculated truth value for the premises of each rule. As the inference rules in the Mamdani method, the minimum (min) operation is used, which «cuts off» the membership function of the rule conclusion by height, which corresponds to the calculated degree of truth of the rule prerequisite.

3. A composition that combines, using the maximum (max) operation, all fuzzy subsets defined for each variable output, and forms one fuzzy subset for each variable output.

4. Defasification, which realizes the scalarization of the composition result, i.e. transition from fuzzy subset to scalar value.

The scheme of the described fuzzy inference system implemented in the MATLAB medium is shown in **Fig. 7.6**.
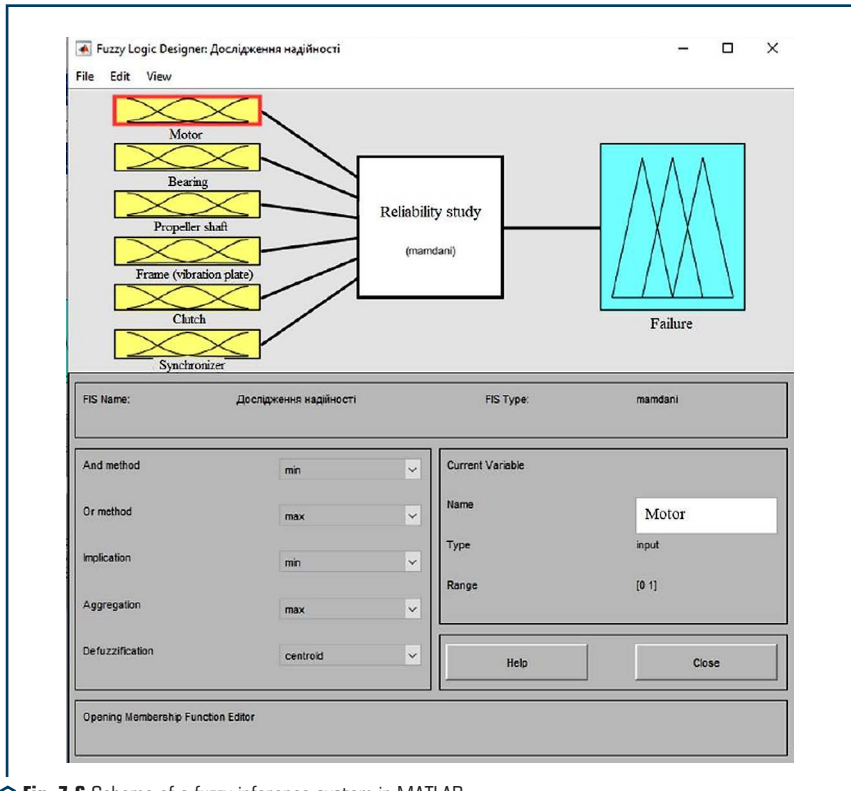
○ **Fig. 7.6** Scheme of a fuzzy inference system in MATLAB

This system makes it possible to assess the failures of vibration platforms based on the input linguistic variable, the parameters of which are shown in **Fig. 7.7**.
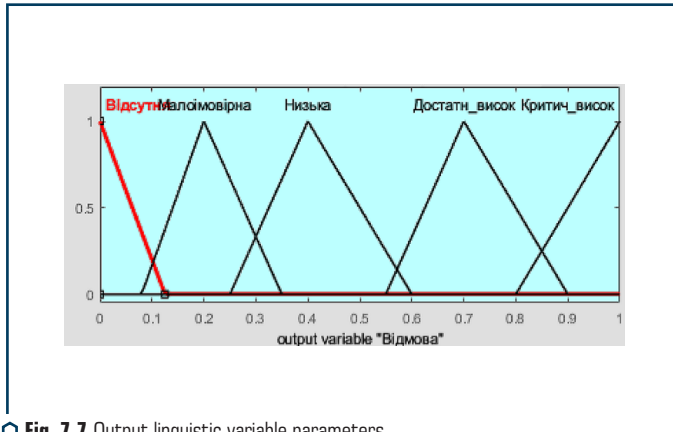
○ **Fig. 7.7** Output linguistic variable parameters

When performing the appropriate calculation, it is possible to preliminarily assume based on certain studies and observations that have input data, namely:

1. Engine – probability of failure 0.2.
2. Bearings – probability of failure 0.7.
3. Propeller shafts – probability of failure 0.7.
4. Frame (vibration plate) – probability of failure is 0.1.
5. Clutch – probability of failure is 0.4.
6. Synchronizer – probability of failure 0.25.

Thus, taking into account the corresponding coefficients, let's obtain the results of constructing fuzzy logic, which in this case will be based on certain 27 rules, according to which the overall failure rate of the vibration platform will be 0.624 (**Fig. 7.8**).

Accordingly, based on this range of values, it can be argued that the level of failure of the vibration platform is at a sufficiently high level.

Conducted similar studies of the presented fuzzy model for different sets of initial data also showed acceptable results (**Fig. 7.9–7.12**).

Failure to operate the vibration platform leads to downtime of the entire technological line and damage to the concrete mixture that has already been supplied to the line. In turn, this approach as a whole gives a clearer idea of which constituent elements need to be paid more attention to during the repair and maintenance of vibration platforms.

The use of this approach can significantly reduce the cost of maintaining vibration platforms and, accordingly, reduce the downtime rate of the production lines of the shop.
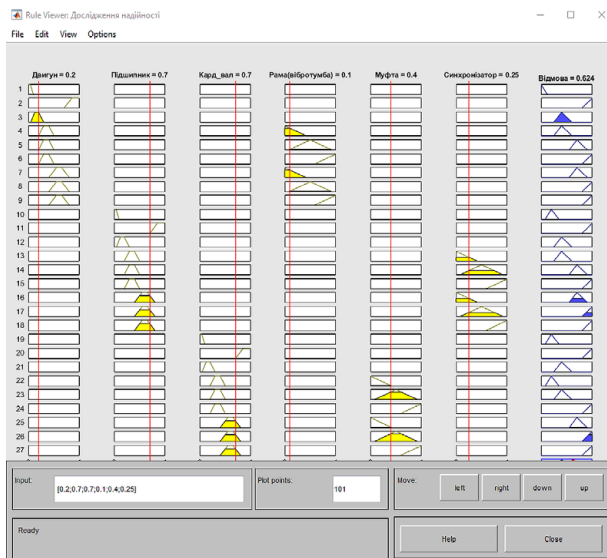
○ **Fig. 7.8** Results of calculating fuzzy logic for 27 rules
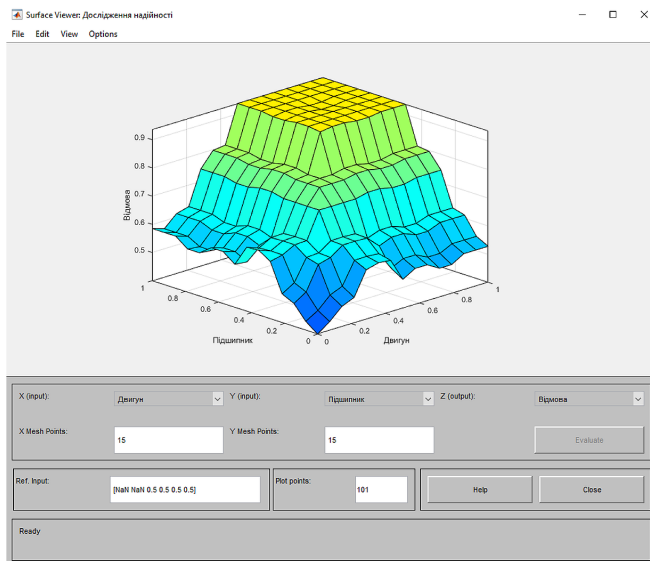
○ **Fig. 7.9** Indicators of the effect of motor and bearings on failure
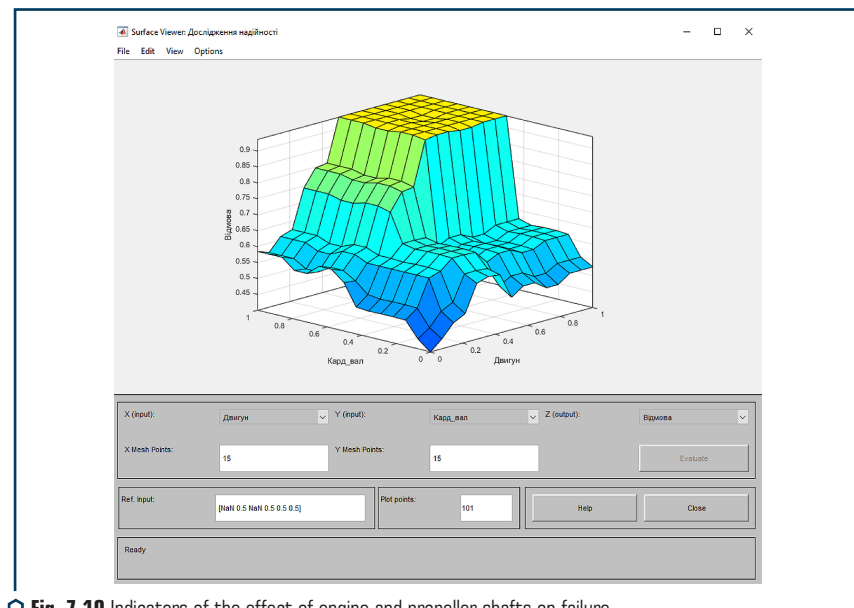
Fig. 7.10 Indicators of the effect of engine and propeller shafts on failure
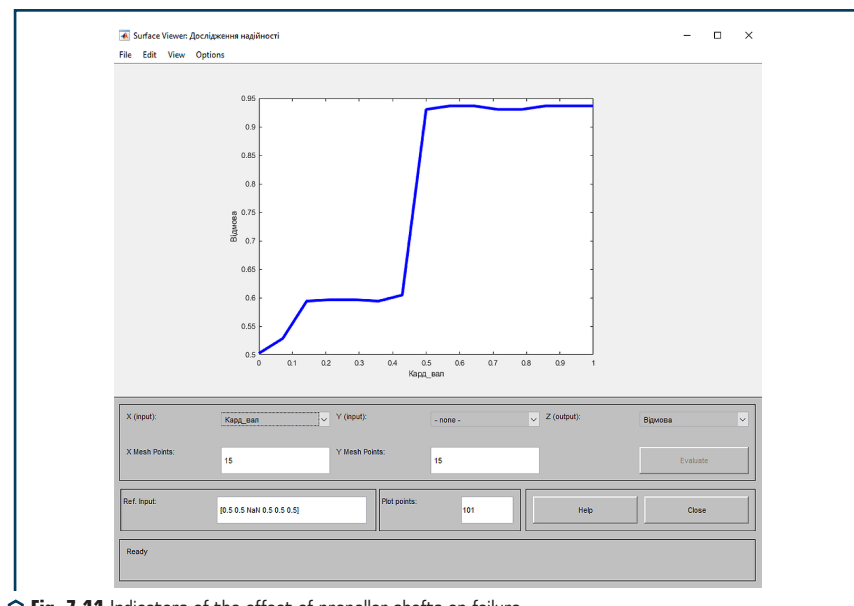
Fig. 7.11 Indicators of the effect of propeller shafts on failure
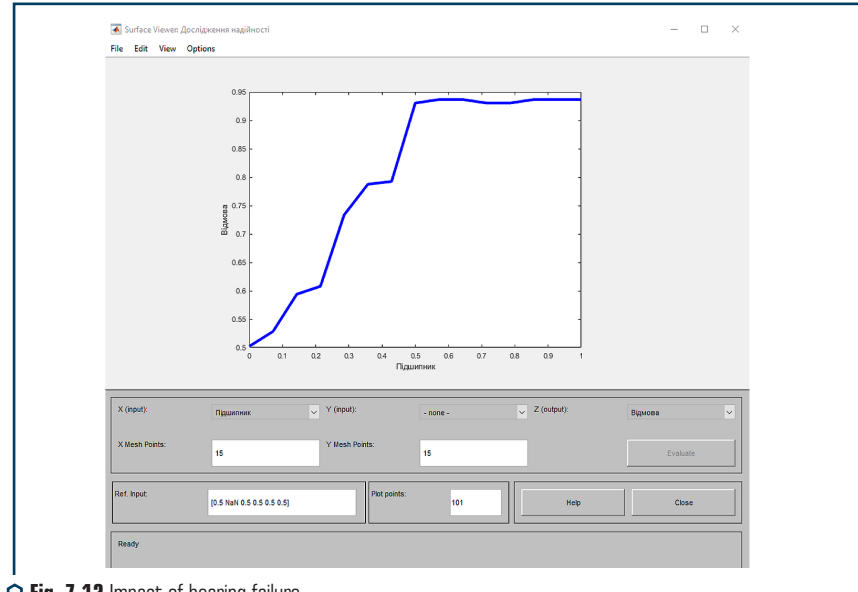
○ Fig. 7.12 Impact of bearing failure

7.4 CALCULATION OF VIBRATION RELIABILITY OF A TECHNICAL SYSTEM

When calculating the vibration reliability of optimal vibration protection, a vibration platform [7] was considered as a system described by the equation of motion:

$$\ddot{u} + 2\varepsilon \cdot \dot{u} + \omega_0^2 \cdot u = -a_0(t).$$

Accordingly, the quality conditions are reflected in the form:

$$\left|u(t)\right| \le u_*, \left|a(t)\right| \le a_*, \tag{7.4}$$

where $a = a_0 + \ddot{u}$ — absolute vibration acceleration. As a criterion for the optimality of the system in terms of reliability, the condition is selected so that the reliability functions (7.4) at the time instant $t = T_*$ acquire a maximum value.

$$P(t) = P\left\{ \begin{matrix} \sup_{\tau} \left\|a(x_j, \tau)\right\| \le a_*, \ \sup_{\tau} \left\|a(x_j, \tau)\right\| \le u_* \\ j = 1,2,\ldots; \qquad \tau \in [0,t] \end{matrix} \right\}. \tag{7.5}$$

Taking into account the high reliability of systems for stationary oscillations, this condition, according to:

$$P(t) \approx 1 - \int_0^t \lambda(\tau)d\tau,$$

is equivalent to the condition $\lambda(\Gamma) = \min$, ε, ω_0, where the average number of emissions per unit time is calculated for a rectangular region of available states (7.5).

It is proposed that the process $a_0(t)$ at the output of the system is narrow-linear with a carrier frequency θ. In **Fig. 7.5** the results of the corresponding calculation data $\lambda(\Gamma)$ are carried out at $u_* = 10^{-3}$ m, $a_* = 20$ m/s^2.

In **Fig. 7.13** a graph is built according to the calculation $\lambda(\Gamma)$ performed for the case of an exponentially correlated process at the input with a correlation $K_{a_0}(\tau) = \sigma_0^2 \cdot \exp(-a|\tau|)$. Considering the above, calculations have been made for the parameter values $m \, \varepsilon/\omega_0 = 0.5$, $a_* = 2\sigma_0$, $U_* = \left(\sigma_0/a^2\right) \cdot 10^{-4}$. Curves 1 in **Fig. 7.5, 7.6** correspond to band emissions $|a| < a_*$, curve 2 – band emissions $|U| < U_*$, curves 3 are plotted for the total number of emissions.
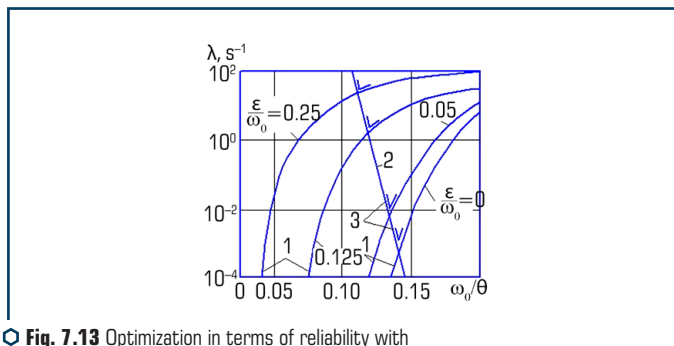
Fig. 7.13 Optimization in terms of reliability with a narrow-linear initial impact
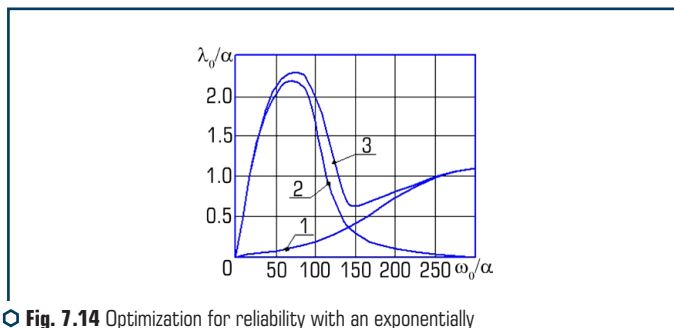
Fig. 7.14 Optimization for reliability with an exponentially correlated initial action

Basically, vibration loading is accompanied by a process of accumulating fatigue damage. The calculation of damages characterized by a one-dimensional process $v(t)$ was carried out accordingly. Accordingly, this process is rather slow, therefore, it requires a transition from $v_{k+1} = v_k + f(v_k, s_k)$ to a continuous analogue – a kinematic level:

$$\frac{dv}{dt} = g(v, s).$$ (7.6)

In such a case, the measure of damage $v(t)$ is an unfortunate function, $0 \le v \le 1$. In the above equation (7.5) $s(t)$ – some characteristic value for the load process $f(t)$, for example, amplitude. Taking this into account, the quality condition was chosen in the form $v < v_* = 1$, $s < s_*(v)$, where $s_*(v)$ – the limiting value of the bearing capacity, taking into account the accumulation of damage. In this case, the reliability function:

$$P(t) = P\left\{v(\tau) < 1, s(\tau) < s_*(v), \tau \in \left[0, t\right]\right\}.$$

As a rule, as the damage caused by the fatigue process takes place:

$$V_k = \sum_{j=1}^{k} \frac{1}{N(S_j)},$$

where $N(S_j)$ – the number of cycles leading to failure with a characteristic S_j, then the condition of fatigued failure takes the form:

$$\sum_j \frac{1}{N(S_j)} = 1.$$

To assess the durability, a value T_* equal to the duration of the load, which is necessary to achieve the condition $v = v_* = 1$, is used. Therefore, with a low dispersion of durability, the value T_* is close to the mathematical expectation $\langle T \rangle$. The value T_* is called the expected durability. Accordingly, if do not take into account the probability of instantaneous destruction due to the process bursting beyond the level $s_*(v)$, then the expression for the expected durability takes the form:

$$T_* = T_e \cdot \left[\int_0^\infty \frac{p(s)ds}{N(s)}\right]^{-1},$$ (7.7)

where T_e – some effective cycle period; $p(s)$ – distribution of the parameter s – the loading process $f(t)$.

Having considered the suitable processes, it can be argued that for stationary normal narrow-linear load processes, the maximum value $m\ s(t) = f_{max}(t)$ is taken as the characteristic value $m\ s(t)$. In this case, the distribution of the maximums of the normal process was found by the formula:

$$p_{max}(v_*) = \frac{1}{\sqrt{2\pi}\beta \cdot \sigma_v} \cdot \left\{ \sqrt{\beta^2 - 1} \cdot \exp\left[-\frac{\beta^2 \cdot (v_* - a)^2}{2(\beta^2 - 1) \cdot \sigma_v^2} \right] + \right.$$

$$\left. + \sqrt{2\pi}\, \frac{v_* - a}{\sigma_v} \cdot \exp\left[-\frac{(v_* - a)^2}{2\sigma_v^2} \right] \cdot \Phi\left(\frac{v_* - a}{\sqrt{\beta^2 - 1}\sigma_v} \right) \right), \tag{7.8}$$

where

$$\beta - \frac{\sigma_{\dot{v}} \cdot \sigma_v}{\sigma_{\dot{v}}^2} = \frac{\lambda_{max}(-\infty)}{\lambda(0)}.$$

Calculations made according to the formula (7.7) with a power-law approximation of the fatigue curve:

$$N = N_1 \cdot \left(\frac{s_1}{s} \right)^m \quad (s \geq s_1),$$

$$N \to \infty, \qquad (s < s_1)$$

give this expression:

$$T_* = \frac{N_1 \cdot X^m \cdot T_e}{2^{m/2} \cdot \Gamma\left(1 + \dfrac{m}{2}\right) \cdot P(X^2, m + 2)},$$

where $X = s_1/\sigma_s$; N_1, s_1, m — empirical constants; $P(X^2, T)$ m function X^2 — Pearson distribution. The same expression, expressed due to an incomplete gamma function $\Gamma(a, x)$, is:

$$T_* = \frac{N_1 \cdot X^m \cdot T_e}{2^{m/2} \cdot \Gamma\left(1 + \dfrac{m}{2}, \dfrac{X^2}{2}\right)}.$$

Accordingly, for wide-linear load processes, there are different ways to select the load parameter, leading to different estimates of durability. To give an example of a cycle, the following maxima, maximum values, half-difference of subsequent maxima and minima, maximum process values at a certain characteristic time interval, etc. are considered. To schematize a given process by a load of some equivalent narrow-linear process, methods have been proposed: outliers (the number of cycles coincides with the average number of process zeros), maxima (the number of cycles is taken as the average number of process maxima), swing (a cycle is characterized by an amplitude equal to half the process increments between adjacent ones), full cycles (a method consisting in the sequential elimination of the process of intermediate cycles with increasing amplitudes), etc.

Having considered the expression for the probability density $p(s)$ of the load parameter $s(t)$ in the case of a stationary normal process $f(t)$, the distribution of the maxima $p_1(s)$ is given by formula (7.8). By emission method:

$$P_0(s) = \frac{s}{\sigma_s^2} \exp\left(-\frac{s^2}{2\sigma_s^2}\right);$$

by calculation method:

$$P_2(s) = \frac{\beta^2 \cdot s}{\sigma_s^2} \cdot \exp\left(-\frac{\beta^2 \cdot s^2}{2\sigma_s^2}\right);$$

by full cycles method:

$$P_3(s) = \begin{cases} \dfrac{\beta^2 \cdot s'}{\sigma_s^2} \cdot \exp\left(-\dfrac{\beta^2 \cdot a^2 \cdot s^2}{2\sigma_s^2}\right) & (s < s_k); \\ \dfrac{c}{\beta} \cdot \dfrac{s}{\sigma_s^2} \cdot \exp\left(-\dfrac{s^2}{2\sigma_s^2}\right) & (s < s_k), \end{cases}$$

where β – coefficient of wide linearity of the process; a, c, s_k – some constants.

The nature of the dependence of the expected durability (7.7) on the nature of the wide linearity β is shown in **Fig. 7.7**.
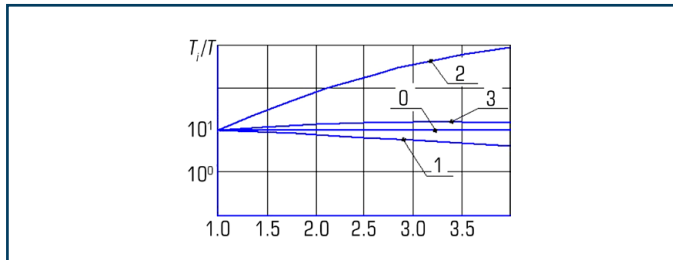
○ **Fig. 7.15** Comparison of estimates of expected durability when schematizing by different methods: 0 – bursting; 1 – maximums; 2 – swings; 3 – full cycles

The expected durability corresponding to the probability density $P_i(s)$ is indicated T_i accordingly. The calculations took into account that $s_1 = 0$, $m = 5$.

The maximum method gives a lower estimate for the expected durability, the swing and full cycles method overestimates this estimate. For narrow-linear processes, all of the above methods lead to practically the same results.

7.5 JUSTIFICATION AND APPLICATION OF THE PROVISIONS OF THE MATHEMATICAL THEORY OF RELIABILITY

Let's consider the exploitation of a number of N elements over time t. Let there be N_p able-bodied and n failed elements by the end of the service life. In this case, the relative number of failures $Q(t)$:

$$Q(t) = \frac{n}{N}. \tag{7.9}$$

If N is large enough, it can be viewed $Q(t)$ as the probability of failure.
Then the probability of failure-free operation is $P(t)$:

$$P(t) = \frac{N_p}{N} = 1 - \frac{n}{N} = 1 - Q(t). \tag{7.10}$$

It follows from (7.10) that:

$$P(t) + Q(t) = 1. \tag{7.11}$$

The distribution of conditions in time is characterized by the distribution density function $f(t)$ of the operating time to failure:

$$f(t) = \frac{dQ(t)}{dt} = \frac{1}{N}\frac{dn}{dt} = \frac{dP(t)}{dt}. \tag{7.12}$$

In this case, the probability of failures and failure-free operation in the density function $f(t)$ is expressed by the dependencies:

$$Q(t) = \int_0^t f(t)dt. \tag{7.13}$$

$$P(t) = 1 - Q(t) = 1 - \int_0^t f(t)dt = \int_t^\infty f(t)dt. \tag{7.14}$$

Failure rate $\lambda(t)$:

$$\lambda(t) = \frac{f(t)}{P(t)} = \left\{ f(t) = -\frac{dP(t)}{dt} \right\} = -\frac{dP(t)}{dt \cdot P(t)}. \tag{7.15}$$

Let's rewrite (7.15) as:

$$-\lambda(t)dt = \frac{dP(t)}{P(t)}. \tag{7.16}$$

Integrating (7.16), let's obtain:

$$\ln P(t) = -\int_0^t \lambda(t)\,dt \quad \text{or} \quad P(t) = e^{-\int_0^t \lambda(t)\,dt}. \tag{7.17}$$

During the period of normal operation, failures have a constant intensity, since worn out (gradual) failures do not appear yet, but only sudden failures occur, i.e.

$$\lambda(t) = \lambda = \frac{1}{m_t} = \text{const}, \tag{7.18}$$

where m_t – mean time to failure, hours.

Probability of failure-free operation:

$$P(t) = e^{-\int_0^t \lambda\,dt} = e^{-\lambda t}. \tag{7.19}$$

It obeys the exponential law of distribution of failure-free operation t and is the same for any equal period of time (**Fig. 7.16**).
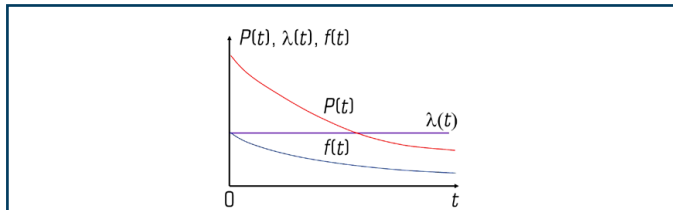
○ **Fig. 7.16** Function of probability $P(t)$ of failure-free operation, probability density $f(t)$ and failure rate $\lambda(t)$ according to exponential distribution during normal operation

The significant advantage of the exponential distribution is its simplicity: it has only one parameter. Distribution density in general:

$$f(t) = -\frac{dP(t)}{dt} = \lambda e^{-\lambda t}. \tag{7.20}$$

7.6 RESEARCH OF INDICATORS OF RELIABILITY OF TECHNICAL SYSTEMS

Experimental studies were carried out on the basis of the collected information on the development of vibration platforms to failure [1, 3]. The received data of malfunctions was carried out

by fixing by groups of prefabricated units, parts and elements, in order to separately determine the data on their operating time. Based on these data, an analysis of the operating time of the main elements between failures and the most frequent failures was carried out.

The studies carried out [2, 7, 10–19] identified the main prefabricated units and parts that fail: engine, gearbox, synchronizer, vibration exciter, propeller shafts, couplings, photographs of such failures are shown in **Fig. 7.17**.
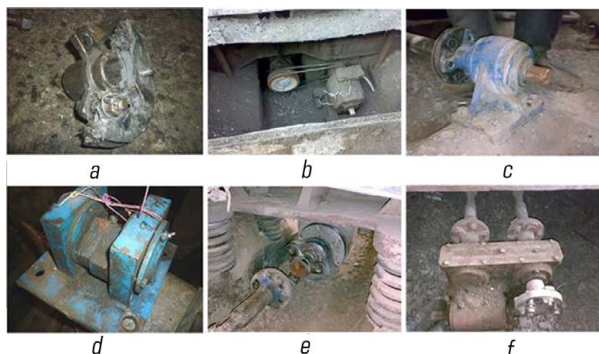
○ **Fig. 7.17** Photo fixation of failures of mechanical assemblies and parts of vibration platforms:
a – failure of the coupling; *b* – failure of the electric motor; *c* – failure of the bearing assembly;
d – failure of the vibration block; *e* – failure of the propeller shaft; *f* – failure of the synchronizer

According to the results of the study, it was found that most often propeller shafts and couplings failed. Destruction of bearings in vibration exciters was recorded only in a few cases.

In the investigated technical objects, depending on the design, the working body can consist of both separate elements such as a vibration plate or a form, and of a welded frame. In the course of research, in this group of elements, frequent defects were found as a result of contact of vibration plates with a form (**Fig. 7.18**).

Based on the results of the performed structural examinations, the main elements were established (**Fig. 7.19**), the failure of which has a direct impact on the reliability and safety of vibration machines.

The research methodology for the operating time of parts to failure consisted in conducting an experiment in real operating conditions of VB-10V vibration platforms.

Due to the frequent fixation of the identified failures of the propeller shafts of vibration platforms, the results of which are shown in **Table 7.2**. The construction of a statistical series for studying the distribution patterns of continuous random variables is possible with a sufficient number of observations. In this case (if $N > 30$) the values obtained during observation in the variation series were grouped, and the entire series of values of the observed trait from t_1 to t_n was divided into ordinary intervals.
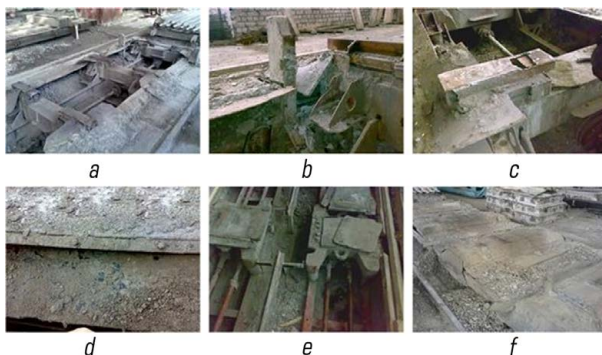
○ **Fig. 7.18** Photo fixation of failures of the working bodies of vibration platforms: *a* – failure of vibration plates; *b* – deformation of the limiters; *c* – damage to the contact platform; *d* – damage to the protective casing; *e* – damage to vibration plates; *f* – blockage of the vibration platform

The number of intervals was determined from the condition of detecting the regularity of the distribution of the indicator values depending on the sample size *N*.

The number of intervals was determined by the formula:

$$K = \sqrt{N}, \tag{7.21}$$

where *N* – the sample size.

For the convenience of further calculations, all intervals are assumed to be equal, targeted and without gaps. However, in some cases, when processing statistical data that are rather unevenly distributed, it is sometimes convenient in the area of the highest distribution density to choose narrower intervals than in the area of the smallest. The value of the interval was determined by the formula:

$$h = \frac{T_{max} - T_{min}}{K - 1}, \tag{7.22}$$

where T_{max} and T_{min} are the highest and lowest values of reliability indicators in the summary table of information.

The left and right boundaries of the distribution area are shifted by $0.5h$ and taken accordingly:

$$t_0 = T_{min} - 0.5h, \tag{7.23}$$

$$t_k = T_{max} + 0.5h, \tag{7.24}$$

where t_0 – the left border of the first interval; t_k – the right border of the last interval.
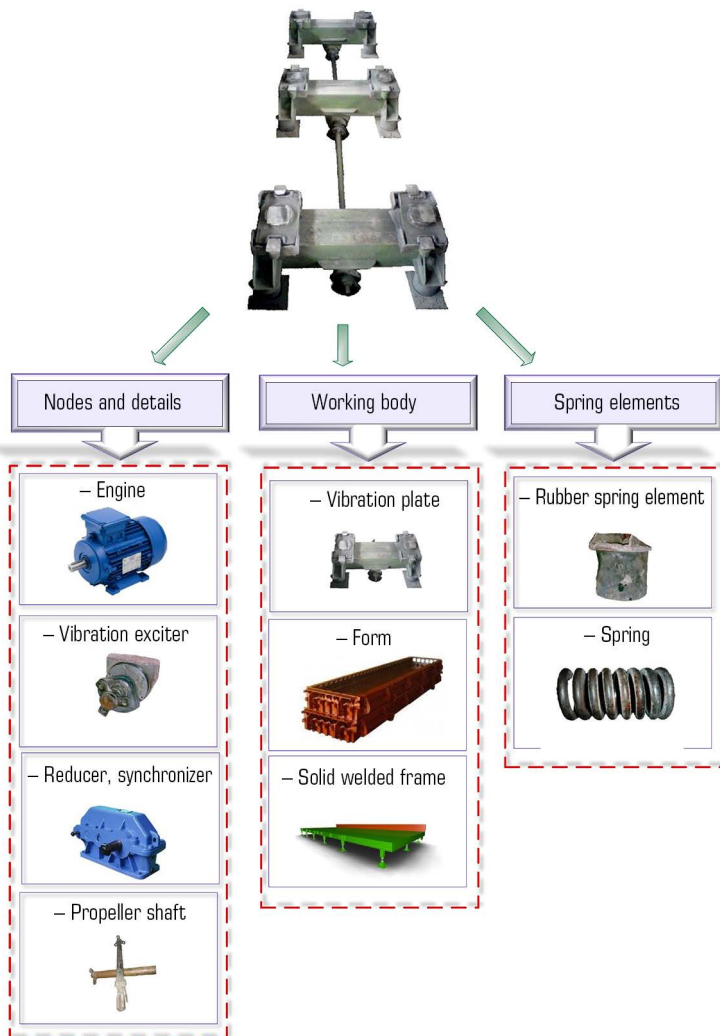
○ **Fig. 7.19** Main structural elements of vibration
platforms affecting reliability

● **Table 7.2** Operating time to failure of propeller shafts

Operating time to failure, h				
125	148	126	131	127
130	155	135	164	133
150	157	145	166	141
162	178	175	192	163
167	184	195	200	182
186	188	202	242	239
199	215	209	252	242
222	226	268	261	271
225	236	272	275	288
287	269	280	288	290

In subsequent calculations, the average value of the interval was taken:

$$t_{avi} = \frac{t_{i-1} + t_i}{2}, \qquad (7.25)$$

where t_i – value of the right limit of the n-interval.

After determining the boundaries of the intervals of the grouping, the frequencies i, the number of observations that fell into each of the intervals $[h_i]$, $i = 1, K$.

The sum of the frequencies of all intervals is equal to the sample size:

$$\sum_{i=1}^{k} n_i = N = 50. \qquad (7.26)$$

Another characteristic of the statistical distribution is the frequency P_t (relative frequency), which is determined for each interval by the ratio of frequency n_i to the total number of observations N:

$$\hat{P} = \frac{n_i}{N}. \qquad (7.27)$$

Empirical distribution density of resources $\overline{f_i}(t)$ in the i-th interval $i = 1,2,3...$

$$\overline{f_i}(t) = \frac{n_i}{N \cdot h_i}. \qquad (7.28)$$

Empirical function:

$$\hat{F}_2(t) = \hat{P}_1 + \hat{P}_2; \ \hat{F}_k(t) = \sum_{i=1}^{k} \hat{P}_i. \qquad (7.29)$$

The average value of the resource $T_{r.av.}$, hours was found by the formula:

$$T_{r.av.} = \frac{\sum\limits_{i=1}^{k} t_{av} n_i}{N}.$$ (7.30)

The standard deviation of the investigated quantity (resource) σ:

$$\sigma = \sqrt{\frac{\sum\limits_{i=1}^{k} t_{av}^{\,2} n_i}{N} - T_{r.av}^2}.$$ (7.31)

The results of processing observational data using the sum method are summarized in **Tables 7.3, 7.4**.

● **Table 7.3** Numerical values of distribution parameters

Interval number	Interval limits	Interval mid point t_{av}	Frequen-cy n_i	T_{av}^2	$T_{av} n_i$	$T_{av}^2 n_i$
1	111.25–138.75	125	7	19 251.6	971.25	134 761.2
2	138.75–166.25	152.5	10	27 639.1	1 662.5	276 391
3	166.25–193.75	180	8	37 539.1	1 550	300 312.8
4	193.75–221.25	207.5	6	48 951.6	1 327.5	293 709.6
5	221.25–248.75	235	7	61 876.6	1 741.25	433 136.2
6	248.75–276.25	525	7	76 314.1	1 933.75	534 198.7
7	276.25–303.75	580	5	92 264.1	1 518.75	461 320.5
			$\Sigma=50$		$\Sigma=10\,705$	$\Sigma=2\,433\,830$

● **Table 7.4** Calculation of characteristics by the method of sums

Interval number	Interval mid point t_{cav}	Frequency n_i	$K_1=110$	$K_2=84$
1	125	7	7	–
2	152.5	10	–	–
3	180	8	33	–
4	207.5	6	25	61
5	235	7	19	36
6	525	7	12	17
7	580	5	5	5
			$\lambda_1 = 94$	$\lambda_2 = 119$

Auxiliary intervals are determined:

$$\mu_1 = k_1 - \lambda_1. \tag{7.32}$$

The average value of the resource $T_{r.av.}$, hours, is found by the formula:

$$T_{r.av} = t_{av.i} - \frac{h\mu_i}{N}. \tag{7.33}$$

The mean square deviation of the resource σ, taking into account the auxiliary intervals:

$$\sigma = h\sqrt{\frac{\mu_2 - \mu_1^2/N}{N}}. \tag{7.34}$$

Variation coefficient:

$$V = \frac{\sigma}{T_{r.av}}. \tag{7.35}$$

Actual value of the criterion λ for extreme points:

$$\lambda_p = \frac{1}{\sigma_t}(t_j - t_{j-1}), \ j = 1, N, \tag{7.36}$$

where t_j and t_{j-1} are adjacent information points. In this case, the condition $\lambda_p < \lambda_T$ is fulfilled.

Thus, as a result of checking the information for outliers, it was found that the minimum and maximum values of the sample are $t_{min} = 125$ and $t_{max} = 126$ with probability $\gamma = 0.95$.

The histogram of relative frequencies (**Fig. 7.20**) indicates that in this case the process is subject to the Weibull distribution law:

$$f(t) = \frac{b}{a}\left(\frac{t}{a}\right)^{b-1} exp\left[-\left(\frac{t}{a}\right)^b\right], \tag{7.37}$$

where a and b are distribution parameters $a \rhd 0$; $b \rhd 0$.

It was found that Pearson's criterion χ^2 with a large number of observations reduces errors to a minimum, which compares favorably with other goodness-of-fit criteria:

$$\chi^2 = N \cdot h_i \cdot \sum_{i=1}^{k} \frac{\left[\hat{f}(t_i) - f(t_i)\right]^2}{f(t_{cpi})}; \tag{7.38}$$

where N – the total number of observations; h_i – width of the i-th interval; k – the number of staking intervals; $\hat{f}(t_i)$, $f(t_i)$ – respectively empirical and theoretical probability density of distribution; $t_{av\,i}$ – midpoint of the i-th interval for a continuous random variable or possible values for a discrete one.
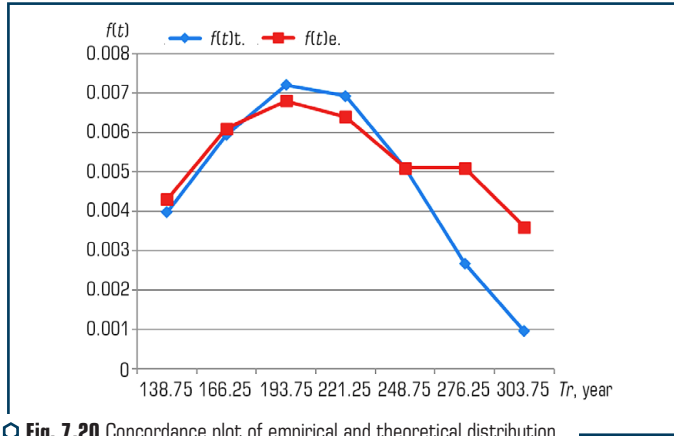
○ **Fig. 7.20** Concordance plot of empirical and theoretical distribution

Therefore, it was found that $P(r, x^2) = 0.99$ exceeding the accepted significance level of 0.95. This gives grounds to assert that the hypothesis that the empirical distribution belongs to cannot be rejected:

$$P(t) = \exp\left[-\left(\frac{t}{a}\right)^b\right].$$

(7.39)

The Weibull distribution law is characterized by the dependences:

$$F(t) = Q(t) = 1 - \exp\left[-\left(\frac{t}{a}\right)^b\right].$$

(7.40)

In relation to these calculations, the possibility of failure and trouble-free operation was obtained (**Fig. 7.21**).
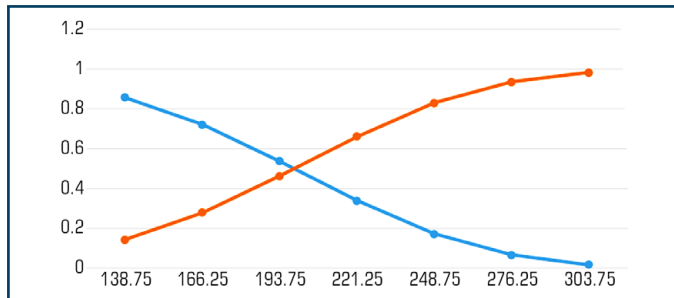
○ **Fig. 7.21** Probability of failure and failure-free operation

7.7 DISCUSSION OF RESEARCH RESULTS

The results of the studies carried out indicate a low level of reliability of the propeller shaft, which leads to long downtime during the unplanned repair time, which is 0.8–1.2 hours, if there are spare parts in stock. As a result of processing the statistical information of the propeller shaft reliability indicators, it was found that the average resource is 262 hours, the standard deviation is equal to $\sigma = 53.2$ hours, the coefficient of variation is $V = 0.27$.

A hypothesis is put forward about the error of the empirical distribution of resource indicators in comparison with the theoretical Weibull's law. The parameters of the Weibull distribution law were determined and graphs were constructed for the model of reliability and failures of propeller shafts, the graphs of the regularities of the distribution of resource indicators $P(t)$ and the distribution function $F(t)$ used in the developed recommendations.

Summarizing the presented calculation method, it is possible to build an algorithm for calculating the determination of the reliability indicators of vibration platforms (7.22).

CONCLUSIONS TO SECTION 7

1. The main states of reliability of a technical system and its elements have been investigated by the example of vibration platforms for compacting concrete mixtures.

2. The model for assessing the reliability has been developed based on fuzzy logic, implemented in the MATLAB b2020 medium.

3. The obtained results of modeling, taking into account the normalized indicators of reliability, show a «sufficiently high» level of failure.

4. When processing statistical data on the operating time to failure of the propeller shafts of vibration platforms, the Weibull distribution law has been established and the possibility of failure-free operation of such structural elements has been determined.

5. The obtained results of experimental data processing can be used in the development of new designs of similar technical systems.

REFERENCES

1. Nazarenko, I. I., Sviderskyi, A. T., Delembovskyi, M. M. (2013). Doslidzhennia nadiinosti kardannykh valiv vibromashyn budivelnoi industrii. Vibratsii v tekhnitsi ta tekhnolohiiakh. VNAU, 3 (71), 72–77.
2. Delembovskyi, M., Klymenko, M., Korniichuk, B. (2020). Doslidzhennia na osnovi nechitkoi lohiky modeli vyiavlennia vidmov vibroploshchadok. Zbirnyk naukovykh prats ΛΌHOΣ, 111–112. doi: https://doi.org/10.36074/25.12.2020.v1.38

3. Delembovskyi, M., Klymenko, M. (2020). Metody pidvyshchennia nadiinosti ta efektyvnosti vibratsiinykh mashyn budivelnoi industrii. ICSR Conference Proceedings, 48–49. doi: http://doi.org/10.36074/23.10.2020.v1.04

4. Delembovskyi, M., Klymenko, M. (2020). Zabezpechennia nadiinosti vibratsiinykh maidanchykiv budivelnoi industrii z urakhuvanniam metodiv analizu. Zbirnyk naukovykh prats ΛΌHOΣ, 26–28. doi: http://doi.org/10.36074/09.10.2020.v2.06

5. Delembovskyi, M., Terentiev, O., Shabala, Ye. (2020). Echnology of implementation of the matlab environment in the investigation model of information security threatS. ΛΌHOΣ mystetstvo naukovoi dumky. doi: http://doi.org/10.36074/2663-4139.15.08

6. Delembovskyi, M., Klymenko, M., Korniichuk, B. (2020). Rozrobka modeli otsinky nadiinosti vibroploshchadky na osnovi nechitkoi lohiky. Zbirnyk naukovykh prats ΛΌHOΣ, 98–102. doi: http://doi.org/10.36074/11.12.2020.v2.28

7. Nazarenko, I., Sviderskii, A. T., Delembovskii, M. M. (2015). Issledovanie nadezhnosti vibromashin stroitelnoi industrii. Mekhanizatsiia stroitelstva, 3, 44–49.

8. Seraya, O. V., Demin, D. A. (2012). Linear Regression Analysis of a Small Sample of Fuzzy Input Data. Journal of Automation and Information Sciences, 44 (7), 34–48. doi: http://doi.org/10.1615/jautomatinfscien.v44.i7.40

9. Domin, D. (2013). Artificial orthogonalization in searching of optimal control of technological processes under uncertainty conditions. Eastern-European Journal of Enterprise Technologies, 5 (9 (65)), 45–53. doi: http://doi.org/10.15587/1729-4061.2013.18452

10. Rogovskii, I. L., Delembovskyi, M. M., Voinash, S. A., Scherbakov, A. P., Teterina, I. A., Sokolova, V. A. (2021). Reliability indexes of vibrating platforms for compaction of construction mixtures. IOP Conference Series: Materials Science and Engineering, 1047 (1), 012026. doi: http://doi.org/10.1088/1757-899x/1047/1/012026

11. Nazarenko, I. I., Ruchynskyi, M. M., Sviderskyi, A. T., Kobylanska, I. M., Harasim, D., Kalizhanova, A., Kozbakova, A. (2019). Development of energy-efficient vibration machines for the buiding-and-contruction industry. Przeglad Elektrotechniczny, 95 (4), 53–59. doi: http://doi.org/10.15199/48.2019.04.10

12. Nazarenko, I., Gavryukov, O., Klyon, A., Ruchynsky, N. (2018). Determination of the optimal parameters of a tubular belt conveyor depending on such an economical. Eastern-European Journal of Enterprise Technologies, 3 (1 (93)), 34–42. doi: http://doi.org/10.15587/1729-4061.2018.131552

13. Nazarenko, I., Gaidaichuk, V., Dedov, O., Diachenko, O. (2017). Investigation of vibration machine movement with a multimode oscillation spectrum. Eastern-European Journal of Enterprise Technologies, 6 (1 (90)), 28–36. doi: http://doi.org/10.15587/1729-4061.2017.118731

14. Nazarenko, I., Mishchuk, Y., Mishchuk, D., Ruchynskyi, M., Rogovskii, I., Mikhailova, L. et. al. (2021). Determiantion of energy characteristics of material destruction in the crushing chamber of the vibration crusher. Eastern-European Journal of Enterprise Technologies, 4 (7 (112)), 41–49. doi: http://doi.org/10.15587/1729-4061.2021.239292

15. Luchko, J., Kovalchuk, V., Kravets, I., Gajda, O., Onyshchenko, A. (2020). Determining patterns in the stresseddeformed state of the railroad track subgrade reinforced with tubular drains. Eastern-European Journal of Enterprise Technologies, 5 (7 (107)), 6–13. doi: http://doi.org/10.15587/1729-4061.2020.213525

16. Kovalchuk, V., Onyshchenko, A., Fedorenko, O., Habrel, M., Parneta, B., Voznyak, O. et. al. (2021). A comprehensive procedure for estimating the stressed-strained state of a reinforced concrete bridge under the action of variable environmental temperatures. Eastern-European Journal of Enterprise Technologies, 2 (7 (110)), 23–30. doi: http://doi.org/10.15587/1729-4061.2021.228960

17. Nazarenko, I., Svidersky, A., Kostenyuk, A., Dedov, O., Kyzminec, N., Slipetskyi, V. (2020). Determination of the workflow of energy-saving vibration unit with polyphase spectrum of vibrations. Eastern-European Journal of Enterprise Technologies, 1 (7 (103)), 43–49. doi: http://doi.org/10.15587/1729-4061.0.184632

18. Bernyk, I., Luhovskyi, O., Nazarenko, I. (2018). Effect of rheological properties of materials on their treatment with ultrasonic cavitation. Materiali in Tehnologije, 52 (4), 465–468. doi: http://doi.org/10.17222/mit.2017.021

19. Luhovskaia, E. A., Yakhno, O. M., Bernyk, Y. N. (2012). Model of Technological Process of Ultrasonic Clearing of Elastic Surfaces Management. Naukovi pratsi Don NTU. Seriia: Hirnycho-elektromekhanichna, 23 (196), 154–166.

8 RESEARCH OF STRESS-STRAIN STATE OF ELEMENTS OF TECHNOLOGICAL TECHNICAL CONSTRUCTIONS

I. Nazarenko, O. Dedov, M. Delembovskyi,
Ye. Mishchuk, M. Nesterenko, I. Zalisko, V. Slipetskyi

ABSTRACT

The distribution of stresses and strains in the elements of vibration structures of machines has been investigated. Vibrograms of changes in the stresses of the forming surface were obtained for individual elements located near the application of a dynamic external force. Comparing the obtained results of the stress-strain state of the forming structure, a new effect of using high frequencies of the operating mode when compacting concrete mixtures was discovered. Due to the application of a spatial forced force to the forming structure, a complex stress-strain state of metal structures is created. And direct contact with the concrete mix helps to reduce energy consumption for the compaction process. The study of the motion of systems related to block structures, the adopted model, which is a two-mass vibration system. The identified transient process is intended to be taken into account when determining the parameters and locations of the vibrators. In such modes, the forms of natural vibrations of the system are realized with large vibration amplitudes and, accordingly, a lower frequency. And this opened up a real opportunity to reduce the energy consumption of vibration machine drives. The stress-strain state of the frame and forms of a vibration unit with spatial vibrations has been investigated. The distribution of stresses in the frame elements is uneven. The concentration of stresses in the welding places of elements having small values in comparison with the ultimate strength of steel has been determined. The static and dynamic loads of the slewing ring of a truck crane have been investigated. The positions of the system and its elements with the highest stresses are established. The results obtained were used in the design of the metal structures of the machines under study.

KEYWORDS

Metal structure, vibration system, stress-strain state, form-generating structure, model, numerical calculations, natural vibration modes, vibrator, spatial vibrations, truck crane, slewing ring.

8.1 STATEMENT OF TASKS AND RESEARCH METHODS

Studying the distribution of stresses and deformations in structural elements of vibration machines will allow analyzing and identifying places of stress concentration, which allows optimization of design solutions.

Based on the existing methods and a certain mathematical description (see Section 2), the problem arises of specifying the constituent elements of the pre-static and dynamic action of the load determined in the study of the machine-medium systems.

Thus, the formulation of the problem of computer modeling is reduced to the construction of a system that replaces and reflects the actual system, and in cognitive processes is in the corresponding similarity with it.

In the general case, any existing or created object can be considered in three-dimensional space both under static and dynamic action on it [1, 2]. Since the entire system is three-dimensional [3, 4], then all elements belonging to it also have three coordinates of displacements and three angles of rotation relative to the axes, that is, six degrees of freedom (DOF).

In accordance with the principles of modeling, the determination of the structural parameters of the elements is based on the ratio of the geometric dimensions and the type of arising (possibly arising) stresses in the structural elements.

So, to simulate a structural element located only in the field of tensile – compression forces (provided that it works in the zone of elastic deformations) and its length with respect to the cross section differs by an order of magnitude, it is enough to consider a one-dimensional problem. Since the processes occurring within the section can be neglected. The model that will reflect the behavior of such a system will look like a bar, the ends of which are clamped by a fixed and movable hinge, respectively.

For structural elements that are in the field of complex types of forces and the ratio of overall dimensions to plane to height are within several orders of magnitude, a system of two-dimensional elements with a thickness – plates – should be considered. Accordingly, structural elements that have overall dimensions of the same order and (or) are in a complex stress-strain state are considered volumetric elements and, accordingly, the system (model) is considered three-dimensional.

Knowledge of the stresses in the sealing layers under the action of a force load allows one to determine the sealing zone and, as a result, to determine the parameters of the sealing equipment with sufficient reasoning.

Improvement of the structures of vibration machines is possible by simulating the operation of this structure under loading, starting from the stage of an unloaded structure and ending with its full load [5, 6]. The study of displacements and deformations of structural elements of technological machines will allow identifying places of stress concentration and optimizing design solutions using finite element analysis [7].

At all nodes, generalized coordinates λ_1 are specified, called nodal offsets, the totality of which for a given element is written in the form of a matrix:

$$\{\lambda\} = \{\lambda_1, \lambda_2, ..., \lambda_N\}^T, \tag{8.1}$$

where N – total number of node displacements of the element; the sign T means the transposition of the matrix. Nodal displacements can represent the components of the vector of displacement of the nodes along the coordinate axes, as well as the angles of rotation of the element at the nodal points.

Within each element, for the components of the displacement vector of any point M, an approximation is set in terms of nodal displacements, which are unknown quantities:

$$u_i = \Phi_{ik}(M)\lambda_k, \ i = 1,2,3, \ k = 1,2\ldots N; \tag{8.2}$$

the same in matrix notation $\{u\} = \{\Phi\}\{\lambda\}$ and vector form:

$$\vec{u} = \Phi_{ik}\vec{e}_k\lambda_k = \{\vec{\Phi}\}\{\lambda\}, \tag{8.3}$$

where $\Phi_{ik}(M)$ values are called functions of the shape of the element and express the relationship between the nodal displacements and the displacement of the point M of the body; polynomials are usually used as a shape function; outside the element, these functions are set equal to zero; $\vec{\Phi}_k = \Phi_{ik}\vec{e}_i$, $\{\vec{\Phi}\} = \{\vec{\Phi}_1, \vec{\Phi}_2, \ldots, \vec{\Phi}_N\}$, $\vec{e}_i$ – unit vectors.

Relations (8.3) are substituted into the body equilibrium equation, from which the nodal displacements $\{\lambda\}$ for each element are determined.

When using the finite element method, it is most convenient to obtain the body balance equation based on the principle of possible displacements. Let $\vec{u}$ is the field of displacements of points of a deformable body under the action of external loads applied to it. By setting each point a small displacement $\delta\vec{u}$ allowed by the constraints imposed on the body (movement is possible). According to this principle, the increase in the work of internal forces is equal to the work of external forces on possible displacements, i.e.:

$$\delta U = \delta W. \tag{8.4}$$

Denoting as $\vec{q}$ the external load distributed over the volume of the body V, and as $\vec{p}$ – the load distributed over its surface S.

Let's obtain:

$$\delta W = \int_V \vec{q} \cdot \delta\vec{u}\,dV + \int_S \vec{p} \cdot \delta\vec{u}\,dS. \tag{8.5}$$

The expression for the work of internal forces has the form:

$$\delta U = \int_V \sigma \cdot \delta\varepsilon\,dV, \tag{8.6}$$

where $\sigma = \sigma_{ij}\vec{e}_i\vec{e}_j$ – stress tensor; $\varepsilon = \varepsilon_{ij}\vec{e}_i\vec{e}_j$ – strain tensor; $\vec{e}_i$ – unit unit vectors, $i, j = 1, 2, 3$.

Then relation (8.4) takes the form:

$$\int_V \sigma \cdot \delta\varepsilon\,dV = \int_V \vec{q} \cdot \delta\vec{u}\,dV + \int_S \vec{p} \cdot \delta\vec{u}\,dS. \tag{8.7}$$

In the case of small deformations of the body:

$$\varepsilon = \nabla \vec{u}, \tag{8.8}$$

where

$$\nabla \vec{u} = \frac{1}{2}\left(\frac{\partial u_i}{\partial x_j} + \frac{\partial u_j}{\partial x_i} \right) \vec{e}_i \vec{e}_j$$

– tensor operator; $i, j = 1, 2, 3$; x_1, x_2, x_3 – coordinate axes directed along the unit vectors $\vec{e}_1, \vec{e}_2, \vec{e}_3$.

Substituting (8.2) into (8.8), let's obtain an expression for the components of the strain tensor in terms of the nodal displacements:

$$\varepsilon_{ij} = \frac{1}{2}\left(\frac{\partial \Phi_{ik}}{\partial x_j} + \frac{\partial \Phi_{jk}}{\partial x_i} \right) \lambda_k. \tag{8.9}$$

or in matrix form:

$$\{\varepsilon\} = \{B\}\{\lambda\}, \tag{8.10}$$

where

$$\{B\} = \{\nabla \vec{\Phi}\} = \left\{ \frac{1}{2}\left(\frac{\partial \Phi_{ik}}{\partial x_j} + \frac{\partial \Phi_{jk}}{\partial x_i} \right) \right\}$$

– matrix associates deformations with nodal displacements. The relationship between the components of stress and strain tensors for an elastic body is expressed by a law:

$$\sigma_{ij} = D_{ijkl}\varepsilon_{kl}, \tag{8.11}$$

where D_{ijkl} – the elastic constants of the body, $i, j, k, l = 1, 2, 3$, or in matrix form $\{\sigma\} = \{D\}\{\varepsilon\}$.

Substituting expression (8.30), let's find the dependence of the stress tensor on nodal displacements:

$$\{\sigma\} = \{D\}\{B\}\{\lambda\}. \tag{8.12}$$

After transformations, let's obtain the equation of equilibrium of an elastic body containing the movement of its points:

$$\int_V D\nabla \vec{u} \cdot \delta(\nabla \vec{u}) dV = \int_V \vec{q} \cdot \delta \vec{u} dV + \int_S \vec{p} \cdot \delta \vec{u} dS. \tag{8.13}$$

Let's apply relation (8.13) to a finite element with some volume V_e bounded by the surface S_e, and find:

$$\delta\lambda_i \left\{ \int\limits_{V_e} \nabla\vec{\Phi}_i \cdot D\nabla\vec{\Phi}_j \cdot \lambda_j dV - \int\limits_{V_e} \vec{q}\vec{\Phi}_i dV - \int\limits_{S_e} \vec{p}\vec{\Phi}_i dS \right\} = 0, \tag{8.14}$$

where $i,j = 1,2,...,N$.

Since $\delta\lambda_i$ — arbitrary nonzero values, the last equality requires all expressions in curly braces to rotate to zero. From these conditions, let's obtain a system of linear algebraic equations expressing the equilibrium conditions for a finite element:

$$\{K\}\{\lambda\} = \{f\}, \tag{8.15}$$

where $K_{ij} = \int \nabla\vec{\Phi}_V \cdot D\nabla\vec{\Phi}_j dV$ — stiffness matrix of the element, which, using relations (8.10) and (8.12), can also be written in the form: $\{K\} = \{B\}^T \{D\}\{B\}$;

$$f_i = \int\limits_{V_e} \vec{q} \cdot \vec{\Phi}_i dV + \int\limits_{S_e} \vec{p} \cdot \vec{\Phi}_i dS$$

— vector of nodal forces of the element, where $i,j = 1,2,...,N$.

The set of equations (8.15) for all elements is supplemented by the equations of ligatures imposed on the body (limiting conditions), which are a system of equations for the equilibrium of the body under consideration, written in a form similar to (8.35):

$$\{\overline{K}\}\{\overline{\lambda}\} = \{\overline{f}\}, \tag{8.16}$$

where $\{\overline{K}\}$ is called the global body stiffness matrix; $\{\overline{\lambda}\}$ and $\{\overline{f}\}$ — vectors of nodal displacements and forces of the whole body.

Equations of the type (8.16) are used for strength analysis of structures under static load. From their solution, the vector of nodal displacements is determined, then, according to relation (8.2), one can find the displacement of the points of the body, and according to (8.8)–(8.11) or (8.13) – deformations and stresses.

From (8.15) it is easy to obtain the equation of motion of the element. By introducing, according to the d'Alembert principle, the volumetric forces of inertia into the integral for the nodal forces (8.15):

$$\vec{q}^{in} = -\rho\frac{\partial^2\vec{u}}{\partial t^2} = -\rho\vec{\Phi}_j \cdot \ddot{\vec{\lambda}}_j, \tag{8.17}$$

let's obtain a system of equations:

$$\{M\}\{\ddot{\lambda}\} + \{K\}\{\lambda\} = \{f\}, \tag{8.18}$$

where $M_y = \int \rho \vec{\Phi}_i \cdot \vec{\Phi}_j dV$ – mass matrix of the element; ρ – material density; $\ddot{\lambda}$ – the second time derivative of the vector of nodal displacements. In the presence of viscous resistance forces in the system, proportional to the speeds of the points, the matrix of damping coefficients $\{B\}$ is introduced into (8.38), after which the equations of motion take the form:

$$\{M\}\{\ddot{\lambda}\} + \{B\}\{\dot{\lambda}\} + \{K\}\{\lambda\} = \{f\}. \tag{8.19}$$

When studying the problems of elastic resistance of structural elements, the equilibrium equation is added taking into account the change in the geometry of the body in the deformed state:

$$\left[\{\bar{K}\} - \beta\{\bar{K}_d\}\right]\{\bar{\lambda}\} = 0, \tag{8.20}$$

where by means of a matrix of geometric stiffness $\{\bar{K}_d\}$, called differential in MSC.vN5W, the work of external forces due to a change in the geometry of the body is taken into account; β – loading parameter.

Equating to zero the determinant of the system (8.40) $\det\left[\{\bar{K}\} - \beta\{\bar{K}_d\}\right] = 0$, let's find the value of the load parameter $\beta_1, \beta_2, \ldots$, at which there are nontrivial displacements for nodal displacements $\{\lambda\}$, i.e. new forms of body balance appear, different from the original. Such values β, called critical, show how many times the critical load F^{cr}, at which the loss of resistance of the original form of body balance occurs, is greater than the current load F:

$$F_i^{cr} = \beta_i F, \ i = 1, 2, \ldots \tag{8.21}$$

The first lowest critical load F_1^{cr} is usually of practical interest, since only it will be realized during the operation of the structure. To study the working process of energy-saving machines and their structural elements for the implementation of specific technological work processes, the following research sequence was established:
   – justification and development of calculation schemes for the machine;
   – analysis of the basic forms, amplitudes and frequencies of vibration of the structure;
   – determination of modes, rational parameters to create a new highly efficient design.

8.2 INVESTIGATION AND DETERMINATION OF STRESSES AND STRAINS IN THE FORMING SURFACE OF THE STRUCTURE OF VIBRATION MACHINES

The search for constructive solutions for the creation of machines with a variable amplitude-frequency oscillation mode is to search for an increase in the efficiency of the working process.

Revealing new phenomena in the operation of compacting machines and taking them into account when modeling work processes. Improvement of models that adequately meet the real conditions of motion of a vibration machine. An effective approach in this direction is the use of continuous models, which make it possible to take into account the propagation of waves, both in the design of a vibration machine and in the compacting mixture. This approach is the basis for determining the real distribution of amplitudes and frequencies of oscillations and the use of multi-mode effects.

So, it is assumed that the design, subject to research and further creation, allows to transfer the maximum amount of energy from the working body to the medium due to the frequency spectrum with different energy components and the use of internal resonance phenomena of the system by choosing an operating mode that is coordinated in elastic-inertial and elastic-viscous properties of the machine and medium.

Thus, on the basis of the created finite element model, studies of the structure were carried out in terms of natural frequencies and vibration modes. The calculation of frequencies and modes of vibration was carried out in two stages. At the first stage, according to the nonlinear theory, static prestressing of the structure by all acting forces is performed, then at the second stage, the frequencies and, accordingly, the vibration modes are calculated.

Studying the distribution of stresses and deformations in structural elements of vibration machines will allow analyzing and identifying places of stress concentration, which allows optimization of design solutions.

To study and determine the stresses and strains in accordance with the goal, the task of calculating the supporting structures of the system in its more critical states is posed. Therefore, for research, the design of a vibration unit was selected, which is a form-forming surface for compacting a concrete mixture. The structure consists of a welded box-section frame mounted on rubber resilient supports and a metal sheet as a shaping surface. Loads of auxiliary structural elements and concrete mix were included in the dynamic component of forces.

The total number of finite elements turned out to be 59 856, the number of nodes – 100 998. It is assumed that the structure frame is rigidly fixed on rubber supports and the materials of all elements are deformed only in the elastic stage.

The nature of the stress-strain state of the structure under the action of external forces and gravity is illustrated in color in **Fig. 8.1**.

The scale of displacement values corresponding to this palette is represented on the left in the form of a colored column. As follows from **Fig. 8.1** the maximum values of the equivalent stresses of the forming surface are 2.5 MPa. Higher values of stresses are concentrated in the area of application and distribution of the driving force.

The frame design accepts a maximum stress of 11.7 MPa (**Fig. 8.2**). The area of action of such stress values is limited by the contact zones of the frame with the supports and is of a local nature. In general, the frame of the structure is in a state of uniform stress distribution.

In order to study the behavior of the forming surface under dynamic action, the distribution of stresses in time is analyzed. In particular, **Fig. 8.3** shows vibrograms of changes in the stresses

of the forming structure for individual elements located near the application of a dynamic external force. As seen from **Fig. 8.3**, at the beginning, a transient process was detected, caused by the exit of the system from a state of rest into oscillatory motion. An increase in the amplitude of stress changes at this stage is a consequence of the transition of the system through resonance modes at lower vibration frequencies.
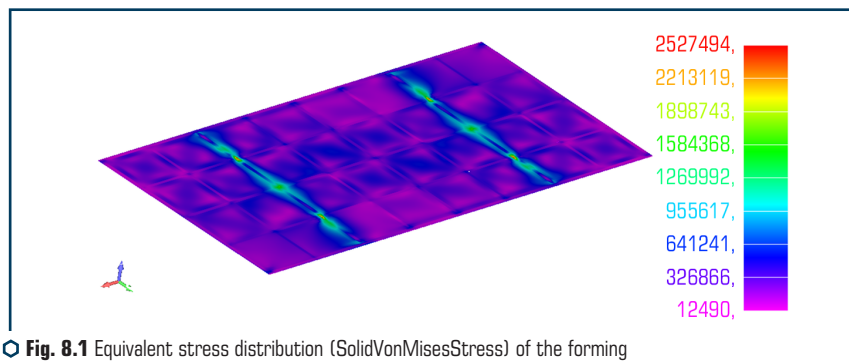

○ Fig. 8.1 Equivalent stress distribution (SolidVonMisesStress) of the forming surface (time 0.0748 s)
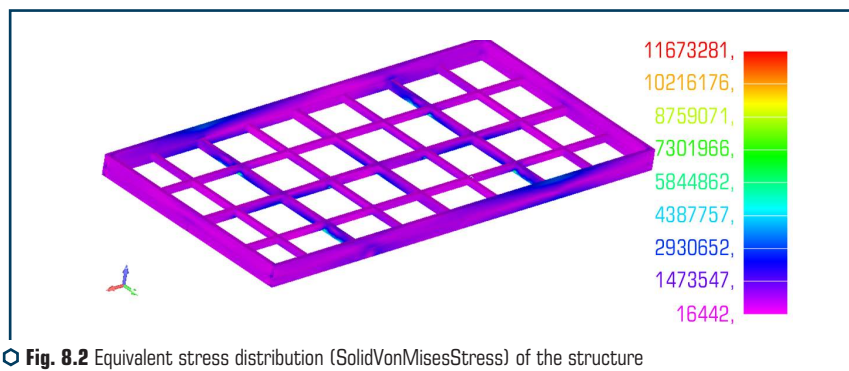
○ Fig. 8.2 Equivalent stress distribution (SolidVonMisesStress) of the structure frame (time 0.0748 s)

In such modes, the forms of natural vibrations of the system are realized with large vibration amplitudes and, accordingly, a lower frequency. When the operating mode is set, negative stress arise in structural element 18 857. The nature of the change in these stresses is periodic and antiphase in comparison with the applied spatial force. The stress of element 48 345 are positive and vary with an offset of $\pi/2$ relative to the applied force. This dependence is explained by the spatial arrangement of the elements in relation to the point of application of the force. But the nature of the change in this force of the force load, since it changes along the two axes of space.

For structural elements 48 114 and 17 290, which are located symmetrically on the opposite side of the applied force, the nature of the change is shown in **Fig. 8.4**. In contrast to the previous vibrograms, one can see the absence of in-phase changes in stress in relation to the forced force. The significant difference can be explained by the dissipation phenomena occurring in the structure.
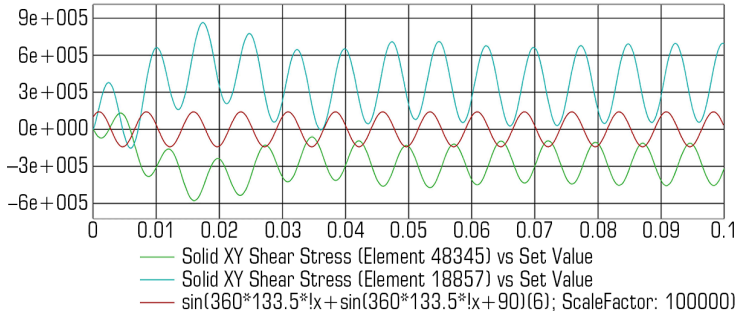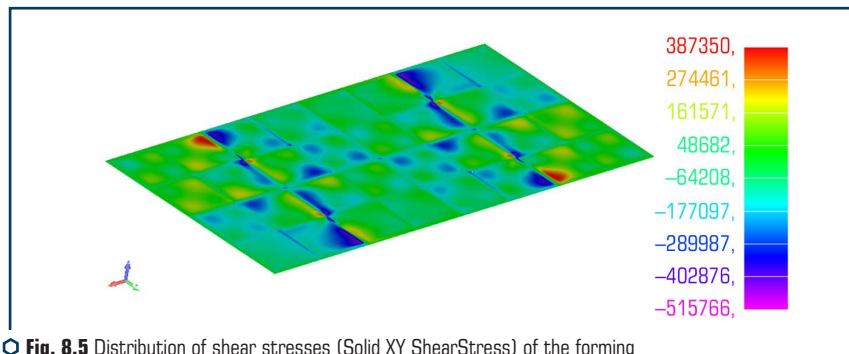

○ **Fig. 8.3** Dependence of shear stresses (Solid XY ShearStress) of the forming surface (elements 48 345 and 18 857) and the vertical component of the driving force
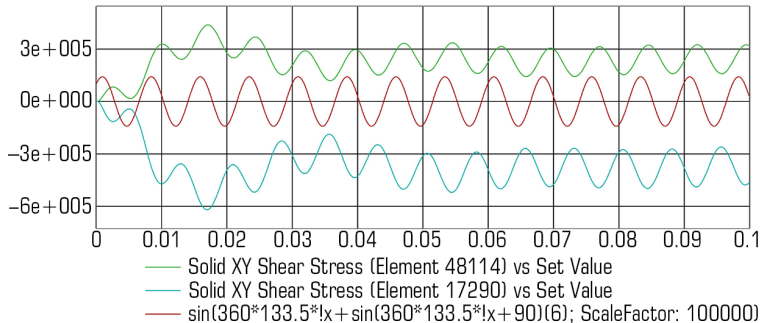
○ **Fig. 8.4** Dependence of shear stresses (Solid XY ShearStress) of the forming surface (elements 48 114 and 17 290) and the vertical component of the driving force

It is quite obvious that the change in the stress-strain state of the system under study is rather difficult. Such a change is associated with the implementation of complex spatial vibrations and the multi-mode of the sealing process. An important criterion for evaluating a design from the point of view of the efficiency of the compaction process is shear stress. Indeed, in the presence of such stresses in the medium, there is an intensive movement of particles and compaction.
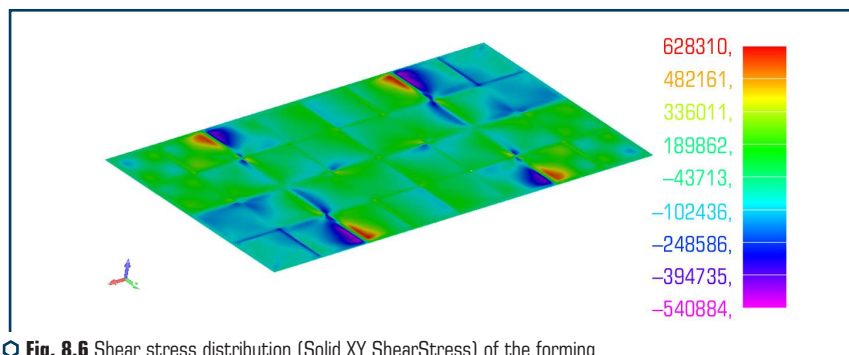
To analyze the shear stresses of the forming surface, time intervals are selected that correspond to 1/4 of the period of oscillation of the driving force. **Fig. 8.5** shows the distribution of stresses in the *XY* plane at a time of 0.0748 s, which is taken as a relative origin.

○ **Fig. 8.5** Distribution of shear stresses (Solid XY ShearStress) of the forming surface (time 0.0750 s)

This is evidenced by the zones with the maximum positive stress values, in which the force is applied. The entire surface is in a complex sign-like stress-strain state.

When the force is turned by an angle of $\pi/4$, the stress distribution changes (**Fig. 8.6**). The appearance of additional zones of maximum stresses indicates the transfer of the load in the horizontal direction and the presence of bending and torsional vibrations. In this case, the middle of the structure is at relative rest.

○ **Fig. 8.6** Shear stress distribution (Solid XY ShearStress) of the forming surface (time 0.0768 s)

When the force returns to an angle of $\pi/4$, almost the entire surface of the forming surface is disturbed (**Fig. 8.7**). Deformation and stress have a sign-like character indicating the presence

of wave phenomena. The transfer of stresses occurs in the direction of the diagonal connecting the points of application of external dynamic forces.
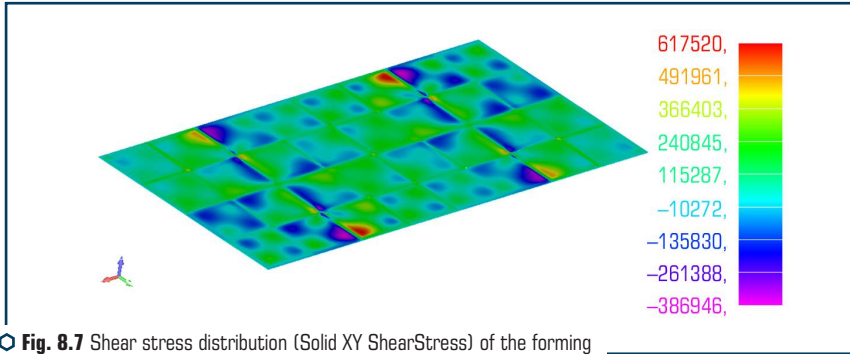
○ **Fig. 8.7** Shear stress distribution (Solid XY ShearStress) of the forming surface (time 0.0786 s)

In the period of time 0.0806 s (3/4π), the propagation of oscillations continues, as evidenced by a change in the stress distribution (**Fig. 8.8**). Deformation and stress are alternating in nature, as in the previous period of time, but their stress distribution is more uniform and orderly. It should be noted that there are zones in the corners of the forming surface. In these zones, the change in stresses is less intense and most of the surface perceives positive stress values. At the same time, the number of surface areas with negative stress values is insignificant.
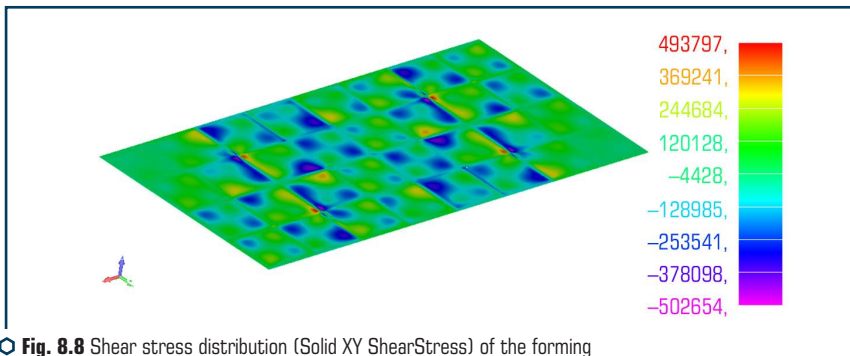
○ **Fig. 8.8** Shear stress distribution (Solid XY ShearStress) of the forming surface (time 0.0806 s)

Comparing the obtained results of the stress-strain state of the forming structure, the following can be noted. The use of high frequencies of the operating mode will allow obtaining a new effect when compacting concrete mixtures. Due to the application of a spatial forced force to the forming

structure, a complex stress-strain state of metal structures is created. And direct contact with the concrete mix helps to reduce energy consumption for the compaction process.

To study the motion of systems related to block structures, a model was adopted (**Fig. 8.9**), which is a two-mass vibration system. The lower mass of the system consists of four vibration blocks resting on elastic elements calculated according to the vibration isolation conditions.

The upper mass simulates the shape with the medium to be processed. Between the upper and lower masses there are elastic elements, the stiffness of which is taken from the condition for the realization of the resonant mode of motion and providing the technological process.

In order to carry out research, the following overall dimensions of the structure were adopted:
– total length 3.30 m;
– width 0.50 m;
– height 0.34 m.

The model was investigated by the finite element method. The finite element model of the structure was compiled by approximating all load-bearing elements, including the forming surface, with two-dimensional finite elements of the PLATE type, elastically deformed under the action of a longitudinal force, bending moments in two planes and a torque.

Vibration isolation supports and elastic elements of the model are adopted as three-dimensional CE of the SOLID type, since the processes occurring in such structural elements are more complex in terms of energy dissipation.

The total number of finite elements was 19 258, the number of nodes was 19 912, and the total number of searched variables was 20 928.

It is assumed that at the extreme points, the supports rest on the foundation and are fixed, therefore, in the model, the extreme nodes of the supports are restrained in the X, Y, Z directions, and rotations in all three axes are also prohibited.

It is believed that the materials of the entire structure are deformed only in the elastic stage.

When checking the strength and determining the functioning of a system that can be subjected to loads that are different in their nature and applied in various combinations, it is advisable to first analyze the behavior of the structure under the simplest loads, and then complicate them with the addition of other disturbances.
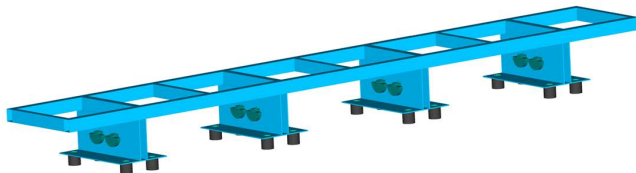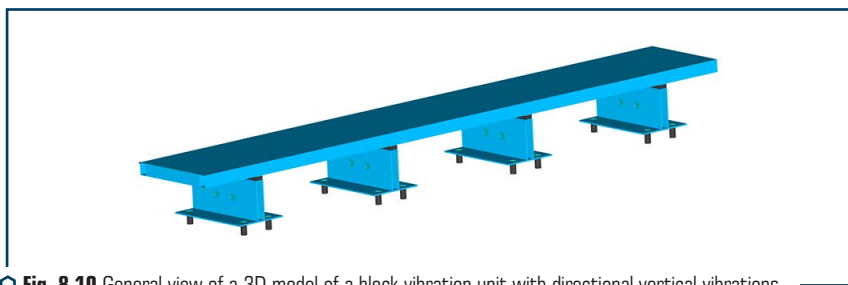

○ **Fig. 8.9** Model of block vibration unit

To check the model and assess its functioning under the action of static and dynamic loads, the following research stages were taken:

– static calculation under the action of the weight of structural elements and the equivalent load of the medium being processed;

– modal analysis;

– dynamic analysis of the structure under the action of a forced force with a vibration frequency close to the natural vibration frequency.

The studies of the unit (**Fig. 8.10**) were carried out in several stages. at the first stage, a modal analysis was carried out in order to determine the main forms and the corresponding vibration frequencies.

○ **Fig. 8.10** General view of a 3D model of a block vibration unit with directional vertical vibrations
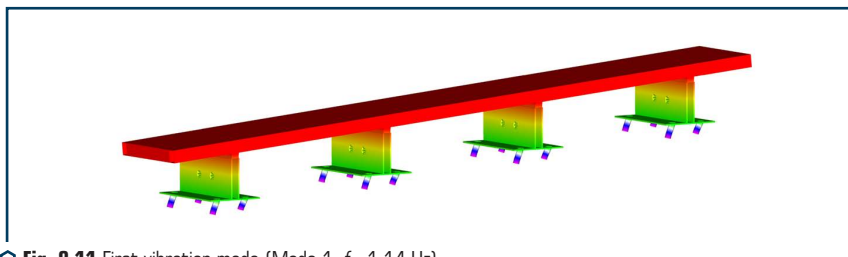

○ **Fig. 8.11** First vibration mode (Mode 1, $f=1.14$ Hz)

So, at an oscillation frequency $f=1.14$ Hz (**Fig. 4.12**), $f=1.32$ Hz (**Fig. 8.12**), the vibration unit will vibrate in the first and second modes of vibration in the horizontal plane (*XY*). This mode of vibration is due to the value of the stiffness of elastic supports, which in the horizontal direction have an insignificant stiffness due to geometric features and physical and mechanical characteristics.

Fig. 8.13 shows the operating mode of the unit at an oscillation frequency $f=2.57$ Hz. In this mode, vibrations are performed in the horizontal plane and have a twisting character.

When the mode is realized at a frequency of $f=4.10$ Hz (**Fig. 8.14**), the oscillations are directional in the vertical direction. This mode corresponds to the resonant mode of vibration, when the vibration frequency corresponds to its own frequency on vibration isolation elastic elements.
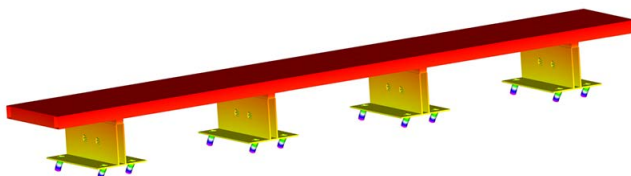
○ **Fig. 8.12** Second vibration mode (Mode 2, $f=1.32$ Hz)
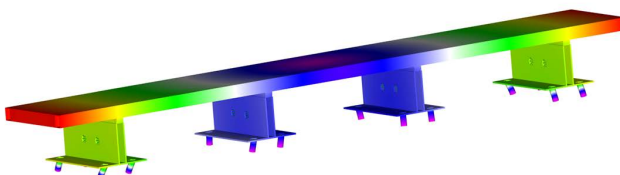
○ **Fig. 8.13** Third vibration mode (Mode 3, $f=2.57$ Hz)
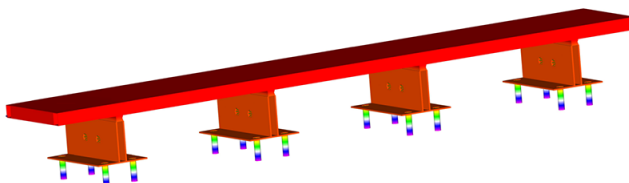
○ **Fig. 8.14** Vibration mode (Mode 8, $f=4,10$ Hz)

The implementation of oscillations according to the mode at a frequency of $f=16.61$ Hz (Mode 23) is a consequence of the influence of the rigidity of the form (**Fig. 8.15**). Oscillations occur due to the bending of the structure in the YZ plane. Such modes are insufficient for the process of compaction of concrete mix. Purely unidirectional oscillations with low frequencies do not cause stresses in the medium that do not exceed the voltage loss of continuity. The operating mode, in which the phase displacement will be realized, is possible when increasing to a frequency of $f=27.40$ Hz (**Fig. 8.16**). This is due to the fact that with increasing frequency, the numerical values of the compressive stresses of the mixture layers and the rupture stress of the layers increase significantly. Also, this mode implements vibrations of the shaping surface, which are realized on elastic elements.
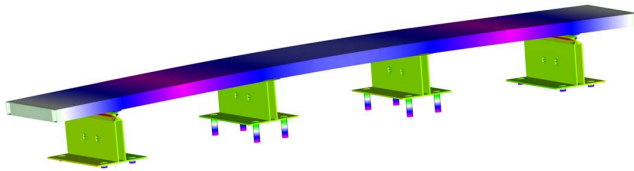
○ **Fig. 8.15** Vibration mode (Mode 23, $f = 16.61$ Hz)
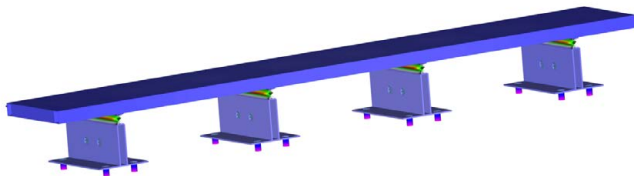
○ **Fig. 8.16** Vibration mode (Mode 29, $f = 27.40$ Hz)

A further increase in vibration frequencies and the implementation of the corresponding vibration modes leads to vibrations of the vibration unit form (**Fig. 8.17**), which is explained by the sufficient stiffness of the form frame and the corresponding stiffness of elastic elements (rubber gaskets).

Since the operating mode of such structures is considered as close to resonance, the choice of the operating mode must be carried out in such a way that the value of the operating frequency is 0.90–0.95 of the natural frequency.

Thus, the operating mode is adopted with a vibration excitation frequency of 25 Hz.

The implementation of the dynamic analysis was carried out in order to obtain the distribution of the vibration amplitudes of the shaping surface along the length of the structure with the application of a driving force on each vibration block.
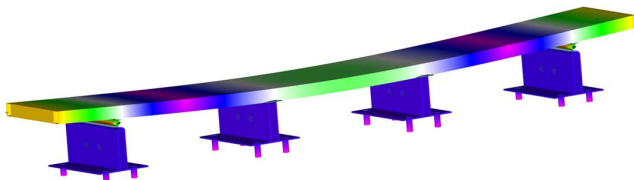

○ **Fig. 8.17** Vibration mode (Mode 31, $f = 35.72$ Hz)

To analyze the dynamics with directional vibrations, the values of displacements in time were obtained.

To study the behavior of the shaping surface, a list and place of points on the surface of the form were determined with the determination of the distribution of vibration amplitudes depending on the location of blocks with vibration exciters (**Fig. 8.18**).

Thus, the implementation of oscillations in one period is shown in **Fig. 8.19**.
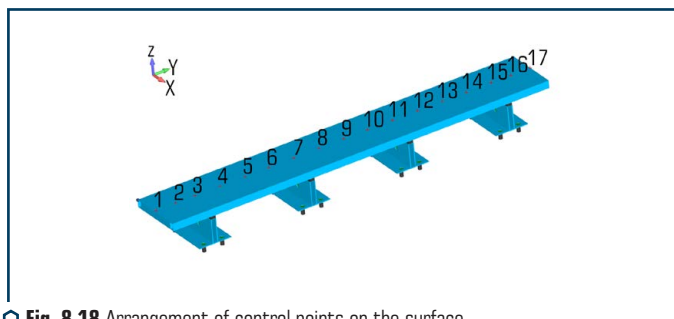
Fig. 8.18 Arrangement of control points on the surface
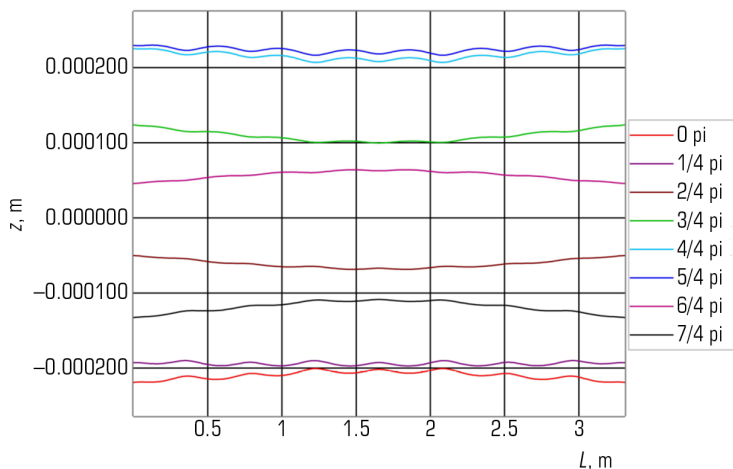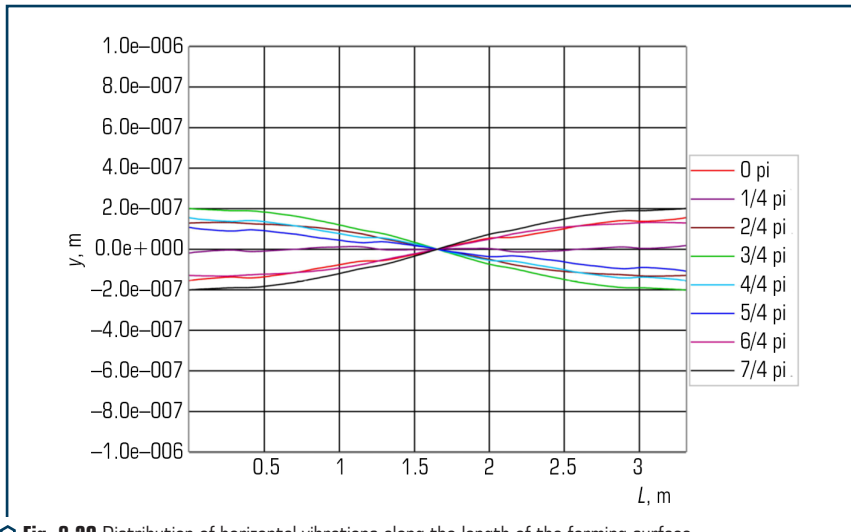

Fig. 8.19 Distribution of vertical vibrations along the length of the forming surface

As can be seen from the distribution, the oscillations are carried out in the vertical plane, which fully confirms the classical approach to modeling such systems with discrete parameters when considering a one-dimensional problem. The maximum value of the vibration amplitude is 0.22–0.25 mm.

So, the implementation of oscillations for one period is shown in **Fig. 8.20**. As can be seen from the distribution, oscillations occur in the vertical plane, which fully satisfies the classical approach to modeling such systems with discrete parameters when considering a one-dimensional problem and thus confirms the adequacy of the created model within the framework of the research. The maximum value of the vibration amplitude is 0.22–0.25 mm.

The analysis of vibrations in the horizontal direction was carried out relative to the Y-axis (**Fig. 8.20**), showed the practical absence of vibrations and displacements of the forming surface. The vibration amplitudes are $2 \cdot 10^{-7}$ m, which is three orders of magnitude less than in the vertical direction and it is quite obvious that such values can be neglected.


Fig. 8.20 Distribution of horizontal vibrations along the length of the forming surface

Likewise, the absence of oscillations along the X axis, since the forcing force is directional and does not act in this direction.

The considered mode of operation of the block structure of the vibration platform with directional vertical vibrations made it possible to analyze the distribution of amplitudes along the length of the forming surface and confirm the adequacy of the adopted model.

To implement the idea of a polyphase oscillation mode, studies of a finite element model have been carried out. Modeling of the vibration unit movement was carried out under two conditions of application of external forces: the first option provided for the application of a driving force with a shift angle of 90° on each vibration unit (**Fig. 3.2**, $\varphi_1 = 0$; $\varphi_2 = 90°$; $\varphi_3 = 180°$; $\varphi_4 = 270°$); the second variant of the load with angles $\varphi_1 = 0$; $\varphi_2 = 60°$; $\varphi_3 = 120°$; $\varphi_4 = 180°$, respectively. The frequency and value of the driving force were similar to the case of directional vertical vibrations.

So, as a result of dynamic analysis, distributions of vibration amplitudes along the Z (**Fig. 8.21, *a***) and Y (**Fig. 8.21, *b***) axes were obtained for the angle $\varphi = 90°$.
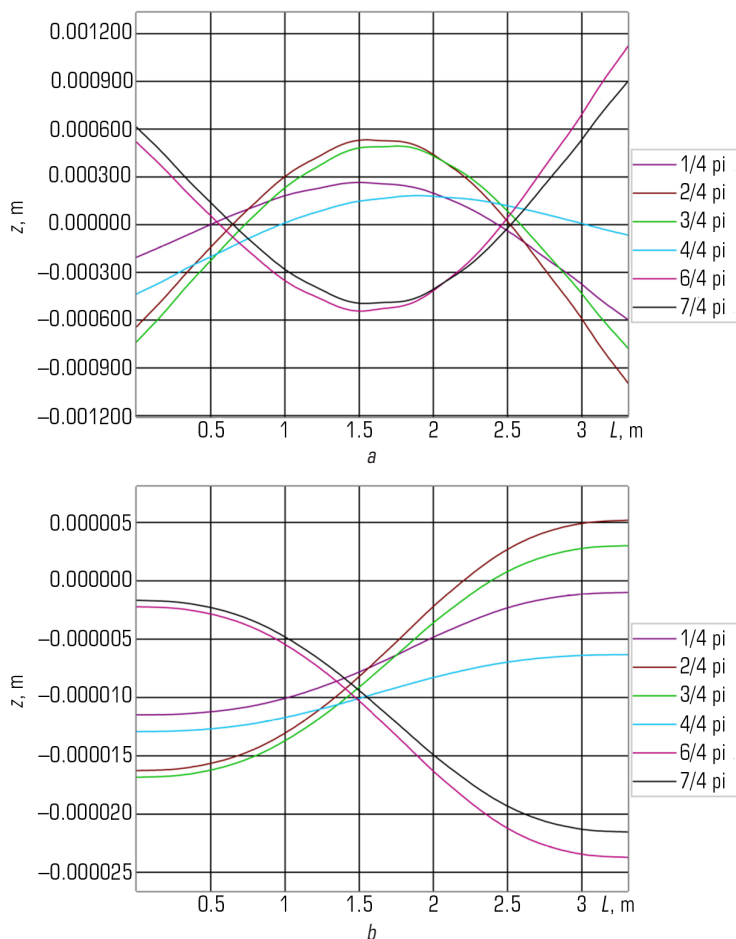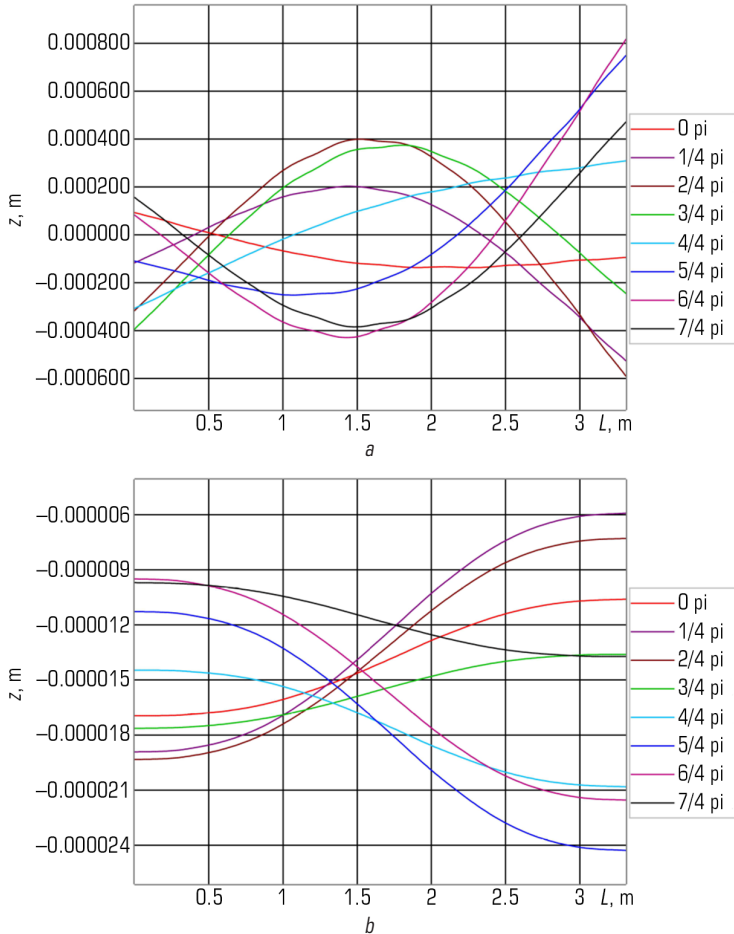

○ Fig. 8.21 Distribution of vibration amplitudes along the length of the structure for one period of vibration (angle=90°): a – X axis; b – Y axis

The maximum value of the vibration amplitude within the framework of the studies performed was obtained at the boundary of the form and, respectively, are 0.6 and 1.1 mm in time intervals from $3/4\pi$ to $7/4\pi$ for oscillations of the Z axis, and for oscillations in the Y direction – $22 \cdot 10^{-6}$ and $5 \cdot 10^{-6}$ mm.

It should be noted that there are points at which vertical vibrations occur to a much lesser extent, but at the same points there are vibrations with a horizontal component, therefore, at these points vibrations are present in both directions and there are all the conditions for compaction of the building mixture.

Distribution of vibration amplitudes at angle $\varphi = 60°$ is shown in **Fig. 8.22** in practice, it is possible to see a similar picture with the previous study, although there is a certain difference, which consists in the fact that there are no points with less vibration intensity.

Fig. 8.22 Distribution of vibration amplitudes along the length of the structure for one period of vibration (angle=60°): a – X axis; b – Y axis

So there are places where the displacements pass through the zero mark, but compared to the previous mode of operation, these points do not have a clear position along the length of the form, but shift with each $\pi/4$ time interval. Thus, transferring vibrations to a larger volume of concrete mix near the contact zone. It should be noted a certain increase in the amplitude of oscillations in the horizontal direction in comparison with the shear angle $\varphi=90°$, as for vertical oscillations, that is, a decrease in the values to 0.6 and 0.8 mm.

Comparing the three operating modes of the block platform ($\varphi=0°$, $\varphi=60°$, $\varphi=90°$), it is possible to note a positive contribution to the qualitative characteristic of oscillations when changing phase angles other than 0. And when comparing the general distribution of amplitudes at an angle of $\varphi=90°$ and $\varphi=60°$, it is obvious that it is the shift angle $\varphi=60°$ that has the advantage.

For a more detailed study of the motion of the shaping surface with this implementation of the model (**Fig. 8.10**), let's consider modeling the motion in time.

The movement of the surface at points 1, 2, 16, 17 (**Fig. 8.18**) in time indicates the presence of different values of the vibration amplitudes (**Fig. 8.23**). So, at point 16, the amplitude of oscillations reaches 0.6 mm, and at point 2, at the same time, it has a value of 0.2 mm, which is evidence of the presence of a wave process.

At other points (**Fig. 8.24**) vibrograms of movement are identical in character to those discussed above. In terms of magnitude, the amplitudes of the oscillations are of lesser importance. At point 14, the magnitude of the amplitude reaches 0.4 mm, and at point 3, in the same period of time, the amplitude of the oscillations is 0.1 mm. At points 14 and 15, there is practically no phase displacement between the vibration amplitudes.
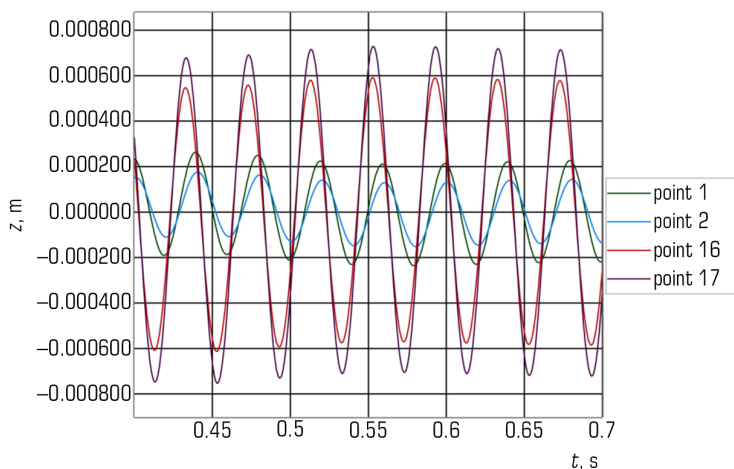
Fig. 8.23 Vibrograms of movement of points 1, 2, 16, 17 in time

Vibrograms of movement at points 5, 6, 12, 13 in time (**Fig. 4.25**) are similar in nature, as for other points (**Fig. 8.24, 8.25**).
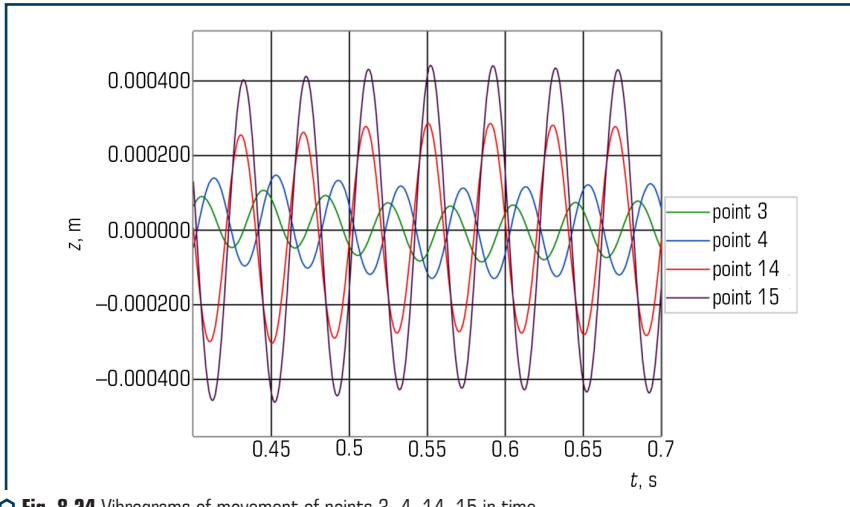

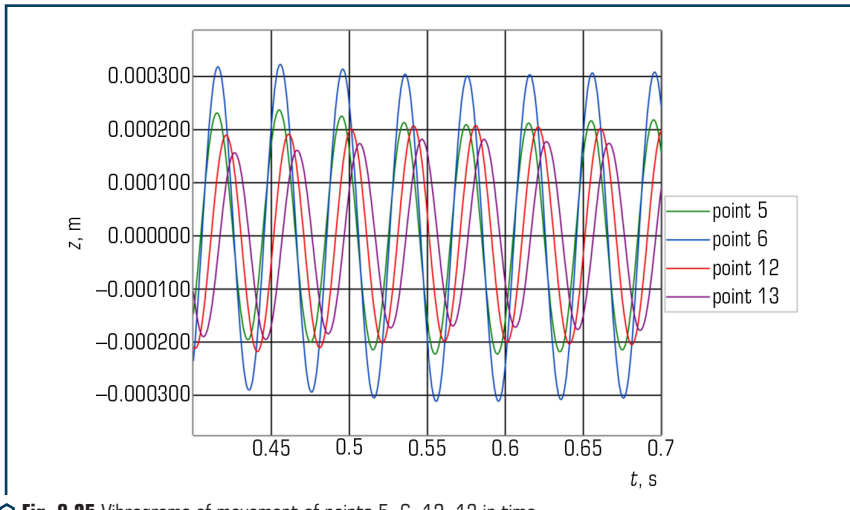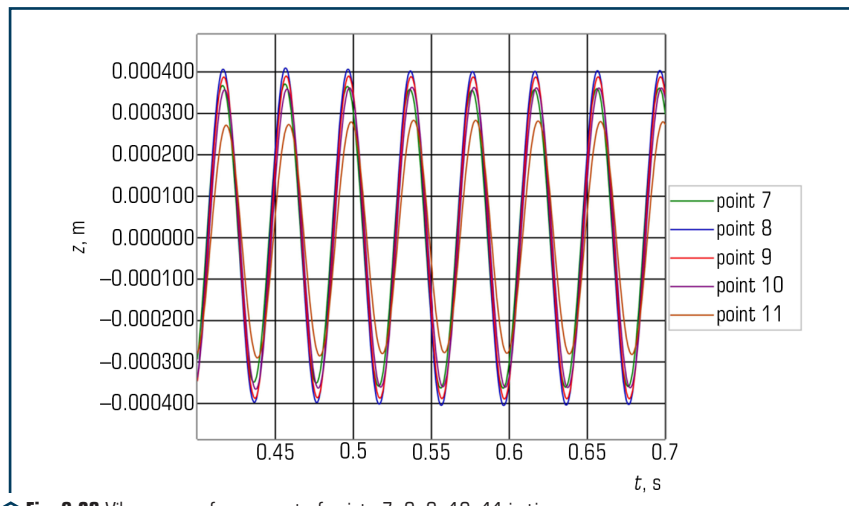**Fig. 8.24** Vibrograms of movement of points 3, 4, 14, 15 in time

Fig. 8.25 Vibrograms of movement of points 5, 6, 12, 13 in time

However, there are also certain differences. So, it was recorded that at points 6, 12 and 13 the vibration amplitudes have similar numerical values within 0.18–0.23 mm. The change in the

oscillation amplitudes at points 7, 8, 9, 10, 11 in time (**Fig. 8.26**) is characterized by a certain deviation in numerical values and in phase.

○ **Fig. 8.26** Vibrograms of movement of points 7, 8, 9, 10, 11 in time

At these points, the amplitudes of oscillations reach values of 0.27—0.40 mm, that is, the limit of change is the smallest in comparison with the movement of points 1, 2 and 16, 17 (**Fig. 8.26**).

The research results indicate the presence of vibration amplitudes different in shape and numerical values over the area of a vibration unit with a polyphase vibration spectrum.

8.3 INVESTIGATION OF THE STRESS-STRAIN STATE OF THE FRAME AND FORMS OF A VIBRATION UNIT WITH SPATIAL VIBRATIONS

8.3.1 MODELING THE STRESS-STRAIN STATE OF VIBRATION PLATFORMS

Determination of the stress-strain state of the vibration platform frame is not an easy task. The complexity of the research is associated with various factors: an increase in the number of finite elements, the use of various types of finite elements in one numerical model, problems of mechanical properties of rubber platform supports, modeling of various types of loads (static and dynamic), modeling of welded joints of a space frame [8, 9].

The following types of finite elements can be used to calculate frames and shapes:

a) the frame elements are modeled with SOLID55 elements. The element is a three-dimensional hexagon with eight nodes located at the corners. This type of element allows the use of

isotropic, plastic and other nonlinear types of materials, with the exception of hyperelastic ones. Elements of this type can take degenerate shapes. Degenerate elements have at first a quadrangular or hexagonal shape, but by combining two or more nodes that take the shape of a triangle for flat elements or a tetrahedron, prism or wedge for volumetric ones;

b) welded seams are taken as idealized and modeled from volumetric finite elements in the form of a six-node triangular prism with the same bases equal to the leg;

c) to model rubber supports, a finite element SOLID185 is used – an element similar to SOLID55, but allows the use of hyperelastic materials.

The displacements of the lower planes of the supports are limited in the X, Y, Z directions, which simulates a rigid clamping of the structure in the foundation. The vibration exciters on the frame are shown conditionally, and their effect on the frame is determined by the driving force. The load on the frame from the form and the concrete mix is simulated by applying a uniformly distributed load.

8.3.2 VIBRATION PLATFORM WITH VERTICAL VIBRATOR

A vibration platform with a horizontal vibrator is divided into finite elements (**Fig. 8.27**). For it, a displacement distribution diagram was obtained (**Fig. 8.28**) in the X, Y, Z directions and a stress distribution diagram (**Fig. 8.29**).

The largest total displacements of the frame elements (**Fig. 8.28**) are observed in the outer frame elements, their maximum value is 0.0615 mm.
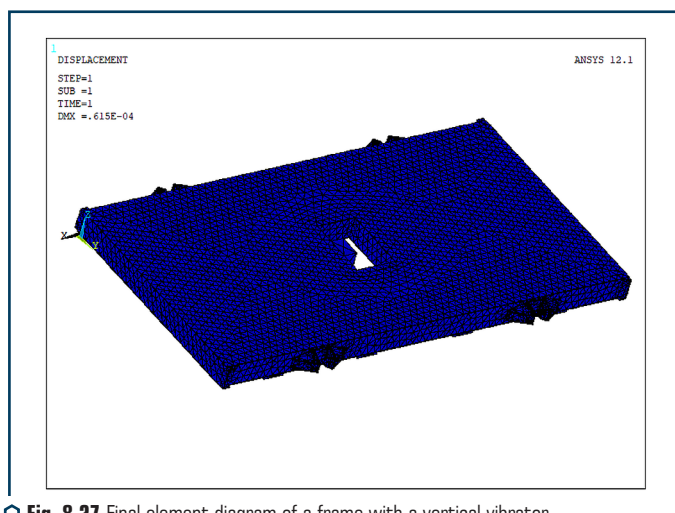

○ **Fig. 8.27** Final element diagram of a frame with a vertical vibrator
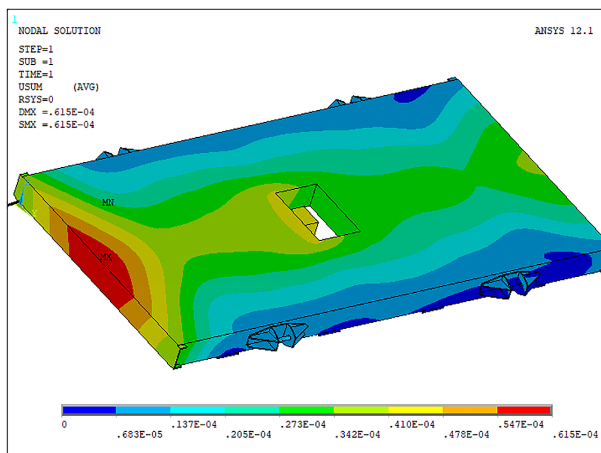
a
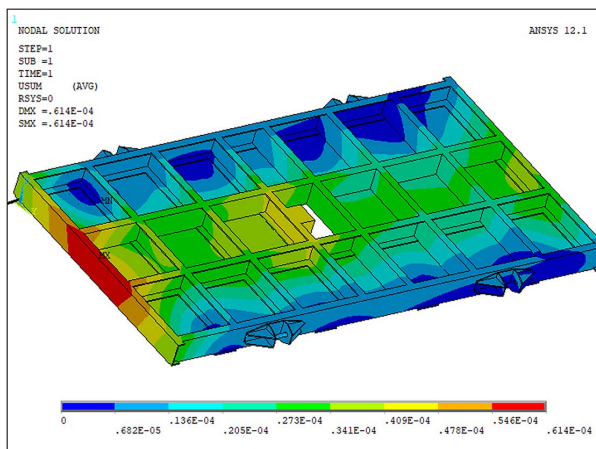
b

○ **Fig. 8.28** Distribution of total displacements:
a – frames with a vertical vibrator; *b* – frames with
a vertical vibrator (the top sheet is conventionally not shown)

Movement in the vertical direction – along the *z*-axis, has both positive and negative values (**Fig. 8.29**), which indicates the presence of small deflections (0.0569 mm) on the cantilever sections of the frame and local bends on the side channels of the frame.
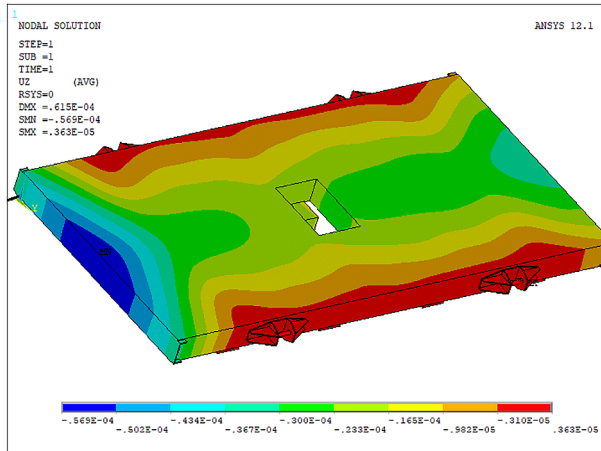
Fig. 8.29 Distribution of vertical displacements:
a – frames with a vertical vibrator; *b* – frames with
a vertical vibrator (the top sheet is conventionally not shown)

The highest values of the equivalent stress reach 10.6 MPa (**Fig. 8.30**). They are observed in the places where vertical and horizontal channels are welded at the place where the vibrator is attached. The values of these stresses are less than the maximum standard stresses, which indicates that the strength of the welded seams is ensured.
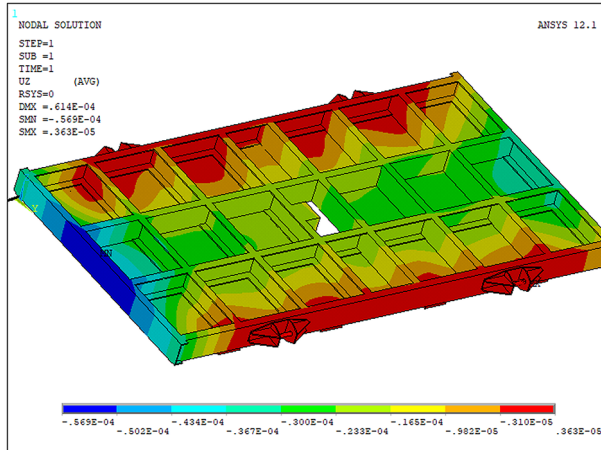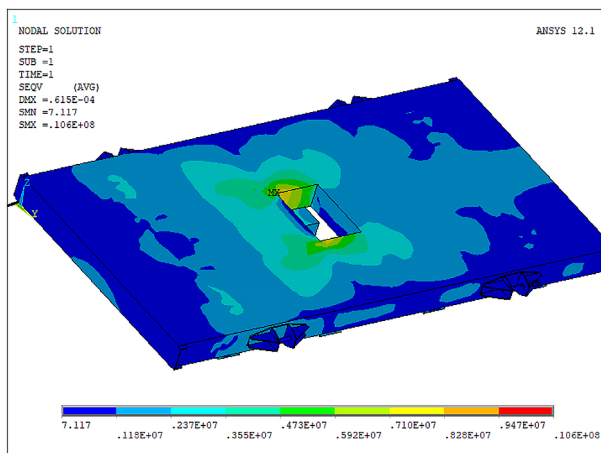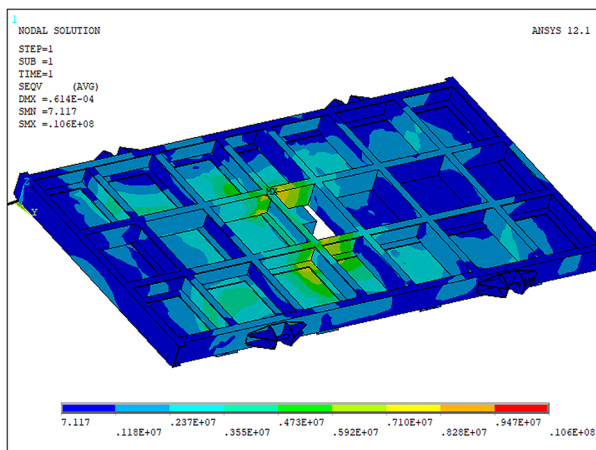
⚪ **Fig. 8.30** Distribution of equivalent stresses:
a – frames with a vertical vibrator; *b* – frames with
a vertical vibrator (the top sheet is conventionally not shown)

In the direction of the *X* axis, the distribution of displacements is circular in nature, with a maximum (0.042 mm) at the place of load application; the outermost parts of the frame are the least deformable.

The distribution of stresses in the frame elements is uneven. The concentration of stresses is observed in the places of welding of elements, but the stress raisers have small values of 4.12 MPa in comparison with the ultimate strength of steel.

The stress in the direction of the X axis is distributed circularly, similar to the distribution of displacements. Moreover, the highest stress values are observed in the two nearest cells to the place of load application.

8.3.3 VIBRATION PLATFORM WITH HORIZONTAL VIBRATOR

The structure of the vibration platform VPGP-6.3×3.6 (**Fig. 8.32**) includes a movable frame with overall dimensions in plan 6.28×3.66, made of channels and a steel sheet made of calm-melting steel st.3sp. In the windows of the moving frame, vibration plates with welded-on M30 nuts are rigidly attached. On the moving frame there are rigid transverse stops for fixing the form with the concrete mixture. The vibration exciter is bolted to the movable frame. With the help of a V-belt transmission, the vibration exciter shaft rotates from an electric motor with a power of 30 kW. The windows of the movable frame are closed with metal covers that prevent particles of the concrete mixture from entering the platform's vibration drive. The movable frame rests on 8 rubber-metal supports attached directly to the foundation of the vibration platform. The supports are attached to the moving frame with the help of protrusions on the supports entering the mounting holes in the moving frame.
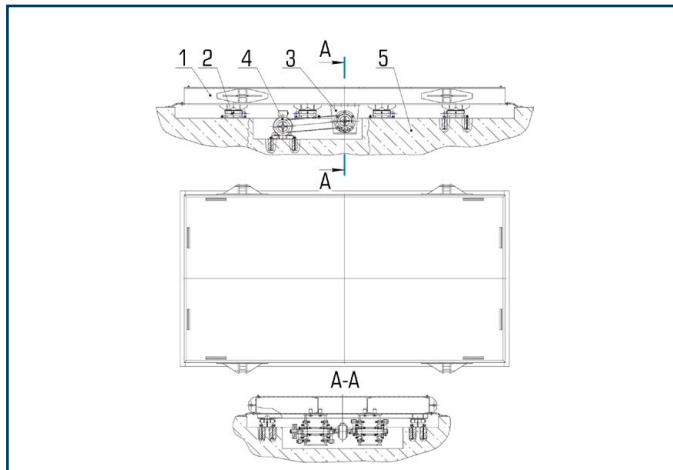
○ **Fig. 8.31** Vibration platform VPGP-6.3×3.6 for the formation of ribbed slabs of coatings with the dimensions of the movable frame in the plan of 6.3×3.6 m: 1 – movable frame, 2 – elastic support, 3 – vibration exciter of torsional vibrations, 4 – electric motor, 5 – foundation

The vibration platform model was loaded with the same uniformly distributed load, but the design and direction of vibration movement were changed.

For this option, a deformed diagram, a displacement distribution diagram (**Fig. 8.32**) and a stress distribution diagram (**Fig. 8.33**) were also obtained.

a

b
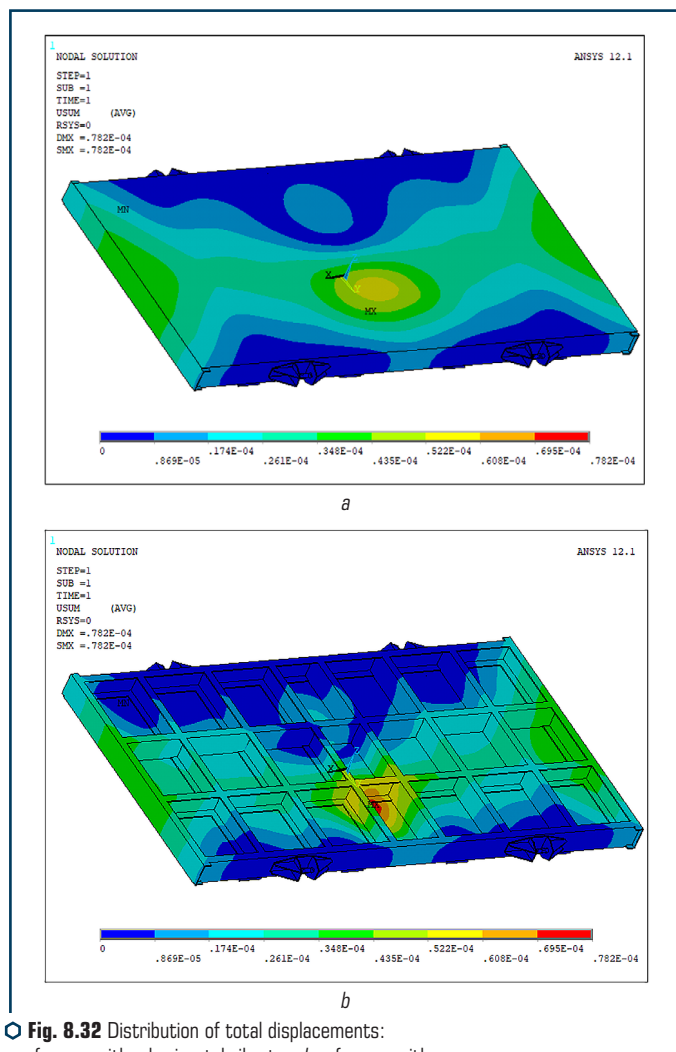
○ **Fig. 8.32** Distribution of total displacements:
a – frames with a horizontal vibrator; *b* – frames with
a horizontal vibrator (the top sheet is conventionally not shown)

The most total displacements of the frame elements are 0.0782 mm (the area is marked in red in the diagram). Such deflections occur in the side channels of the frame on the cantilever sections free from supports (**Fig. 8.33**). In the center of symmetry of the frame, local deflections of up to 0.0608 mm are also observed.

○ **Fig. 8.33** Distribution of equivalent stresses:
a – frames with a horizontal vibrator; *b* – frames with
a horizontal vibrator (the top sheet is conventionally not shown)
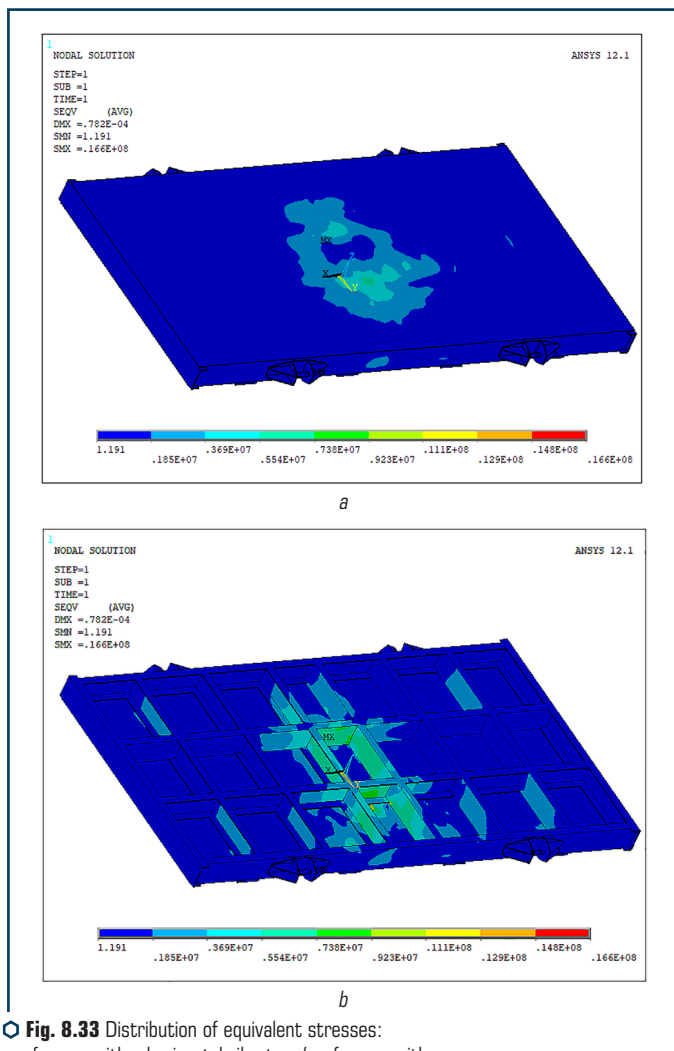
Equivalent stresses have a maximum value of 16.6 MPa (**Fig. 8.33**). These values can be seen in the channels located above the frame supports and in the welds at the vibrator attachment points.

Dynamic calculation of the form [10] (**Fig. 8.34**) is performed in the ANSYS/LS-Dyna finite element analysis program. The program simulates the compaction of a mixture in a metal form during the operation of a shock-vibration unit. For the numerical model, two types of finite elements are used that implement the elastic and plastic properties of the metal form and mixture (**Fig. 8.35**).

The force resulting from the fall of the form from a height of 8 mm, taking into account the acceleration of gravity and the static and dynamic action of the loader on the metal form, is taken as the maximum load.

○ **Fig. 8.34** Metal form
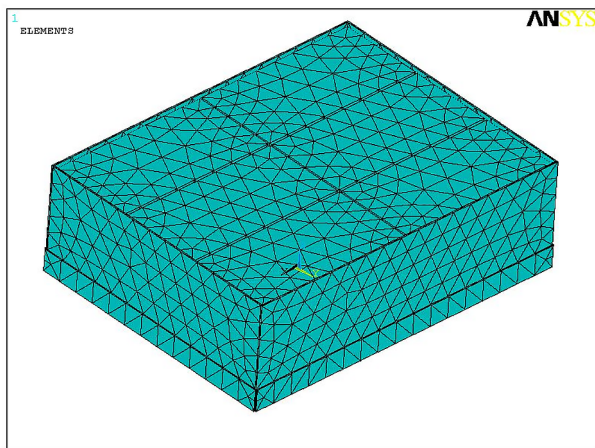
○ **Fig. 8.35** Numerical model of the form with wood concrete mixture

Fig. 8.37 shows the picture of stress distribution on a deformed structure diagram. The loader is not shown in the **Fig. 8.37**, since the distribution of stresses and strains in it is not important for the task at hand. As can be seen from the **Fig. 8.37**, the stress in the elements of the form is on average 15–60 kPa, and the subsidence of the concrete mixture during compaction is about 38 mm, as shown in the work.

○ **Fig. 8.36** Stress distribution in structural members
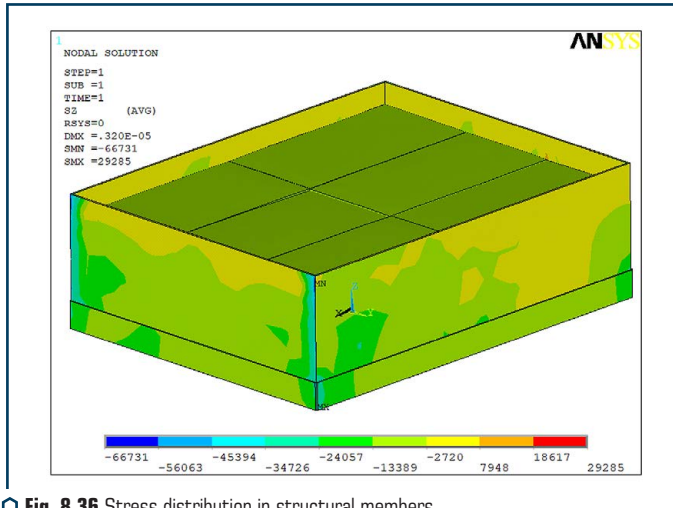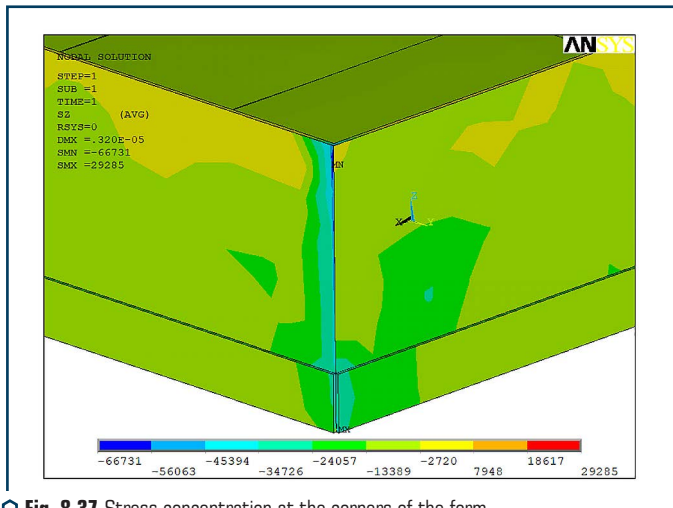

○ **Fig. 8.37** Stress concentration at the corners of the form

The greatest deformation and stress concentration (60–65 kPa) occurs in the corners of the form, where the welded seams of the structure are located (**Fig. 8.37**).

8.4 INVESTIGATION OF THE STRESS-STRAIN STATE OF CRANES METAL STRUCTURES

The study of static dynamic loads of the slewing ring of a truck crane was carried out in order to establish the position of the system and its elements with the highest stresses. The basic laws of the theory of elasticity and plasticity were used to construct a computational mathematical model of a loaded support-rotary contour. Equations of motion were drawn up taking into account the behavior of structural elements and the machine as a whole under the simultaneous action of various loads. The design model was taken in the form of a structure consisting of rods rigidly connected to each other at the nodes. For each bar, this section is shown with geometric characteristics. As a calculation method, the finite element method was used with the definition of displacement (deformation), force (stress) at the mesh nodes of structural elements of the support-rotary contour. The distribution of stresses for each structural element was obtained depending on the type of load.

In the theoretical studies [7–11], a scientific hypothesis was proposed according to which the development of reliable and most efficient machines for various technological purposes is based on the establishment and general purposeful use of the regularities of changes in the internal properties of the working bodies of machines and the technological load, which is a processing material. The implementation of the hypothesis is provided by the solution of a scientific idea [11]. Recently, the development and creation of the design of machines for various technological purposes is carried out in the direction of searching for design solutions with a changing operating mode. In the process of operation of such machines, the maximum allowable use of the internal resources of the machine structure is assumed, which in turn necessitates ensuring strength and reliability with specified dynamic parameters. An integral assessment of the state of metal structures of the finished product can be carried out on the basis of dynamic tests. The idea of such tests is to find the actual dynamic characteristics of the structure (natural frequency, vibration amplitude, etc.) with the subsequent comparison of these characteristics with the characteristics obtained by the method of mathematical modeling of the given structure system. The mathematical model should be created in such a way as to adequately describe the real structure and its behavior under various loads, and also be able to reflect the modeling of various kinds of imperfections associated with manufacturing and direct operation as intended.

Under dynamic loads on structural elements inherent in most machines for technological purposes, the main type of damage is the formation and development of cracks due to the accumulation of fatigue stresses. Durability in case of tedious destruction is determined by the long-term cyclicity of the action of loads on the supporting structures of the machine and its individual elements, as a result of which a crack is formed, which gradually develops and leads to destruction.

The solution to the problem of determining the study of the stress-strain state is carried out by using an integrated approach that combines analytical calculations, mathematical modeling and experimental research directly.

For the implementation of these tasks, the following sequence of research was envisaged:

— analysis of the behavior of structural elements of the machine from the point of view of taking into account all types of loads that were carried out during its operation and determining the possible combination of loads acting on the elements;

— development of a computational model of the research object, taking into account the general or individual most loaded nodes or structural elements;

— drawing up equations of motion, taking into account the behavior of structural elements and the machine as a whole under the simultaneous action of various loads;

— assessment of real loads for the development of an algorithm for determining the stress-strain state, identification of the most stressed structural elements;

— development on a computer model of a matrix of control points for the limiting values of the integral characteristics of the state of the structure for subsequent use in field tests;

— carrying out computer calculations to determine stresses and strains by applying a number of possible loads to the model;

— development and implementation of experimental studies on samples reflecting the real operating conditions of a part or machine unit;

— adjusting the computer model until the comparison of the integral characteristics obtained by measurements at control points during the experiment and during simulation can differ from each other within the permissible error (the computer model obtained in this way will be adequate to the real design within the limits). points of adequacy — points of control of integral characteristics);

— development of recommendations for improving the existing or creating a new design, corresponding to the basic idea of the equal strength of stress distribution, regardless of the applied forces on the elements of the loaded product. The analysis of possible loads was carried out on the basis of the studies carried out using the example of truck cranes. This is due to the fact that these machines are a classic example of the structure of a system in which static and dynamic loads are organically combined, which require correct accounting for safe crane operation under real load conditions. The basic laws of the theory of elasticity and plasticity were used to construct a computational mathematical model of a loaded SC [11–14]. Equations of motion were drawn up taking into account the behavior of structural elements and the machine as a whole under the simultaneous action of various loads. In the case of a dynamic effect on its metal structure (**Fig. 8.38**) as a linear elastic body, the equations of motion in the adopted coordinate system (**Fig. 8.39**) are as follows:

$$z_{i,j,j} + F_i = \rho \cdot U_i, \tag{8.21}$$

where $z_{i,j,j}$ — stress tensors, $(i, j = 1, 2, 3)$; F_i — components of volumetric forces; ρ — material density; U_i — displacement vector.
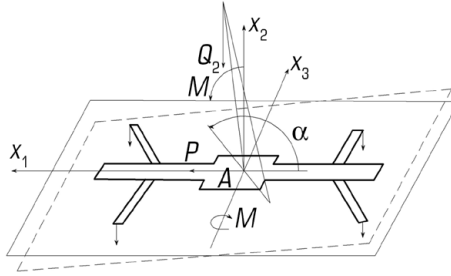
○ **Fig. 8.38** Design diagram of the support contour of a truck crane
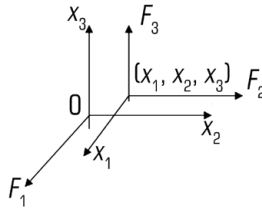
○ **Fig. 8.39** Coordinate system of the acting forces
on the support contour of the truck crane

If to take into account the viscous properties, then let's replace the operator from (21):

$$\rho \cdot \frac{\partial^2}{\partial t^2} \Leftrightarrow \rho \cdot \left(\frac{\partial^2}{\partial t^2} \right) + k \frac{\partial}{\partial t},$$

(8.22)

where k – viscosity coefficient.

Equation (22) in this form remains unchanged.

Let's introduce designations for the speeds of wave propagation in the SC:

$$C_1^2 = \frac{1-v}{(1+v)(1-2v)} \cdot \frac{E}{\rho}; \, C_2^2 = \frac{1}{2(1+v)} \cdot \frac{E}{\rho}.$$

(8.23)

For the case when the force $F(t)$ is ordinary and acts along the $OX1$ axis (at the origin of the coordinate system):

$$U_1\left(x_1, x_2, x_3, t\right) = \frac{1}{4\pi\rho R} \times$$

$$\times \left[\frac{1}{C_1^2} \cdot \frac{x_1^2}{R^2} \cdot P\left(t - \frac{1}{C_1}\right) + \frac{1}{C_1^2} \cdot \left(1 - \frac{x_1^2}{R^2}\right) P\left(t - \frac{1}{C_1}\right) - \left(1 - 3\frac{x_1^2}{R^2}\right) \cdot \int_{\frac{1}{C_1}}^{\frac{1}{C_2}} \lambda P(t - \lambda R) d\lambda \right]; \quad (8.24)$$

$$U_2\left(x_1, x_2, x_3, t\right) = \frac{x_1 x_2}{4\pi\rho R} \cdot \left[\frac{1}{C_1^2} \cdot P\left(t - \frac{R}{C_1}\right) - \frac{1}{C_1^2} \cdot P\left(t - \frac{R}{C_2}\right) + 3\int_{\frac{1}{C_1}}^{\frac{1}{C_2}} \lambda P(t - \lambda R) d\lambda \right]; \quad (8.25)$$

If the force acts along the $OX2$ axis, then it is necessary to replace the indices:

$$y(22) \Rightarrow \begin{cases} 1 \to 2; \\ 2 \to 3; \\ 3 \to 1. \end{cases}$$

If the force acts along the $OX3$ axis, then it is necessary to replace the indices:

$$y(22) \Rightarrow \begin{cases} 1 \to 3; \\ 2 \to 1; \\ 3 \to 2. \end{cases}$$

For a plane problem $(x3=0)$; for a one-dimensional problem: $(x1 \neq 0; x2=x3=0)$.

The SC design scheme is taken in the form of a structure consisting of rods rigidly connected to each other at the nodes (**Fig. 8.40**) in a rectangular coordinate system X, Y, Z and is built along a line connecting the centers of gravity of the cross-sections of the rods.

Each element is designated by small circles numbered with Arabic numerals. The serial number of the bar (element) is shown in a circle. For each bar, this section is shown with geometric characteristics. As a calculation method, the finite element method was used with the definition of displacement (deformation), force (stress) at the nodes of the mesh of structural elements of the SC structure (**Fig. 8.41**).

The correctness of the results of mathematical modeling largely depends on the mechanical characteristics of structural materials and the study of the operation of complex assemblies of load-bearing structural elements. Experimental studies of the connection of parts to each other (**Fig. 8.42, a**) and nodes (**Fig. 8.42, b**) were carried out by the test method for determining the mechanical characteristics to check the results of analytical calculations. Tests on these stands allowed to propose the design of the elements used in real structures of the defense industry complex.
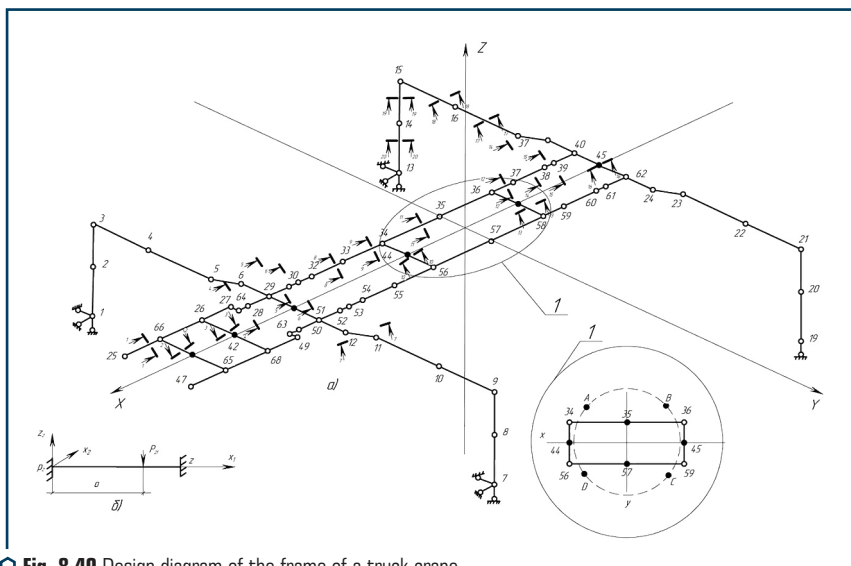
Fig. 8.40 Design diagram of the frame of a truck crane

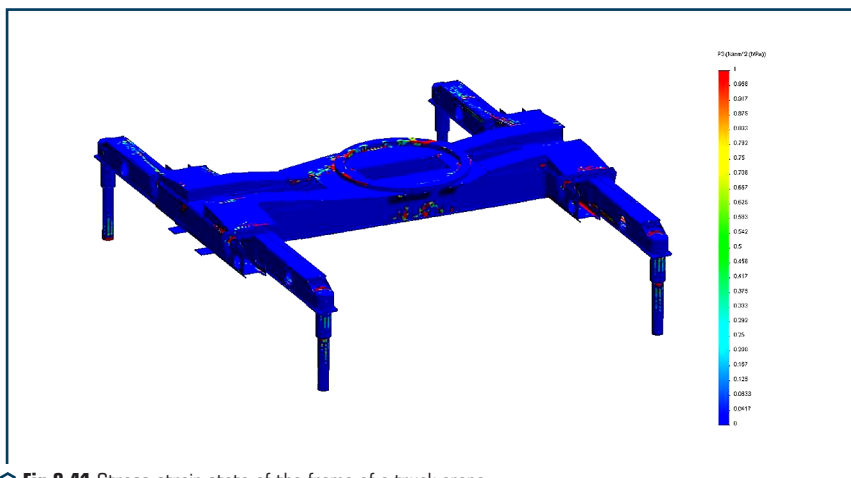**Fig 8.41** Stress-strain state of the frame of a truck crane

It is found that the maximum loads occur in the position of the crane unit perpendicular to the main axis of the vehicle on which the crane unit is fixed. At the same time, it is found that of all the nodes of the crane unit, the greatest stresses arise in the support contour (SC), which ensures the rotation of the lifting mechanism by 360 degrees.

Fig. 8.42 Testing of structural elements of metal structures:
a – tensile welded joint; *b* – bracket test

By changing the dynamic and static loads and analyzing the results obtained, similar to **Fig. 8.41**, the research results were introduced into the SC structure in such a way that all the elements had the same order of numerical values of stresses, which in the final design solution made it possible to reduce the SC mass by 30 %.

8.5 DISCUSSION OF RESEARCH RESULTS

The research results (**Fig. 8.1**) indicate that the maximum values of the equivalent stresses of the forming surface are 2.5 MPa. Higher values of stresses are concentrated in the area of application and distribution of the driving force. The frame design accepts a maximum stress of 11.7 MPa (**Fig. 8.2**). The area of action of such stress values is limited by the contact zones of the frame with the supports and is of a local nature. Vibrograms of changes in the stresses of the forming surface are given for individual elements located near the application of a dynamic external force. This is a fundamentally new result. It consists in the fact that the detected transient process is intended to be taken into account when determining the parameters and locations of the vibrators. In such modes, the forms of natural vibrations of the system are realized with large vibration amplitudes and, accordingly, a lower frequency. And this opens up a real opportunity to reduce the energy consumption of the drives of the vibration machine. The stresses for structural elements located symmetrically on the opposite side from the applied force are investigated (**Fig. 8.5**). In contrast to the previous vibrograms, there is no in-phase change in stresses in relation to the forcing force, which confirms the inclusion of dissipative forces in the design model. An important

criterion for evaluating a design from the point of view of the efficiency of the compaction process is shear stress. Indeed, in the presence of such stresses in the medium, there is an intensive movement of particles and compaction. To analyze the shear stresses of the forming structure, time intervals were selected corresponding to 1/4 of the period of oscillation of the driving force (**Fig. 8.6**). The zones with the maximum positive stress values, in which the force is applied, have been determined. A complex sign-like stress-strain state of the structure under the action of a spatial load has been confirmed. This study has a limitation in terms of the adopted law of the change of dissipative forces.

A fundamentally new result has been obtained, which consists in the fact that the implementation of a complex vibration mode as an effective method of accelerated compaction of concrete mixtures is ensured by the arrangement of unbalances at a certain angle on each separate vibration unit. As a result, energy consumption is reduced by 30 %, and the process of forming a concrete product is reduced by 20 %. The presence of different forms of the polyphase spectrum is confirmed by the vibration modes (**Fig. 8.11–8.17**) and the distribution of the vibration amplitudes of the form surface along the length of the structure for one period of vibration. The use of such effects is determined by the overall dimensions of the product in terms of plan and height, which affects not only the phase deployment of the unbalances along the central axis of the vibration unit, but also the magnitude of the static moment of the unbalances.

The design diagram of an energy-saving vibration plant with a polyphase vibration spectrum has been substantiated. Modeling of the working process of a vibration plant is based on the use of the finite element method using the MSC.NASTRAN calculation complex (MSC.Software, Germany).

As a result of the research, the main modes of vibration have been determined by the numerical values of the frequencies of 1.32 Hz, 4.10 Hz, 16.61 Hz, 27.40 Hz. The calculated value of the oscillation frequency of the operating mode is 25 Hz. The most effective in the framework of the research carried out is the vibration form of 24.31 Hz. The implementation of this form of vibration provides an energy-saving mode of operation of the vibration unit.

A polyphase spectrum of vibrations of the unit has been established and proposedat an excitation frequency of 25 Hz, according to which vibration amplitudes of 0.27…0.6 mm are realized. The investigated vibration mode of the computational model is a confirmation of the energy-saving mode, which is a prerequisite for calculating and creating a new class of vibration unit.

Analysis of the stress-strain state of frames with horizontal and vertical vibrators shows that in the elements of the proposed frame structures during the operation of vibration platforms, stresses arise significantly less than the design resistance of steel, which provides the condition for the strength of the structure. The deflections in the frame elements are much less than permissible, which indicates the sufficient planar and spatial stiffness of the created frames and metal forms.

Frames with a vertically positioned vibrator work in tension and bending. The movements of the frame members are distributed circularly from the vibrator location. The greatest stresses arise at the welding points of the longitudinal and transverse channels and the top sheet in the vibrator attachment area. Their maximum values are 11.4 MPa.

For the distribution of displacements of frames with horizontally located vibrators, areas of both positive and negative deflections are characteristic. At the junction of the vibrator with the frame, a wave-like bend is observed, and in the cantilever sections, deflections of 0.0672 mm are observed. The maximum stress in the vertical direction is 16.6 MPa.

In the manufacture of frames of such structures, special attention should be paid to the quality of welded seams in the area of the vibrator and in the attachment points of the supports in order to minimize the possibility of cracks in them.

CONCLUSIONS TO SECTION 8

1. In the course of the research, finite element models of vibration machines have been developed to implement the transfer of energy in the vertical direction with a fixed frequency, with a polyphase direction of external forces, with a spatial direction of movement in the vertical and horizontal planes.

2. The study of the nature of the distribution and the numerical values of stresses and strains has been done in the forming structure of the unit, depending on the angle of instantaneous action of the external force of the vibrators and vibration frequencies.

3. The maximum values of the equivalent stresses of the forming surface are 2.5 MPa. Higher values of stresses are concentrated in the zone of application and distribution of force, the maximum stresses are 11.7 MPa.

4. The results obtained indicate the presence of vibration amplitudes of different shapes and numerical values over the area of a vibration unit with a polyphase vibration spectrum.

5. Stress concentrators in structural elements of machines for technological purposes have been determined, taking into account the working loads.

6. The static and dynamic loads of the support contour of a truck crane have been investigated.

7. The obtained research results are taken into account when making further design decisions when creating such machines.

REFERENCES

1. Petrov, A. A. (2002). Teoriia i proektirovanie vibratsionnykh mashin impulsnogo i rezonansnogo deistviia. Khmelnitskii: Tekhnologicheskii un-t Podoliia, 182.
2. Nazarenko, I., Gaidaichuk, V., Dedov, O., Diachenko, O. (2017). Investigation of vibration machine movement with a multimode oscillation spectrum. Eastern-European Journal of Enterprise Technologies, 6 (1 (90)), 28–36. doi: http://doi.org/10.15587/1729-4061.2017.118731
3. Bazhenov, V. A., Dashchenko, A. F., Orobei, V. F., Surianov, N. H. (2004). Chyselnie metodi v mekhanyke. Odessa: Draft, 564.

4. Bathe, K. J. (1996). Finite Element Procedures. New-York: Prentice Hall, 1037.

5. Lanets, O., Derevenko, I., Borovets, V., Kovtonyuk, M., Komada, P., Mussabekov, K., Yeraliyeva, B. (2019). Substantiation of consolidated inertial parameters of vibrating bunker feeder. Przeglad Elektrotechniczny, 95 (4), 47–52. doi: http://doi.org/10.15199/48.2019.04.09

6. Gursky, V., Kuzio, I., Lanets, O., Kisała, P., Tolegenova, A., Syzdykpayeva, A. (2019). Implementation of dual-frequency resonant vibratory machines with pulsed electromagnetic drive. Przegląd Elektrotechniczny, 95 (4), 43–48. doi: http://doi.org/10.15199/48.2019.04.08

7. Nazarenko, I. I., Nesterenko, T. M., Nesterenko, M. M., Marchenko, I. A. (2020). Kompiuterne modeliuvannia elementiv vibratsiinykh mashyn. Kompiuterna matematyka v nautsi, inzhenerii ta osviti (CMSEE-2020), 36–38.

8. Nazarenko, I. I., Smirnov, V. M., Fomin, A. V., Sviderskyi, A. T., Kosteniuk, O. O., Diedov, O. P., Zukhba, A. H.; Nazarenko, I. I. (Ed.) (2010). Osnovy teorii vzaiemodii robochykh orhaniv budivelnykh mashyn iz napruzheno-deformovanym seredovyshchem. Kyiv: «MP Lesia», 216.

9. Nesterenko, M. M., Nesterenko, T. M., Mahas, N. M. (2017). Method of calculation of shock-vibrating machinefor manufacturing products from light concrete for energy efficient reconstruction buildings in Ukraine. Naukovyi visnyk budivnytstva, 88 (2), 178–182.

10. Nazarenko, I. I., Dedov, O. P., Sviderski, A. T., Ruchinski, N. N. (2017). Research of energy-saving vibration machines with account of the stress-strain state of technological environment. The IX International Conference HEAVY MACHINERY HM 2017, 21–24.

11. Nazarenko, I., Gaidaichuk, V., Dedov, O., Diachenko, O. (2018). Determination of stresses and strains in the shaping structure under spatial load. Eastern-European Journal of Enterprise Technologies, 6 (7 (96)), 13–18. doi: http://doi.org/10.15587/1729-4061.2018.147195

12. Nazarenko, I., Gavryukov, O., Klyon, A., Ruchynsky, N. (2018). Determination of the optimal parameters of a tubular belt conveyor depending on such an economical. Eastern-European Journal of Enterprise Technologies, 3 (1 (93)), 34–42. doi: http://doi.org/10.15587/1729-4061.2018.131552

13. Luchko, J., Kovalchuk, V., Kravets, I., Gajda, O., Onyshchenko, A. (2020). Determining patterns in the stresseddeformed state of the railroad track subgrade reinforced with tubular drains. Eastern-European Journal of Enterprise Technologies, 5 (7 (107)), 6–13. doi: http://doi.org/10.15587/1729-4061.2020.213525

14. Kovalchuk, V., Onyshchenko, A., Fedorenko, O., Habrel, M., Parneta, B., Voznyak, O. et. al. (2021). A comprehensive procedure for estimating the stressed-strained state of a reinforced concrete bridge under the action of variable environmental temperatures. Eastern-European Journal of Enterprise Technologies, 2 (7 (110)), 23–30. doi: http://doi.org/10.15587/1729-4061.2021.228960

Edited by
Ivan Nazarenko

DYNAMIC PROCESSES IN TECHNOLOGICAL TECHNICAL SYSTEMSS

Ivan Nazarenko, Oleg Dedov, Iryna Bernyk, Andrii Bondarenko, Andrii Zapryvoda,
Maxim Nazarenko, Ivan Pereginets, Yevhen Mishchuk, Mykola Kyzminec,
Serhii Oryshchenko, Oleg Fedorenko, Sergii Tsepelev, Artur Onyshchenko, Liudmyla Titova,
Ivan Rogovskii, Mykola Ruchynskyi, Anatoly Svidersky, Volodymyr Slipetskyi,
Maksym Delembovskyi, Igor Zalisko, Mykola Nesterenko

Monograph

Technical editor I. Prudius
Desktop publishing T. Serhiienko
Cover photo Copyright © 2021 Canva